OCTREOTATE: A NEW SOMATOSTATIN ANALOGUE FOR TUMOR IMAGING AND RADIONUCLIDE THERAPY

Joseph Thomas Edward Bugaj

Front Cover: Corresponding images of a CA20948 tumor bearing rat by fluoresence imaging using Cytate (right) and ^{111}In-DTPA-Tyr^{3}-Octreotate (left)

Bibliografische Information Der Deutschen Bibliothek

Die Deutsche Bibliothek verzeichnet diese Publikation in der Deutschen Nationalbibliografie; detaillierte bibliografische Daten sind im Internet über <http://dnb.ddb.de> abrufbar.

Dissertation, Erasmus Universiteit Rotterdam
ISBN 3-89820-422-7

Nordendstr. 75, 13156 Berlin • ☎ 030 - 45 49 48 66
http://www.menschundbuch.de • info@menschundbuch.de

OCTREOTATE: A NEW SOMATOSTATIN ANALOGUE FOR TUMOR IMAGING AND RADIONUCLIDE THERAPY

OCTREOTATE: EEN NIEUW SOMATOSTATINE ANALOGON VOOR TUMORVISUALISATIE EN RADIONUCLIDENTHERAPIE

PROEFSCHRIFT

ter verkrijging van der graad van doctor aan
de Erasmus Universiteit Rotterdam
op gezag van de rector magnificus
Prof.dr.ir. J.H. van Bemmel
en volgens het besluit van het College voor Promoties.

De openbare verdediging zal plaats vinden op
donderdag 28 november 2002 om 13:30 uur door

Joseph Thomas Edward Bugaj

geboren te New York (USA)

Dedication:

To my parents, Joseph and Helen

To Maggie

"Any day now, any day now, I shall be released".....

(Bob Dylan)

Promotiecommissie

Promotor:	Prof.dr. E.P. Krenning
Overige leden:	Prof.dr.ir. T.J. Visser
	Prof.dr. S.W.J. Lamberts
	Prof.dr. S. Pauwels
Co-Promotor:	Dr.ir. M. de Jong

Paranimfen: H.F. Bernard and Wouter A. Breeman

The studies conducted in this thesis were largely performed at the laboratories of Mallinckrodt/Tyco Healthcare, Saint Louis, Missouri and are hereby acknowledged.

Publication of this thesis was made possible due to the generous financial support of **Schering AG** and **I.D.B. Holland B.V.**

CONTENTS

List of Abbreviations

ALA	5-aminolevulinic acid
AR42-J	Rat acinar pancreatic tumor line
CA20948	Rat acinar pancreatic tumor line
CCD	Cooled coupled device
CMDTPA	Carboxymethyl diethylenetriaminepentacetic acid
DMF	Dimethylformamide
DNA	Deoxyribonucleic acid
DOTA	Polyazamacrocycle
DTPA	Diethylenetriaminepentacetic acid
Gy	Gray
HPLC	High pressure liquid chromatography
$hSST_2$	Human somatostatin receptor subtype-2
IC_{50}	Inhibitory concentration at 50% saturation
ICG	Indocyanine green
%ID/g	Percent injected dose per gram of tissue
%ID/o	Percent injected dose per whole organ
keV	Thousand electron volts
LC-MS	Liquid Chromatography-Mass Spectroscopy
mCi	Millicurie
MBq	Megabecquerel (10^6 Bq)
MeV	Million electron volts
mmol	Millimole

MURR	Missouri University Research Reactor
nM	Nanomolar
NMR	Nuclear magnetic resonance spectroscopy
PDT	Photodynamic therapy
Phe	Phenylalanine
SA	Specific activity
SCID	Severe combined immunodeficient
sst_2	Somatostatin receptor subtype-2
$t_{1/2}$	Half-life
TFA	Trifluroacetic acid
Tyr	Tyrosine
µCi	Microcurie
µmol	Micromole

CHAPTER 1

INTRODUCTION AND BRIEF HISTORY OF RADIONUCLIDE THERAPY

INTRODUCTION

The use of radionuclides for therapeutic applications first began nearly 50 years ago with the use of iodine-131 (I-131), phosphorus-32 (P-32) and strontium-89 (Sr-89). These early indications were primarily for metastatic bone pain and thyroid malignancies. I-131 was and still is used for the treatment of thyrotoxicosis and differentiated thyroid (papillary and follicular) carcinoma (Chatal et al., 1999, Park 1997). Palliation of bone pain from skeletal metastases by treatment with Sr-89 was first attempted by Pecher in 1942 (Hoefnagel 1991). Since then, there has been a resurgence in the management of bone pain using isotopes including P-32, Sm-153, and Re-186 usually complexed with a variety of bisphosphonate ligands that seek and bind with high affinity to the hydroxyapatite surface of bone (Volkert et al., 1991, Hoefnagel 1991, Chatal et al., 1999, Syed et al., 1999). P-32 orthophosphate has been used as early as 1936 for the treatment of myleoproliferative disorders including polycythemia vera and thrombocythemia (Chatal et al., 1999). However, the use of targeted radiotherapy has only recently become increasingly popular in the areas of oncology, endocrinology and rheumatology. This heightened interest can be attributed in part to an increasing number of radionuclides for therapy and the advent of specific tumor seeking agents that direct the radiolabel to the tissue of choice (Hoefnagel 1998, Chatal et al.; 1999; Park 1997; Murtha 2000).

Therapeutic nuclear medicine is rapidly expanding as an adjunct modality in oncology to conventional chemotherapy and external beam therapy. This type of therapy offers a systematic but very selective delivery of radiation to target tissues with a relatively low frequency of immediate and latent side effects. An additional advantage to this approach is that tumor uptake and retention can be assessed by a

tracer study prior to the administration of the therapeutic dose. As a result of new developments in carrier molecules that provide greater selective tumor targeting properties, the specific metabolic characteristics and biological properties of tumors are now the focus for targeted radionuclide therapy, as opposed to only diagnostic imaging and staging procedures (Hoefnagel 1991). Effective radiation therapy depends on the total absorbed radiation dose and the sensitivity of the lesion that is being targeted. Successful radiation therapy depends upon high and selective uptake of the isotope at the target site, and a long retention time to allow for effective cell kill. A relatively simplistic calculation using the formula $D_{(\beta^-)}(Gy) = 19.9 \times C \times E \times T_{(eff)}$ is used to estimate absorbed radiation dose from a β^- emitting radionuclide with uniform distribution throughout the tumor mass (Hoefnagel 1991). In this formula C is the concentration in MBq per gram of tissue, E is the effective β^- energy in Mev and $T_{(eff)}$ is the effective half-life in days. Three key factors should be considered when deciding on a particular radionuclide for a therapeutic application: (1) the chemical and physical properties of the radionuclide, (2) the production methods of the radionuclide and (3) the biological behavoir of the radionuclide, especially if the complex is unstable and in vivo disassociation occurs (Zweit 1996). The half-life, mode of decay and the type and intensity of the energy emitted are associated with the physical properties. The chemical form refers to the nature of the agent, which can be as simple as the ionic form (I^- or Sr^{+2}), to as complex as radiolabeled monoclonal antibodies (MoAbs). As such, the more ideal agents would exhibit in vivo inertness with respect to disassociation, transchelation and redox chemistry. Overall radionuclidic purity and high specific activity are essential qualities that relate to the production of the radionuclide. Radionuclides that have been evaluated as potential radiotherapy indications include the following three modes of decay: (1) alpha

emitting radionuclides, (2) beta emitting radionuclides and (3) Auger electron and Coster-Kronig electron emitting radionuclides following electron capture (Volkert et al., 1991). Since each type of particle that is emitted will have a different range, effective distance and relative biologic effectiveness (RBE), careful selection of the radionuclide to fit a particular therapeutic regimen needs to be strongly considered to adequately match the biological properties of the target to the physical properties of the radionuclide to maximize the therapeutic index. Though the focus of this thesis will be on the use of low to medium β^- emitting radionuclides for therapy of somatostatin receptor expressing tumors, a brief description of the three general categories of decay is provided.

Alpha particle emitters: Alpha particles are high-energy helium nuclei producing high density ionizing radiation. They are monoenergetic particles that deposit their energy over a relatively short range (McDevitt et al. 1998). For a 5-8 MeV alpha emitter a range of only 40-80μm would be expected. Despite this short range associated with alpha particles, they are attractive candidates for certain limited therapeutic applications. The high linear energy transfer (LET) of alpha particle radiation is especially effective in limiting the cell's ability to repair itself at the level of DNA, particularly under hypoxic conditions. The high RBE requires that only a few particles are needed to promote cell death in comparison to the higher number of beta particles. The distinct disadvantage of this type of therapy is that the agent must be tightly bound to the carrier and be in very close proximity to the tumor cell, and not to normal non-target cells to avoid undesirable toxicities. The two most studied alpha emitters to date are bismuth-213 (Bi-213) and astatine-211 (At-211). Bi-213 is available from a generator with radon-224 as the parent, while At-211 is produced in an accelerator facility. Three other alpha emitters with clinical therapeutic potential

include bismuth-212 (Bi-212), fermium-255 (Fe-255) and actinium-225 (Ac-225). Both Bi-213 and At-211 have been largely complexed to monoclonal antibodies for radioimmunotherapy, but recently Bi-213 has been evaluated with smaller peptides when incorporated into DOTA like ligand systems. Both of these radionuclides suffer from short half-lives of 45 minutes and 7.2 hours respectively. The more favorable properties of Ac-225 with a $t_{1/2}$ of 10 days and a release of 4 alpha emissions in the decay chain resulting in 28MeV total energy release, make this radionuclide very attractive for therapy (Sgouros 2000; Kennel et al., 2000). Because of the tremendous release of energy, very stable chelates for Ac-225 are required, but the advent of the macrocylic systems including HEHA has shown in vivo stability when chelated to Ac-225 (Deal et al., 1999). Table 1 describes briefly the primary alpha emitting candidate radionuclides and their salient properties.

Table 1: Candidate Alpha (α)-emitting Radionuclides for Radiotherapy

Radionuclide	Half-Life	Mean Energy	%Emitted/decay (Particle)
Bi-213	45.6 min	6.0 MeV	2% (α); 98% (β)
Bi-212	60.5 min	7.8 MeV	36% (α); 64% (β)
At-211	7.21 hr	6.76 MeV	42% (α); 19% (γ)
Fm-255	20.1 hr	7.02 MeV	93% (α)
Ac-225	10 d	6.0 MeV (X4)	100% (α)

Beta Particle Emitters: Beta particles are negatively charged electrons emitted from the nucleus with a wide energy spectrum range (Zweit 1996). Generally, the range of energies for β^- particles is much greater compared to α-particles, and the low or sparse ionization density is the reason for their low LET (Volkert et al., 1991). The

energies are usually listed as the average energy in MeV ($B_{(avg)}$) which is approximately one-third the value of the maximum energy ($B_{(max)}$). Beta emitters are classified as low energy, medium energy and high energy emitting radionuclides with corresponding $E_{(avg)}$ values of 0.08-0.18MeV, 0.23-0.36 MeV and 0.5-1.0MeV respectively (Zweit 1996). These types of radionuclides are primarily produced in nuclear reactors using an N,γ reaction to produce neutron-rich isotopes, although a few are produced in charged particle accelerators (Volkert et al., 1991). Because of the ready supply of a variety of beta emitters a relatively large number of potential candidates have been evaluated clinically. The larger range in energy for beta emitters allows for greater flexibility in comparison to alpha emitters with regard to the choice of the preparation of a potential therapeutic agent. For example, radionuclides that can be produced in low specific activity such as Sm-153, Re-186, Ho-166 and Sr-89 are all effective agents for palliation of bone pain. The first three radioisotopes are complexed to ligands (EDTMP, HEDP and DOTMP) at high ligand to metal ratios. The high selectivity of these ligands for the skeletal system and their rapid urinary clearance from non-osseous tissues has shown clinical efficacy, and the samarium agent was approved as a commercial product in 1997 (Maxon et al., 1988, Goeckler et al., 1998; Turner et al., 1989). High specific activity beta emitters include rhodium-105, lutetium-177, gold-199 and promethium-149, and are good potential candidates as receptor targeted radionuclides complexed to smaller molecules like peptides (Zewit 1996). Non-carrier added (NCA) radioisotopes produced from a generator system include yttrium-90 and rhenium-188. Both are high-energy beta emitters (E_{max} 2.27MeV and 2.10MeV respectively), with Y-90 forming stable complexes with DOTA like ligands and Re-188 stably chelating to N_3S ligand systems. Additionally, both radionuclides have been complexed to monoclonal antibodies (MoAbs) for indications in radioimmunotherapy (Hoefnagel 1991). The

longer path length of the beta ray from isotopes like Y-90 and Re-188 is approximately 10-12 mm and is considered ideal for larger tumors with a non-uniform distribution of radioactivity ("cold spots") by some investigators. This is in comparison to lower energy radioisotopes, which are considered to be more efficacious for treating smaller tumor masses (Humm et. al., 1986, Zweit 1996). Table 2 describes briefly the primary beta emitting candidate isotopes and their physical properties.

Table 2: Candidate Beta (β^-)-emitting Radionuclides for Radiotherapy

Radionuclide	Half-Life	$E_{(max)}$(MeV)	E(γ)(keV)	Range(mm)
I-131	8.1 (d)	0.61	364	2.4
P-32	14.3 (d)	1.73	---	8.7
Sr-89	52.1 (d)	1.49	---	5.7
Re-186	3.8 (d)	1.07; 0.93	137	3.6
Sm-153	46.8 (h)	0.82; 0.71; 0.64	103	2.7
Lu-177	6.6 (d)	0.497	208	2.5
Ho-166	1.13 (d)	1.84	80	8.7
Rh-105	1.4 (d)	0.57	319	2.85
Pm-149	2.2 (d)	1.07	286	5.35
Au-199	3.2 (d)	0.46	158	2.3
Re-188	17 (h)	2.1	155	10.5
Y-90	64 (h)	2.27	---	11.5

Auger electron/Coster-Kronig electron emitters: Radionuclides that decay by electron capture or isomeric transition emit low energy Auger and Coster-Kronig electrons which have a very short range (<1μm). Therefore, in order to be effective, their therapeutic application is limited to situations in which the carrier localizes in or very

near the cell nucleus (Zweit 1996, Volkert et al.,1991). This resulting concentrated shower of low energy Auger and Coster-Kronig electrons with energies ranging from only a few to several hundred electron volts occurs in an extremely small volume of nuclear DNA producing a high "LET like environment" and which is independent of oxygen concentration (Volkert et al., 1991). A successful therapeutic agent based on this mechanism necessitates that the carrier be incorporated into the tumor cell target, and then be selectively guided further in the direction of the cell nucleus (Hornick et al., 2000). Agents of this general category include radiolabeled DNA intercalators that have shown to be highly effective cell killing agents and internalizing antibodies (Kassis et al., 1989; Behr et al., 2000). Auger and Coster-Kronig electron emitting radionuclides include europium-165, platinum-193m, iodine-125, indium-111 and rhodium-103. Table 3 briefly describes the main candidate Auger and Coster-Kronig electron emitting radionuclides with therapeutic potential.

Table 3: Auger and Coster-Kronig Electron Emitting Radioisotopes for Radiotherapy

Radionuclide	Half-life
I-125	60 (d)
Er-165	10.3 (h)
Pt-193m	4.3 (d)
Rh-103	59 (min)
In-111	67.3 (h)

Radioimmunotherapy: An area that has received a considerable amount of attention over the past 15 years is the use of radiolabeled antibodies (MoAbs) for the purpose of radioimmunotherapy. With the advent of the development of the hybridoma technology of Kohler and Milstein in 1975, the number of monoclonal antibodies against a large number of tumor antigens became possible (Hoefnagel 1991; Chatal et al., 1999; Hoefnagel 1998). The subsequent separation of whole antibodies into Fab and $F(ab')_2$ fragments offered even greater promise for this approach allowing for

faster blood clearance and a reduced human anti-mouse antibody (HAMA) response. Monoclonal antibodies (MoAbs) were first used as diagnostic scintigraphic agents (radioimmunoscintigraphy), but therapeutic applications directed against various antigens of specific tumor types quickly followed (Chatal et al., 1999; Park 1997). Radionuclides that have been complexed to antibodies for radioimmunotherapy include I-131, Re-186, Re-188, Y-90, Cu-67, At-211, Bi-212 and Bi-213 (Park 1997). Results with solid tumors has been disappointing resulting in an objective response rate of <2% (Chatal et al., 1999; Hoefnagel 1998). These poor results have been attributed to the low uptake of antibody in the tumor, relative radio-resistance of the tumors treated and short retention of the antibody at the tumor site (Humm et al., 1990; Hoefnagel 1991/1998, DeNardo et al., 1999). Therefore, this approach has not lived up its initial expectations. More recent positive results using I-131 anti-CD 20 antibody for the treatment of leukemia and lymphoma (liquid tumors) has resulted in objective response rates of nearly 70%, and a high number of patients achieving complete remission (Hoefnagel 1998). Major drawbacks to radioimmunotherapy in general include acute toxicities, HAMA response, and bone marrow toxicity (Humm et al., 1990; Hoefnagel 1991). The encouraging results in liquid tumors show that radioimmunotherapy has a definite place in the clinic, but the approach to solid tumor radioimmunotherapy may not be a reality in the near future. Table 4 is a summary of the current status of radionuclide therapies which are available and/or are in clinical progress that relate directly to the oncology area. Additionally, their respective targeting mechanisms are listed.

Of the draw-backs mentioned regarding the use of monoclonal antibodies for radioimmunotherapy (RAIT), a major concern is the amount of time required for these types of molecules clear from the normal non-target tissues. High-energy

radionuclides like Y-90 would impose a high radiation burden on normal tissue as a result of the high degree of non-specific localization of the radioactivity (Goodwin et al., 1999). More recently, there has been a concerted effort to improve the targeting moiety to solid tumors and significantly reduce non-specific background radiation, which would permit faster imaging of the malignancy, but more importantly reduce the non-specific radiation burden from the non-target tissues. The methods used to achieve the reduction in background has been termed "pre-targeting" and the experimental results in animal models have been impressive thereby resurrecting the concept of RAIT.

Successful pretargeting combines the slow clearance of the target molecule (MoAb) with the rapidly clearing effector molecule, which results in high tumor uptake with correspondingly lower non-target retention, which reduces the toxicity as a result. The most popular pre-targeting approaches have employed either the biotin/avidin or hapten/antibody systems (Yao et al., 1998). These approaches allow for separate administration of antibody and effector molecule, which separate or decouple the pharmocokinetics of the antibody from the radionuclide (Axworthy et al., 2000). By separating these two, high uptake of the antibody at the target site can occur followed by injection of the rapidly clearing effector (radionuclide) molecule. Pairing of the appropriate receptor-ligand-combination results in shorter whole body residence time of the radionuclide permitting administration of higher doses of radioactivity. Axworthy used the avidin/biotin system of pretargeting showed that the conjugate NRLU-10/SA injected into nude mice bearing human xenografts were cured (10/10 mice) after a single dose of 600-800μCi of 90Y-DOTA-Biotin (Axworthy et al., 2000).

A second approach to pre-targeting is known as the Affinity Enhancement System (AES) which uses bispecific antibodies and radiolabeled bivalent haptens to target cells. The system promotes cooperative binding of the haptens to target cells thereby delivering increased radiation doses to tumors and increasing residence times at the site (Barbet et al., 1999). Preliminary clinical results with MTC and certain lung cancers look promising.

Table 4: Therapeutic Applications of Nuclear Medicine in Oncology

Treatment	Targeting Mechanism	Indication
I-131(as iodide)	Thyroid Hormone Synthesis	Thyroid Cancer
P-32 Phosphate	Incorporation into DNA of rapidly proliferating cells	Polycythemia vera Thrombocythemia
I-131-MIBG	Active uptake in granular storage	Neuroblastoma Pheochromocytoma Paraganglioma MTC
In-111/Y-90 Octreotide	Somatostatin receptor binding	Neuroendocrine, SCLC
I-131 anti-CD20 I-131 MoAbS	Antigen binding	Lymphoma, Renal cell Carcinoma, Thyroid cancers Lymphoma MTC, NSCLC
Sr-89 Chloride Re-186 HEDP Sm-153 EDTMP Sn-117m DTPA	Bone metastases	Bone Pain Palliation
Y-90 microspheres I-131 Lipidol	Intravascular trapping	Hepatocellular ca. Liver metastases
Intracavity MoAbs	Antigen binding	Malignant effusions Craniopharyngioma
Intratumoral MoAbs P-32 Colloids	Direct intratumoral injection	Glioma Pancreatic and liver Tumors

(Source: Hoefnagel 1998)

Somatostatin Receptor Targeted Radiotherapy: Almost 30 years after the discovery and identification of somatostatin, the therapeutic potential of this target remains to be adequately exploited (Berelowitz 1995). Somatostatin is a cyclic disulfide containing peptide hormone consisting of 14 amino acids that is present on the hypothalamus, cerebral cortex, brain stem and pancreas (Breeman et al. 1996). The hormone was first isolated in 1973 by Guillemin at the Salk Institute, and the somatostatin receptor has been found in the gastrointestinal tract, CNS, and many cells of neuroendocrine origin (Reubi et al., 1982; Patel et al., 1982). In the CNS somatostatin acts as a neurotransmitter and the hormonal activities include inhibition of the release of growth hormone, insulin, glucagon and gastrin (Brazeau et al., 1986). The inhibitory effects on secretion by somatostatin yielded a possible therapeutic application, but the tetradecapeptide was unstable after intravenous administration with an effective half-life of only ~3 minutes as a result of rapid enzymatic degredation (Breeman et al., 1996). The more recent synthesis of stable somatostatin analogues by the introduction of D-amino acids and shortening of the core binding sequence produced the octapeptide Octreotide (Figure 1a). The visualization of tissues containing somatostatin receptors was first demonstrated in rats and humans beginning in 1987 using first ^{123}I-Tyr^3-octreotide, and later with ^{111}In-DTPA-octreotide (Krenning et al., 1989, Bakker et al., 1990; Breeman et al., 1996). This agent, OctreoScan, became the first commercial nuclear medicine product to receive FDA approval in which the mechanism was based on receptor targeting, and since it's market introduction in 1994 this agent has remained the "Gold Standard" for somatostatin receptor scintigraphy (Krenning et al., 1995; Reubi et al., 2000). To date five human subtypes have been identified and cloned and are labeled as sst_1 through sst_5. All five subtypes bind somatostatin-14 and somatostatin-28 with high affinity,

while octreotide binds to sst_2 with high affinity and to sst_5 with lower affinity. It has a lower affinity for subtype sst_3, and no affinity for subtypes 1 and 4 (Breeman et al., 1995, Reubi et al., 2000).

Figure 1: Structures of Somatostatin Derivatives

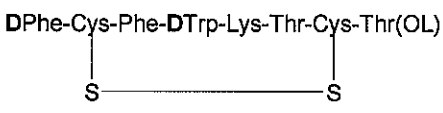

1a: Octreotide

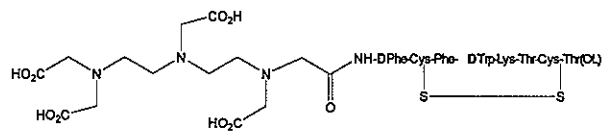

1b: DTPA-Octreotide

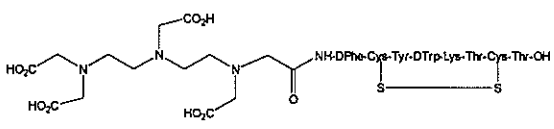

1c: DTPA-Tyr^3-Octreotate

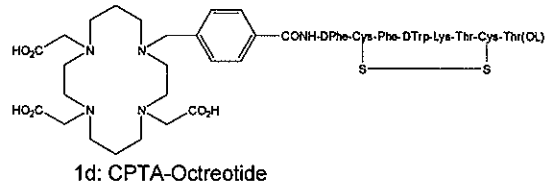

1d: CPTA-Octreotide

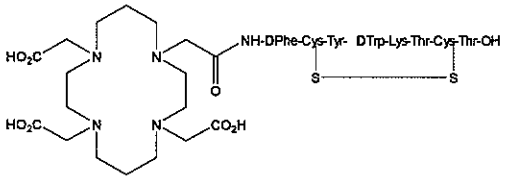

1e: TETA-Tyr^3-Octreotate

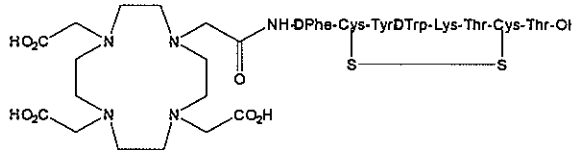

1f: DOTA-Tyr^3-Octreotate

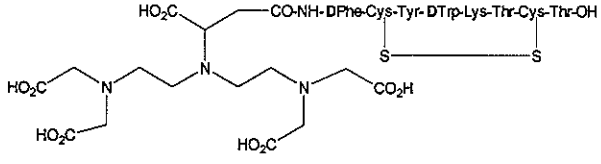

1g:CMDTPA-Tyr^3-Octreotate

The favorable imaging and pharmacokinetics of ^{111}In-DTPA-Octreotide (OctreoScan) as a scintigraphic agent quickly gave rise to the idea of using Octreotide as a potential ligand for radiotherapy. At that time a suitable chelate for a β^- emitting radionuclide such as Y-90 did not exist, as DTPA is insufficient to prevent the disassociation of the metal complex in vivo (Krenning et al., 1994). Therefore, the initial therapeutic attempts with Octreotide were begun using In-111 with the idea that the Auger and Coster-Kronig electrons would exhibit a sufficient therapeutic effect on a human neuroendocrine tumor based on the internalization of OctreoScan (Krenning et al., 1994, Breeman PhD Thesis 1995). In-111 yields several low energy Auger and Coster-Kronig electrons in the range of ~3.0 keV (Auger) and 175 keV (conversion electrons). A second human study was done in 1996 designed to treat midgut carcinoma syndrome (Fjalling et al., 1996). In animal studies using the CA20948 flank and liver models, de Jong and Breeman were able to show a significant reduction in tumor masses (flank model) and in the number of hepatic metastases (liver model) using ^{111}In-DTPA-octreotide at 370MBq dosing regimens (de Jong et al.,1999).

The lack of an objective response using this approach led to the idea that the radionuclide terbium-161 (Tb-161) may have improved therapeutic properties over In-111 and be chelated to DTPA-Tyr^3-Octreotide (de Jong et al., 1995). Tb-161 has a half-life of 6.91 days and emits β^- rays of 135, 154 and 180keV. Tumor bearing rat studies showed that the terbium complex may be a more promising candidate for both intraoperative scanning and radiotherapy (de Jong et al., 1995).

In that same year Anderson introduced the potential of copper-64 (Cu-64) complexed to Octreotide through the more stable TETA (Figure 1e) and CPTA (Figure 1d) ligand systems. Cu-64 has a short half-life of 12.8 hours and emits a β^- of 0.573 MeV and a β^+ of 0.656 MeV that is useful for PET imaging (Anderson et al., 1995). In vitro cell binding data indicted that both ^{64}Cu-Octreotide complexes bound with greater affinity on AT20 mouse pituitary carcinoma cells, and also showed greater tumor uptake in a Lewis tumor model (CA20948) compared to ^{111}In-DTPA-Octreotide. The very high hepatobiliary metabolism of the CPTA ligand precluded its use as an agent, but the TETA derivative exhibited favorable biological characteristics in vivo. The TETA complex was prepared at high specific activity (1500-3000Ci/mmol) in yields >95%. Radiotherapy studies were conducted in Lewis rats bearing the CA20948 pancreatic tumor line with single doses of 15mCi/rat or fractionated doses (15mCi) of 2-3 doses per animal. Inhibition of tumor growth was observed in all treatment groups, however a significantly greater effect on tumor growth inhibition was noted when dose fractionation was employed as the regimen. Tumor growth was delayed from 50-100% for only 10-15 days over untreated controls, but after 25 days post treatment significant re-growth of the tumors occurred in all treatment groups (Anderson et al., 1998). No apparent toxicity was observed in any of the treatment groups. Despite the large (mCi) dosage and the very short inhibition of tumor growth, the researches propose that ^{64}Cu-TETA-Octreotide is a promising radiopharmaceutical for targeted radiotherapy for somatostatin positive tumors (Anderson et al., 1998).

In an impressive study Stoltz described the use of Y-90 chelated to Tyr^3-Octreotide using the DOTA ligand (Figure 1f) targeted to the same rat tumor model (Stoltz et al., 1998). In this study five of seven animals treated with a single dose of 10mCi/kg (2.5mCi/rat) resulted in complete tumor remission, with no re-growth of tumor noted

up to eight months post treatment. Other than transient loss in body weight, no significant toxicity was observed using this regimen. This study was the first to demonstrate that a somatostatin targeted radionuclide agent could effectively induce tumor remission in this animal model. Due to the high homology (94%) between human and rat sst_2, the predominant subtype on human somatostatin expressing malignancies, (Reubi et al., 1996) this agent is quite promising for radionuclide therapy. Attempts by de Jong to reproduce this finding were not successful, however, as only a transient delay in tumor re-growth was observed. After a single injection of 3.0 mCi of Y-90 a delay in tumor growth of 28 days was observed, and with two doses of 3.0 mCi a delay of only 65 days was noted before re-growth was observed (de Jong et al., 1999). In this reference it was noted that this difference in the results may be due to size of the tumors targeted and the relative difference in radiosensitivity, even though the tumor line (CA20948) used in both studies was the same.

The concept of using low to medium energy beta emitting radionuclides chelated to small peptide molecules emerged with the discovery of DTPA-Y^3-Octreotate (Figure 1c). The peptide was modified to replace the threoninol with the natural amino acid threonine. This modification resulted in a greater than three fold increase in uptake of the sst_2 positive tumor CA20948 and a 50% reduction in the kidney dose (deJong et al.,1998; Srinivasan et al., 1998). The biodistribution and pharmacokinetic profile of this molecule offer a significant improvement over octreotide. The idea of using radionuclides such as samarium-153 (Sm-153) and lutetium-177 (Lu-177) was first attempted with the idea of reducing kidney toxicity, while evaluating the potential of these low-medium energy beta emitters as therapeutic radionuclides. The palliative effects of Sm-153 chelated to EDTMP are well documented, and the product

Quadramet was approved by the US FDA in 1995 for the palliation of bone pain associated with metastatic bone cancer (Goeckler et al., 1998 Turner et al., 1989). The stable chelation of Sm-153 to the peptide Octreotate required a ligand other than DTPA, and as a result the ligand DTPA' or CMDTPA (Figure 1g) was synthesized and evaluated in CA20948 tumor bearing Lewis rats. The results indicated good tumor uptake and retention, corresponding low kidney retention and 75% renal clearance of the agent at 24 hours post injection. Based on these results several therapy studies were initiated evaluating the potential of the peptide chelate to inhibit tumor growth in the CA20948 rat model. Preliminary studies indicated that even a single bolus dose of 0.5 mCi/rat had a therapeutic effect on tumor growth. The most efficacious results were obtained with multiple dosing regimens of either 3 x 5mCi/rat or 5 x 5mCi/rat dosed over a period of 3 to 5 weeks. In these studies tumor regression was prolonged 150% and 400% respectively over untreated control animals (Bugaj et al., 2001). However, even after five treatments all animals eventually succumbed to latent tumor growth. These results indicated that low-medium energy beta rays can be effective in promoting tumor regression, but it was believed that Sm-153 suffered from two major draw backs: (1) low specific activity (<300Ci/mmol) and (2) relative short half-life (46.8 h) that reduces the overall effective therapeutic payload. To counteract these shortcomings, the radionuclide Lu-177 was investigated. This radionuclide has a slightly lower E_{max} (0.497MeV/78% abundance) but the $t_{1/2}$ of 6.7 days is substantially greater than that of Sm-153. The potential specific activity of >3000Ci/mmol is significantly greater than that of Sm-153. This radionuclide also emits a gamma ray of 0.208MeV that is an excellent tracer for scintigraphy and for calculating dosimetry (Meredith et al., 1996). This lanthanide has similar physiochemical properties as Sm-153, however stable complexes of Lu-177 in vivo require that the DOTA ligand system be employed over

DTPA or CMDTPA type of ligand systems. The DOTA ligand has been used extensively with Y-90, and the synthesis of DOTA-linked peptides by standard Fmoc solid phase synthesis has been readily achieved.

The biodistribution and clearance properties of ^{177}Lu-DOTA-Tyr^3-Octreotate were compared to the Octreotide analogue directly in CA20948 tumor bearing Lewis rats. The Octreotate derivative showed significantly ($P<0.05$) higher uptake in the sst_2 expressing organs compared to Octreotide. Overall clearance properties and excretion patterns were similar for both compounds, however the Octreotate compound indicated significantly less kidney retention compared to Octreotide, which makes this molecule more attractive as a potential therapeutic by reducing the potential radiotoxicity to the kidneys accordingly (Erion et al. 1999, de Jong et al., 1998). The therapeutic efficacy of this agent was tested in CA20948 Lewis rat model based on the favorable biodistribution and clearance properties exhibited in the aforementioned studies. Tumor bearing rats were treated with one or three doses (37, 92.5, 185MBq per dose) 30 days between dosing, at a specific activity of ~1200Ci/mmol. Tumor regression was observed in all treatment groups. The highest percentage of surviving animals was observed in the groups that received multiple treatments. Fifty percent of the animals (n = 8) receiving 3 x 92.5 MBq survived more than 18 months post implant. Animals treated with three doses of 185MBq showed that 100% of the animals (n = 8) survived 12 months post implant, but began to exhibit signs of morbidity (weight loss, loss of appetite and poor grooming) from 12-15 months post implant (Erion et al., 1999). By 16 months post implant all animals in this group had died, and necropsy results revealed a high prevalence of renal carcinoma in the treatment group (Bugaj et al., 2001). However, the renal toxicity issues presented here require closer examination with regard to additional design in

treatment regimens and the use of amino acid infusion to reduce radiotoxicity to the kidneys (de Jong et al., 1998; Behr et al., 1995; Bernard et al., 1996).

In a parallel study design, de Jong reproduced these findings with a similar dose regimen of ^{177}Lu-DOTA-Y^{3}-octreotate in the CA20948 Lewis rat model (de Jong et al., 2001). In this study complete remission of tumor growth was noted over a period of 150 days post treatment, at which time the study was terminated and the animals sacrificed to evaluate possible toxicity associated with the treatment.

This approach to receptor-targeted radiotherapy was expanded through the introduction of two novel sst_2 positive rat tumor models, and demonstrated a pronounced radiotherapeutic effect using ^{177}Lu-DOTA-Y^{3}-octreotate (Bugaj 2002). Based on the AR42-J cell line, pre-weaned Lewis rats were successfully manipulated into hosting this quasi-murine cell line in both the flank and the liver metastases models. All prior use of the AR42-J cell line was limited with either athymic nude or SCID mice, both animal models that require expensive and elaborate housing requirements in a sterile barrier. Pre-weaned Lewis rats bearing the AR42-J flank tumor treated with either 3 x 2.5mCi or 4 x 5.0mCi showed a significant reduction in tumor growth compared to untreated controls. However, unlike the complete remissions observed by Erion and de Jong using the CA20948 rat model, latent re-growth was observed in all the AR42-J tumor-bearing animals treated with ^{177}Lu-DOTA-Y^{3}-octreotate at 75-100 days. The new flank model was, therefore, thought to represent a novel animal model for more radio-resistant neuroendocrine tumors bearing the sst_2 receptor subtype.

The second animal model introduced was the AR42-J liver metastases model, patterned after the CA20948 liver model of Breeman and de Jong (de Jong et al., 2000). In this study animals were inoculated with 2.5 x 10^6 AR42-J cells directly into the portal vein of young (4 week old) Lewis rats. They were subsequently treated with 3 x 5.0mCi of ^{177}Lu-DOTA-Y^3-octreotate at 7, 14 and 28 days post injection of cells. Using this dosing regimen treated animals at 34 days post injection of cells upon necropsy showed virtually no presence of tumor involvement of the liver (<2%) compared to ~80% liver involvement for the untreated control group.

A novel in vivo sst_2 expression system was created in the rat mammary tumor line, Mat-B, using a series of plasmid vectors encoding for the human $hsst_2$ receptor gene. The approach is similar to the methodology of Rogers and Zinn, for the gene expression of sst_2 using adenoviral vectors (Rogers et al., 1999; Zinn et al., 1999). The Mat-B tumor line is normally negative for the expression of sst_2. Transfection of the vector resulted in the expression of $hsst_2$ receptors in the Mat-B tumor line. The tumor was then implanted into Fischer-344 rats and the novel model was evaluated for uptake of Tyr^3-octreotate radiolabeled with In-111. Following validation of the model system, radiotherapy using ^{177}Lu-DOTA-Tyr^3-octreotate was performed and a therapeutic effect was observed. This model allows for the expression of human receptors in a rat model as opposed to athymic nude or SCID mice bearing human xenografts., and can be applied to other receptors including bombesin or CCK (Bugaj et al., 2002).

The examples provided confirm the hypothesis that low-medium beta particle emitting radionuclides can be effective for radiotherapy of somatostatin tumors, and that the radionuclide, Lu-177, is particularly attractive for radiotherapy due to its

favorable physiochemical properties. The pre-clinical data presented here has helped lead to the evaluation of the ^{177}Lu-DOTA-Y^{3}-Octreotate in a clinical setting. The compound has now been administered to over 100 patients at Erasmus Medical Center with neuroendocrine indications. To date the data indicate a complete or partial response rate of 36% (CR +PR) and stable disease (SD) in 42%. These response rates Indicate a large improvement over ^{90}Y-Octreother, and clinical consensus is that this radiolabeled peptide is most promising for the treatment of tumors of neuroendocrine origin (Kwekkeboom et al., 2002).

Applications to Biomedical Optics: The use of low beta emitting radionuclides chelated to Tyr^{3}-Octreotate was extended to the targeting of sst_2 positive tumors using fluorescent probes as opposed to radionuclides. This work was conducted using modified indocyanine green conjugated to Tyr^{3}-octreotate, creating a molecule termed Cytate. CA20948 and AR42-J tumor animals were injected with the Cytate dye-conjugate, and imaged using a simple CCD camera interfaced to a standard computer system. Following injection, the animal was excited at a wavelength of 780nm and fluorescence emission was captured at 810nm. When injected into tumor bearing Lewis rats, intense localization of the Cytate dye was observed in the tumor, with little background fluoresence observed elsewhere in the animal (Achilefu et al., 2000; Bugaj et al., 2001). The localization of the dye exceeded 36 hours in the sst_2 positive tissues of the pancreas, adrenals and tumor, but almost no fluoresence was observed in non-target tissue including blood, spleen, heart and kidneys.

The logical extension of this use of fluorescent probes targeted to the somatostatin receptor is the conjugation of a therapeutic dye to the peptide. These molecules, termed Photodynamic Therapy (PDT) agents, release singlet oxygen or free radicals upon excitation, and produce a therapeutic effect as a result (van den Boogert-Kluin

1999). Thus far, the clinical success has largely been limited to the condition known as Barrett's esophagus when treated with 5-aminolevulinic acid (Gossner et al., 1999; van den Boogert-Kluin, 1999; Overholt et al., 1999). The use of acridine orange as a PDT agent for the treatment of osteosarcoma in an experimental mouse model has also been reported (Kusuzaki et al., 1999). None of the systems utilize the targeted peptide conjugate approach, thereby limiting the therapeutic dose delivered to the target tissue. Additionally, these agents are rather toxic and prevent the patient from exposure to natural sunlight for extended periods of time (van den Boogert-Kluin, 1999). The use of targeted PDT agents based on a peptide conjugate approach would largely eliminate unnecessary toxicity, and deliver a substantially larger amount of dose to the targeted tissues.

Conclusion: The studies presented in the thesis confirm the utility of low-medium energy beta emitting radionuclides for radiotherapy of somatostatin positive tumors, and demonstrates that the optimal peptide for somatostatin imaging and therapy is Tyr^3-Octreotate. The potential of this peptide for use in PDT conjugated with fluorescent agents was also demonstrated in vivo.

REFERENCES

1. Achilefu, S., Dorshow, R.B., Bugaj, J.E., and Rajagopalan, R., (2000), Novel Receptor-Targeted Fluorescent Contrast Agents for In Vivo Tumor Imaging, *Investigative Radiology*, 35, 479-485.

2. Akizawa, H., Arano, Y., Uezono, T., Ono, M., Fujioka, Y., Uehara, T., Yokoyama, A., Akaji, K., Kiso, Y., Koizumi, M. and Saji, H. (1998) Renal Metabolism of 111In-DTPA-(D)Phe^1-Octreotide In Vivo, *Bioconjugate Chem*, 9, 662-670.

3. Anderson, C. J., Pajeau, T. S., Edwards, W. B., Sherman, E. L., Rogers, B. E. and Welch, M. J. (1995) In Vitro and In Vivo Evaluation of Copper-64-Octreotide Conjugates, *J Nucl Med*, 36, 2315-2325.

4. Anderson, C. J., Jones, L. A., Bass, L. A., Sherman, E. L., McCarthy, D. W., Cutler, P. D., Lanahan, M. V., Cristel, M. E., Lewis, J. S. and Schwarz, S. W. (1998) Radiotherapy, Toxicity and Dosimetry of Copper-64-TETA-Octreotide in Tumor-Bearing Rats, *J Nucl Med,* 39, 1944-1951.

5. Andersson, P., Forssell-Aronsson, E., Johanson, V., Wangberg, B., Nilsson, O., Fjalling, M. and Ahlman, H. (1996) Internalization of Indium-111 into Human Neuroendocrine Tumor Cells after Incubation with Indium-111-DTPA-D-Phe^1-Octreotide, *J Nucl Med*, 37, 2002-2006.

6. Axworthy, D. B., Reno, J. M., Hylarides, M. D., Mallett, R. W., Theodore, L. J., Gustavson, L. M., Su, F. M., Hobson, L. J., Beaumier, P. L. and Fritzberg, A. F. (2000) Cure of Human Carcinoma Xenografts by a Single Dose of Pretargeted Yttrium-90 with Negligible Toxicity, *PNAS*, 97, No. 4, 1802-1807.

7. Bakker, W. H., Krenning, E. P., Breeman, W. A., Koper, J. W., Kooij, P. P., Reubi, J-C, Klijn, J. G., Visser, T. J., Docter, R. and Lamberts, S. W. (1990) Receptor Scintigraphy with Radioiodinated Somatostatin Analogue: Radiolabeling, Purification, Biologic Activity and In Vivo Application in Animals, *J Nucl Med*, 31, 1501-1509.

8. Barbet, J., Kraeber-Bodere, F., Vuillez, J-F, Gautherot, E., Rouvier, E. and Chatal, J.F. (1999) Pretargeting with the Affinity Enhancement System for Radioimmunotherapy, *Cancer Biotherapy & Radiopharmaceuticals*, 14, No. 3, 153-166.

9. Behr, T. M., Sharkey, R. M., Juweid, M. E., Blumenthal, R. D., Dunn, R. M., Griffiths, G. L., Bair, H. J., Wolf, F. G., Becker, W. S. and Goldenberg, D. M. (1995) Reduction of the Renal Uptake of Radiolabeled Monoclonal Antibody Fragments by Cationic Amino Acids and Their Derivatives, *Cancer Research*, 55, 3825-3834.

10. Behr, T.M., Behe, M., Lohr, M., Sgorous, G., Angerstein, C., Wehrmann, E., Nebendahl, K. and Becker, W., (2000) Therapeutic advantages of Auger electron-over B-emitting radiometals or radioiodine when conjugated to internalizing antibodies, *E J Nucl Med*, 27, 753-765.

11. Berelowitz, M.: (1995) Editorial: The Somatostatin Receptor-A Window of Therapeutic Opportunity?, Endocrinology, Vol. 136, No. 9, 3695-3697.

12. Bernard, B. F., Krenning, E. P., Breeman,W. A., Rolleman, E. J., Bakker, W. H., Visser, T. J., Macke, H. and de Jong, M. (1996) D-Lysine Reduction of Indium-111 Octreotide and Yttrium-90 Octreotide Renal Uptake, *J Nucl Med*, 38, 1929-1933.

13. Brazeau, P. (1986) Somatostatin: A Peptide with Unexpected Physiologic Activities, *Am J Med*, 81 (supp. 6B) 8-13.

14. Breeman, W. A., Bakker, W. H., de Jong M., Hofland, L. J., Kewkkeboom, D. J, Kooij, P. P., Visser, T. J. and Krenning, E. P. (1996) Studies on Radiolabeled Somatostatin Analogues in Rats and Patients, Q. J. Nucl Med, Vol. 40, 209-220.

15. Bugaj, J. E., Erion, J. L., Johnson, M. A., Schmidt, M. A. and Srinivasan, A. (2001) Radiotherapeutic Efficacy of ^{153}Sm-CMDTPA-Tyr^3-Octreotate in Tumor-Bearing Rats, *Nucl Med Biol*, 28, 327-334.

16. Bugaj, J.E., Achilefu, S., Dorshow, R.B., and Rajagopalan, R., (2001) Novel fluorescent contrast agents for optical imaging of in vivo tumors based on a receptor-targeted dye-peptide conjugate platform, *J Biomedical Optics*, 6, 122-133.

17. Bugaj, J. E., Erion, J. L., Johnson, M. A. and de Jong, M. (2002) Radiotherapeutic Efficacy of ^{177}Lu-DOTA-Tyr^3-Octreotate in Novel Rat Tumor Animal Model Systems, *E J Nucl Med* (in press).

18. Bugaj, J. E., de Jong, M. and Erion, J. L. (2001) Chronic Renal Toxicity in Rats Treated with ^{177}Lu-DOTA-Tyr^3-Octreotate, *(Submitted)*.

19. Chatal, J.F. and Hoefnagel, C.A.; (1999) Radionuclide Therapy, *The Lancet*, 354, 931-935.

20. Deal, K.A., Davis, I.A., Mirzadeh, S., Kennel, S.J. and Brechbiel, M.W., (1999) Improved in Vivo Stability of Actinium-225 Macrocyclic Complexes, *J. Med. Chem*, 42, 2988-2992.

21. De Jong, M., Breeman, W. A., Bernard, B. F., Rolleman, E. J., Hofland, L. J., Visser, T. J., Setyono-Han, B., Bakker, W. H., van der Pluijm, M. E. and Krenning, E. P. (1995) Evaluation in vitro and in Rats of ^{161}Tb-DTPA-Octreotide, a Somatostatin Analogue with Potential for Intraoperative Scanning and Radiotherapy, *E J Nucl Med*, 22, 608-616.

22. De Jong, M., Rollemann, E. J., Bernard, B. F., Visser, T. J., Bakker, W. H., Breeman, W. A. and Krenning, E. P. (1995) Inhibition of Renal Uptake of Indium-111-DTPA-Octreotide In Vivo, *J Nucl Med*, 37, 1388-1392.

23. De Jong, M., Breeman, W. A., Bakker, W. H., Kooij, P. P., Bernard, B. F., Hofland, L. J., Visser, T. J., Srinivasan, A., Schmidt, M. A., Erion, J. L., Bugaj, J. E., Macke, H. R. and Krenning, E. P. (1998) Comparison of ^{111}In-Labeled Somatostatin Analogues for Tumor Scintigraphy and Radionuclide Therapy, *Cancer Research*, 58, 437-441.

24. De Jong, M., Breeman, W. A., Bernard, H. F., Kooij, P. P., Slooter, G. D., Van Eijck, C. H., Kwekkeboom, D. J., Valkema, R., Macke, H. R. and Krenning, E. P. (1999) Therapy of Neuroendocrine Tumors with Radiolabeled Somatostatin-Analogues, *Q J Nucl Med*, 43, 356-366.

25. De Jong, M., Breeman, W. A., Bernard, H. F., Bakker, W. H., Schaar, M., van Gameren, A., Bugaj, J. E., Erion, J. L., Schmidt, M. A., Srinivasan, A. and Krenning, E. P. (2001) [^{177}Lu-DOTA^{0}, Tyr^{3}] Octreotate for Somatostatin Receptor-Targeted Radionuclide Therapy, *Int. J Cancer*, 92, 628-633.

26. DeNardo, G.L., O'Donnell, R.T., Kroger, L.A., Richman, C.M., Goldstein, D.S., Shen, S. and DeNardo, S.J., (1999 Suppl.) Strategies for Developing Effective Radioimmunotherapy for Solid Tumors, *Clinical Cancer Research*, 5, 3219s-3223s.

27. Erion, J. L., Srinivasan, A., Schmidt, M. A., Bugaj, Wilhelm, R.R., and Bugaj , J. E., (1999) High Radiotherapeutic Efficacy of [177Lu]-DOTA-Y^{3}-Octreotate in a Rat Tumor Model, *J Nucl Med*, 40, (Supp):223P.

28. Fjalling, M., Andersson, P., Forssell-Aronsson, F., Gretarsdottir, J., Johansson, V., Tisell, L. E., Wangberg, B., Nilsson, O., Berg, G., Michanek, A., Lindstedt, G. and Ahlman, H. (1996) *J Nucl Med*, 37, 1519-1521.

29. Goeckeler, W. F., Edwards, B., Volkert, W. A., Holmes, R. A., Simon, J., and Wilson, D.; (1998) Skeletal Localization of Samarium-153 Chelates: Potential Therapeutic Bone Agents, *J Nucl Med*, 28, 495-504.

30. Goodwin, D. A. and Mears, C. F.; (1999) Pretargeted Peptide Imaging and Therapy, Cancer Biotherapy & Radiopharmaceuticals, Vol. 14, No. 3, 145-152.

31. Gossner, L., Stolte, M., Sroka, R., Rick, K., May, A., Hahn, E.G. and Ell, Christian, (1998) Photodynamic Ablation of High-Grade Dysplasia and Early Cancer in Barrett's Esophagus by Means of 5-Aminolevulinic Acid, 114, 448-455.

32. Hnatowich, D. J., Virzi, F., and Rusckowski, M. (1987) Investigations of Avidin and Biotin for Imaging Applications, *J Nucl Med*, 28, 1294-1302.

33. Hoefnagel, C. A., (1991) Radionuclide Therapy Revisited, *Eur J Nucl Med*, 18, 408-431.

34. Hoefnagel, C. A., (1998) Radionuclide Cancer Therapy, *Ann. Nucl. Med.*, 12, No. 2, 61-70.

35. Hofland, L. F., Koetsveld, P. M., Waaijers, M., Zuyderwijk, J., Breeman, W, A. and Lamberts S. W. (1995) Internalization of the Radioiodinated Somatostatin

Analog [^{125}I-Tyr^{3}]Octreotide by Mouse and Human Pituitary Tumor Cells: Increase by Unlabeled Octreotide, *Endocrinology*, 136, No. 9, 3698-2006.

36. Hornick, C.A., Anthony, C.T., Hughey, S., Gebhardt, B.M., Espenan, G.D. and Woltering, E.A. (2000)Progressive Nuclear Translocation of Somatostatin Analogs, *J Nucl Med*, 41, 1256-1263.

37. Humm, J. L.; (1986) Dosimetric Aspects of Radiolabeled Antibodies for Tumor Therapy, *J Nucl Med*, 27, 1490-1497.

38. Humm, J. L. and Cobb, L. M.; (1989) Nonuniformity of Tumor Dose in Radioimmunotherapy, *J Nucl Med*, 31, 75-83.

39. Kassis, A. I., Fayad, F., Kinsey, B. M., Sastry, K. S. and Adelstein, S. J.; (1989) Radiotoxicity of an ^{125}I-Labeled DNA Intercalator in Mammalian Cells, *Radiat Res*, 118, 283-294.

40. Kennel, S.J., Chappell, L.L., Dadachova, K., Brechbiel, M.W., Lankford, T.K., Davis, I.L., Stabin, M. And Mirzadeh, S., (2000) Evaluation of ^{225}Ac for Vascualr Targeted Radioimmunotherapy of Lung Tumors, *Cancer Biotherapy & Radiopharmaceuticals*, 15, 235-244.

41. Krenning, E. P., Kooij, P. P., Bakker, W. H., Breeman, W. A., Postema, P. T., Kwekkwboom, D. J., Oei, H. Y., de Jong, M., Visser, T. J., Reijs, A. E., and Lamberts, S. W. (1994) Radiotherapy with a Radiolabelled Somatostatin Analogue, [^{111}In-DTPA-D-Phe^{1}]Octreotide, *Ann NY Acad Sci*, 733, 496-506.

42. Kusuzaki, K., Aomori, K., Suginoshita, T., Minami, G., Takeshita, H., Murata, H., Hashiguchi, S., Ashiara, T. And Hirasawa, Y. (2000) Total Tumor Cell Elimination with Minimum Damage to Normal Tissues in Musculoskeletal Sarcomas following Photodynamic Therapy with Acridine Orange, *Oncology*, 59, 174-180.

43. Kwekkeboom, D.J., Bakker, W.H., Kooij, P.M., Srinivasan, A., Erion, J.L., Schmidt, M.A., Bugaj, J.E., de Jong, M. and Krenning, E.P.; (2001) [^{177}Lu-DOTA^{0},Tyr^{3}]octreotate: comparison with [^{111}In-DTPA^{0}]octreotide in patients, *Eur J Nucl Med*, 28, 1319-1325.

44. Maxon, H. R., Deutsch, E. A., Thomas, S. R., Libson, K., Lukes, S. J., Williams, C. C. and Alo, S.; (1988) Re-186 (Sn)-HEDP for Treatment of Multiple Metastatic Foci in Bone: Human Biodistribution and Dosimetric Studies, *Radiol*, 166, 501-507.

45. McDevitt, M. R., Sgouros, G., Finn, R. D., Humm, J. L., Jurcic, J. G., Larson, S. M., and Scheinberg, D. A.; (1998) Radioimmunotherapy with Alpha-Emitting Nuclides, *Eur J Nucl Med*, 25, 1341-1351.

46. Murtha, A.D., (2000) Radiobiology of Low-Dose-Rate Radiation Relevant to Radioimmunotherapy, , Cancer Biotherapy & Radiopharmaceuticals, 15, 7-14.

47. Overholt, B., Panjehpour, M. and Haydek, J.M., (1999) Photodynamic therapy for Barrett's esophagus: follow-up in 100 patients, *Gastrointestinal Endoscopy*, 49, 1-7.

48. Park, C. H.; (1997) The Role of Radioisotopes in Radiation Oncology, *Seminars in Oncology*, 24, No. 6, 639-654.

49. Patel, Y. C., Amherdt, M. and Orci, L. (1982) Quantitative Electron Microscopic Autoradiography of Insulin, Glucagon and Somatostatin Binding on Islets, *Science*, 217, 1155-1156.

50. Reubi, J-C. and Maurer, R.: (1982) Autoradiographic Mapping of Somatostatin Receptors in Rat CNS and Pituitary, *Neuroscience*, 15, 1183-1193.

51. Reubi, J-C., Schaer, J.C., Waser, B. and Mengod, G., (1994) Expression and localization of somatostatin receptor SSTR1, SSTR2 and SSTR3 messenger RNAs in primary human tumors using in situ hybridization, *Cancer Research*, 54, 3455-3459.

52. Reubi, J-C., Schar, J-C., Waser, B., Wenger, S., Heppeler, A., Schmitt, J. S., and Macke, H. R. (2000) Affinity Profiles for Human Somatostatin Receptor Subtypes SST1-SST5 of Somatostatin Radiotracers Selected for Scintigraphic and Radiotherapeutic Use, *E J Nucl Med*, 27, 273-282.

53. Rogers, B.E., McLean, S.F., Kirkman, R.L., Olsen, C.C., Bright, S.J., Myracle, A.D., Mayo, M.S., Curiel, D.T., and Buchsbaum, D.J., (1999) *In Vivo* Localization of [^{111}In]-DTPA-D-Phe^{1}-Octreotide to Human Ovarian Tumor Xenografts Induced to Express the Somatostatin Receptor Subtype 2 Using an Adenoviral Vector, *Clinical Cancer Research*, 5, 383-393.

54. Sgouros, G. (2000) Long-lived Alpha Emitters in Radiotherapy: The Mischievous Progeny, *Cancer Biotherapy & Radiopharmaceuticals*, 15, 219-221.

55. Shah-Syed, G.M., Maken, R.N., Muzzaffar, N., Shah, M.A. and Rana, F., (1999) Effective and economical option for pain palliation in prostate cancer with skeletal metastases: ^{32}P therapy revisited, *Nucl Med Comm*, 20, 697-702.

56. Srinivasan, A., Bugaj, J. E., Marmion, M. and Erion, J. L., (1998) U.S. Patent # 5, 804, 157, Peptide Compositions and Method of Radiolabeling.

57. Stolz, B., Weckbecker, G., Smith-Jones, P. M., Albert, R., Raulf, F. and Bruns, C. (1998) The Somatostatin Receptor-Targeted Radiotherapeutic [^{90}Y-DOTA-(D)Phe^{1}, Tyr^{3}]Octreotide (^{90}Y-SMT 487) Eradicates Experimental Rat Pancreatic CA20948 Tumours, *E J Nucl Med*, 25, 668-674.

58. Turner, J. H., Martindale, A. A., Sorby, P., Hetherington, E. L., Fleay, R. F., Hoffman, R. F. and Claringbold, P. G.; (1989) Samarium-153 EDTPM Therapy of Disseminated Skeletal Metastasis, *Eur J. Nucl Med*, 15, 784-795.

59. Van den Boogert-Kluin, J. (1999) Photodynamic Therapy fpr Barrett's Esophagus with Use of 5-Aminolevulinic Acid, Ph.D Thesis, Erasmus University Rotterdam

60. Volkert, W. A., Goeckeler, W. F., Ehrhardt, G. J., and Ketring, A. R., (1991) Therapeutic Radionuclides: Production and Decay Property Considerations, *J Nucl Med*, 32, 174-185.

61. Yao, Z., Zhang, M., Sakhara, H., Saga, T., Kobayshi, H., Nakamoto, Y., Toyama, S., and Konishi, J., (1998) Increased Streptavidin Uptake in Tumors Pretargeted with Biotinylated Antibody Using a Conjugate of Streptavidin-Fab Fragment, *Nucl Med Biol*, 25, 557-560.

62. Zweit, J., (1996) Radionuclides and Carrier Molecules for Therapy, *Phys. Med. Biol*, 41, 1905-1914.

63. Zinn, K.R., Buchsbaum, D.J., Chaudhuri, T.R., Mountz, J.M., Grizzle, W.E., and Rogers, B.E., (1999) Noninvasive Monitoring of Gene Therapy Using a Reporter Receptor Imaged with a High-Affinity Peptide Radiolabeled with ^{99m}Tc or ^{188}Re, *J Nucl Med*, 41, 887-895.

CHAPTER 2

COMPARISON OF ^{111}IN-LABELED SOMATOSTATIN ANALOGUES FOR TUMOR SCINTIGRAPHY AND RADIONUCLIDE THERAPY

Cancer Research, 58, 437-441, (1998)

Comparison of ^{111}In-labeled Somatostatin Analogues for Tumor Scintigraphy and Radionuclide Therapy[1]

Marion de Jong,[2] Wout A. P. Breeman, Willem H. Bakker, Peter P. M. Kooij, Bert F. Bernard, Leo J. Hofland, Theo J. Visser, Ananth Srinivasan, Michelle A. Schmidt, Jack L. Erion, Joseph E. Bugaj, Helmut R. Mäcke, and Eric P. Krenning

Departments of Nuclear Medicine [M. d. J., W. A. P. B., W. H. B., P. P. M. K., B. F. B., E. P. K.] and Internal Medicine III [L. J. H., T. J. V., E. P. K.], University Hospital Dijkzigt, 3015 GD Rotterdam, the Netherlands; Mallinckrodt Medical, St. Louis, Missouri 63134 [A. S., M. A. S., J. L. E., J. E. B.]; and Department of Nuclear Medicine, Kantonspital Basel, CH-4031 Basel, Switzerland [H. R. M.]

ABSTRACT

We evaluated the following ^{111}In-labeled somatostatin (SS) analogues (diethylenetriaminepentaacetic acid, DTPA; tetraazacyclododecanetetraacetic acid, DOTA): [DTPA^0]octreotide, [DTPA^0,Tyr^3]octreotide, [DTPA^0,D-Tyr^1]octreotide, [DTPA^0,Tyr^3]octreotate [Thr(ol) in octreotide replaced with Thr], and [DOTA^0,Tyr^3]octreotide, *in vitro* and *in vivo*.

***In vitro*, all compounds showed high and specific binding to SS receptors in mouse pituitary AtT20 tumor cell membranes, and IC_{50}s were in the nanomolar range. Furthermore, all compounds showed specific internalization in rat pancreatic tumor cells; uptake of [^{111}In-DTPA^0,Tyr^3]octreotate was the highest of the compounds tested, and that of [^{111}In-DTPA^0,D-Tyr^1]octreotide was the lowest. Biodistribution experiments in rats showed that, 4, 24, and 48 h after injection of [^{111}In-DTPA^0,Tyr^3]octreotide, [^{111}In-DTPA^0,Tyr^3]octreotate, and [^{111}In-DOTA^0,Tyr^3]octreotide, radioactivity in the octreotide-binding, receptor-expressing tissues and tumor-to-blood ratios were significantly higher than those after injection of [^{111}In-DTPA^0]octreotide. Uptake of [^{111}In-DTPA^0,Tyr^3]octreotate in the target organs was also, *in vivo*, the highest of the radiolabeled peptides tested, whereas that of [^{111}In-DTPA^0,D-Tyr^1]octreotide was the lowest. Uptake of [^{111}In-DTPA^0,Tyr^3]octreotide, [^{111}In-DTPA^0,Tyr^3]octreotate, and [^{111}In-DOTA^0,Tyr^3]octreotide in target tissues was blocked by >90% by 0.5 mg of unlabeled octreotide, indicating specific binding to the octreotide receptors. Blockade of [^{111}In-DTPA^0,D-Tyr^1]octreotide was >70%. In conclusion, radiolabeled [DTPA^0,Tyr^3]octreotide and, especially, [DTPA^0,Tyr^3]octreotate and their DOTA-coupled counterparts are most promising for scintigraphy and radionuclide therapy of SS receptor-positive tumors in humans.**

INTRODUCTION

Radiolabeled tumor receptor-binding peptides can be used for *in vivo* scintigraphic imaging. An example is SS,[3] which binds to its receptors on tumors of neuroendocrine origin (1). The native peptide, however, is susceptible to very rapid enzymatic degradation (2) and is, therefore, not useful for *in vivo* application. Therefore, more stable synthetic SS analogues have been developed; *e.g.*, the octapeptide octreotide (Fig. 1; Ref. 3). Because octreotide cannot be radiolabeled easily with a γ-emitting radionuclide, Tyr^3-octreotide was developed, allowing radioiodination of the molecule (Fig. 1). This compound, radiolabeled with ^{125}I or ^{123}I, was the first used in *in vitro* SS receptor studies (4), tumor scintigraphy in animals (4), and in humans (1, 5). [^{111}In-DTPA^0]octreotide, consisting of the octapeptide octreotide and the chelator DTPA (Fig. 1), enabling radiolabeling with a radiometal like ^{111}In, was the next SS analogue to be synthesized for scintigraphy of SS receptor-positive lesions *in vivo*. We have described its advantages over radioiodinated Tyr^3-octreotide and its use for scintigraphic imaging of SS receptor-positive lesions (6, 7).

A new and fascinating application is the use of radiolabeled octreotide for radionuclide therapy. Promising results with regard to tumor growth inhibition have been reported in humans using [^{111}In-DTPA^0]octreotide (8). A β^- particle emitter, such as ^{90}Y, may, in certain cases, appear more suitable for this purpose than the Auger electron emitter ^{111}In. However, ^{90}Y-DTPA is unstable, resulting in hematopoietic toxicity *in vivo*; therefore, Tyr^3-octreotide has been derivatized with the DOTA chelator (Fig. 1), enabling stable radiolabeling with ^{90}Y and ^{111}In. (Pre)clinical studies with [DOTA^0,Tyr^3]octreotide showed favorable biodistribution and tumor uptake characteristics (9–11).

The success of the therapeutic strategy relies upon the amount of radioligand, which can be concentrated within tumor cells, and this will, among other things, be determined by the rates of internalization, degradation, and recycling of both ligand and receptor. We have evaluated and compared the different mentioned ^{111}In-chelator-peptide constructs, and we have also studied some new, recently synthesized SS analogues, with regard to binding to octreotide receptors on mouse pituitary tumor cell membranes and internalization in rat pancreatic tumor cells. Furthermore, biodistribution in tumor-bearing rats was investigated *in vivo*. The newly synthesized analogues tested were [DTPA^0,D-Tyr^1]octreotide and [DTPA^0,Tyr^3]octreotate (structures shown in Fig. 1).

MATERIALS AND METHODS

Labeling of Octreotide Derivatives. [DTPA^0]octreotide and $^{111}InCl_3$ were provided by Mallinckrodt Medical (Petten, the Netherlands), and octreotide was supplied by Sandoz (Basel, Switzerland). [DOTA^0,Tyr^3]octreotide was synthesized by H. R. M., and [DTPA^0,D-Tyr^1]octreotide, [DTPA^0,Tyr^3]-octreotide, and [DTPA^0,Tyr^3]octreotate were synthesized by A. S. ^{111}In labeling of the DTPA-analogues was as described for [DTPA^0]octreotide (12), and ^{111}In-labeling of [DOTA^0,Tyr^3]octreotide (9) and ^{125}I-labeling of [Tyr^3]octreotide (4) were performed as described.

***In Vitro* Receptor Binding Studies.** Receptor binding assays were carried out using [^{125}I-Tyr^3]octreotide (2200 Ci/mmol) as radioligand using mouse AtT20 pituitary tumor cell membranes (13).

Internalization. AR42J cells were grown in RPMI 1640 (Life Technologies, Inc., Grand Island, NY), CA20948 cells were grown in DMEM (Life Technologies, Inc.), and ARO cells were grown in DMEM/F12 (Life Technologies, Inc.); for all cell lines, medium was supplemented with 2 mM glutamine and 10% FCS. Before the experiment, subconfluent cell cultures were transferred to six-well plates.

The binding of the radiolabeled peptides to tumor cells and subsequent internalization were studied essentially as described (14). In short, before the experiments, cells were washed, and incubation was started by addition of 1 ml of internalization medium/well (culture medium without FCS but with 1% BSA) with 80 kBq of peptide (0.1 nM concentration). Cells were incubated at 37°C for indicated periods of time. To determine nonspecific internalization, cells were incubated with an excess unlabeled octreotide (0.1 μM). Cellular

Received 8/6/97; accepted 12/3/97.

The costs of publication of this article were defrayed in part by the payment of page charges. This article must therefore be hereby marked *advertisement* in accordance with 18 U.S.C. Section 1734 solely to indicate this fact.

[1] This work was supported by Swiss National Science Foundation Grant 31-42516/94 and the "Regionale Krebsliga beider Basel" (both to H. R. M.).

[2] To whom requests for reprints should be addressed, at Department of Nuclear Medicine, V220, University Hospital Rotterdam, 3015 GD Rotterdam, the Netherlands. Phone: 31 10 4635781; Fax: 31 10 4635997; E-mail: dejong@nuge.azr.nl.

[3] The abbreviations used are: SS, somatostatin; DTPA, diethylenetriaminepentaacetic acid; DOTA, tetraazacyclododecanetetraacetic acid; AUC, area under the curve; %ID, percentage injected dose.

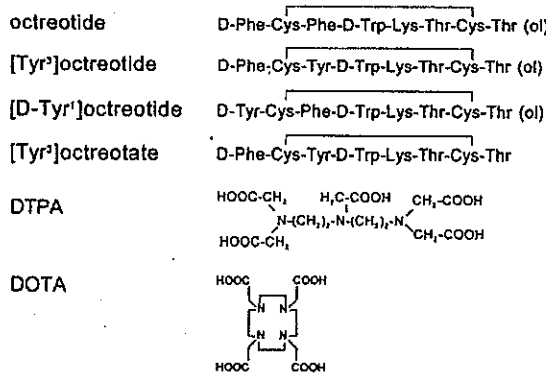

Fig. 1. Structures of octreotide, D-Tyr¹-octreotide, Tyr³-octreotide, Tyr³-octreotate, DTPA, and DOTA.

Table 1 *IC_{50} of unlabeled peptides*

Binding of [^{125}I-Tyr^3]octreotide to mouse AtT20 pituitary cell membranes. Results are means of triplicate measurements in a representative experiment.

Unlabeled peptide	IC_{50} (nM)
[DTPA^0]octreotide	3
[DTPA^0,Tyr^3]octreotide	3.2
[DTPA^0,D-Tyr^1]octreotide	6.3
[DTPA^0,Tyr^3]octreotate	3.6
[DOTA^0,Tyr^3]octreotide	0.6

uptake was stopped by removing medium from the cells and washing with 2 ml of ice-cold PBS. To discriminate between internalized and noninternalized (surface-bound) radiopharmaceuticals, intact cells were incubated with 1 ml of 20 mM sodium acetate. The internalized and noninternalized fractions were determined by measuring radioactivity in a LKB-1282-Compugammasystem. The internalized fraction was expressed as percentage of the applied dose per mg of cellular protein. The latter was determined using a commercially available kit (Bio-Rad, Veenendaal, the Netherlands).

***In Vivo* Tissue Distribution.** Animal experiments were performed in compliance with regulations of our institution and with generally accepted guidelines governing such work. Male Lewis rats, bearing the CA20948 pancreatic tumor or Wistar male rats (200–250 g) were used in the experiments. Rats were injected under ether anesthesia with 3 MBq (0.5 μg) of ^{111}In-labeled peptide in 200 μl of saline into the dorsal vein of the penis. To determine nonspecific binding of the radiopharmaceutical, a separate group of rats was injected s.c. with 0.5 mg of octreotide in 1 ml of 0.05 M acetic acid in saline, 30 min before injection of the radiolabeled peptide. At the indicated time points, rats were sacrificed under ether anesthesia. Organs and blood were collected, and the radioactivity in these samples was determined using a LKB-1282-Compugammasystem. Statistical evaluation was performed using one-way ANOVA, followed by comparison among class means and Student's *t* test, corrected for multiple pairwise comparisons between means.

RESULTS

Radiolabeling. ^{111}In-labeling efficiency of the different peptides and radioiodination efficiency of [Tyr^3]octreotide ranged from 97 to 100%.

***In Vitro* Receptor Binding Studies.** Table 1 shows that unlabeled peptides had high and specific binding for the octreotide-binding receptors (mostly sst_2) on AtT20 membranes; the IC_{50} values were all in the nanomolar range. [DOTA^0,Tyr^3]octreotide showed the highest affinity.

***In Vitro* Internalization Studies.** Table 2 shows specific internalization, that is, total internalization corrected for internalization in the presence of a blocking dose of octreotide of the ^{111}In-labeled peptides in the octreotide receptor-positive rat pancreatic cell lines after a 60-min incubation at 37°C. Data were expressed as percentages of specific internalization of [^{125}I-Tyr^3]octreotide. As is shown, internalized radioactivity of [^{111}In-DTPA^0,Tyr^3]octreotate was the highest of the compounds tested, whereas that of [^{111}In-DTPA^0,D-Tyr^1]octreotide was the lowest.

Tissue Distribution in Rats. Fig. 2 presents radioactivity in octreotide binding receptor-positive (mostly sst_2) organs, including pancreas, adrenals, pituitary, and CA20948 rat pancreatic tumors, 4, 24, and 48 h after injection of the radiolabeled peptides. Uptake in these octreotide receptor-expressing organs at the time points tested was highest for [^{111}In-DTPA^0,Tyr^3]octreotate and lowest for [^{111}In-DTPA^0,D-Tyr^1]octreotide.

Table 3 shows that uptake of ^{111}In-labeled peptides in these octreotide receptor-positive target organs represented mostly specific binding to the octreotide receptors because uptake was decreased to less than 7% of control by pretreatment of the rats with 0.5 mg of unlabeled octreotide, except for [^{111}In-DTPA^0,D-Tyr^1]octreotide, for which uptake was decreased to about 30% of control.

In Table 4, radioactivity in octreotide receptor-negative organs and blood 24 h after injection of the tested ^{111}In-labeled peptides is shown. Clearance from the blood was rapid and comparable for all peptides. The radiolabeled peptides were excreted in the urine very rapidly and mostly intact; over 95% of the excreted radioactivity after 24 h was intact radiolabeled peptide (data not shown). Furthermore, the low uptake of [^{111}In-DTPA^0,Tyr^3]octreotate in the liver is worth mentioning, which is favorable, especially in combination with the rapid blood clearance and high uptake of this compound in the target organs.

The data obtained *in vivo*, as shown in Fig. 2 and Table 4, are summarized in Fig. 3, in which the AUC (h·%ID/g) for each group between 4 and 48 h post injection is shown. The top panel shows that radioactivity/g tissue in this time period was low in blood, liver, and spleen and higher in kidneys, tumor, and octreotide receptor (sst_2)-positive organs. The bottom panel shows the same data but expressed as percentage of the AUC of [^{111}In-DTPA^0]octreotide in the different organs. In the sst_2-negative organs, AUC is comparable for the peptides, except for the low liver AUC of [^{111}In-DTPA^0,Tyr^3]octreotate. In the sst_2-positive organs, the AUC of [^{111}In-DTPA^0,Tyr^3]octreotate is the highest.

DISCUSSION

Compared to ^{123}I-Tyr^3-octreotide, [^{111}In-DTPA^0]octreotide was the preferred analogue for *in vivo* scintigraphy because it has several advantages: general availability, simple one-step method of radiolabeling, longer physiological half-life in plasma, and a more suitable metabolism (5). A new field of application of radiolabeled SS ana-

Table 2 *Comparison of specific internalization of [^{111}In-DTPA^0]octreotide, [^{111}In-DTPA^0,D-Tyr^1]octreotide, [^{111}In-DTPA^0,Tyr^3]octreotide, [^{111}In-DTPA^0,Tyr^3]octreotate, and [^{111}In-DOTA^0,Tyr^3]octreotide after a 60-min incubation at 37°C*

Data for each experiment expressed as percentage of specific [^{125}I-Tyr^3]octreotide internalization (range, 6.5 ± 0.8%–9.2 ± 1.1% dose) tested in the same experiment. Data are the means of those obtained in at least two different experiments in the two octreotide receptor-positive cell lines used (CA20948 and AR42J).

Compound	Mean (SD)
[^{125}I-Tyr^3]octreotide	100 (12)
[^{111}In-DTPA^0]octreotide	8.2 (0.7)[a]
[^{111}In-DTPA^0,D-Tyr^1]octreotide	2.2 (1.1)[a]
[^{111}In-DTPA^0,Tyr^3]octreotide	40.2 (4.5)[a]
[^{111}In-DTPA^0,Tyr^3]octreotate	211.5 (12)[a]
[^{111}In-DOTA^0,Tyr^3]octreotide	14.6 (1.1)[a]

[a] $P < 0.001$ *versus* [^{125}I-Tyr^3]octreotide.

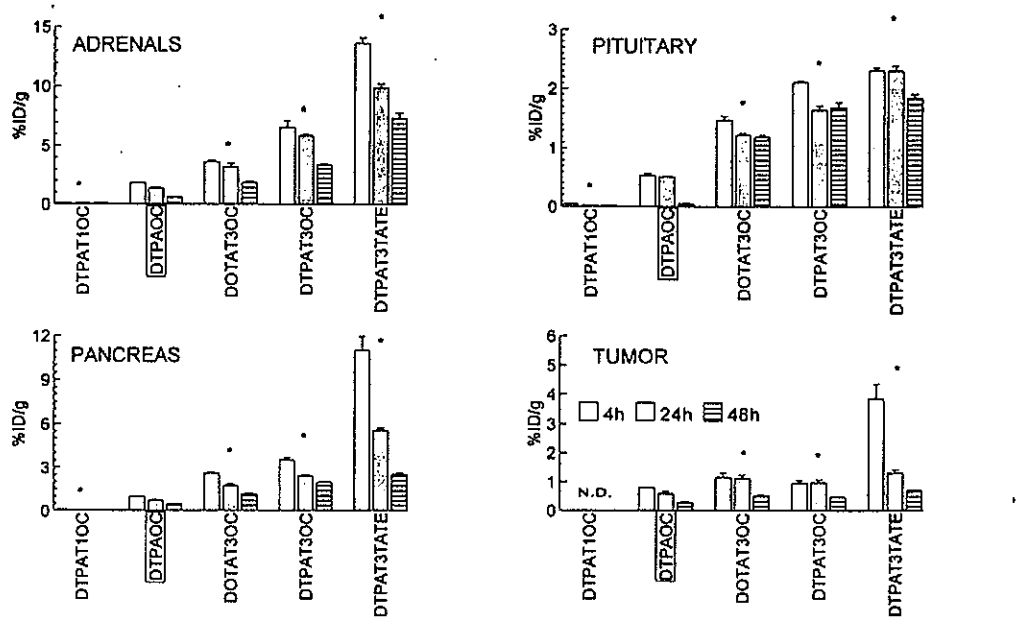

Fig. 2. Radioactivity in octreotide receptor-expressing organs 4, 24, and 48 h after injection of the ^{111}In-labeled peptides in rats. *Columns*, mean %ID/g ($n \geq 6$); *bars*, SE. *ND*, not determined; *DTPAOC* [DTPA^0]octreotide; *DTPAT1OC*, [DTPA^0,D-Tyr^1]octreotide; *DTPAT3OC*, [DTPA^0,Tyr^3]octreotide; *DTPAT3TATE*, [DTPA^0,Tyr^3]octreotate; *DOTAT3OC*, [DOTA^0,Tyr^3]octreotide. *, $P < 0.001$ *versus* [^{111}In-DTPA^0]octreotide, for all time points tested.

Table 3 *Radioactivity in SS receptor-positive organs of octreotide-pretreated rats 24 h after administration of the ^{111}In-labeled peptides*

Labeled compound was injected 30 min after s.c. injection of 0.5 mg of unlabeled octreotide or vehicle (control). Tissue radioactivity in octreotide-pretreated rats is expressed as a percentage of that in controls [for each group $n \geq 6$ mean (SE)].

Treatment	Pituitary	Pancreas	Adrenals	Tumor
[DTPA^0]octreotide	6.9 (0.7)[a]	3.5 (0.03)[a]	1.5 (0.02)[a]	4.3 (0.3)[a]
[DTPA^0,D-Tyr^1]octreotide	22.2 (4.5)[a]	27.9 (1.4)[a]	29.6 (1.1)[a]	ND[b]
[DTPA^0,Tyr^3]octreotide	4.7 (0.4)[a]	0.9 (0.03)[a]	4.0 (0.3)[a]	4.8 (0.4)[a]
[DTPA^0,Tyr^3]octreotate	3.2 (0.4)[a]	2.6 (0.4)[a]	0.7 (0.1)[a]	6.3 (0.9)[a]
[DOTA^0,Tyr^3]octreotide	1.6 (0.04)[a]	1.0 (0.02)[a]	1.0 (0.04)[a]	3.6 (0.3)[a]

[a] $P < 0.001$ *versus* control.
[b] ND, not determined.

logues is the use of radiolabeled peptide for radionuclide therapy of receptor-positive lesions. Currently, this application was explored successfully by repeated administration of high doses of [^{111}In-DTPA^0]octreotide in humans (8). However, a β^- particle emitter, such as ^{90}Y, may, in certain cases, appear more suitable for this purpose than the Auger electron emitter ^{111}In. Radiotherapeutic use of ^{90}Y-labeled peptide will lead to a higher and more evenly distributed radiation dose to the tumor because of its larger particle range and tissue penetration. Even tumors with an nonhomogeneous cellular distribution of receptors, such as breast tumors, may respond favorably to treatment with such a ^{90}Y-labeled radiopharmaceutical, whereas treatment with ^{111}In-labeled peptide will not be successful because of the particle range of the Auger electrons, which is only about one cell diameter. Because ^{90}Y-DTPA is unstable, introduction of the DOTA chelator was necessary, enabling stable radiolabeling with ^{90}Y and ^{111}In.

We investigated receptor binding, internalization and biodistribution characteristics of several SS analogues, all labeled with ^{111}In: [DTPA^0]-octreotide, [DTPA^0,Tyr^3]octreotide, [DTPA^0,D-Tyr^1]octreotide, [DOTA^0,Tyr^3]octreotide, and [DTPA^0,Tyr^3]-octreotate. Phe residues were replaced with Tyr to increase the hydrophilicity of the peptides. Furthermore, [DTPA^0,Tyr^3]octreotate, with the C-terminal threonine, was synthesized to investigate the effects of an additional negative charge on clearance and cellular uptake.

For the success of radionuclide therapy, it is important that the radiopharmaceutical is internalized by the tumor cells after binding to the receptor. Internalization of [^{111}In-DTPA^0]octreotide into human neuroendocrine tumor cells was described recently (15). Here, we also observed specific internalization of the tested ^{111}In-labeled peptides. Internalized radioactivity of all radiolabeled peptides was higher than that of [^{111}In-DTPA^0]octreotide, except that of [^{111}In-DTPA^0,D-Tyr^1]octreotide.

The results of the *in vitro* binding studies demonstrated that all unlabeled peptides showed high and specific binding for the octreotide receptors. *In vivo*, uptake of the ^{111}In-labeled peptides in octreotide receptor-expressing tissues was also demonstrated to be highly specific. Our findings further showed that specific uptakes of ^{111}In-labeled [DTPA^0,Tyr^3]octreotide, [DOTA^0,Tyr^3]octreotide, and [DTPA^0,Tyr^3]octreotate in octreotide receptor-expressing tissues were significantly higher than that of [^{111}In-DTPA^0]octreotide at the

Table 4 *Radioactivity in SS receptor-negative organs and blood of rats 24 h after administration of the ^{111}In-labeled peptides*

Tissue radioactivity is expressed as %ID/g [for each group $n \geq 6$, mean (SE)].

Treatment	Blood	Liver	Kidney	Spleen
[DTPA^0]octreotide	0.003 (0.000)	0.05 (0.003)	1.91 (0.11)	0.03 (0.002)
[DTPA^0,D-Tyr^1]octreotide	0.003 (0.001)	0.03 (0.001)[a]	1.52 (0.05)[a]	0.03 (0.002)
[DTPA^0,Tyr^3]octreotide	0.003 (0.001)	0.06 (0.004)	1.39 (0.08)[a]	0.03 (0.002)
[DTPA^0,Tyr^3]octreotate	0.003 (0.000)	0.02 (0.001)[a]	1.96 (0.11)	0.02 (0.001)
[DOTA^0,Tyr^3]octreotide	0.002 (0.001)	0.05 (0.000)	2.32 (0.13)[a]	0.04 (0.001)

[a] $P < 0.01$ *versus* [^{111}In-DTPA^0]octreotide.

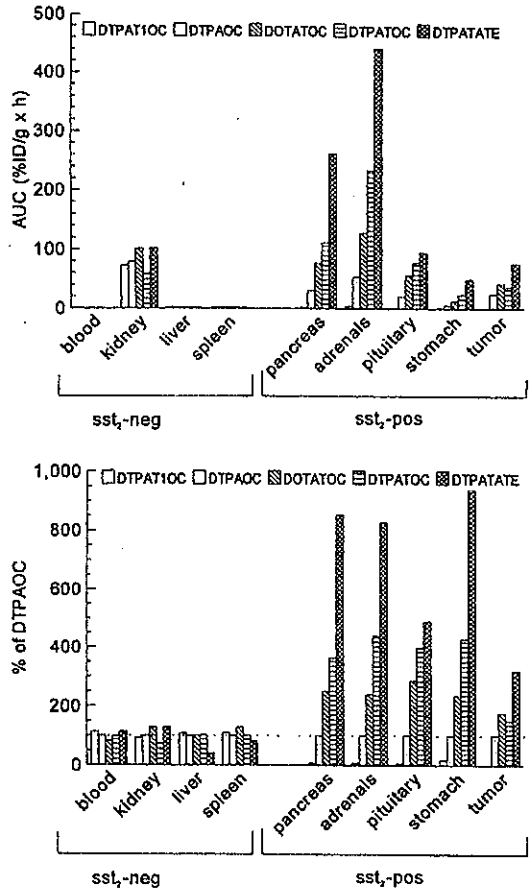

Fig. 3. *Top*, AUC of radioactivity between 4 and 48 h after injection of the different ^{111}In-labeled peptides in rats. *Columns*, mean h×%ID/g. *DTPAOC*, [DTPA^0]octreotide; *DTPAT1OC*, [DTPA^0,D-Tyr^1]octreotide; *DTPAT3OC*, [DTPA^0,Tyr^3]octreotide; *DTPATJTATE*, [DTPA^0,Tyr^3]octreotate; *DOTAT3OC*, [DOTA^0,Tyr^3]octreotide. *Bottom*, same as *top*, except data represent percentage of [DTPA^0]octreotide AUC (*columns*).

time points tested. Uptake of [^{111}In-DTPA^0,D-Tyr^1]octreotide was significantly lower, in accordance with the lower internalization rate found *in vitro*. In our *in vivo* animal model, [^{111}In-DTPA^0,Tyr^3]octreotate showed the highest uptake in the octreotide receptor-positive organs and tumor of the ^{111}In-labeled peptides tested, also in accordance with the *in vitro* internalization studies. Because blood radioactivity was comparable for all radiolabeled peptides, we also found that [^{111}In-DTPA^0,Tyr^3]octreotate had the highest tumor-to-blood ratio. Uptake of [DTPA^0,Tyr^3]octreotide was higher than that of [DOTA^0,Tyr^3]octreotide, both *in vitro* and *in vivo*, in the octreotide receptor-positive organs; however, uptake in the target, the tumor, was not significantly different for these two radiolabeled peptides; therefore, the therapeutic index of [Tyr^3]octreotide has not been impaired significantly by the replacement of DTPA for DOTA, necessary for ^{90}Y studies (11). We are currently investigating the relationship of the injected peptide mass and uptake in target organs for these two peptides to further elucidate the consequences of the DTPA-to-DOTA replacement.

At radiotherapeutic levels, the high uptake of radioactivity in the octreotide receptor-positive normal organs, such as adrenals and pituitary, should also be considered. We are performing radionuclide therapy studies in normal rats with [DOTA^0,Tyr^3]octreotide radiolabeled with different radionuclides to investigate possible radiotoxic effects on normal organs. However, until now, no radiotoxicity was found in these organs.

The ^{111}In-labeled peptides are rapidly cleared from the body, mostly by the kidneys. However, a significant amount of the dose accumulated in the kidneys, reducing both the scintigraphic sensitivity for detection of small tumors in the perirenal region in the abdomen and the application for radionuclide therapy. It has been reported that renal accumulation of peptides or proteins labeled with radiometals can be reduced by both L- and D-lysine (16–19). Recently, we described that D-lysine administration resulted in a significant reduction of labeled [DTPA^0]octreotide, [DTPA^0,Tyr^3]octreotide, and [DOTA^0,Tyr^3]octreotide uptake in the kidneys without affecting uptake in receptor-positive tissues, which is favorable for both visualization of lesions in the kidney region and for radionuclide therapy, thus bringing these applications further within reach (10).

It can be concluded that ^{111}In-labeled [DTPA^0,Tyr^3]octreotide and, especially, [DTPA^0,Tyr^3]octreotate and their DOTA-coupled counterparts are most promising for scintigraphy and, after coupling to therapeutic radionuclides, for radionuclide therapy of octreotide receptor-positive tumors in humans.

REFERENCES

1. Krenning, E. P., Bakker, W. H., Breeman, W. A. P., Koper, J. W., Kooij, P. P. M., Ausema, L., Lamérls, J. S., Reubi, J. C., and Lamberts, S. W. J. Localisation of endocrine-related tumors with radioiodinated analogue of somatostatin. Lancet, *i:* 242–244, 1989.
2. Patel, Y. C., and Wheatley, T. *In vivo* and *in vitro* plasma disappearance and metabolism of somatostatin-28 and somatostatin-14 in the rat. Endocrinology, *112:* 220–225, 1983.
3. Pless, J., Bauer, W., Briner, U., Doepfner, W., Marbach, P., Maurer, R., Petcher, T. J., Reubi, J. C., and Vonderscher, J. Chemistry and pharmacology of SMS 201–995, a long-acting analogue of somatostatin. Scand. J. Gastroenterol., *21:* 54–64, 1986.
4. Bakker, W. H., Krenning, E. P., Breeman, W. A. P., Koper, J. W., Kooij, P. P. M., Reubi, J. C., Klijn, J. G., Visser, T. J., Docter, R., and Lamberts, S. W. J. Receptor scintigraphy with a radioiodinated somatostatin analogue: radiolabeling, purification, biologic activity and *in vivo* application in animals. J. Nucl. Med., *31:* 1501–1509, 1990.
5. Bakker, W. H., Krenning, E. P., Breeman, W. A. P., Kooij, P. P. M., Reubi, J. C., Koper, J. W., De Jong, M., Lamérls, J. S., Visser, T. J., and Lamberts, S. W. J. *In vivo* use of a radioiodinated somatostatin analogue: dynamics, metabolism, and binding to somatostatin receptor-positive tumors in man. J. Nucl. Med., *32:* 1184–1189, 1991.
6. Krenning, E. P., Bakker, W. H., Kooij, P. P. M., Breeman, W. A. P., Oei, H. Y., De Jong, M., Reubi, J. C., Visser, T. J., Bruns, C., Kwekkeboom, D. J., Reijs, A. E. M., Van Hagen, P. M., Koper, J. W., and Lamberts, S. W. J. Somatostatin receptor scintigraphy with [^{111}In-DTPA-D-Phe^1]-octreotide in man: metabolism, dosimetry and comparison with [^{123}I-Tyr^3]-octreotide. J. Nucl. Med., *33:* 652–658, 1992.
7. Krenning, E. P., Kwekkeboom, D. J., Bakker, W. H., Breeman, W. A. P., Kooij, P. P. M., Oei, H. Y., Van Hagen, M., Postema, P. T. E., De Jong, M., Reubi, J. C., Visser, T. J., Reijs, A. E. M., Hofland, L. J., Koper, J. W., and Lamberts, S. W. J. Somatostatin receptor scintigraphy with [^{111}In-DTPA-D-Phe^1]- and [^{123}I-Tyr^3]-octreotide: the Rotterdam experience with more than 1000 patients. Eur. J. Nucl. Med., *20:* 716–731, 1993.
8. Krenning, E. P., Kooij, P. P. M., Pauwels, S., Breeman, W. A. P., Postema, P. T. E., De Herder, W. W., Valkema, R., and Kwekkeboom, D. J. Somatostatin receptor scintigraphy and radionuclide therapy. Digestion, *57:* 57–61, 1996.
9. De Jong, M., Krenning, E. P., Bakker, W. H., Breeman, W. A. P., Van der Pluijm, M. E., Bernard, H. F., Visser, T. J., Jermann, E., Béhé, M., Powell, P., and Mäcke, H. R. ^{90}Y and ^{111}In labelling, receptor binding and biodistribution of [DOTA^0,D-Phe^1, Tyr^3]octreotide, a promising somatostatin analogue for radionuclide therapy. Eur. J. Nucl. Med., *24:* 368–371, 1997.
10. De Jong, M., Bakker, W. H., Breeman, W. A. P., Bernard, W. H., Hofland, L. J., Visser, T. J., Srinivasan, A., Schmidt, M., Béhé, M., Mäcke, H. R., and Krenning, E. P. Preclinical comparison of [DTPA^0]octreotide, [DTPA^0,Tyr^3]-octreotide, and [DOTA^0,Tyr^3]octreotide, as carriers for octreotide receptor-targeted scintigraphy and radionuclide therapy. Int. J. Cancer, in press, 1998.
11. Otte, A., Jermann, E., Béhé, M., Goetze, M., Bucher, H. C., Roser, H. W., Heppeler, A., Müller-Brand, J., and Mäcke, H. R. DOTATOC: a powerful new tool for receptor-mediated radionuclide-therapy. Eur. J. Nucl. Med., *24:* 792–795, 1997.
12. Bakker, W. H., Albert, R., Bruns, C., Breeman, W. A. P., Hofland, L. J., Marbach, P., Pless, J., Pralet, D., Stolz, B., Koper, J. W., Lamberts, S. W. J., Visser, T. J., and

Krenning, E. P. [^{111}In-DTPA-D-Phe^1]-octreotide, a potential radiopharmaceutical imaging of somatostatin receptor-positive tumors: synthesis, radiolabeling and *in vitro* validation. Life Sci., *49:* 1583–1591, 1991.

13. Hofland, L. J., Van Koetsveld, P. M., Wouters, N., Waaijers, M., Reubi, J. C., and Lamberts, S. W. J. Dissociation of antiproliferative and antihormonal effect of the somatostatin analogue octreotide on 7315b pituitary tumor cells. Endocrinology, *131:* 571–577, 1992.
14. Hofland, L. J., Van Koetsveld, P. M., Waaijers, M., Zuyderwijk, J., Breeman, W. A. P., and Lamberts, S. W. J. Internalization of a radioiodinated somatostatin analogue, [^{125}I-Tyr^3]octreotide, by mouse and human pituitary tumour cells. Endocrinology, *136:* 3698–3706, 1995.
15. Andersson, P., Forssel-Aronsson, E., Johanson, V., Wangberg, B., Nilsson, O., Fjalling, M., and Ahlman, H. Internalization of In-111 into human neuroendocrine tumor cells after incubation with Indium-111-DTPA-D-Phe^{1}octreotide. J. Nucl. Med., *37:* 2002–2006, 1996.

Gwilliam, M. E., Peters, A. M., Myers, M. J., Gibbey, S. G., Bloom, S. R., and Calam, J. Amino acid infusion blocks renal tubular uptake of an indium-labelled somatostatin analogue. Br. J. Cancer, *67:* 1437–1439, 1993.

17. Pimm, M. V., and Gribben, S. J. Prevention of renal tubule re-absorption of radiometal (indium-111) labelled Fab fragment of a monoclonal antibody in mice by systemic administration of lysine. Eur. J. Nucl. Med., *21:* 663–665, 1994.
18. Behr, T. M., Sharkey, R. M., Juweid, M. E., Blumenthal, R. D., Dunn, R. M., Griffith, G. L., Bair, H-J., Wolf, F. G., Becker, W. S., and Goldenberg. D. M. Reduction of the renal uptake of radiolabelled monoclonal antibody fragments by cationic amino acids and their derivatives. Cancer Res., *55:* 3825–3834, 1995.
19. De Jong, M., Rolleman, E. J., Bernard, H. F., Visser, T. J., Bakker, W. H., Breeman, W. A. P., and Krenning, E. P. Inhibition of renal uptake of ^{111}In-DTPA-octreotide *in vivo*. J. Nucl. Med., *37:* 1388–1392, 1996.

CHAPTER 3

RADIOTHERAPEUTIC EFFICACY OF ^{153}SM-CMDTPA-TYR^3-OCTREOTATE IN TUMOR-BEARING RATS

Nuclear Medicine and Biology, 28, 327-334, (2001)

Radiotherapeutic efficacy of ^{153}Sm-CMDTPA-Tyr^3-octreotate in tumor-bearing rats☆

Joseph E. Bugaj, Jack L. Erion, Michael A. Johnson, Michelle A. Schmidt, Ananth Srinivasan

Mallinckrodt Inc., Department of Discovery Research, PO Box 5840, St. Louis, Missouri 63134, USA

Received 13 August 2000; received in revised form 4 November 2000; accepted 30 December 2000

Abstract

A number of radiolabeled somatostatin analogs have been evaluated in animal tumor models for radiotherapeutic efficacy. The majority of the agents tested have used either high-energy beta-emitters, such as Y-90 or Re-188, or the Auger electron-emitting radionuclide, In-111. Because a medium-energy beta-emitter might have equivalent efficacy compared to high-energy emitters, and lower toxicity to non-target tissues, we have evaluated the therapeutic potential of the beta-emitting nuclide, Sm-153, chelated to the somatostatin analog, CMDTPA-Tyr^3-octreotate. Using an in vitro binding assay, this octreotate derivative was shown to have high affinity for the somatostatin subtype-2 receptor (IC_{50} = 2.7 nM). Biodistribution studies in CA20948 tumor-bearing Lewis rats demonstrate that the Sm-153 labeled compound has high uptake and retention in tumor tissue (1.7% injected dose/g tissue, 4 hrs post injection) and has rapid overall clearance properties from non-target tissue. Radiotherapy studies were carried out using ^{153}Sm-CMDTPA-Tyr^3-octreotate and CA20948 tumor bearing Lewis rats at 7 days post implant. Dose regimens consisting of single and multiple i.v. injections of 5.0 mCi/rat (185 MBq) were employed over a time span of 7 days. Suppression of tumor growth rate was observed in all treated animals compared to untreated controls. Greater inhibition of tumor growth was observed in animals that received multiple doses. These studies indicate that medium-energy beta-emitting isotopes have considerable potential for the treatment of somatostatin receptor-positive tumors.

Keywords: Octreotate; Octreotide; Samarium; Somatostatin; Peptides; Radiotherapy

1. Introduction

The use of peptides as a means of targeting radionuclides to specific tissues has recently become more promising in both diagnostic and therapeutic applications. The wider use and acceptance of small peptide-based molecules has resulted from the ability to design compounds that have favorable biological characteristics, such as rapid blood clearance, low toxicity, high uptake into tumor tissue, and low immunogenicity [3,30,37,38]. The clinical use of OctreoScan® (^{111}In-DTPA-octreotide) is a specific example of a peptide-based imaging agent. The development of this diagnostic agent for use as a targeted radiotherapeutic has been reported [8,16,17,19,33]. Various octreotide derivatives radiolabeled with isotopes, including Y-90, and Re-188, have been reported to inhibit tumor growth in animals [16,33,38,39]. While high-energy (>1–2 MeV) beta-emitters have been used in these studies, there may be advantages to using lower energy beta-emitting radionuclides (<1 MeV). A low-energy particle should still be sufficient to kill targeted (and nearby) tumor cells but would be less damaging to non-target tissues. In this study, the radionuclide samarium-153 was used to test this premise.

The potential application of Sm-153 in peptide-targeted radiotherapy is indicated by its successful use in both bone palliation [4,13,22,24] and in radiation synovectomy [11, 20,22,23]. Sm-153 ($T_{1/2}$ = 46.3 hr) is a medium-energy beta-emitter (0.808 MeV, 17.5%; 0.705 MeV, 49.6%; 0.635 MeV, 32.2%) with a 30% abundance gamma emission (103 keV) that is suitable for use in scintigraphy [23]. In addition

☆An abstract containing a portion of the work presented in this paper was presented at the SNM meeting in Los Angeles, June 1999: J.E. Bugaj, J.L. Erion, M.A. Schmidt, R.R. Wilhelm, S.I. Achilefu, A.J. Srinivasan, J. Nucl. Med. (40) (1999) 223.

* Corresponding author. Tel.: +1-314-654-7344; fax: +1-314-654-8900.

E-mail: jebugaj@mkg.com (J.E. Bugaj).

Abbreviations: ACN, acetonitrile; TFA, trifluoroacetic acid; CMDTPA, carboxymethyldiethylenetriaminepentaacetic acid; sst_2, somatostatin subtype-2 receptor

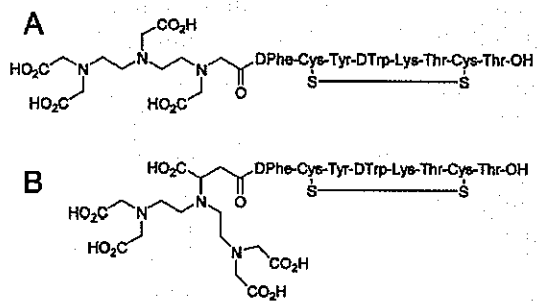

Fig. 1. Structures of (A) DTPA-Tyr^3-octreotate and (B) CMDTPA-Tyr^3-octreotate.

to the desirable emission properties of Sm-153, this lanthanide also readily forms complexes with DTPA-type chelates that can be conjugated to small peptide based molecules [32].

In previous work [21], it was demonstrated that even small variations in the structure of a DTPA-type ligand could have significant effects on the biodistribution properties of a Sm-153 labeled somatostatin peptide derivative. In other studies, we have shown that a substitution of the carboxy-terminal threoninol in octreotide with the natural amino acid threonine to generate a derivative termed, octreotate, substantially enhances the uptake and retention of a radiolabeled derivative in somatostatin receptor-expressing tumors [17,21]. In this study, we evaluated the therapeutic potential of one of these optimized derivatives, ^{153}Sm-CMDTPA-Tyr^3-octreotate (Fig. 1), in a rat tumor model.

2. Materials and methods

2.1. Preparation of somatostatin analogs

Solid phase peptide synthesis of CMDTPA-Tyr^3-octreotate and other octreotate derivatives was carried out with an Applied Biosystems 432A *Synergy* peptide synthesizer (Foster City, CA) employing Fmoc (9-fluorenylmethoxycarbonyl) strategy, utilizing 25 μmol of Fmoc-Thr(OtBu) Wang resin and 75 μmol of subsequent Fmoc-protected amino acids. Activation was accomplished using N-hydroxy-benzotriazole (HOBt) and 2-(1H-benzotriazole-1-yl)-1,1,3,3-tetramethyluronium hexafluorophosphate (HBTU). Penta-*t*-butyl carboxymethyl DTPA (protected CMDTPA) or tri-*t*-butyl DTPA was incorporated at the N-terminus in the same manner. Penta-*t*-butyl CMDTPA was prepared by a modification of a procedure described by Williams and Rappaport [35]. These authors carried out the bis *N*-alkylation of *p*-nitrophenylalanine benzyl ester with di-*t*-butyl [*N*-(bromoethyl)amino]diacetate using a phosphate buffer/acetonitrile reaction medium. This phenylalanine derivative was substituted here with L-aspartic acid β-benzyl, α-*t*-butyl ester. The benzyl ester of the resulting product was then cleaved via hydrogenolysis in methanol using 10% Pd/C as the catalyst to generate penta-*t*-butyl CMDTPA. Tri-*t*-butyl DTPA was prepared according to our previously published procedure [31]. Upon completion of the linear peptide, disulfide cyclization was performed manually by suspension of the resin-bound peptide in DMF (2 mL) containing 75 μmol thallium(III) trifluoroacetate (3 hr reaction at room temperature). After washing the resin with DMF and THF, the peptide was cleaved from the resin and deprotected with 85% trifluoroacetic acid/5% thioanisole/5% phenol/5% water (6 hrs). The peptide was precipitated with 10 mL t-butyl methyl ether and centrifuged. The peptide/resin pellet was then washed with 4 × 10 mL of t-butyl methyl ether. Acetonitrile/water (2:3) was finally added to dissolve the peptide, and the mixture was filtered to remove the resin. Crude peptide solutions were lyophilized prior to purification by HPLC. Final purification was accomplished by reverse phase HPLC on a Vydac C18 column using an acetonitrile/water gradient containing 0.1% TFA. Molecular weights were determined by mass spectrometry operating in the electrospray ionization mode.

2.2. Radiochemistry

$^{153}SmCl_3$ in 0.05N HCl was obtained from MURR (Columbia, MO) at a specific activity of ~700 Ci/mmol (25.9 TBq/mmol). Radiolabeling was carried out in 25 mM NaOAc, 12.5 mM sodium ascorbate (pH 5.0, room temperature). Small-scale reactions (10 mCi) were carried out by addition of 25 μL of $^{153}SmCl_3$ (400 mCi/ml in 0.05 N HCl) to 50 μL buffer (50 mM NaOAc, 25 mM sodium ascorbate) and 25 μL CMDTPA-Tyr^3-octreotate (1.1 molar excess peptide: Sm, 30 to 45 μg peptide in water). Reactions were incubated at room temperature for 30 min. For larger scale reactions (50 mCi), proportions identical to the small-scale reaction were used. The specific activity of radiolabeled peptide ranged from 300 to 500 Ci/mmol (11.1–18.5 TBq/mmol). For in vivo studies, ^{153}Sm-CMDTPA-Tyr^3-octreotate was diluted to 10 mCi/ml (370 MBq/ml) in phosphate-buffered saline containing 5% ethanol. Radiochemical yield (typically >98%) and purity (>95%) were determined by reverse phase HPLC on a Nova-Pak C18 column, 3.9 × 150 mm (Waters, MA), using a 15-min linear gradient of 0 to 70% solvent B at 1 ml/min (solvent A, 5% ACN/25 mM triethylamine pH 6.0; solvent B, 90% ACN/25 mM triethylamine, pH 6.0). The ^{153}Sm radiolabeled peptide eluted with a retention time of 13.2 min.

2.3. Receptor binding assays

Receptor binding assays were performed using membranes prepared from CA20948 tumors harvested from implanted Lewis rats [3]. Assays were carried out using the Millipore Multiscreen system (Bedford, MA) with ^{111}In-DTPA-Tyr^3-octreotate as the trace and unlabeled CMDTPA-Tyr^3-octreotate or other peptide derivatives as

the cold competitor. Radiolabeling of DTPA-Tyr^3-octreotate was performed by combining 1.0 μg peptide (1.0 mg/ml) with 1.0 mCi of $^{111}InCl_3$ (100 mCi/ml, Mallinckrodt Inc., St. Louis) and 10 μL buffer (50 mM NaOAc, 25 mM sodium ascorbate). After incubation at room temperature for 15 minutes, the peptide radiochemical yield (>99%) and purity (>95%) were determined by reverse phase HPLC. IC_{50} values were calculated using a four-parameter curve fitting routine using the program GraFit (Erithacus Software, UK).

2.4. Animal tumor model

All animal studies were conducted in compliance with the Mallinckrodt Inc. Animal Welfare Committee requirements. Male Lewis rats (120–140 g) were purchased from Harlan (Indianapolis, IN). The somatostatin subtype-2 (sst_2) receptor positive pancreatic acinar tumor line, CA20948, was maintained by serial passage in Lewis rats [3,27,28]. Tumor tissue was implanted into the left flank of the animal, and after approximately 2 weeks, tumor volumes were adequate for use in biodistribution studies. For therapy studies, tumor-implanted animal were used at 7 days post implant, at which time, tumors were palpable.

2.5. Tissue biodistribution studies

Biodistribution studies were carried out using male Lewis rats bearing CA20948 tumors (20-days post implant). Anesthetized (Metofane) animals received 25 μl (25 μCi [0.925 MBq]) of radiolabeled compound via the jugular vein. The animals were sacrificed in three groups (n = 3) at 1, 4, and 24 hours post injection by cervical dislocation. The tissues and organs of interest were removed, weighed, and radioactivity measured in a Packard Cobra gamma-scintillation counter.

2.6. Radiotherapy studies

CA20948 tumor tissue was implanted into the left flank of Lewis rats as described above. At 7-days post implant, animals were randomly divided into three study groups. The presence of a tumor was confirmed in all animals by palpation of the animal's left flank. For each treatment group a set of negative control tumor-implanted animals (n = 6/group) was maintained. Negative control animals received no treatment, and the three treated groups receiving ^{153}Sm-CMDTPA-Tyr^3-octreotate were as follows: (1) single i.v. dose of 5.0 mCi (185 MBq), (2) three doses of 5.0 mCi each with 7-day intervals between doses, (3) five doses of 5.0 mCi each with 7-day intervals between doses. Tumor volume measurements were performed on a weekly basis and calculated using the formula for an ellipsoid ($v = \pi/6[l \cdot w \cdot h]$).

Dosimetry calculations are based on the residence times of the radiolabeled peptide in organs and tumor tissue determined from biodistribution data, and the percent dose uptake per gram tissue. MIRD s-values were calculated assuming spherical geometry using energy tables from the Lawrence Berkeley National Laboratory database [10]. Tumor and organ doses correspond to self-absorbed dose only and do not include contributions from other organs.

Gamma scintigraphy was performed using a Picker 300 SX gamma camera interfaced to a dedicated Odyssey Imaging Processor. The gamma images of the rats injected with Sm-153 were obtained with a large field of view camera fitted with a general-purpose low-energy collimator for 100 K counts with the peak energy centered at 103 keV. The same conditions were used for obtaining In-111 images with the exception that the collimator was a medium-energy collimator, and the peak energies were centered at 171 and 245 keV. When used in this latter configuration, the gamma-camera does not detect Sm-153 gamma emissions. All rats were imaged in the prone position.

3. Results

3.1. In vitro assays

The CA20948 pancreatic acinar tumor line expresses high levels of the sst_2 receptor [3,17,28,33]. We have used membrane preparations from this tumor line in an in vitro assay to screen a number of somatostatin analogs with chemical modifications made in both the peptide and chelate segment of the molecule. Fig. 2 shows the data for several compounds analyzed using this assay. The estimated IC_{50} for CMDTPA-Tyr^3-octreotate was found to be essentially the same as that determined for DTPA-octreotide (2.8 and 2.5 nM, respectively). This compound was therefore selected as a promising candidate for further testing because of its high binding affinity and improved samarium chelating properties [21].

3.2. Tissue biodistribution study

The tissue biodistribution properties of ^{153}Sm-CMDTPA-Tyr^3-octreotate were studied in CA20948 tumor-bearing Lewis rats (Table 1, Fig. 3). At 1, 4, and 24 h post injection (p.i.) of the compound the amount of radioactivity that accumulated in the tumor tissue was 1.45, 1.73, and 0.74% of the injected dose per gram (%ID/g). Significant uptake was also observed in the pancreas and adrenal glands, both sst_2 receptor positive tissues. Pancreas uptake was 3.43, 3.02, and 1.74 %ID/g, and the adrenal tissue was 0.18, 0.17, and 0.15% of the injected dose per whole organ (%ID/o) at 1, 4, and 24 h p.i., respectively. Non-somatostatin receptor expressing tissues including the liver, muscle, spleen, and heart exhibited low accumulation of the radiotracer. The kidneys were the only non-receptor positive tissue in which high uptake was observed (3.34, 3.03 and 2.51% ID/gram; 1, 4, 24 h respectively). Scintigraphs at all

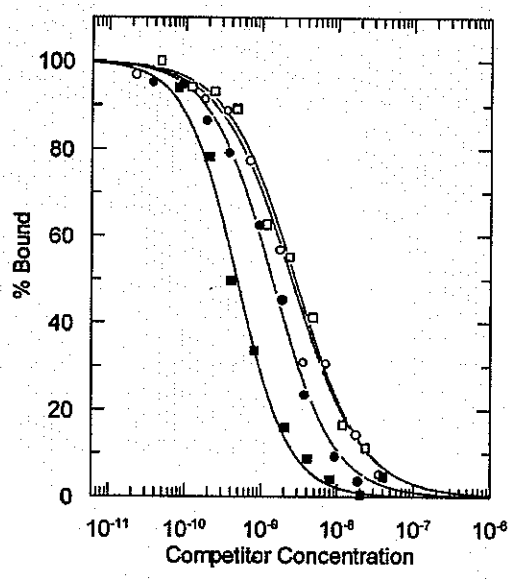

Fig. 2. Graph of competition binding of ^{111}In-DTPA-Tyr^3-octreotate to CA20948 tumor membranes in the presence of increasing concentration of unlabeled somatostatin analogs: ●, DTPA-Tyr^3-octreotate; ○, DTPA-octreotide; □, CMDTPA-Tyr^3-octreotate; ■, Tyr^3-octreotate. The corresponding calculated IC_{50} values are 1.39 nM, 2.51 nM, 2.77 nM, and 0.48 nM, respectively.

time points confirmed the strong localization of the agent in the tumor with no significant uptake observed in other non-sampled tissues or organs (data not shown). At 24 h, the predominant route of clearance was urinary (75.2%) with only 4.5% of the radioactivity recovered in the feces. The rapid distribution and excretion of this agent resulted in high target to non-target tissue ratios, except as noted for the kidneys. The tumor to tissue ratios calculated from %ID/g values at 24 h p.i. were 737 for blood, 369 for muscle, 9 for liver, and 0.3 for kidneys.

3.3. Radiotherapy

Preliminary studies were carried out to assess the dose levels required for ^{153}Sm-CMDTPA-Tyr^3-octreotate to affect the growth rate of CA20948 tumors in Lewis rats. It was found that relatively small doses (0.5 mCi/animal) measurably reduced the growth rate of tumors, but that higher doses (3.0–5.0 mCi) were necessary to either decrease tumor volumes or significantly delay tumor regrowth (data not shown). To further determine the therapeutic potential of this agent, three separate dosing regimens were tested using a 5.0 mCi dose with one, three, and five treatments. Treatments were spaced 7 days apart because the biological clearance of the agent was essentially complete by this time. The effect of repeat doses on the biodistribution of the radiolabeled peptide was not determined. However, an evaluation of the mass effects of peptide (6 ng to 250 μg) on the biodistribution of ^{111}In-DTPA-Tyr^3-octreotate (data not shown) indicates that the amount of peptide used in each treatment (~15 μg) was insufficient to block the uptake of a subsequent dose by more than 50% of levels found in a normal biodistribution study [17]. Similar results have been demonstrated by others [7,18] with DTPA-octreotide. Our data also show that when tumors re-emerged they continued to express high levels of the somatostatin receptor (Fig. 5B and C). Additionally, as determined from the aforementioned mass effects study, it was not feasible to compare the effect of a single cumulative dose with the multiple dose regimens because the level of peptide required for 15 and 25 mCi doses at 500 Ci/mmol (40 to 70 μg) would significantly attenuate the uptake of radiolabel into tumor tissue. An untreated control group of tumor-implanted animals (n = 6) was maintained for each treatment group to limit uncertainties arising from possible variability in tumor growth rates or in somatostatin receptor expression following serial passages of tumor tissue.

Fig. 4 shows the results of the single and multiple dose administration of ^{153}Sm-CMDTPA-Tyr^3-octreotate in tumor-bearing Lewis rats. In all three studies, untreated tu-

Table 1
Biodistribution of ^{153}Sm-CMDTPA-Tyr^3-octreotate in CA20948 tumor-bearing Lewis rats (%ID/gram tissue, n = 3)

	Time post injection		
Tissue sample	1 Hour	4 Hours	24 Hours
Blood	0.083 ± 0.011	0.006 ± 0.001	0.001 ± 000.0
Liver	0.072 ± 0.008	0.079 ± 0.011	0.084 ± 0.007
Kidneys	3.344 ± 0.454	3.031 ± 0.112	2.510 ± 0.190
Skeletal Muscle	0.018 ± 0.002	0.004 ± 000.0	0.002 ± 0.001
Spleen	0.042 ± 0.004	0.036 ± 0.013	0.030 ± 0.004
Heart	0.044 ± 0.004	0.011 ± 0.001	0.007 ± 000.0
Pancreas	3.425 ± 0.264	3.023 ± 0.082	1.736 ± 0.110
Small Int	0.307 ± 0.077	0.395 ± 0.132	0.125 ± 0.011
Stomach	0.275 ± 0.047	0.392 ± 0.044	0.107 ± 0.011
Bone	0.138 ± 0.012	0.129 ± 0.010	0.134 ± 0.005
Tumor	1.453 ± 0.371	1.726 ± 0.332	0.737 ± 0.053

Table 2
Biodistribution and excretion of ^{153}Sm-CMDTPA-Tyr^3-octreotate in CA20948 tumor-bearing Lewis rats (%ID/total tissue, n = 3)

Tissue sample	Time post injection		
	1 Hour	4 Hours	24 Hours
Blood	1.010 ± 0.130	0.071 ± 0.009	0.017 ± 0.004
Liver	0.683 ± 0.071	0.734 ± 0.076	0.954 ± 0.084
Kidneys	6.535 ± 0.523	5.852 ± 0.244	5.214 ± 0.225
Skeletal Muscle	1.986 ± 0.224	0.400 ± 0.019	0.224 ± 0.060
Spleen	0.025 ± 0.002	0.020 ± 0.005	0.016 ± 0.002
Heart	0.035 ± 0.003	0.009 ± 0.001	0.006 ± 0.001
Pancreas	3.620 ± 0.106	2.742 ± 0.178	1.584 ± 0.022
Stomach	1.085 ± 0.029	0.968 ± 0.148	0.543 ± 0.057
Bone	1.937 ± 0.177	1.790 ± 0.074	1.944 ± 0.114
Adrenals	0.180 ± 0.003	0.167 ± 0.002	0.145 ± 0.009
Thyroid	0.004 ± 0.001	0.003 ± 0.001	0.001 ± 0.000
Tumor	3.208 ± 1.627	6.177 ± 2.620	1.921 ± 0.435
Total Urine			75.217 ± 4.983
Total Feces			4.512 ± 0.655
Total Excreted			79.728 ± 5.054
Total Recovered			92.298 ± 4.401

mor-bearing rats showed similar tumor growth rates. The majority of control animals were sacrificed at approximately 35 days p.i. due to the state of tumor progression. A significant delay in tumor growth occurred in both single and multiple treatment groups. This suppression of tumor growth is seen in Fig. 5A, which shows comparative scintigraphs (50 μCi ^{111}In-DTPA-Tyr^3-octreotate/rat) of untreated (−) and treated animals (+, 3 × 5 mCi dose of ^{153}Sm-CMDTPA-Tyr^3-octreotate), 2 days after the final treatment dose (30 days post tumor implant). The biodistribution pattern of the ^{111}In-DTPA-Tyr^3-octreotate is also seen by scintigraphy to be very similar to ^{153}Sm-CMDTPA-Tyr^{3}octreotate (Fig. 5D). Measured tumor volumes (Fig. 4)

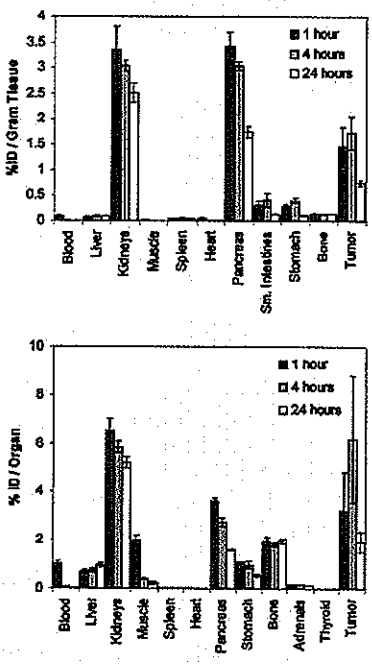

Fig. 3. The biodistribution of ^{153}Sm-CMDTPA-Tyr^3-octreotate in CA20948 tumor-bearing Lewis rats. Animals were injected with 25 μCi of radiolabeled peptide (n = 3 per time point) and sacrificed at 1, 4, and 24 hours post injection. See text for details.

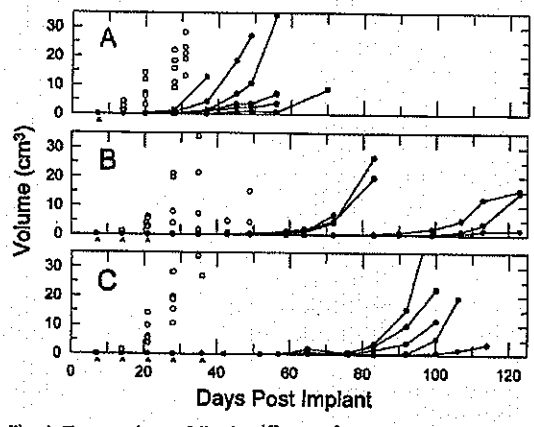

Fig. 4. Tumor volumes following ^{153}Sm-Tyr^3-octreotate radiotherapy of CA20948 tumor-bearing rats. Panels: A, single dose of 5.0 mCi; B, 3 doses of 5.0 mCi at seven day intervals; C, 5 doses of 5.0 mCi at seven day intervals. Carets on time axis indicate dose administration. Symbols: ○, Tumor-implanted untreated controls; ●, Tumor-implanted rats with indicated treatments. Calculated mean survival of untreated control animals was: A, 31 days ± 0; B, 40 days ± 7; C, 32 days ± 4; and treated animals was: A, 54 days ± 10; B, 101 days ± 22; C, 101 days ± 9.

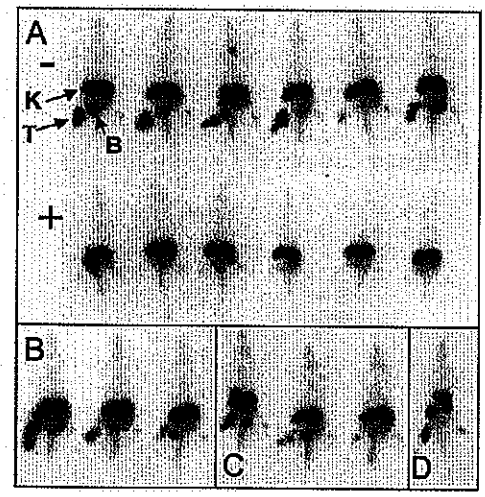

Fig. 5. Gamma-scintigraphy of treated or untreated CA20948 tumor-implanted Lewis rats. A, scintigraphs of rats treated with 3 × 5 mCi (+) of ^{153}Sm-CMDTPA-Tyr^3-octreotate and the corresponding control group (−) were imaged at 30 days post tumor implant. Symbols on scintigraphs indicate position of (T) tumor, (K) kidney, and (B) bladder. B, scintigraphs of 3 of 5 surviving rats treated with a single 5 mCi dose of ^{153}Sm-CMDTPA-Tyr^{3}octreotate at 37 days post treatment. C, scintigraphs of 3 of 6 surviving rats treated with 5 × 5 mCi doses of ^{153}Sm-CMDTPA-Tyr^3-octreotate at 78 days post tumor implant. A, B, C, Animals were injected with 50 μCi of ^{111}In-DTPA-Tyr^3-octreotate and imaged at 3 hours post injection. D, scintigraph of tumor bearing Lewis rat (3 wks post implant) at 3 hrs post injection of 250 μCi ^{153}Sm-CMDTPA-Tyr^3-octreotate.

were consistent with the observed tumor uptake of ^{111}In-DTPA-Tyr^3-octreotate suggesting uptake was not compromised by receptor saturation from previous doses. Multiple treatments improved efficacy over a single 5 mCi dose; at 95 days post tumor implant there were 50% surviving rats treated with 3 × 5 mCi and 100% surviving rats treated with 5 × 5 mCi. Tumor regrowth was, however, observed in all treated animals with no animal surviving more than 125 days post tumor implant (Fig. 4). In all cases, the tumors that eventually developed in animals treated with either single or multiple doses still expressed high levels of the sst_2 receptor as shown in scintigraphs of animals imaged with ^{111}In-DTPA-Tyr^{3}octreotate (Fig. 5B and C). Dosimetry estimates for the tumor and organs with significant uptake were calculated using the percent uptake and residence times determined from the biodistribution data. For a single 5 mCi treatment, doses to the tumor, kidney and pancreas are calculated to be 8.7 Gy, 29.5 Gy, and 18.7 Gy respectively.

4. Discussion

The studies presented here demonstrate the radiotherapeutic potential of the medium-energy beta-emitting radionuclide, Sm-153, chelated to the somatostatin analog CMDTPA-Tyr^3-octreotate. This agent's high affinity for the somatostatin sst_2 receptor and its long-term retention in tumor tissue are properties that are required for effective radiotherapy. The biodistribution data of ^{153}Sm-CMDTPA-Tyr^3-octreotate in CA20948 tumor-bearing Lewis rats showed that this compound has high uptake and retention in tumor tissue expressing the sst_2 receptor. The tumor uptake is greater than that observed for ^{111}In-DTPA-octreotide [16, 17], and is similar to that reported for ^{90}Y-DOTA-Tyr^3-octreotide [16]. Higher tumor uptake has been reported for ^{111}In-DTPA-Tyr^3-octreotate [17], but we found the corresponding ^{153}Sm-DTPA complex to be somewhat less stable in vivo than the ^{153}Sm-CMDTPA complex. The tumor uptake of the DTPA- or CMDTA-Tyr^3-octreotate compounds radiolabeled with Sm-153 was not significantly different (data not shown). There was low uptake/retention of ^{153}Sm-CMDTPA-Tyr^3-octreotate in most non-target tissues with only the observed kidney uptake representing a limiting factor to dose escalation [1]. It has been demonstrated, however, that a significant reduction of the kidney retention of other similar somatostatin metal-chelate analogues can be achieved by the use of amino acid i.v. infusion [5,17]. The pancreas is an sst_2 receptor positive organ in which potentially undesirable uptake was observed. Additional studies are necessary to determine whether the high pancreatic uptake observed in rats will also be found in humans. Results with other octreotate derivatives in primates, where no apparent pancreas uptake is observed in scintigraphs, suggest that this will not be the case [25]. Moreover, all animals from the high multiple dose treatment group were examined at death and no visual signs of tissue pathology were noted in kidneys or pancreas. Other overt parameters such as weight gain and grooming behavior during the course of the study were also normal in these animals. In addition to the overall favorable biodistribution properties of ^{153}Sm-CMDTPA-Tyr^3-octreotate, the compound also has excellent clearance properties with almost 80% of the injected dose excreted within 24 hours, predominately via the renal system.

The radiotherapeutic efficacy of ^{153}Sm-CMDTPA-Tyr^3-octreotate is demonstrated here by our finding that even a single 5 mCi dose per animal was sufficient to attenuate tumor growth as compared to untreated controls. More pronounced suppression of tumor regrowth was observed when multiple dose regimens were administered. With three or five doses of 5 mCi at one-week intervals, we observed a mean survival of 101 days post tumor implant as compared to <40 days for untreated controls. In all cases, however, treated rats ultimately succumbed to regrowth of latent tumor cells. Despite this, the therapeutic effect was significant and similar or superior to results achieved by workers using other radiolabeled somatostatin analogs. For example, Anderson *et al.* [3] reported the therapeutic effect of ^{64}Cu-TETA-octreotide in the same tumor model employed here. In their studies, treatment of tumor-bearing rats

with one or two, 15 mCi doses of radiolabeled peptide also resulted in delayed tumor growth; however, at two weeks post treatment, tumor volumes in treated animals were comparable to untreated controls [3]. De Jong *et al.* reported a transient tumor response in rats (CA20948 tumors) following treatment with 2 × 3 mCi of ^{90}Y-DOTA-Tyr^3-octreotide with rats surviving 65 days on average post treatment [19]. Using the latter agent in the same animal tumor model, Stolz *et al.* reported complete remission in 5 of 7 animals with a single treatment of 2.5 mCi per animal [33]. These data indicate that identical tumor models can behave differently when maintained in separate laboratories. The variables that alter tumor radiosensitivity, such as volume and growth rate, which may account for the discrepancies, have not yet been evaluated.

5. Conclusion

The recent search for the ideal radionuclide for targeted radiotherapy using somatostatin analogs has resulted in the evaluation of Y-90, Cu-64, In-111, Re-188, I-131, and now Sm-153 [2,3,17,19,33,38,39]. The beta emission energy of Sm-153 is similar to that of I-131, an extensively used therapeutic radionuclide. Sm-153 also emits a partial low-energy gamma emission (30%, 103 keV), which allows for scintigraphic imaging, useful in staging radionuclide therapy and performing dosimetric calculations. A low or medium-energy beta emission as compared to the high-energy emissions of Y-90 or Re-188, for example, is expected to be less toxic to critical non-target organs. Additionally, peptide degradation due to radiolysis is easier to prevent in compounds radiolabeled with Sm-153 than with high-energy beta-emitters. Though there are advantages to using Sm-153, the relatively low specific activity (~700 Ci/mmol) results in some limitations, especially if an agonist-targeting agent is used, which may have negative physiological effects at high concentrations. Additional studies are necessary to determine whether these limitations can be overcome, or whether they can be circumvented using other low to medium-energy beta-emitting radionuclides.

Acknowledgments:

The authors thank Randy Wilhelm for mass spec analysis of peptides, and Dr. C.J. Anderson, Washington Univ., St. Louis, for seed CA20948 tumor tissue.

References

[1] Y. Akizawa Arano, T. Uezono, M. Ono, Y. Fujioka, T. Uehara, A. Yokoyama, K. Akaji, Y. Kiso, M. Koizumi, H. Saji, Renal metabolism of ^{111}In-DTPA-DPhe^1-octreotide in vivo. Bioconjugate Chem. (9) (1998) 662–670.

[2] C.J. Anderson, T.S. Pajeau, W.B. Edwards, E.L. Sherman, B.E. Rogers, M.J. Welch, In vitro and in vivo evaluation of copper-64-octreotide conjugates. J. Nucl. Med. (36) (1995) 2315–2325.

[3] C.J. Anderson, L.A. Jones, L.A. Bass, E.L. Sherman, D.W. McCarthy, P.D. Cutler, M.V. Lanahan, M.E. Cristel, J.S. Lewis, S.W. Schwarz, Radiotherapy, toxicity and dosimetry of copper-64-TETA-octreotide in tumor-bearing rats. J. Nucl. Med. (39) (1998) 1944–1951.

[4] J.E. Bayouth, D.J. Macey, L.P. Kasi, F.V. Fossella, Dosimetry and toxicity of samarium-153-EDTMP administered for bone pain due to skeletal metastases. J. Nucl. Med. (35) (1994) 63–69.

[5] T.M. Behr, R.M. Sharkey, M.E. Juweid, R.D. Blumenthal, R.M. Dunn, G.L. Griffiths, H.J. Bair, F.G. Wolf, W.S. Becker, D.M. Goldenberg, Reduction of the renal uptake of radiolabeled antibody fragments by cationic amino acids and their derivatives. Cancer Res. (55) (1995) 3825–3834.

[6] W.A. Breeman, P.M. van Hagen, D.J. Kwekkeboom, T.J. Visser, E.P. Krenning, Somatostatin receptor scintigraphy using [^{111}In-DTPA^0]RC-160 in humans: a comparison with [^{111}In-DTPA^0]octreotide. Eur J Nucl. Med. (25) (1998) 182–186.

[7] W.A. Breeman, M. de Jong, B.F. Bernard, W.H. Bakker, E.J. Rolleman, D.J. Kwekkeboom, T.J. Visser, E.P. Krenning, Effects of ligand priming and multiple-dose injection on tissue uptake of ^{111}In-pentetreotide in rats. Nucl. Med. Biol. (24) (1997) 749–753.

[8] M.E. Caplin, W. Mielcarek, J.R. Buscombe, A.L. Jones, P.L. Crossdale, M.S. Cooper, A.K. Burroughs, A.W. Hilson, Toxicity of high-activity ^{111}In-octreotide therapy in patients with disseminated neuroendocrine tumours. Nucl. Med. Comm. (21) (2000) 97–102.

[9] M. Chinol, S. Vallabhajosula, S.J. Goldsmith, M.J. Klein, K.F. Deutsch, L.K. Chinen, J.W. Brodack, E.A. Deutsch, B.A. Watson, A.J. Tofe, Chemistry and biological behavior of samarium-153 and rhenium-186 labeled hydroxyapatite particles: potential radiopharmaceuticals for radiation synovectomy. J. Nucl. Med. (34) (1993) 1536–1542.

[10] S.Y.F. Chu, L.P. Ekstrom, R.B. Firestone, WWW Table of Radioactive Isotopes, database version 2/28/99 from URL http://nucleardata.nuclear.lu.se/nucleardata/toi/

[11] G. Clunie, D. Lui, I. Cullum, J.C. Edwards, P.J. Ell, Samarium-153-particulate hydroxyapatite radiation synovectomy: biodistribution data for chronic knee synovectomy. J. Nucl. Med. (36) (1995) 51–57.

[12] G. Clunie, D. Lui, I. Cullum, Clinical outcome after one year following samarium-153 particulate hydroxyapatite radiation synovectomy. Scand. J. Rheumatology (25) (1996) 360–366.

[13] C. Collins, J.F. Eary, G. Donaldson, C. Vernon, N.E. Bush, S. Petersdorf, R.B. Livingston, E.E. Gordon, C.R. Chapman, F.R. Appelbaum, Samarium-153-EDTMP in bone metastases of hormone refractory prostate carcinoma: a phase I/II trial. J. Nucl. Med. (34) (1993) 1839–1844.

[14] M. De Jong, W.A. Breeman, B.F. Bernard, E.J. Rolleman, L.J. Hofland, T.J. Visser, B. Setyono-Han, W.H. Bakker, M.E. van der Pluijm, E.P. Krenning, Evaluation in vitro and in rats of ^{161}Tb-DTPA-octreotide, a somatostatin analogue with potential for intraoperative scanning and radiotherapy. Eur. J. Nucl. Med. (22) (1995) 608–616.

[15] M. De Jong, E.J. Rolfsmann, B.F. Bernard, T.J. Visser, W.H. Bakker, W.A. Breeman, E.P. Krenning, Inhibition of renal uptake of indium-111-DTPA-octreotide in vivo. J. Nucl. Med. (37) (1996) 1388–1392.

[16] M. De Jong, W.H. Bakker, E.P. Krenning, W.A. Breeman, M.E. van der Pluijm, B.F. Bernard, T.J. Visser, E. Jermann, M. Behe, P. Powell, H.R. Macke, Yttrium-90 and indium-111 labelling, receptor binding and biodistribution of [DOTA^0,D-Phe^1,Tyr^3]octreotide, a promising somatostatin analogue for radionuclide therapy. Eur. J. Nucl. Med. (24) (1997) 368–371.

[17] M. De Jong, W.A. Breeman, W.H. Bakker, P.M. Kooij, B.F. Bernard, L.J. Hofland, T.J. Visser, A. Srinivasan, M.A. Schmidt, J.L. Erion, J.E. Bugaj, H.R. Macke, E.P. Krenning, Comparison of ^{111}In-labeled

somatostatin analogues for tumor scintigraphy and radionuclide therapy. Cancer Res. (58) (1998) 437–441.

[18] M. De Jong, W.A. Breeman, B.F. Bernard, A. van Gameren, E. de Bruin, W.H. Bakker, M.E. van der Pluijm, T.J. Visser, H.R. Macke, E.P. Krenning, Tumour uptake of the radiolabelled somatostatin analogue [DOTA^0,Tyr^3]octreotide is dependent on the peptide amount. Eur. J. Nucl. Med. (26) (1999) 693–698.

[19] M. De Jong, W.A. Breeman, B.F. Bernard, P.M. Kooij, G.D. Slooter, C.H. van Eijck, D.J. Kwekkeboom, R. Valkema, H.R. Macke, E.P. Krenning, Therapy of neuroendocrine tumors with radiolabeled somatostatin-analogues. Q. J. Nucl. Med. (43) (1999) 356–366.

[20] E.A. Deutsch, J.W. Brodack, K.F. Deutsch, Radiation synovectomy revisited. Eur. J. Nucl. Med. (20) (1993) 1113–1127.

[21] J.L. Erion, A. Srinivasan, M.A. Schmidt, R.R. Wilhelm, J.E. Bugaj, Radiolabeled ligand-octreotate conjugates: evaluation of potential diagnostic and therapeutic radiopharmaceutical agents targeted to somatostatin receptors. J. Nucl. Med. (Suppl. 38) (1997) 813.

[22] M. Farhangi, R.A. Holmes, W.A. Volkert, K.W. Logan, A. Singh, Samarium-153-EDTMP: pharmacokinetic, toxicity and pain response using an escalating dose schedule in treatment of metastatic bone cancer. J. Nucl. Med. (33) (1992) 1451–1458.

[23] W.F. Goeckeler, B. Edwards, W.A. Volkert, R.A. Holmes, J. Simon, D. Wilson, Skeletal localization of samarium-153 chelates: potential therapeutic bone agents. J. Nucl. Med., (28) (1987) 495–504.

[24] J.C. Lattimer, L.A. Corwin, J. Stapleton, W.A. Volkert, G.J. Ehrhardt, A.R. Kelring, S.K. Anderson, J. Simon, W.F. Goeckeler, Clinical and clinicopathologic response of canine bone tumor patients to treatment with samarium-153-EDTMP. J. Nucl. Meet. (31) (1990) 1316–1325.

[25] J.S. Lewis, A. Srinivasan, M.A. Schmidt, C.J. Anderson, In vitro and in vivo evaluation of ^{64}Cu-TETA-tyr3-octreotate. A new somatostatin analog with improved target tissue uptake. Nucl. Med. Biol. (26) (1999) 267–273.

[26] K.W. Logan, W.A. Volkert, R.A. Holmes, Radiation dose calculations in persons receiving injection of samarium-153 EDTMP. J. Nucl. Med. (28) (1987) 505–509.

[27] D.S. Longnecker, H.S. Lilja, J. French, E. Kuhlmann, W. Noll, Transplantation of azaserine-induced carcinomas of pancreas in rats. Cancer Lett. (4) (1979) 197–202.

[28] J-C. Reub, L. Kvols L., Somatostatin receptors in human renal cell carcinomas. Cancer Res. (52) (1992) 6074–6078.

[29] J-C. Reubi, J.C. Schar, B. Waser, S. Wenger, A. Heppeler, J.S. Schmitt, H.R. Macke, Affinity profiles for human somatostatin receptor subtypes SST-1-SST-5 of somatostatin radiotracers selected for scintigraphic and radiotherapeutic use. Eur. J. Nucl. Med. (27) (2000) 273–282.

[30] P.M. Smith-Jones, B. Stolz, R. Albert, H. Knecht, C. Bruns, Synthesis, biodistribution and renal handling of various chelate-somatostatin conjugates with metabolizable linking groups. Nucl. Med. Biol. (24) (1997) 761–769.

[31] A. Srinivasan, M.A. Schmidt, Tri-*t*-butyl DTPA: A versatile synthon for the preparation of DTPA-containing peptides by solid phase synthesis, in Peptides: frontiers of peptide science. Proceedings of the 15th American peptide symposium, edited by J.P. Tam, P.T.P. Kaumaya, (1997) 267–268.

[32] J.B. Stimmel, F.C. Kull, Samarium-153 and lutetium-177 chelation properties of selected macrocyclic and acyclic ligands. Nucl. Med. Biol. (25) (1998) 117–125.

[33] B. Stolz, G. Weckbecker, P.M. Smith-Jones, R. Albert, F. Raulf, C. Bruns, The somatostatin receptor-targeted radiotherapeutic [^{90}Y-DOTA-DPhe^1,Tyr^3-octreotide (^{90}Y-SMT 487) eradicates experimental rat pancreatic CA20948 tumors. Eur. J. Nucl. Med. (25) (1998) 668–674.

[34] J.H. Turner, A.A. Martindale, P. Sorby, E.L. Hetherington, R.F. Fleay, R.F. Hoffman, P.G. Claringbold, Samarium-153 EDTMP therapy of disseminated skeletal metastasis. Eur. J. Nucl. Med. (15) (1989) 784–795.

[35] M.A. Williams, H. Rapoport, Synthesis of enantiomerically pure diethylenetriaminepentaacetic acid analogs. L-Phenylalanine as the educt for substitution at the central acetic acid. J. Org. Chem. (58) (1993) 1151–1158.

[36] M. Windoren, I. Kjonniksen, O. Fodstad, Pronounced therapeutic effect of samarium 153-ethylenediaminetetramethylene phosphonate in an orthotopic human osteosarcoma tibial tumor model. J. Nat. Cancer Inst. (87) (1995) 221–222.

[37] G.A. Wiseman, L.K. Kvols, Therapy of neuroendocrine tumors with radiolabeled MIBG and somatostatin analogues. Sem. Nucl. Med. (3) (1995) 272–278.

[38] P.O. Zamora, S. Gulhke, H. Bender, D. Diekmann, B.A. Rhodes, H.J. Biersack, F.F. Knapp Jr, Experimental radiotherapy of receptor-positive human prostate adenocarcinoma with ^{188}Re-RC-160, a directly-radiolabeled somatostatin analogue. Int. J. Cancer (65) (1996) 214–220.

[39] P.O. Zamora, H. Bender, S. Gulhke, M.J. Marek, R.R. Knapp, B.A. Rhodes, H.J. Biersack, Pre-clinical experience with Re-188-RC-160, a radiolabeled somatostatin analog for use in peptide-targeted radiotherapy. Anticancer Res. (17) (1997) 1803–1808.

CHAPTER 4A

LONG TERM SURVIVAL OF TUMOR-IMPLANTED LEWIS RATS TREATED WITH ^{177}LU-DOTA-Y^{3}-OCTREOTATE

Jack. L. Erion, Joseph E. Bugaj, Michelle A. Schmidt and Ananth Srinivasan

ABSTRACT

Biodistribution and clearance properties of ^{177}Lu-DOTA-Y^{3}-Octreotate and ^{177}Lu-DOTA-Y^{3}-Octreotide were evaluated in CA20948 tumor implanted Lewis rats. The Octreotate derivative was shown to have substantially higher uptake in somatostatin receptor expressing tissue than the Octreotide counterpart (tumor uptake of Octreotate compound was 2.5%id/gram tissue vs. 0.81%id/gram for the Octreotide compound at 24 hours post injection). Overall clearance and excretion of the two compounds was similar, but uptake and retention in non-target tissue differed in that the kidney/tumor ratios for the Octreotide based radiopharmaceutical ranged from 1.7 to 2.5 at 1, 4 and 24 hour time points, whereas, the ratios for the Octreotate based compound were only 0.3 to 0.5 for the same time points evaluated.

Because of the improved biological properties compared to Octreotide, the radiotherapeutic efficacy of Lu-177 labeled DOTA-Y^{3}-Octreotate, a somatostatin receptor-targeted peptide, was tested in a CA20948 Lewis rat tumor model. The long-term survival of treated animals was further studied to determine the efficacy of this therapeutic agent, and to assess the potential negative effects of relatively high doses of Lu-177. Tumor-bearing Lewis rats were treated with one or three doses (37, 92.5, or 185 MBq per dose) of DOTA-(Tyr^{3})-Octreotate radiolabeled with Lu-177 to a specific activity of ~44 TBq/mmol. Tumor regression was observed in all treatment groups. Complete tumor ablation and long-term survival occurred only in animals that received 92.5 or 185 MBq of Lu-177 radiolabeled compound. The highest percentage of survivors occurred in the treatment groups that received multiple doses. Fifty percent of the rats (n=8) treated with 3 x 92.5 MBq survived more than 18 months post tumor implant. Rats treated with three doses of 185 MBq

showed the highest percentage of survivors (100%, n=8) at 12 months post tumor implant, but began to show signs of morbidity (weight loss, poor grooming) at 12 to 15 months post implant. Within a 4-month time span all animals in this treatment group died. These animals showed evidence of renal disease as determined by post mortem examination. These long-term survival studies further underscore the therapeutic potential of ^{177}Lu-DOTA-Y^{3}-Octreotate for treatment of somatostatin receptor-positive tumors. However, issues of renal toxicity may require closer examination in order to design appropriate treatment regimens that reduce radiation exposure to the kidney.

Introduction

Recent studies have demonstrated the potential radiotherapeutic efficacy of various high-energy beta-emitting radionuclides complexed with somatostatin analogs, which are targeted to tumors that over-express somatostatin subtype-2 (sst_2) receptors (1-3).

Additionally, ^{111}In-DOTA-Y^{3}-Octreotate was shown to have superior uptake and retention in receptor positive tumors compared to a number of other somatostatin analogs (6-9). Our studies using either samarium-153 or lutetium-177 labeled DTPA derivatives of Y^{3}-Octreotate have shown that relatively low energy ß$^{-}$ emitting isotopes have a significant radiotherapeutic effect on rats implanted with the sst_2 receptor positive tumor line CA20948 (4).

The radionuclide lutetium-177 has improved properties over samarium-153; most notable are a medium energy beta emission (78% 497 keV), a relatively long half-life (6.7 days), and the potential for high radio-specific activity (>3000 Ci/mmol). Lu-177

also has a low abundance gamma emission (11%, 208 keV), which allows scintigraphic imaging and provides a convenient tracer emission for quantitation in biodistribution studies and dosimetry determinations. As a reactor product produced from Lu-176, Lu-177 presents a number of additional advantages in cost, scalability, and availability over radionuclides produced by other means.

In an ongoing study ^{177}Lu-DOTA-Y^3-Octreotate (Fig. 1) has been shown to be a highly effective SS derivative for use as a radiotherapeutic agent (5). The long-term fate of animals treated with single and multiple doses of this agent are presented here.

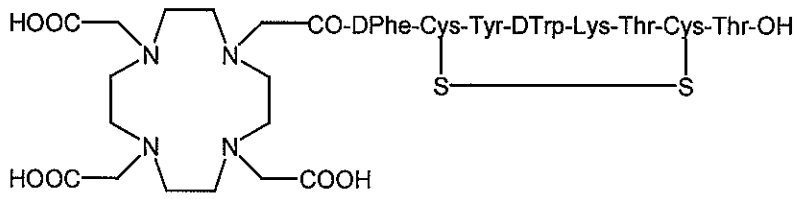

Figure 1: Structure of DOTA-Tyr^3-octreotate

Methods

Peptides and Radiochemistry

The DOTA conjugate of Y^3-Octreotate was synthesized as previously described (8) Lutetium-177 was obtained from MURR, Columbia, MO (specific activity >3000 Ci/mmol). Labeling reactions were performed at 80°C in 30 mM NaOAc, 15 mM NaAscorbate, pH 5.5. Peptides were labeled to a radiospecific activity of

1200 Ci/mmol. Radiochemical yield (>99.5%) and radiochemical purity (>95%) were determined by reverse phase chromatography on a C18 Vydac column using a acetonitrile/0.1% TFA gradient (5% to 70% acetonitrile over 20 minutes) at a flow rate of 1 ml/min. Samples were coinjected in 2.5 mM DTPA to chelate unincorporated metal. The Lu-177 radiolabeled peptide has a retention time of 14.8 minutes under these conditions. The Lu-177-DTPA complex elutes at 3.0 minutes.

Receptor Binding Assays

Receptor binding assays were performed using membranes prepared from CA20948 tumors harvested from implanted Lewis rats (3). Assays were carried out using the Millipore Multiscreen system (Bedford, MA) with ^{111}In-DTPA-Tyr^3-octreotide as the trace and unlabeled DOTA-Tyr^3-octreotate or other peptide derivatives as the cold competitor. IC_{50} values were calculated using a four-parameter curve fitting routine using the program GraFit (Erithacus Software, UK).

Animal Model

All animal studies were conducted in compliance with the Mallinckrodt Inc. Animal Welfare Committee requirements. Male Lewis rats (120-140 g) were purchased from Harlan (Indianapolis, IN). The somatostatin subtype-2 (sst_2) receptor positive pancreatic acinar tumor line, CA20948, was maintained by serial passage in Lewis rats (3). Tumor tissue was implanted subcutaneously into the left flank of the animal, and after approximately 2 weeks, tumor volumes were adequate for use in biodistribution and therapy studies.

Biodistribution Studies

The overall biodistribution properties of ^{177}Lu-labeled DOTA linked peptides were determined in CA20948 tumor implanted Lewis rats. Rats were injected via the jugular vein with 250 µCi of radiolabeled peptide (1200 Ci/mmol) in phosphate buffered saline, 5% ethanol. Groups of animals (3 per time point) were sacrificed by cervical dislocation at indicated times. Following scintigraphy, selected tissues and organs were removed, weighed, and radioactivity measured in a Packard Cobra gamma-scintillation counter (Canberra).

Radiotherapy

Radiotherapy studies were initiated at 14 days post implant of the CA20948 pancreatic tumor cell line. For each treatment group a set of untreated, tumor implanted animals was maintained (n = 6 for single dose study, n = 8 for multidose study). Animals were injected with up to 5 mCi of ^{177}Lu-DOTA-Y^3-Octreotate (1200 Ci/mmol, 1Ci/ml) via the jugular vein. Animals received either single doses of radiolabeled peptide, or multiple doses administered at 30-day intervals. Control animals with tumor implants received no treatments. A blocking dose of unlabeled peptide (1mg/kg) was administered to an additional group (n=3) to demonstrate the receptor specificity of the radiotherapeutic effect. Tumor volume was determined by measurement with calipers 2 to 3 time per week during treatment periods follow by weekly measurements (or monthly for long term survivors) post treatment. Also recorded were the weight and overt health of the animal.

Gamma scintigraphy was performed using a Picker300 SX gamma camera interfaced to an Odyssey imaging processor. The gamma images of the rats injected with Lu-177 radiolabeled peptides were obtained with a large field of view camera

fitted with a general purpose medium-energy collimator with the peak energy centered at 208 keV. All rats were imaged in the prone position.

Results

Our previous evaluations of ^{153}Sm-DTPA'-Y^3-Octreotate (CMDTPA) and ^{177}Lu-iDTPA-Y^3-Octreotate established the radiotherapeutic potential of a medium energy ß$^-$ emitting radionuclide in a rat tumor model expressing somatostatin subtype-2 receptors (4) The short half-life and low specific activity of Sm-153 were found, however, to be major limiting factors for clinical use. The availability of Lu-177 overcomes these limitations, and when used with DOTA-linked peptides eliminates concerns regarding chelate stability.

Table I. Table of Competitive Binding of ^{111}In-DTPA-Tyr^3-octreotate to CA20948 Tumor Membranes in the Presence of Unlabeled Somatostatin Analogues. (IC_{50} values are in nM)

Peptide	IC_{50} (nM)
DTPA-Octreotide	2.5
DTPA-Tyr^3-octreotate	1.4
CMDTPA-octreotate	2.8
Tyr^3-octreotate	0.5
DOTA-Tyr^3-octreotate	4.0

In Vitro Assays

The CA20948 pancreatic acinar tumor line expresses high levels of the sst_2 receptor (3). We have used membrane preparations from this tumor line in an in vitro assay to screen a number of somatostatin analogs with chemical modifications made in both the peptide and chelate segment of the molecule. Table I shows the data for several compounds analyzed using this assay. The estimated IC_{50} for the DOTA-

Tyr^3-octreotate and the DOTA-Tyr^3-Octreotide compounds is approximately 1 nM. A small loss of binding affinity occurs as the result of the addition of the DOTA chelate moiety to the Tyr^3-octreotide or Tyr^3-octreotate peptide (IC_{50} = 0.22 and 4.0 nM respectively).

Biodistribution Studies

The biodistribution properties of ^{177}Lu-DOTA-Tyr^3-octreotide (1, 4 and 24 hour study) and ^{177}Lu-DOTA-Tyr^3-octreotate (1, 4, 12, 24, 48, 72 hour study) were determined in CA20948 tumor bearing Lewis rats (Figures 2 and 3, Tables 2-5). These data show that the octreotate peptide has substantially greater uptake and retention in somatostatin receptor positive tumors than the corresponding octreotide derivative. Significantly higher uptake is also observed in the pancreas, a somatostatin receptor positive tissue. Retention of ^{177}Lu-DOTA-Y^3-Octreotate in non-target tissues was reduced. Kidney retention of the octreotate derivative, for example, was approximately 41% less than the retention of the octreotide counterpart at the 24 hour time point (1.29 versus 2.19% ID/gram tissue). Total excretion at 24 hours was greater for the Octreotide peptide (86% vs. 73%), but most of the difference can be accounted for by the increased uptake of octreotate in the tumor and pancreas. Total excreted, plus pancreas and tumor retained radioactivity at 24 hours post injection was 90% for octreotide and 84% for octreotate. Figure 3B are scintigrams of animals injected with ^{177}Lu-DOTA-Tyr^3-octreotate at the indicated time points of the biodistribution.

Table 2. Biodistribution of ^{177}Lu-DOTA-Y^{3}-Octreotide in CA20948 Tumor Bearing Lewis Rats
(Percent Injected Dose / gram ± SE)

Tissue	1 hour	4 hours	24 hours
Blood	0.113±0.012	0.004±0.001	0.001±0.000
Kidney	2.413±0.018	2.324±0.049	2.186±0.115
Pancreas	2.664±0.028	2.400±0.152	1.463±0.072
Tumor	1.401±0.035	1.307±0.063	0.862±0.050

Table 3. Biodistribution of ^{177}Lu-DOTA-Y^{3}-Octreotide in CA20948 Tumor Lewis Bearing Rats
(Percent Injected Dose / organ ± SE)

Tissue	1 hour	4 hours	24 hours
Blood	1.417±0.119	0.052±0.014	0.013±0.001
Liver	0.893±0.042	0.697±0.052	0.551±0.024
Kidneys	5.328±0.046	5.005±0.224	4.814±0.265
Muscle	2.398±0.141	0.387±0.024	0.313±0.070
Pancreas	2.811±0.163	2.750±0.134	1.405±0.090
Adrenals	0.391±0.014	0.271±0.016	0.261±0.009
Stomach	0.740±0.067	0.814±0.233	0.519±0.191
Bone	1.677±0.030	1.005±0.040	0.918±0.050
Tumor	3.488±0.486	5.824±1.659	2.844±0.332
Urine			78.62±1.721
Feces			7.217±1.689
Total Excreted			85.84±2.113
Total Recovered			97.49±2.420

The clearance rates determined for kidney, pancreas, and tumor tissue all displayed biphasic patterns. In all cases, a large portion of the retained radiolabel had a clearance half-life greater than 10 days. In tumor tissue, for example, 59% of the radiolabel cleared with a half-life of 14 hours. The remaining radioactivity cleared with a half-life greater than 27 days.

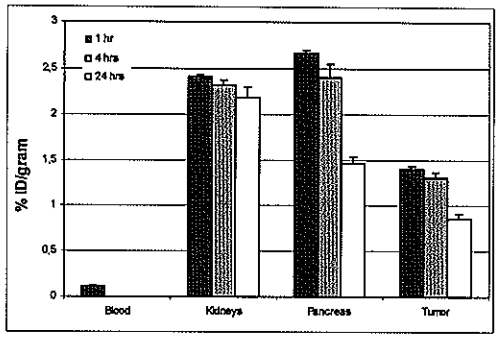

Figure 2: Biodistribution of ^{177}Lu-DOTA-Tyr^3-octreotide in CA20948 tumor bearing rats (n = 3 per time point). Animals were sacrificed at indicated time points and selected tissues assayed for radioactivity.

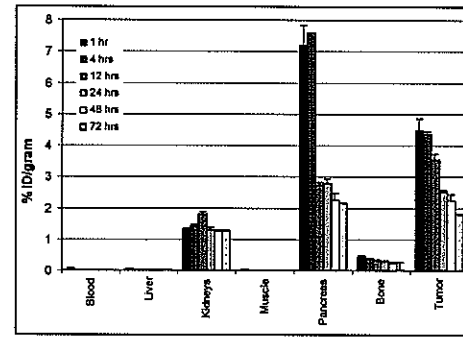

Figure 3A: Biodistribution of ^{177}Lu-DOTA-Tyr^3-octreotide in CA20948 tumor bearing rats (n = 3 per time point). Animals were sacrificed at indicated time points and selected tissues assayed for radioactivity.

In vivo blocking studies demonstrated that uptake and retention in the sst_2 positive tissues of the tumor, pancreas, adrenals, bone and stomach were all blocked by 90% or greater by with a co-injection of cold peptide (data not shown). These blocking studies confirm the receptor mediated specificity of Octreotate for the sst_2 subtype.

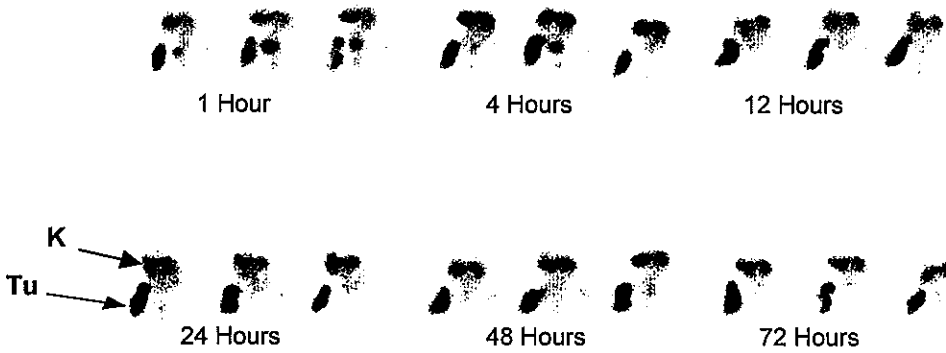

Figure 3B: Scintigrams from biodistribution of ^{177}Lu-DOTA-Tyr^3-octreotate in CA20948 tumor bearing rats at indicated time points. Location of (**K**) kidneys and (**Tu**) tumor noted by arrows.

Radiotherapy Studies: Single Dose Study

Radiotherapy studies were performed using CA20948 tumor bearing Lewis rats at 14 days post implant (average tumor volume ~1.5 cm^3). In a dose range study (Fig. 4),

rats were injected with a single dose of either 1.0, 2.5, or 5.0 mCi of ^{177}Lu-DOTA-Y^3-Octreotate (n=6 per group). In all cases, there was a rapid decrease in tumor volume 1-3 weeks post treatment. Animals receiving a 5.0 mCi dose showed the most rapid regression in tumor volume (Fig 4C and D). At 14 days post treatment, tumors in all treated animals regressed to less than 5% of original tumor volume with several animals (2.5 and 5.0 mCi doses) showing no evidence of palpable masses. Average tumor growth in untreated animals increased over 750% of original tumor volume over the same time span (Fig. 4A). At approximately 30 days post treatment, all animals receiving a 1 mCi dose showed tumor regrowth (Fig. 4B). In both the 2.5 and 5 mCi dose groups, approximately 50% of the animals remained tumor free over 5 months. At eight months 50% of the 5 mCi treatment group remained tumor free (Figs. 4C and 4D).

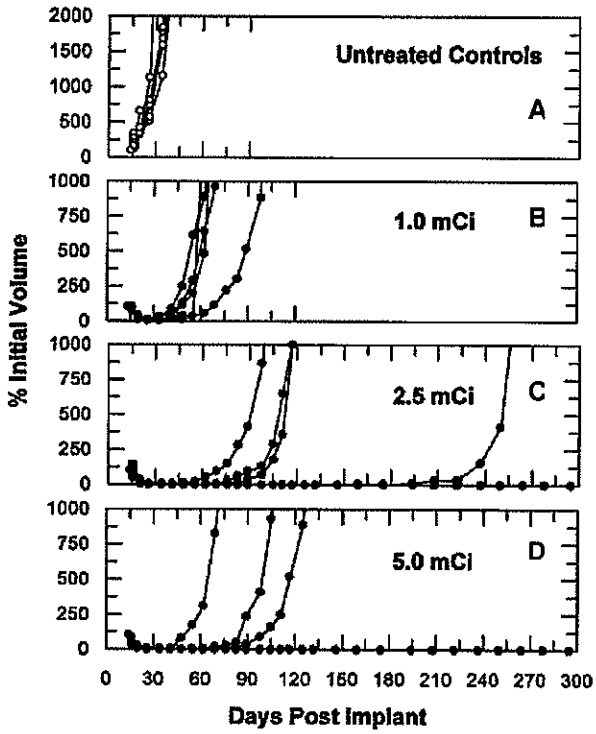

Figure 4:

Radiotherapeutic effect of single dose administration of ^{177}Lu-DOTA-Tyr^3-octreotate in CA20948 tumor bearing rats. **A**. untreated control group, **B**: 1.0mCi; **C**: 2.5mCi; **D**: 5.0mCi

Multiple Dose Study

In a second study (Fig. 5), tumor-bearing rats received multiple doses of ^{177}Lu-DOTA-Y^3-Octreotate at 30-day intervals (3 doses total of 2.5 and 5 mCi/dose, n=8

per group). Tumor regression in both groups was similar to that observed in the single dose study above. Cumulative dosing was found to be beneficial as there was a progressive increase in the number of tumor free animals after each treatment. In the 3X2.5 mCi treatment group, 75% of the treated rats were tumor free at 3.5 months post tumor implant with 25% of those animals subsequently showing tumor regrowth by the 7th month (Fig. 5C; 50% tumor free at 8 months post implant). Complete tumor regression occurred in 50% of the rats in the 5 mCi treatment group after the first dose. All animals were tumor free after the third 5mCi dose (Fig. 5D) and remained so up to 12 months post implant. Tumor growth in rats that received a 1 mg/kg blocking dose of cold peptide in addition to a single 2.5 mCi dose was identical to the growth observed in untreated animals (Fig. 5A and 5 B), showing that the radiotherapeutic effect is indeed receptor mediated.

Long Term Survival

Long-term survival was observed in animals treated with single or multiple doses of 2.5 or 5.0 mCi of ^{177}Lu-DOTA-Y^{3}-Octreotate. At the highest multiple dose regimen (3 x 5 mCi) abrupt weight loss occurred at approximately 12 months post final dose of treatment. All animals in this group died within a 4-month time frame. Post mortem examination of these rats indicated that most suffered from renal disease, characterized by the presence of fibrous nodules. In most cases, nodules were viewed as small, discolored lesions on the surface of the kidney, although in some cases, multiple large masses were found, suggesting a possibly malignant state (Long term toxicity MS in progress).

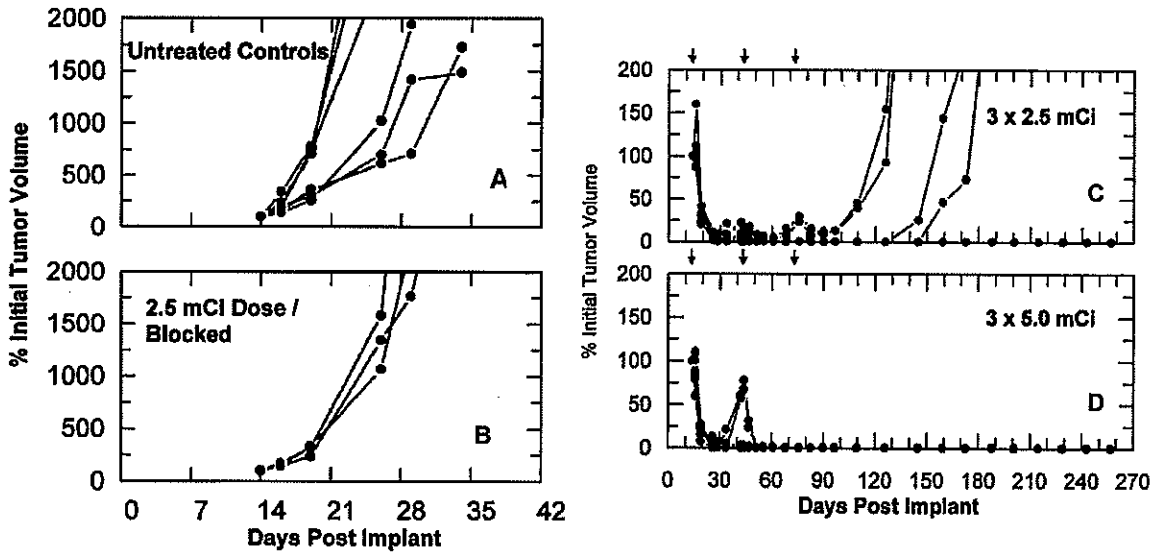

Figure 5: Radiotherapeutic effect of multiple dose administrations of ^{177}Lu-DOTA-Tyr^3-octreotate in CA20948 tumor bearing rats. A: untreated controls; B: rats received 2.5mCi of radiolabeled peptide plus 1.0mg/kg of unlabeled peptide; C: rats (n = 8) received 2.5mCi of radiolabeled peptide x 3 doses; D: rats (n = 8) received 5.0mCi radiolabeled peptide x 3 doses. Dosing indicated by arrows.

No tumor regrowth at the initial site of tumor implant was observed in these animals. No significant premature weight loss was observed in the long-term survivors of the 3 x 2.5 mCi or with any of the single dose treatment groups. Significant weight loss (preceding death) that occurred in these latter treatment groups is within the life expectancy of *ad lib* fed male Lewis rats determined from previous reports (12, 13). Based on these studies, we estimate a normal life span for the male Lewis rats in our facility to be 26 months ± 5 months. Comparisons of the survival for all treatment groups showed that only the long-term survivors of the highest dose treatment group (3 x 5.0 mCi) had an attenuated life span (approximately 65% of normal).

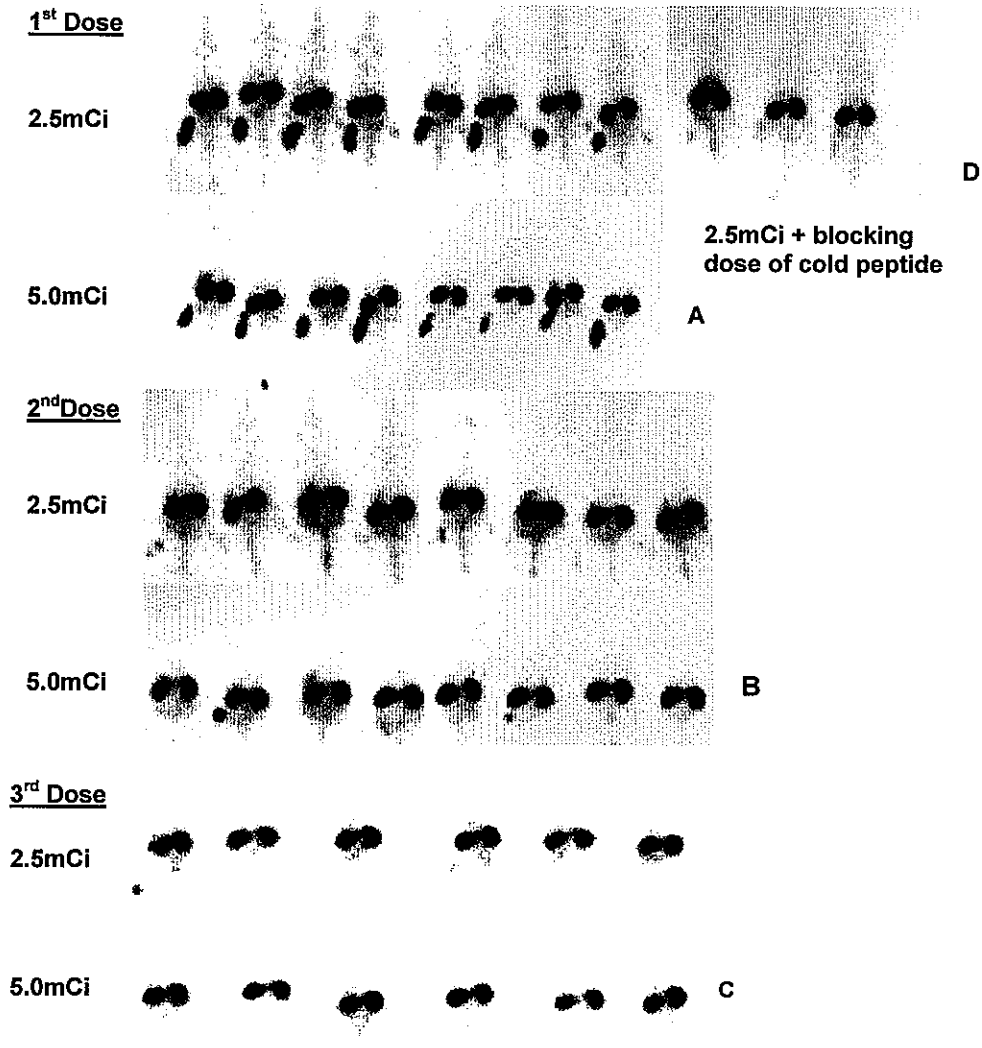

Figure 6: Scintigraphy performed at 24 hours post injection of radiolabeled peptide. Scintigrams represent multiple doses at either 2.5mCi (top rows) or 5.0mCi (bottom rows) of ^{177}Lu-DOTA-Tyr^3-octreotate administered at 30 day intervals. **A**: 1st dose; **B**: after 2nd dose, **C**: after 3rd dose; **D**: animals received 2.5mCi plus 1.0mg/kg cold peptide.

Table 4: Biodistribution of ^{177}Lu-DOTA-Y^{3}-Octreotate in CA20948 Tumor Bearing Lewis Rats at 1, 4, 12, 24, 48 and 72 Hours Post Injection (Percent Injected Dose/gram ± SE)

Tissue	1 hour	4 hours	12 hours
Blood	0.060±0.001	0.005±0.000	0.003±0.000
Liver	0.048±0.003	0.039±0.001	0.038±0.001
Kidneys	1.313±0.040	1.424±0.062	1.801±0.077
Muscle	0.015±0.002	0.004±0.001	0.003±0.000
Pancreas	7.184±0.665	7.591±0.010	2.726±0.090
Bone	0.457±0.023	0.393±0.003	0.334±0.009
Tumor	4.483±0.387	4.367±0.090	3.553±0.178

Tissue	24 hours	48 hours	72 hours
Blood	0.002±0.000	0.001±0.000	0.001±0.000
Liver	0.032±0.001	0.026±0.002	0.029±0.003
Kidneys	1.293±0.063	1.267±0.031	1.251±0.050
Muscle	0.002±0.000	0.002±0.000	0.002±0.000
Pancreas	2.779±0.136	2.267±0.214	2.148±0.022
Bone	0.295±0.014	0.253±0.021	0.248±0.015
Tumor	2.521±0.052	2.244±0.196	1.792±0.042

Table 5. Biodistribution of ^{177}Lu-DOTA-Y^{3}-Octreotate in CA20948 Tumor Bearing Lewis Rats at 1, 4, 12, 24, 48 and 72 Hours Post Injection (Percent Injected Dose/organ ± SE)

Tissue	1 hour	4 hours	12 hours
Blood	0.777±0.039	0.059±0.001	0.030±0.004
Liver	0.500±0.021	0.358±0.015	0.348±0.008
Kidneys	2.606±0.018	2.706±0.077	3.609±0.099
Muscle	1.615±0.190	0.394±0.077	0.311±0.001
Pancreas	6.415±0.403	7.964±0.272	2.454±0.144
Bone	6.547±0.199	5.352±0.099	4.417±0.125
Adrenals	0.623±0.049	0.580±0.010	0.457±0.030
Tumor	11.88±0.944	11.21±1.645	13.78±0.720

Tissue	24 hours	48 hours	72 hours
Blood	0.020±0.004	0.012±0.000	0.012±0.000
Liver	0.335±0.008	0.304±0.010	0.343±0.024
Kidneys	2.778±0.123	2.672±0.139	2.564±0.088
Muscle	0.258±0.037	0.218±0.006	0.219±0.005
Pancreas	2.666±0.140	2.126±0.123	2.207±0.171
Bone	4.163±0.194	3.510±0.273	3.468±0.260
Adrenals	0.411±0.013	0.330±0.019	0.277±0.012
Tumor	8.373±1.137	7.740±0.993	5.847±1.250
Urine	66.61±0.445	66.08±0.445	70.17±1.384
Feces	6.225±0.758	10.19±0.143	12.16±0.731
Excreted	72.83±1.007	76.80±0.433	82.32±1.544
Recovered	92.71±0.606	94.65±0.930	98.15±0.671

Figure 7: Survival graph for rats treated with ^{177}Lu-DOTA-Y^3-octreotate in the multidose regimen of 3 x 2.5mCi and 3 x 5.0mCi per rat at 30 day intervals compared to negative control (untreated) animals. Days are post implant of tumor.

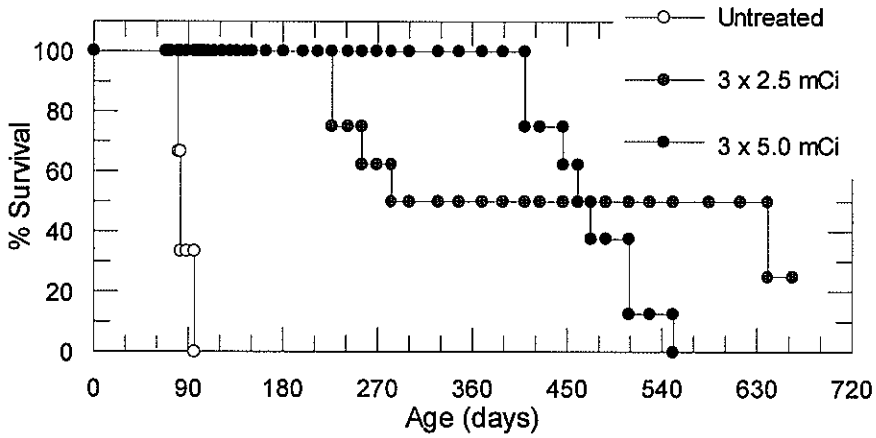

Conclusions

Biodistribution studies demonstrate that ^{177}Lu-DOTA-Y^3-Octreotate has substantially higher tumor uptake and retention than the corresponding Octreotide derivative. Further, uptake and retention of the former compound into non-target organs, such as kidneys, is less than that observed for ^{177}Lu-DOTA-Y^3-Octreotide. Considerably higher uptake of the octreotate compound is observed in the pancreas. The clinical relevance of this observation is not presently known. No apparent pancreatic uptake was observed in baboons imaged by positron emission tomography (PET) with an analogous Tyr^3-Octreotate derivative labeled with ^{64}Cu, a positron-emitting radioisotope (^{64}Cu-TETA-Tyr^3-Octreotate). Current clinical studies suggest that a similar situation exists in humans. Nevertheless, somatostatin receptors are known to be expressed in pancreatic islet cells, and it is also known that there are different subtype expression levels in rodent and human pancreas, although sst_2 receptors are present in both. In any case, it is reasonable to expect that the higher tumor

localization and reduced kidney retention achieved with ^{177}Lu-DOTA-Tyr^3-octreotate will enhance the selective targeting of somatostatin receptor rich tumors while minimizing the radiation dose delivered to kidneys. Ample evidence exists in the literature to support the reduction of kidney uptake by the administration of amino acid infusion cocktails. Up to a 50% reduction has been reported, and current clinical trials evaluating ^{90}Y-DOTA-Tyr^3-Octreotide have employed this procedure to minimize long term renal toxicity.

Long-term survival of tumor-implanted rats is observed after treatment with single or multiple doses of ^{177}Lu-DOTA-Y^3-Octreotate. The results are comparable or superior to studies, which have used other radiolabeled somatostatin analogs (2-6). None of the previous studies, however, have reported survival data beyond 8 months.

Some apparent radiotoxic effects are observed at the highest multiple dose regimens at approximately 12 months post treatment. Renal lesions (nodules and large neoplasms) were observed during macroscopic inspection of the kidneys in the multiple dose treatment group, indicating that the kidney is the critical organ for toxicity.

The current results demonstrate the therapeutic potential of ^{177}Lu-DOTA-Y^3-Octreotate. Further studies to determine the value of this radiopharmaceutical for the treatment of human cancers over expressing somatostatin subtype-2 receptors are in progress.

REFERENCES

1. Otte A, Jermann E, Behe M, Goetze M, Bucher HC, Roser HW, Heppeler A, Mueller-Brand, Macke HR. DOTATOC: a powerful new tool for receptor-mediated radionuclide therapy. *Eur J Nucl Med* 1997; 24:792-795.

2. Stolz B, Weckecker G, Smith-Jones P, Rainer A, Raulf F, Bruns C. The somatostatin receptor-targeted radiotherapeutic [^{90}Y-DOTA-dPhe1,Tyr^{3}]octreotide (^{90}Y-SMT 487) eradicates experimental rat pancreatic CA 20948 tumors. *Eur J Nucl Med* 1998: 25:668-674.

3. Zamora PO, Bender H, Gulhke S, Marek MJ, Knapp FF Jr, Rhodes BA, Biersack HJ. Pre-clinical experience with Re-188-RC-160, a radiolabeled somatostatin analog for use in peptide-targeted radiotherapy. *Anticancer Res* 1997; 17(3B):1803-1808.

4. Bugaj JE, Erion JL, Schmidt MA, Wilhelm RR, Achilefu SI, Srinivasan A. Biodistribution and radiotherapy studies using samarium-153 and lutetium-177 DTPA conjugates of Y3-Octreotate. *J Nucl Med* 1999; 40(Supp):Abstract 996.

5. Erion JL, Bugaj JE, Schmidt MA, Wilhelm RR, Srinivasan A. High Radiotherapeutic Efficacy of [^{177} Lu]-DOTA-Y^{3}-Octreotate in a Rat Tumor Model. *J Nucl Med* 1999; 40(Supp):223P.

6. Anderson CJ, Jones LA, Bass LA, Sherman EL, McCarthy DW, Cutler PD, Lanahan MV, Cristel ME, Lewis JS, Schwarz SW. Radiotherapy, toxicity and dosimetry of copper-64-TETA-octreotide in tumor-bearing rats. *J Nucl Med* 1998; 39:1944-1951.

7. Erion JL, Srinivasan A, Schmidt MA, Wilhelm R, Bugaj JE. Radiolabeled ligand octreotate conjugates: evaluation of potential diagnostic and therapeutic radiopharmaceutical agents targeted to somatostatin receptors. *J Nucl Med* 1997; 38(Supp): 813.

8. de Jong M, Breeman WA, Bakker WH, Kooij PP, Bernard BF, Hofland LJ, Visser TJ, Srinivasan A, Schmidt MA, Erion JL, Bugaj JE, Macke HR, Krenning EP. Comparision of ^{111}In-labeled somatostatin analogues for tumor scintigraphy and radionuclide therapy. *Cancer Res* 1998; 58:437-441.

9. de Jong M, Bakker WH, Krenning EP, Breeman WAP, Van der Pluijm ME, Bernard BF, Visser TJ, Jermann E, Béhé M, Powell P, Mäcke HR. Yttrium-90 and indium-111 labeling, receptor binding and biodistribution of [DOTA, d-Phe1, Try^{3}]octreotide, a promising somatostatin analogue for radionuclide therapy. *Eur J Nucl Med* 1997; 24:368-371.

10. Reubi JC, Laissue J, Krenning E, Lamberts SW. Somatostatin receptors in human cancer: incidence, characteristics, functional correlates and clinical implications. *J Steroid Biochem Mol Biol* 1992; 43:27-35.

11. Reubi JC, Schaer JC, Waser B, Mengod G. Expression and localization of somatostatin receptor SSTR1, SSTR2 and SSTR3 messenger RNAs in primary human tumors using in situ hybridization. *Cancer Res* 1994; 54:3455-3459.

12. Baum A, Pohlmeyer G, Rapp KG, Deerberg F. Lewis rats of the inbred strain LEW/Han: life expectancy, spectrum and incidence of spontaneous neoplasms. *Exp Toxicol Pathol* 1995, 47:11-8.

13. Thurman JD, Bucci TJ, Hart RW, Turturro A. Survival, body weight, and spontaneous neoplasms in ad libitum-fed and food-restricted Fischer-344 rats. *Toxicol Pathol* 1994, 22:1-9.

CHAPTER 4B

[^{177}LU-DOTA^{0}, TYR^{3}] OCTREOTATE FOR SOMATOSTATIN RECEPTOR-TARGETED RADIONUCLIDE THERAPY

International Journal of Cancer, 92, 628-633 (2001)

[^{177}LU-DOTA^0,TYR^3]OCTREOTATE FOR SOMATOSTATIN RECEPTOR-TARGETED RADIONUCLIDE THERAPY

Marion DE JONG[1]*, Wout A.P. BREEMAN[1], Bert F. BERNARD[1], Willem H. BAKKER[1], Michael SCHAAR[1], Arthur VAN GAMEREN[1], Joe E. BUGAJ[2], Jack ERION[2], Michelle SCHMIDT[2], Ananth SRINIVASAN[2] and Eric P. KRENNING[1,2]

[1]*Department of Nuclear Medicine, University Hospital and Erasmus University Rotterdam, Rotterdam, The Netherlands*
[2]*Department of Internal Medicine, University Hospital and Erasmus University Rotterdam, Rotterdam, The Netherlands*
[3]*Mallinckrodt Medical Inc., St. Louis, MO, USA*

Receptor-targeted scintigraphy using radiolabeled somatostatin analogs such as octreotate is being used with great success to demonstrate the *in vivo* presence of somatostatin receptors on various tumors. A new and promising application for these analogs is radionuclide therapy. Radionuclides suitable for this application include the Auger electron-emitter ^{111}In and the β-emitters ^{90}Y (high energy) and ^{177}Lu (low energy). We investigated [DOTA^0,Tyr^3]octreotate, labeled with the lanthanide ^{177}Lu, in biodistribution and radionuclide therapy experiments using male Lewis rats bearing the somatostatin receptor-positive rat CA20948 pancreatic tumor. Biodistribution studies in Lewis rats showed the highest uptake in the rat pancreatic CA20948 tumor and sst$_2$-positive organs, which include the adrenals, pituitary and pancreas, of [^{177}Lu-DOTA^0,Tyr^3]octreotate in comparison with ^{86}Y- and ^{111}In-labeled analogs. Kidney uptake of [^{177}Lu-DOTA^0,Tyr^3]octreotate could be reduced by approximately 40% by co-injection of 400 mg/kg D-lysine. In radionuclide therapy studies, a 100% cure rate was achieved in the groups of rats bearing small (≤1 cm^2) CA20948 tumors after 2 doses of 277.5 MBq or after a single dose of 555 MBq [^{177}Lu-DOTA^0,Tyr^3]octreotate. A cure rate of 75% was achieved after a single administration of 277.5 MBq. In rats bearing larger (≥1 cm^2) tumors, 40% and 50% cure rates were achieved in the groups that received 1 or 2 277.5 MBq injections of [^{177}Lu-DOTA^0,Tyr^3]octreotate, respectively. After therapy with [^{177}Lu-DOTA^0,Tyr^3]octreotide in rats bearing small tumors, these data were 40% cure after 1 injection with 277.5 MBq and 60% cure after 2 repeated injections. In conclusion, [^{177}Lu-DOTA^0,Tyr^3]octreotate has demonstrated excellent results in radionuclide therapy studies in rats, especially in animals bearing smaller tumors. This candidate molecule shows great promise for radionuclide therapy in patients with sst$_2$-expressing tumors.

Key words: *^{177}Lu; octreotate; radionucleitide therapy; receptor; tumour*

[DTPA^0]octreotide, consisting of the stable somatostatin analog octreotide and the chelator DTPA (diethylenetriaminepentaacetic acid), enabling radiolabeling with a radiometal such as ^{111}In, was synthesized for scintigraphy of receptor-positive lesions, mostly of neuro-endocrine origin.[1,2] A new somatostatin analog is Tyr^3-octreotate, where the alcohol Thr(ol) at the C-terminus is replaced with the natural amino acid Thr (Fig. 1). This analog was found to have a very high affinity for the somatostatin receptor subtype 2 (sst$_2$) and showed the highest uptake in the rat pancreatic CA20948 tumor in a biodistribution study in rats using different ^{111}In-labeled somatostatin analogs.[3]

A new and fascinating application of radiolabeled peptides is radionuclide therapy. Studies with an Auger (^{111}In) or a high-energy β$^-$ particle-emitter (^{90}Y) complexed to an octreotide analog have been reported. Promising results with regard to tumor growth inhibition were shown in preclinical studies and in patient studies using [^{111}In-DTPA^0]octreotide[1,4,5] or [^{90}Y-DOTA^0,Tyr^3]octreotide.[3,6–10]

In our study, we investigated the therapeutic potential of the low energy β$^-$ particle-emitter ^{177}Lu. For this purpose, Tyr^3-octreotate has been derivatized with the DOTA chelator (tetraazacyclododecanetetraacetic acid, Fig. 1), enabling stable radiolabeling with ^{90}Y, ^{177}Lu and ^{111}In. Here we describe the biodistribution of [^{177}Lu-DOTA^0,Tyr^3]octreotate in CA20948 pancreatic tumor-bearing rats, in comparison with the ^{111}In- and ^{88}Y-labeled peptide. The reactor product ^{177}Lu was chosen for radionuclide therapy because it emits low-energy β$^-$ particles (497 keV, 78%) with a long half-life (6.7 days). It also emits gamma radiation (208 keV, 11%) with an energy suitable for scintigraphy and dosimetry studies using this same compound. Also, *ex vivo* autoradiography was performed and possible reduction of kidney uptake of [^{177}Lu-DOTA^0,Tyr^3]octreotate using 400 mg/kg D-lysine was investigated. Finally, we started radionuclide therapy studies with [^{177}Lu-DOTA^0,Tyr^3]octreotate using the rat pancreatic CA20948 tumor model. Based on previous reports of the efficacy of [^{177}Lu-DOTA^0,Tyr^3]octreotate to eradicate rat tumors,[11] we compared the therapeutic effects of [^{177}Lu-DOTA^0,Tyr^3]octreotate and [^{177}Lu-DOTA^0,Tyr^3]octreotide. Additionally, we investigated the therapeutic efficacy of [^{177}Lu-DOTA^0,Tyr^3]octreotate as a function of tumor size at the start of therapy.

MATERIAL AND METHODS

Compounds

$^{111}InCl_3$ was from Mallinckrodt Medical BV (Petten, The Netherlands). $^{88}YCl_3$ was from IDB (Baarle Nassau, The Netherlands). ^{177}Lu was from MURR (Columbia, MO). [DOTA^0,Tyr^3]octreotide (DOTA = tetraazacyclododecanetetraacetic acid) was synthesized as reported.[12] [DOTA^0,Tyr^3]octreotate was synthesized by AS. Octreotide was supplied by Novartis (Basel, Switzerland). ^{177}Lu-labeling of [DOTA^0,Tyr^3]octreotide was performed as previously described for [^{90}Y-DOTA^0,Tyr^3]octreotide.[13] D-lysine (as monochloride salt) was obtained from Sigma Chemical (St. Louis, MO). TissueTek was from Sakura (Zoeterwoude, The Netherlands).

Autoradiography

The presence of radioactivity in tumor and normal tissues after injection of [^{177}Lu-DOTA^0,Tyr^3]octreotate in rat pancreatic CA20948 tumor-bearing rats was investigated by *ex vivo* autoradiography. Tumor and normal organs were isolated 24 hr post-injection, embedded in TissueTek and processed for cryosectioning. Tissue sections (10 μm) were mounted on glass slides and stored at −20°C for at least 1 day to improve adhesion of the tissue to the slide. From each organ and the tumor, several slides were used to make autoradiographs, whereas the adjacent sections were hematoxilin-eosin stained. The sections were exposed to phosphor imaging screens (Packard Instruments, Meriden, CT) for 1 day in X-ray cassettes. The screens were analyzed using a Cyclone phos-

*Correspondence to: Department of Nuclear Medicine, University Hospital Rotterdam, 3015 GD Rotterdam, The Netherlands.
Fax: +31-10-463-5997. E-mail:dejong@nuge.azr.nl

Received 3 September 2000; Revised 22 December 2000; Accepted 15 January 2001

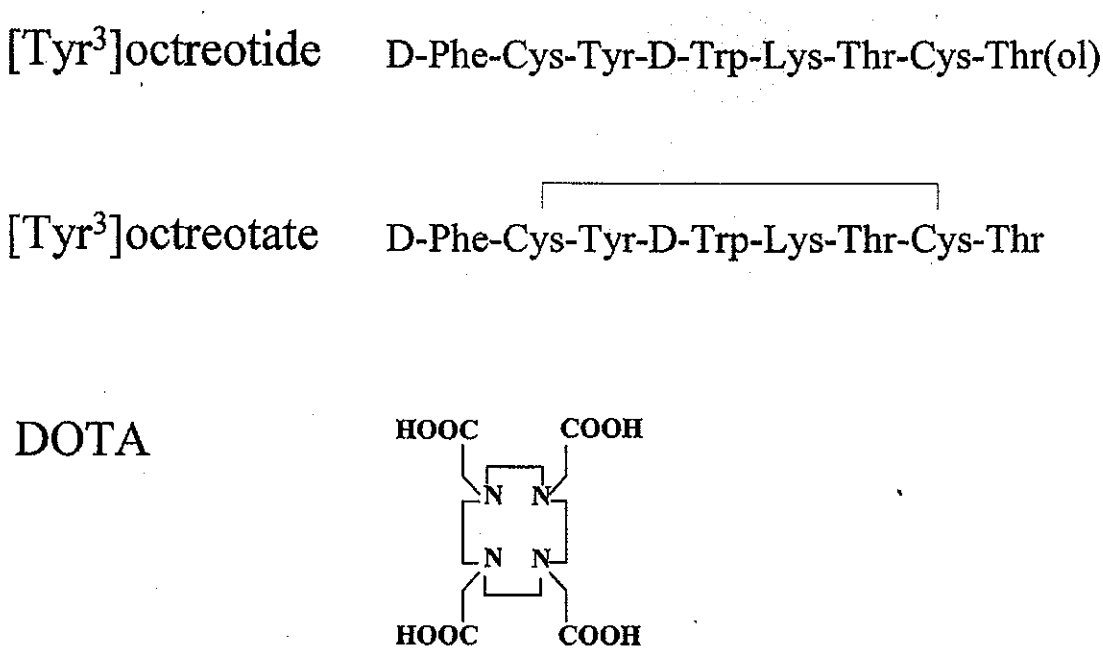

FIGURE 1 – Structures of [Tyr^3]octreotide, [Tyr^3]octreotate and DOTA.

phor imager and a computer-assisted OptiQuant 03.00 image processing system (Packard Instruments, Groningen, The Netherlands).

In vivo *biodistribution and reduction of kidney uptake*

Animal experiments were performed in compliance with regulations of our institution and with generally accepted guidelines governing such work. Male Lewis rats (Harlan, The Netherlands; 200–300 g), bearing the rat CA20948 pancreatic tumor in their flank, were used in the experiments. Rats were injected under ether anesthesia with 3 MBq (0.5 μg) ^{111}In-, ^{88}Y- or ^{177}Lu-labeled [DOTA^0,Tyr^3]octreotate in 200 μl saline into the dorsal vein of the penis. To determine nonspecific binding of the radiopharmaceutical, a separate group of rats was co-injected with 0.5 mg octreotide. For reduction of kidney uptake, D-lysine was given intravenously in a dose of 400 mg/kg, as a single co-injection with the radiolabeled peptide. At the indicated time points (see Figures), rats were sacrificed under ether anesthesia. Organs and blood were collected and the radioactivity in these samples was determined using an LKB-1282-Compu-gamma-system.

For all groups: $n \geq 4$, data are expressed as mean ± SD.

Statistical analysis was performed using Student's *t*-test or analysis of variance.

Acute toxicity study of unlabeled peptide

On experimental day 0, 4 treatment groups of 5 Wistar rats and of 5 Balb-c mice were injected intravenously with saline, and 10×, 100× and 1,000× the human dose of unlabeled peptide (15 μg/75 kg body weight) of [DOTA^0,Tyr^3]octreotate. All test solutions were injected through the penile vein at a rate not exceeding 1 ml/min. During 24 hr after injection, the animals were monitored for changes in behavior (eating, sleeping, motion, posture). All rats were euthanized 24 hr after injection by ether narcosis and subjected to macroscopic post-mortem examination. After external examination, the chest and abdomen were opened by a midline incision. Thoracic and abdominal viscera were examined for abnormalities and aberrations were recorded. Organs were investigated macroscopically (*e.g.*, for hemorrhage). Liver, kidneys, stomach, spleen, lungs and intestines were isolated and fixed in 4% buffered formalin. The organs were sectioned, stained and evaluated by light microscopy.

Radionuclide therapy experiments using [^{177}Lu-DOTA^0,Tyr^3]octreotate

Male Lewis rats bearing pancreatic CA20948 flank tumors were injected with [^{177}Lu-DOTA^0,Tyr^3]octreotate or [^{177}Lu-DOTA^0,Tyr^3]octreotide into the dorsal vein of the penis. Different therapeutic groups ($n = 6–10$) received either a single intravenous injection or 2 injections (1 week apart) of 277.5 MBq or a single injection of 555 MBq [^{177}Lu-DOTA^0,Tyr^3]octreotate or [^{177}Lu-DOTA^0,Tyr^3]octreotide as indicated. Specific activity of [^{177}Lu-DOTA^0,Tyr^3]octreotate and [^{177}Lu-DOTA^0,Tyr^3]octreotide was 37 MBq/1.6–1.8 μg peptide. The control group did not receive radiolabeled peptide.

Tumor growth, animal condition and body weight were determined at regular intervals. At a more progressed stage of the CA20948 tumor, central necrosis may occur with rupture to the surface. Besides loss of more than 10% of original body weight and tumor growth beyond about 20 cm^2, tumor rupture was an indication to sacrifice the rats.

Responses were defined according to the criteria of the South-West Oncology Group (SWOG): partial response (PR) as at least 50% reduction of the product of the 2 largest perpendicular tumor diameters vs. pretreatment values, whereas complete response (CR) was defined as 100% reduction of this product, lasting for at least 150 days.

GraphPad Prism (GraphPad Prism Software, San Diego, CA) was used to plot survival curves for the different groups.

Dosimetry

The dose to the rat tumors in Gy was calculated using the tumor uptake data from the biodistribution experiments and assuming uniform distribution of radioactivity in a spherical mass. Tumor-to-tumor dose was taken into account only and S-values (mean absorbed dose per unit cumulated activity) for ^{177}Lu in spheres of 1 and 10 g were used as described.[14]

RESULTS

Autoradiography

Figure 2 presents *ex vivo* autoradiographs of some rat organs and CA20948 tumor, showing that the energies emitted by ^{177}Lu are suitable for autoradiography. Organs and tumor were isolated 24 hr post-injection of [^{177}Lu-DOTA^0,Tyr^3]octreotate. Adrenals, pituitary, stomach and CA20948 tumor all express sst_2 (see also blocking experiment in Fig. 3). In the adrenal glands, radioactivity is mostly localized in the zona glomerulosa, in the pituitary it is found only in the frontal lobe, and in the stomach radioactivity is found in the mucosa. In the CA20948 tumor, a nearly homogenous uptake is observed. Though the kidneys of the rat are sst_2-negative, a high amount of radioactivity is found in these organs because of reabsorption of the peptide in the cells of the proximal tubules after glomerular filtration The highest amount of radioactivity is found in the cortex of the kidneys, whereas much less radioactivity is found in the medulla.

In vivo *biodistribution and reduction of kidney uptake*

Figure 3 presents radioactivity in rat sst_2-positive organs: pancreas, adrenals, pituitary and CA20948 rat pancreatic tumor, 4, 24 and 48 hr after injection of ^{111}In-, ^{88}Y- or ^{177}Lu-labeled [DOTA^0,Tyr^3]octreotate. Uptake in the sst_2-expressing organs and tumor at these time points was the highest for [^{177}Lu-DOTA^0,Tyr^3]octreotate, whereas kidney uptake was lower for ^{177}Lu- and ^{88}Y- than for ^{111}In-labeled [DOTA^0,Tyr^3]octreotate. Co-injection of an excess of cold octreotide, to block the sst_2, reduced uptake in the sst_2-positive organs and tumor to a large extent as measured at 24 hr post-injection, as shown in the fourth group of bars in each panel of Figure 3. This indicates that uptake of the radiolabeled peptides in these rat sst_2-positive targets represented specific binding to the octreotide (sst_2) receptors. Further data obtained for [^{177}Lu-DOTA^0,Tyr^3]octreotate 24 hr post-injection are shown in Table I.

D-lysine (400 mg/kg), co-injected with [^{177}Lu-DOTA^0,Tyr^3]-octreotate, reduced kidney uptake from 1.37 ± 0.16% of the injected dose per *g* kidney in the control rats to 0.7 ± 0.13% of the injected dose per *g* kidney ($p<0.001$). No significant effect of D-lysine was found on [^{177}Lu-DOTA^0,Tyr^3]octreotate clearance from blood and uptake in the other sst_2-positive organs and tumor (not shown).

Acute toxicity study

No abnormalities were found with regard to animal behavior during the 24 hr period after injection. No macroscopic pathology was observed. Microscopic examination of representative tissue sections from rats treated with [DOTA^0,Tyr^3]octreotate did not reveal any abnormalities that could be attributed to the treatment.

In vivo *radionuclide therapy experiments using ^{177}Lu-labeled somatostatin analogs*

[^{177}Lu-DOTA^0,Tyr^3]octreotate in animals bearing tumors ≤1 cm². Survival curves for the control and treatment groups are shown in Figure 4*a*. Tumors of the rats in the negative control group grew excessively. Treatment with a single dose of 277.5 MBq [^{177}Lu-DOTA^0,Tyr^3]octreotate resulted in complete remission of tumor growth in most animals after 1–2 weeks. At 150 days post-tumor implantation, 75% of the rats in this group were still alive and tumor-free ($p<0.001$ vs. control). For the groups that received either the multidose regimen, *i.e.*, 2 injections of 277.5 MBq, or the single dose of 555 MBq, the survival curves of animals were even more impressive. All animals were alive and tumor-free 150 days post-tumor implantation ($p<0.001$ vs. control). The tumor responses of these groups are shown in Figure 4*b*. The lowest single dose resulted in 75% CR and 25% PR in that group of rats, increasing to 100% CR in the higher-dose groups.

[^{177}Lu-DOTA^0,Tyr^3]octreotate in animals bearing tumors ≥1 cm². Completely responding tumors regressed to unpalpable tumors in 4–5 weeks. Figure 5 shows that a 40% CR was found after a single administration of 277.5 MBq [^{177}Lu-DOTA^0,Tyr^3]-octreotate, and this response rate was 50% in the group that received the multiple-dose regimen of 2 × 277.5 MBq. These data indicate a more favorable response rate in rats bearing smaller tumors (Fig. 4*b*) compared with those bearing larger tumor masses (Fig. 5).

[^{177}Lu-DOTA^0,Tyr^3]octreotide in animals bearing tumors ≤1 cm². Survival curves for the control and therapeutic groups are shown in Figure 6*a*. Treatment with a single dose of 277.5 MBq [^{177}Lu-DOTA^0,Tyr^3]octreotide resulted in a significant increase of the survival of the rats in this group. At 150 days post-implant, 40% of the rats in this group were still alive and tumor-free

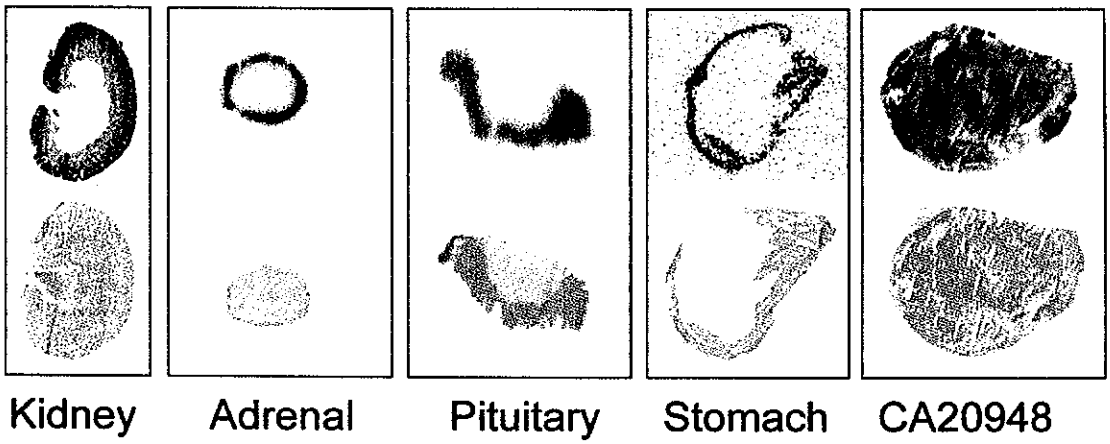

FIGURE 2 – *Ex vivo* autoradiographs and hematoxilin-eosin staining of adjacent sections of indicated organs and CA20948 tumor. Organs and tumor were isolated from the rat (for specifics, see Fig. 3) 24 hr post-injection of [^{177}Lu-DOTA^0,Tyr^3]octreotate (0.5 μg, 3 MBq).

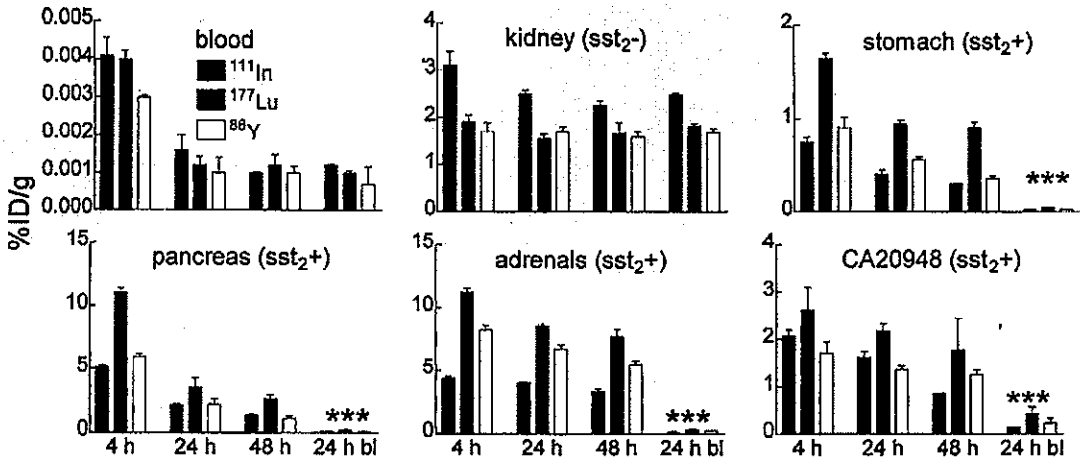

FIGURE 3 – Biodistribution at indicated time points of [DOTA^0,Tyr^3]octreotate, labeled with either ^{111}In, ^{88}Y or ^{177}Lu (0.5 μg, 3 MBq), in male Lewis rats bearing the rat pancreatic CA20948 tumor. The fourth group of bars in each panel shows the effect at 24 hr post-injection of co-injection of 0.5 mg unlabeled octreotide to block receptor binding. *p < 0.001 vs. control (24 hr).

TABLE 1 – RADIOACTIVITY, EXPRESSED AS % OF THE INJECTED DOSE PER GRAM TISSUE IN DIFFERENT ORGANS AND TUMOUR OF CA20948 TUMOUR-BEARING RATS, 24 HR AFTER INJECTION OF [^{177}LU-DOTA^0, TYR^3]OCTREOTATE

Organ	24 hr
Blood	0.002 (0.000)
Spleen	0.023 (0.003)
Pancreas	3.590 (0.980)
Adrenals	8.562 (0.262)
Kidney	1.561 (0.158)
Liver	0.032 (0.001)
Stomach	0.948 (0.067)
Muscle	0.002 (0.000)
Femur	0.275 (0.024)
CA20948 tumour	2.173 (0.284)

(p<0.001 vs. control). Of the animals that received the repeated-dose regimen, *i.e.*, 2 injections of 277.5 MBq, about 60% were alive and tumor-free at 150 days post-implant. The tumor responses of these groups are shown in Figure 6*b*. The lowest single dose gave 40% CR and 60% PR, increasing to 60% CR with 40% PR for the highest dose.

Dosimetry

Estimation of tumor dose of [^{177}Lu-DOTA^0,Tyr^3]octreotate was based on the biodistribution results in this rat model, taking into account the %ID/g radioactivity in the tumor at 72 hr post-injection [1.80 (0.04) %] and a 50% lower uptake in the tumor as a result of the lower specific activity of the radiolabeled peptide as used in the radionuclide therapy studies. This resulted for [^{177}Lu-DOTA^0,Tyr^3]octreotate in an absorbed dose of 96 mGy/MBq for a 1 g tumor and 97 mGy/MBq for a 10 g tumor.

Based on these data, the absorbed doses in the small tumors are 58 Gy for the 2 × 277.5 MBq dose and 50 Gy for the 555 MBq single dose because of the somewhat lower specific activity of the latter therapy dose.

DISCUSSION

Our results show impressive radiotherapeutic effects of ^{177}Lu-labeled [DOTA^0,Tyr^3]octreotate in the rat pancreatic CA20948

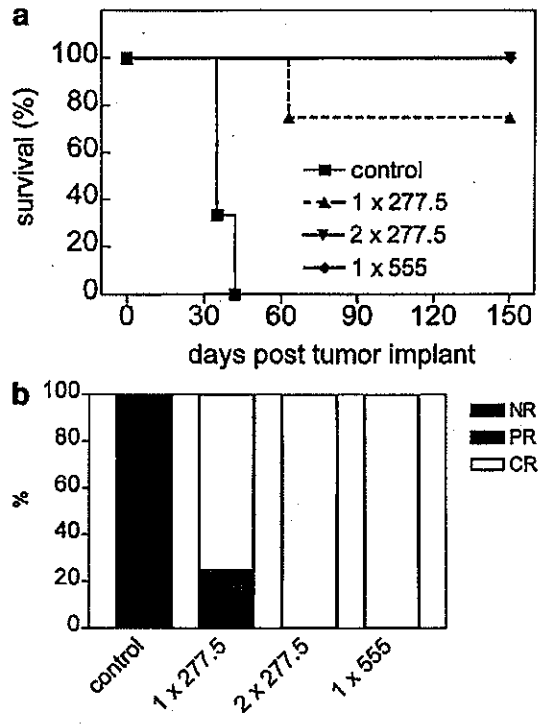

FIGURE 4 – *(a)* Survival curves of groups of rats bearing CA20948 tumors smaller than 1 cm^2 after indicated doses in MBq of [^{177}Lu-DOTA^0,Tyr^3]octreotate (control group n = 6; other groups n = 8). *(b)* Tumor size responses found in groups of rats bearing CA20948 tumors smaller than 1 cm^2 after indicated doses in MBq of [^{177}Lu-DOTA^0,Tyr^3]octreotate. NR, no response; PR, partial response; CR, complete response (control group n = 6; other groups n = 8).

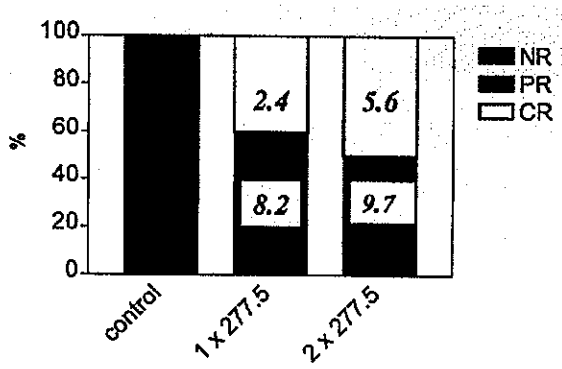

FIGURE 5 – Tumor size responses found in groups of rats bearing CA20948 tumors larger than 1 cm^2 after indicated doses in MBq of [^{177}Lu-DOTA^0,Tyr^3]octreotate. NR, no response; PR, partial response; CR, complete response (control group n = 6; 277.5 MBq group n = 10; 2 × 277.5 MBq group n = 6). The figures in the bars indicate the size of the tumors in cm^2 at the beginning of therapy.

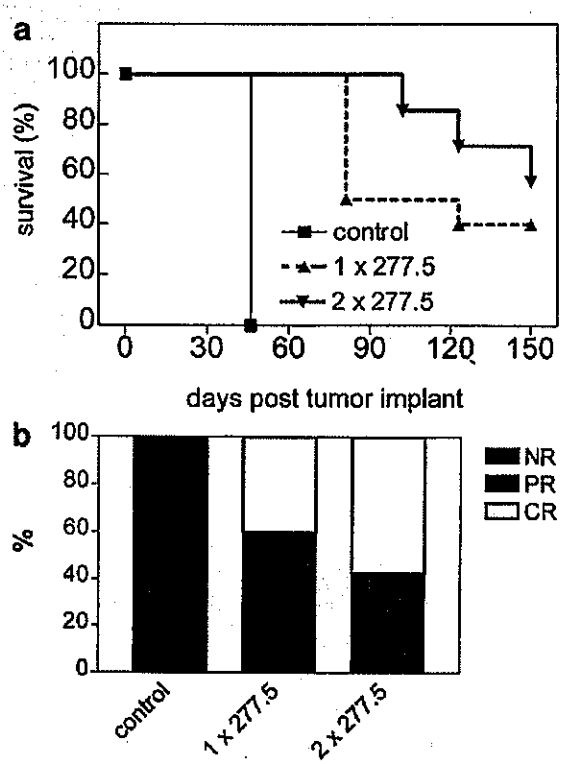

FIGURE 6 – *(a)* Survival curves of groups of rats bearing CA20948 tumors smaller than 1 cm^2 after indicated doses in MBq of [^{177}Lu-DOTA^0,Tyr^3]octreotide (control group n = 6; 277.5 MBq group n = 10; 2 × 277.5 MBq group n = 7). *(b)* Tumor size responses found in groups of rats bearing CA20948 tumors smaller than 1 cm^2 after indicated doses in MBq of [^{177}Lu-DOTA^0,Tyr^3]octreotide. NR, no response; PR, partial response; CR, complete response (control group n = 6; 277.5 MBq group n = 10; 2 × 277.5 MBq group n = 7).

tumor model. All animals bearing small but clearly palpable tumors showed complete regression of tumor mass after a total dose of 555 MBq [^{177}Lu-DOTA^0,Tyr^3]octreotate. In animals bearing larger tumors and treated with this 555 MBq [^{177}Lu-DOTA^0,Tyr^3]octreotate or in animals bearing the small tumors and treated with 555 MBq [^{177}Lu-DOTA^0,Tyr^3]octreotide, the effects were less impressive; 50% to 60% of the animals responded with complete remission of tumor growth. The latter finding is in accordance with the observation that radiolabeled octreotide analogs, including [^{177}Lu-DOTA^0,Tyr^3]octreotide, have a lower tumor uptake in this tumor model compared with the corresponding octreotate analogs,[3,11] thereby resulting in a significantly lower tumor radiation dose in radionuclide therapy studies.

With regard to the better results found in smaller tumors in comparison with larger tumors, we also found a difference in the response rate after radionuclide therapy with ^{111}In- and ^{90}Y-labeled octreotide, showing better results in smaller than in larger CA20948 tumors.[15] Further studies using ^{90}Y-labeled octreotide indicated that 100% cure could be achieved in medium-sized tumors with a mean size of 7.8 cm^2 tumor size, whereas the % cure in smaller tumors (≤ 1 cm^2) and bigger tumors (≥12 cm^2) was less impressive (data not shown). In smaller tumors, a large part of the radiation energy of ^{90}Y will be deposited outside the tumor as a result of the large particle ranges (up to 12 mm) of the high-energy electrons emitted by ^{90}Y. ^{177}Lu is therefore more suitable for treatment of smaller tumors, as shown here. In large tumors, on the other hand, more hypoxic cells are expected to be present, being more radioresistant than well-oxygenated tumor cells, limiting the potential cure rate. Studies are being designed to investigate if this parameter also influenced our results.

The data observed here for [^{177}Lu-DOTA^0,Tyr^3]octreotate point to the importance of early onset of radionuclide therapy during tumor development.

A problem during radionuclide therapy may arise because of the high uptake of ^{177}Lu-labeled peptide in the kidneys, resulting in a higher dose to these radiosensitive organs, thereby limiting the possibilities for radionuclide therapy. This nonspecific renal uptake is restricted to the cortex, as shown in the autoradiography studies, covering about 50% of the kidney. Therefore, the radiation dose on this part of the kidney will be about twice that calculated in dosimetry estimations based on the whole kidney. We showed that the renal uptake of radiolabeled octreotide analogs in rats could be reduced by about 50% by single intravenous administration of 400 mg/kg L- or D-lysine.[16,17] In our study, we found that D-lysine administration also resulted in a significant reduction of [^{177}Lu-DOTA^0,Tyr^3]octreotate uptake in the kidneys without affecting uptake in receptor-positive tissues and tumor, thus enlarging the therapeutic window during radionuclide therapy.

The rat CA20849 flank tumor, which expresses 2 of the 5 existing somatostatin-receptor subtypes, *i.e.*, rat sst_2 and to a lesser extent rat sst_3, has been shown to be a very good model for radionuclide therapy studies using radiolabeled somatostatin analogs with affinity for these 2 receptor subtypes.[4,5,9,11,18,19] Significant tumor growth delay but no cure was found in rats bearing small tumors after radionuclide therapy with [^{64}Cu-TETA]octreotide or [^{64}Cu-TETA,Tyr^3]-octreotate.[18,19] Tumor growth inhibition in this model was also found after treatment of CA20948 tumor-bearing rats with [^{90}Y-DTPA^0-benzyl-acetamido,Tyr^3]-octreotide.[20] Using 370 MBq/kg of [^{90}Y-DOTA^0,Tyr^3]octreotide, the same group observed complete tumor reduction in 5 of 7 rats.[9]

Here we present impressive data on radionuclide therapy in rats using DOTA-octreotate in comparison with octreotide using ^{177}Lu as the radionuclide, resulting in up to 100% CR, in accordance with an earlier radionuclide therapy study using [^{177}Lu-DOTA^0,Tyr^3]octreotate.[11] This study shows the good characteristics of [^{177}Lu-DOTA^0,Tyr^3]octreotate for treatment of rat sst_2-expressing tumors, underscoring the potential of the low-energy β$^-$ particles of ^{177}Lu for radiotherapeutical use. The impressive therapeutic results can be explained by the very high affinity (in the low nM range) of chelated [Tyr^3]octreotate for both the rat and

human sst_2,[3,21] its very high internalization rate[3] and, as shown by the autoradiography and biodistribution studies, the high uptake in the tumor. Other advantages of this radiopharmaceutical include the suitable gamma energy emitted by ^{177}Lu, enabling scintigraphy, dosimetry and radionuclide therapy using this very radionuclide and the fact that the energy emitted is suitable for autoradiography.

In conclusion, radionuclide therapy with octreotate and the low energy β^- emitter ^{177}Lu as radionuclide is most feasible. Acute toxicity studies using this somatostatin analog in rats and mice did not reveal any abnormalities, making it a very promising new treatment modality for sst_2-overexpressing human tumors.

ACKNOWLEDGEMENTS

The authors thank Prof. HR Mäcke (Basel, Switzerland) for the supply of [DOTA^0,Tyr^3]octreotide.

REFERENCES

1. Krenning EP, de Jong M, Kooij PP, Breeman WA, Bakker WH, de Herder WW, et al. Radiolabelled somatostatin analogue(s) for peptide receptor scintigraphy and radionuclide therapy. Ann Oncol 1999;10: S23–9.
2. Krenning EP, Kwekkeboom DJ, Bakker WH, Breeman WA, Kooij PP, Oei HY, et al. Somatostatin receptor scintigraphy with [111In-DTPA-D-Phe1]- and [123I- Tyr3]-octreotide: the Rotterdam experience with more than 1000 patients. Eur J Nucl Med 1993;20:716–31.
3. De Jong M, Breeman WA, Bakker WH, Kooij PP, Bernard BF, Hofland LJ, et al. Comparison of (111)In-labeled somatostatin analogues for tumor scintigraphy and radionuclide therapy. Cancer Res 1998;58:437–41.
4. De Jong M, Breeman WA, Bernard HF, Kooij PP, Slooter GD, Van Eijck CH, et al. Therapy of neuroendocrine tumors with radiolabeled somatostatin- analogues. Q J Nucl Med 1999;43:356–66.
5. Slooter GD, Breeman WA, Marquet RL, Krenning EP, van Eijck CH. Anti-proliferative effect of radiolabelled octreotide in a metastases model in rat liver. Int J Cancer 1999;81:767–71.
6. Otte A, Herrmann R, Heppeler A, Behe M, Jermann E, Powell P, et al. Yttrium-90 DOTATOC: first clinical results. Eur J Nucl Med 1999;26:1439–47.
7. Otte A, Mueller-Brand J, Dellas S, Nitzsche EU, Herrmann R, Maecke HR. Yttrium-90-labelled somatostatin-analogue for cancer treatment [letter]. Lancet 1998;351:417–8.
8. Paganelli G, Zoboli S, Cremonesi M, Macke HR, Chinol M. Receptor-mediated radionuclide therapy with 90Y-DOTA-D-Phe1-Tyr3- Octreotide: preliminary report in cancer patients. Cancer Biother Radiopharm 1999;14:477–83.
9. Stolz B, Weckbecker G, Smith-Jones PM, Albert R, Raulf F, Bruns C. The somatostatin receptor-targeted radiotherapeutic [90Y-DOTA-DPhe1, Tyr3]octreotide (90Y-SMT 487) eradicates experimental rat pancreatic CA 20948 tumours. Eur J Nucl Med 1998;25:668–74.
10. Valkema R, Jamar F, Jonard P, Bakker WH, Norenberg J, Hadley J, et al. Targeted radiotherapy with 90Y-SMT487 (OctreoTher): a phase I study. J Nucl Med 2000;41:111P.
11. Erion JL, Bugaj JE, Schmidt MA, Wilhelm RR, Srinivasan A. High radiotherapeutic efficacy of [Lu-177]-DOTA-Y3-octreotate in a rat tumor model. J Nucl Med 1999;40:223p.
12. Heppeler A, Froidevaux S, Mäcke HR, Jermann E, Béhé M, Powell P, et al. Radiometal-labelled macrocyclic chelator-derivatised somatostatin analogue with superb tumour-targeting properties and potential for receptor-mediated internal radiotherapy. Chem Eur J 1999;5: 1974–81.
13. De Jong M, Bakker WH, Breeman WA, Bernard BF, Hofland LJ, Visser TJ, et al. Pre-clinical comparison of [DTPA0] octreotide, [DTPA0,Tyr3] octreotide and [DOTA0,Tyr3] octreotide as carriers for somatostatin receptor- targeted scintigraphy and radionuclide therapy. Int J Cancer 1998;75:406–11.
14. Siegel JA, Stabin MG. Absorbed fractions for electrons and beta particles in spheres of various sizes. J Nucl Med 1994;35:152–6.
15. De Jong M, Breeman WAP, Bernard HF, Van Gameren A, Schaar M, Bakker WH, et al. Response to radionuclide therapy using 90Y- and 111In-labeled somatostatin analogs is dependent on tumor size. J Nucl Med 2000;41:111P.
16. Bernard BF, Krenning EP, Breeman WA, Rolleman EJ, Bakker WH, Visser TJ, et al. D-lysine reduction of indium-111 octreotide and yttrium-90 octreotide renal uptake. J Nucl Med 1997;38:1929–33.
17. De Jong M, Rolleman EJ, Bernard BF, Visser TJ, Bakker WH, Breeman WA, et al. Inhibition of renal uptake of indium-111-DTPA-octreotide in vivo. J Nucl Med 1996;37:1388–92.
18. Anderson CJ, Jones LA, Bass LA, Sherman EL, McCarthy DW, Cutler PD, et al. Radiotherapy, toxicity and dosimetry of copper-64-TETA-octreotide in tumor-bearing rats. J Nucl Med 1998;39:1944–51.
19. Lewis JS, Lewis MR, Cutler PD, Srinivasan A, Schmidt MA, Schwarz SW, et al. Radiotherapy and dosimetry of 64Cu-TETA-Tyr3-octreotate in a somatostatin receptor-positive, tumor-bearing rat model. Clin Cancer Res 1999;5:3608–16.
20. Stolz B, Smith-Jones P, Albert R, Tolcsvai L, Briner U, Ruser G, et al. Somatostatin analogues for somatostatin-receptor-mediated radiotherapy of cancer. Digestion 1996;57:17–21.
21. Reubi JC, Schar JC, Waser B, Wenger S, Heppeler A, Schmitt JS, et al. Affinity profiles for human somatostatin receptor subtypes SST1-SST5 of somatostatin radiotracers selected for scintigraphic and radiotherapeutic use. Eur J Nucl Med 2000;27:273–82.

CHAPTER 5

RADIOTHERAPEUTIC EFFICACY OF ^{177}Lu-DOTA-Tyr^3-OCTREOTATE IN NOVEL RAT TUMOR ANIMAL MODELS

Joseph E. Bugaj, Jack L. Erion, Michael A. Johnson and Marion de Jong

Submitted to: E J Nucl Med

ABSTRACT

A number of somatostatin analogs have been recently evaluated in animal models as potential radiotherapeutic agents for ablation of neuroendocrine tumors. These analogs have been chelated with beta emitting isotopes such as Y-90, and Re-188, and more recently increased efficacy using Lu-177 has been demonstrated. The majority of these agents have been evaluated for therapeutic efficacy in the rat flank tumor model, CA20948 tumor bearing Lewis rats, or in athymic nude or SCID mice bearing the AR42-J flank model. We have developed two novel tumor models in the Lewis rat based on the exocrine acinar pancreatic cell line AR42-J. These models represent a flank model induced by serial implantation of solid tumor material in pre-weaned animals, and a liver model mimicking smaller *in vivo* metastases. Biodistribution studies in the flank model showed that the compound, ^{177}Lu-DOTA-Tyr^3-Octreotate, has high uptake and retention of the agent in the tumor (8.0% ID/gram at 4 hrs. p.i.), and an *in vivo* blocking study confirmed the receptor specificity of this agent for the sst_2 receptor. The radiotherapeutic efficacy of this agent was evaluated in both model systems. In animals bearing the flank tumor at 9 days post implant multi-dose regimens of 2.5mCi/rat and 5.0mCi/rat significantly suppressed tumor growth compared to untreated control animals. In the liver model, a significant reduction in the total number of metastases and overall tumor involvement of the livers was observed in animals treated with three doses of 5.0mCi/rat compared to the untreated control group. All animals in the flank model groups showed latent tumor re-growth after ~90 days, indicating that this new tumor model is more difficult to treat therapeutically than CA20948, and therefore represents a potentially new model of radio-resistant neuroendocrine tumors.

INTRODUCTION

Small peptides chelated with a growing number of beta particle and Auger electron emitting radionuclides is becoming a promising means of specifically targeting cancerous tissues for the purpose of radiotherapy. This wider acceptance of peptides is predicated on the favorable biological characteristics that include rapid blood clearance, low toxicity, and high specificity for tumor tissue and low immunogenicity [1-4]. The successful use of OctreoScan as a clinical radio-diagnostic was the initial example of a peptide-based agent for the specific identification of certain neuroendocrine tumors [5]. Since then a variety of octreotide analogs radiolabeled with Y-90, Re-188, Sm-153, Cu-64, In-111 and more recently Lu-177, have all demonstrated efficacy in inhibiting tumor growth in tumor bearing animal models [1, 4, 6-10] The radionuclide, Lu-177, has superior properties over the radionuclides mentioned, most notably a low β^- emission (497keV), a relatively long half-life (6.7 d) and the potential for high radio-specific activity (>3000Ci/mmol). Lu-177 also possesses a low abundance γ emission (11%, 208keV) which is quite suitable for scintigraphic imaging and provides a very convenient tracer emission for biodistribution studies and dosimetry calculations [11]. Being a reactor product produced from Lu-176, this radionuclide presents a number of advantages with regard to cost, scalability and availability over radionuclides produced by other means.

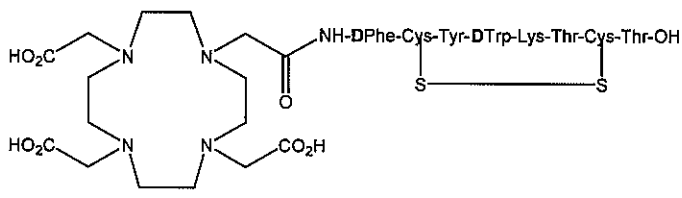

Figure 1: Structure of DOTA-Tyr^3-Octreotate

It has been shown that the substitution of the carboxy-terminal threoninol in octreotide with the natural amino acid threonine substantially increases both the uptake and retention of the radiolabeled derivative in somatostatin positive (sst_2) tumors [9, 11]. This superior uptake and retention in this derivative, termed octreotate, led to the synthesis and evaluation of ^{177}Lu-DOTA-Tyr^3-Octreotate in the CA20948 tumor bearing Lewis rat model as a potential radiotherapeutic agent. Using this model with a multi-dose regimen of 3 X 5.0mCi/rat at 30 day intervals, Erion et al. were able to demonstrate the complete remission of tumor growth for 16-24 months [11]. De Jong has reproduced this result by demonstrating complete remission of tumor growth in the same animal model for 150 days post injection, at which time the animals were sacrificed for histological evaluation to assess possible toxicological effects of the treatment [12].

The majority of the studies that establish therapeutic efficacy of various sst_2 agents employ either Lewis rats bearing the CA20948 tumor in the flank model or athymic nude or SCID mice using AR42-J cell inoculations to establish palpable tumor masses. The CA20948 flank model has been extensively used to evaluate octreotide derivatives chelated to In-111, Cu-64, Sm-153, Y-90 and Lu-177 [6-9, 11-13]. This model is quite attractive, as it is easy to establish and maintain in Lewis rats, and produces tumors that consistently achieve 1-3 grams in size 16-20 days post implant [1, 7, 8]. This tumor line is of rat acinar pancreatic origin and is known to express a high number of sst_2 membrane bound receptors that readily recycle by the mechanism of receptor mediated endocytosis [9, 13, 14]. De Jong and Breeman have also demonstrated that these cells can be injected directly into the vena porta to produce a metastatic liver model in Lewis rats that has been used to evaluate the radiotherapeutic efficacy of In-111 and Y-90 labeled octreotide derivatives [15].

A second sst_2 tumor model used to evaluate diagnostic and therapeutic potential of novel agents is the athymic nude or SCID mouse model injected with AR42-J cultured rat cells in the flank area. This cell line is positive for the expression of a number of membrane bound receptors including sst_2, bombesin, VIP, CCK, EGF, and as a result has been used to test a variety of radiolabeled peptides chelated to Tc-99m and Re-188 [16]. Because of their compromised immune systems, both the athymic nude and SCID mouse models require housing within a sterile barrier, and as a result, these models are not readily available to all research sites due to the expense and increased maintenance and housing requirements for this type of facility.

In this work we introduce two novel rat models that produce AR42-J tumors in the flank and the liver that over-express the sst_2 receptor. We then evaluated the therapeutic potential of ^{177}Lu-DOTA-Tyr^3-Octreotate (Figure 1) in both animal models.

MATERIALS AND METHODS

Tumor Models

Flank Model: All animal studies were conducted in compliance with the Mallinckrodt Inc. Animal Welfare Committe requirements. Pre-weaned male Lewis rats weighing approximately 40 grams and 20 days old were first injected subcutaneously in the left flank area with 2.5 x 10^6 AR42-J cells. After 12-14 days palpable masses were present, and were allowed to reach a mass of a 2-3 grams. This material was aseptically harvested and placed into a petri dish on ice containing Media 199 (Gibco Co.). The tumor was further diced into smaller pieces (2 x 2 mm), placed into the bevel of a cancer implant needle and then directed subcutaneously to the center of

the left flank of each recipient animal. These animals were also pre-weaned Lewis rats weighing 40 grams anesthetized with Halothane. Palpable masses resulted with 9-11 days and consecutive generations (>30) have been serially passaged *in vivo* by this technique.

Liver Metastases Model: Donor animals were initially obtained from Lewis rats bearing AR42-J flank tumors described previously. The tumor material was aseptically removed, placed into a petri dish containing Media 199 and kept on ice. The tumor mass was passed through a sieve to remove capsular debris and then suspended in PBS at a concentration of 5 x 10^6 cells/ml. Young (4 week old) male Lewis rats were injected directly into the portal vein with 500µl of cell suspension. Metastatic tumor growth confined to the liver occurred within 30 days. The transplantable line was maintained in successive generations by direct portal vein injection into naive animals.

Radiochemistry

The preparation of DOTA-Tyr^3-Octreotate has been previously described in detail [9, 11, 12]. The Lu-177 was obtained from MURR at a specific activity of ~3000Ci/mmol. Labeling reactions were performed at 80^{o}C in 30mM NaOAc, 15mM NaAscorbate at pH 5.5. The peptide was labeled to a radio-specific activity of 1200Ci/mmol. Radiochemical yields (>99.5%) and radiochemical purity (>98%) were determined by reverse phase chromatography on a Vydac C18 column using acetonitrile/0.01% TFA gradient (5% to 70% ACN) over a 20 minute time span at 1.0 ml/minute. Samples were coinjected with 2.5mM DTPA to chelate unincorporated metal. The radiolabeled complex has a retention time of 14.8 minutes.

Receptor Binding Assays

Receptor binding assays were carried out using membranes prepared from CA20948 tumors harvested from Lewis rats [6, 7]. Assays were performed using the Millipore Multiscreen system (Bedford, Mass) with ^{111}In-DTPA-Tyr^3-Octreotate as the trace and unlabeled DOTA-Tyr^3-octreotate as the cold competitor. Radiolabeling of DTPA-Tyr^3-octreotate was performed by combining 1.0 µg peptide (1.0mg/ml) with 1.0 mCi of $^{111}InCl_3$ (100 mCi/ml, Mallinckrodt Inc., St. Louis) and 10 µl buffer (50mM NaOAc, 25mM sodium ascorbate). After incubation at room temperature for 15 minutes, the peptide radiochemical yield (> 99%) and purity (> 95%) were determined by reverse phase chromatography. IC_{50} values were calculated using a four-parameter curve fitting routine using the program GraFit (Erithacus, UK).

Tissue Distribution and Blocking Study

A biodistribution study was carried out using the AR42-J Lewis rat flank model at 14 days post implant. Anesthetized (Halothane) animals received 25 µl (250 µCi/9.25 MBq) of ^{177}Lu-DOTA-Tyr^3-octreotate via the jugular vein. The animals were divided into three groups (n = 3/group) and sacrificed at 1, 4 and 24 hours post injection by cervical dislocation. Scintigraphic images were obtained using a Picker 300SX gamma camera interfaced to a dedicated Odyssey image processor. A large field of view camera using a general-purpose medium energy collimator with the peak energy centered at 208keV was used to collect images for 100K counts. The tissues and organs of interest were removed, weighed and the radioactivity measured in a Packard Cobra gamma-scintillation counter.

A blocking study was performed in the same animal model. The positive control group (n = 3) was pre-treated with a subcutaneous injection of cold Tyr^3-octreotide at

1.3 mg/kg 45 minutes prior to injection of ^{177}Lu-DOTA-Tyr^3-octreotate. The negative control group (n = 3) received a subcutaneous injection of saline 45 minutes prior to injection with the test article. Three hours post injection of agent the animals were sacrificed by cervical dislocation and imaged for 100K counts. Tissues and organs of interest were removed, weighed and the radioactivity measured in a Packard Cobra gamma-scintillation counter.

Radiotherapy Studies

Flank Model: Radiotherapy studies were initiated in animals at 9 days post implant of AR42-J solid tumor. Animals were randomly divided into study groups (n = 6/group) and received either three doses of 2.5 mCi or four doses 5.0 mCi of ^{177}Lu-DOTA-Tyr^3-octreotate via the jugular vein at 14 day intervals. Presence of tumor mass was first confirmed by palpation of the flank area. The control group (n = 6) received no treatment. Tumor volumes were measured with calipers initially twice per week, followed by weekly measurements after receiving the final treatment dose.

Liver Metastases Model: Male Lewis rats were inoculated with 2.5×10^6 viable cells by direct injection into the portal vein. Two groups of animals were randomly divided with the treatment group (n = 6) receiving three doses of 5.0 mCi of ^{177}Lu-DOTA-Tyr^3-octreotate via the jugular vein at 7, 14 and 28 days post injection of cells. The negative control group (n= 5) received no treatment. The animals were weighed weekly, and their general health was periodically monitored for overt signs of

morbidity. At 34 days post injection of cells, the animals were sacrificed, all livers excised, weighed and graded by four independent investigators ranking the extent of metastatic involvement (from 0 to 5+), while blinded from treatment regimen.

Statistical Analysis

Statistical analysis was performed using a one tailed students t-test, and the level of statistical significance was set at $p < 0.05$.

RESULTS

In Vitro Binding Assay

The CA20948 pancreatic acinar tumor line expresses high levels of sst_2 receptor [1, 13, 17]. We have used membrane preparations from this tumor line to screen a number of somatostatin analogs with chemical modifications made in both the peptide and chelate

segment of the molecule [7]. Figure 2 shows the data for several analogs analyzed using this method, and the IC_{50} value for DOTA-Tyr^3-octreotate was found to be 4.0nM, very similar to that for DTPA-Octreotide (2.5nM) and CMDTPA-Tyr^3-Octreotate (2.8nM). This compound was therefore evaluated as a promising agent for testing of radiotherapeutic potential in these model systems based on its high in vitro binding affinity, improved Lu-177 chelating properties and promising radiotherapeutic effect demonstrated previously in the CA20948 Lewis rat tumor model [11, 12].

Table 1. Table of Competitive Binding of ^{111}In-DTPA-Tyr^3-octreotate to CA20948 Tumor Membranes in the Presence of Unlabelled Somatostatin Analogues. IC_{50} values are in nM.

Peptide	IC_{50} (nM)
DTPA-octreotide	2.5
DTPA-Tyr^3-octreotate	1.4
CMDTPA-octreotate	2.8
Tyr^3-octreotate	0.5
DOTA-Tyr^3-octreotate	4.0

Tissue Distribution and Blocking Studies

The tissue biodistribution properties of ^{177}Lu-DOTA-Tyr^3-octreotate were studied in the AR42-J Lewis rat flank model. The complete tissue distribution is listed in Tables 2 and 3 and is represented graphically in Figure 2. At 1, 4 and 24 hours post injection (p.i.) of the agent the amount of activity accumulated in the tumor tissue was 7.7%, 8.0% and 5.3% of the injected dose per gram of tissue (%ID/g). Significant uptake was also observed in the pancreas and adrenal glands, both sst_2 receptor positive tissues. Pancreas uptake was 23.0%, 14.0% and 4.2% ID/g, and the adrenal tissue was 0.59, 0.57 and 0.43%-injected dose per whole organ (ID/o). Non-somatostatin receptor expressing tissues which includes the liver, spleen, heart and muscle all exhibited low uptake of the radiotracer. Scintigraphs at the three sacrifice points confirm the strong localization of the agent in the tumor with no significant uptake in any non-sampled tissues or organs (Figure 4). At 24 hours p.i. the predominant route of excretion was urinary with 62% excreted via the renal system and 15% excreted fecally (Table 2). The rapid distribution and excretion of the agent coupled with the high specificity for the sst_2 receptor resulted in very high target to non-target tissue ratios. The tumor to tissue ratios calculated from %ID/g values at 24 hours were 1776 for blood, 1333 for muscle and 66 for liver, and the pancreas to tissue ratios from

%ID/g values were 1392 for blood, 1044 for muscle and 52 for liver. These ratios validate the specificity of the agent for tumor tissue in this novel animal model.

The kidney was the only non-sst_2 positive organ to show significant uptake and retention of the agent. Kidney retention remained relatively constant at 2.5% ID/gram at 4 and 24 hours post injection. The mechanism for this non-receptor mediated uptake is the result of the metabolism of octapeptide to the ^{177}Lu-DOTA-(D)Phe^1, that is retained in the renal tubules of the kidneys [18].

Table 2. Biodistribution of ^{177}Lu-DOTA-Y^3-Octreotate in AR42-J Tumor Bearing Rats (Percent Injected Dose / gram ± SE)

Tissue	1 hour	4 hours	24 hours
Blood	0.076±0.013	0.008±0.001	0.003±0.000
Liver	0.080±0.004	0.086±0.012	0.081±0.009
Kidneys	1.652±0.086	1.844±0.079	1.394±0.125
Muscle	0.019±0.004	0.006±0.000	0.004±0.000
Spleen	0.085±0.009	0.095±0.019	0.069±0.008
Heart	0.060±0.007	0.022±0.001	0.011±0.001
Pancreas	23.01±1.454	14.00±2.029	4.176±0.229
Sm. Intes.	0.727±0.077	0.970±0.127	0.269±0.037
Stomach	2.094±0.326	1.044±0.104	0.785±0.059
Bone	1.175±0.157	0.925±0.030	0.811±0.020
Tumor	7.732±0.690	8.048±0.376	5.330±0.557

Table 3. Biodistribution of ^{177}Lu-DOTA-Y^3-Octreotate in AR42-J Tumor Bearing Rats (Percent Injected Dose / organ ± SE)

Tissue	1 hour	4 hours	24 hours
Blood	0.436±0.083	0.043±0.003	0.018±0.002
Liver	0.422±0.014	0.366±0.034	0.423±0.020
Kidneys	1.856±0.131	1.869±0.007	1.702±0.028
Muscle	0.996±0.200	0.293±0.003	0.227±0.012
Spleen	0.033±0.003	0.031±0.006	0.023±0.000
Heart	0.028±0.004	0.010±0.001	0.006±0.000
Pancreas	13.03±1.470	7.740±0.735	2.615±0.136
Adrenals	0.586±0.029	0.570±0.009	0.432±0.025
Stomach	2.316±0.154	1.553±0.036	0.846±0.019
Bone	7.821±1.131	5.760±0.222	5.547±0.451
Tumor	12.54±3.019	15.06±1.781	6.451±0.535
Urine			61.95±1.411
Feces			14.95±2.310
Total Excreted			76.901±2.510
Total Recovered			95.104±3.072

Table 4 and Figures 4 and 5 confirm the receptor specificity of this agent for the sst_2 receptor. In the animals receiving cold peptide to block receptor uptake of the radiotracer the pancreas, adrenals and tumor tissues showed a reduction of 85% or greater in uptake compared to saline treated animals at three hours post injection.

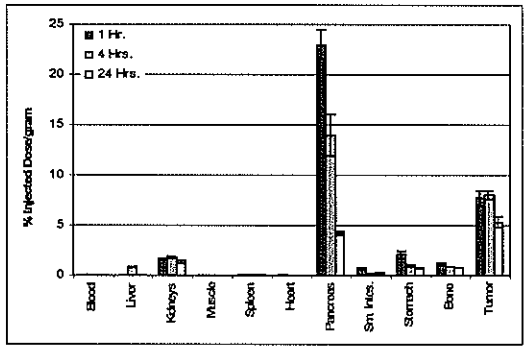

Figure 2: Biodistribution of ^{177}Lu-DOTA-Tyr^3-octreotate in AR42-J tumor bearing rats at 1, 4 and 24 hours post injection (expressed as %ID/gram of tissue).

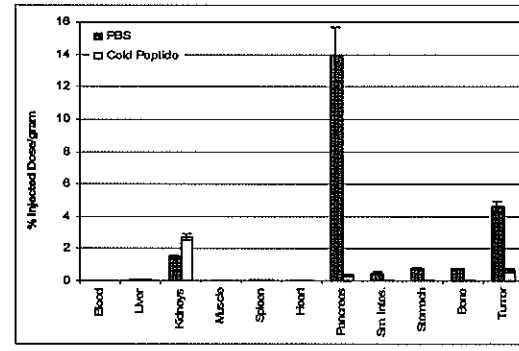

Figure 4: Blocking study in AR42-J tumor bearing rats pre-treated with PBS or cold peptide 3 hours post injection with ^{177}Lu-DOTA-Tyr^3-octreotate (expressed as %ID/gram of tissue).

Table 4. Biodistribution of ^{177}Lu-DOTA-Y^3-Octreotate in AR42-J Tumor Bearing Rats 3 Hours Post Injection after Pre-treatment with PBS or Cold Peptide (Percent Injected Dose / gram ± SE)

Tissue	PBS	(+) Cold Peptide
Blood	0.011±0.001	0.007±0.001
Liver	0.052±0.004	0.069±0.006
Kidneys	1.492±0.092	2.702±0.202
Muscle	0.005±0.000	0.008±0.000
Spleen	0.055±0.002	0.034±0.002
Heart	0.023±0.002	0.010±0.001
Pancreas	13.99±1.668	0.328±0.055
Sm. Intes.	0.459±0.105	0.052±0.007
Stomach	0.768±0.054	0.061±0.025
Bone	0.730±0.008	0.043±0.004
Tumor	4.592±0.360	0.626±0.120

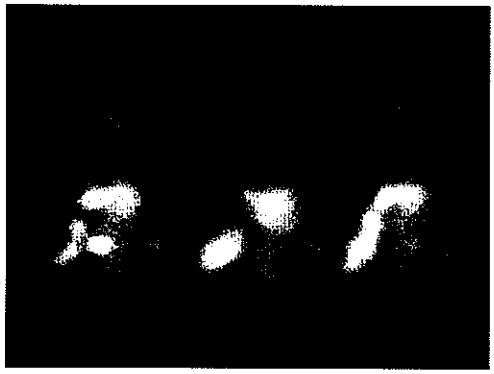

1 hour

4 hours

24 hours

Figure 3: Scintigraphs of AR42-J tumor bearing Lewis rats at 1, 4 and 24 hours post injection of 250μCi ^{177}Lu-DOTA-Tyr^3-octreotate. Images were obtained with a Picker 300SX gamma camera using medium energy collimation centered on a peak energy of 208keV.

Other tissues known to express sst_2 naturally include the stomach and bone, both tissues that exhibited a significant blocking effect in this study. The non-somatostatin expressing tissues of the blood, muscle, spleen and liver did not exhibit any blocking effect as a result of the administration of cold peptide. Scintigraphs from representative animals (Figure 5) shows the dramatic reduction in the localization of the agent in tumor tissue in the animals that received a blocking dose of cold peptide versus animals receiving saline.

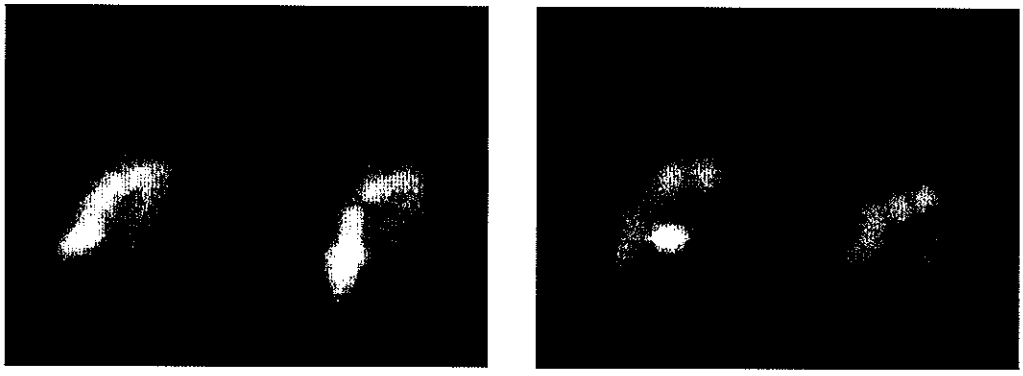

Figure 5: Scintigraph of blocking study comparing animals pretreated with 1.3mg/kg of cold Tyr^3-octreotate (Right) or saline (left) 45 minutes prior to injection with ^{177}Lu-DOTA-Tyr^3-octreotate.

Radiotherapy Studies

Flank Model: Figure 6 shows the survival curves for animals treated with 3 x 2.5mCi/rat and 4 x 5.0mCi/rat at 14 day intervals compared to untreated control animals. In both studies the untreated animals show similar tumor growth rates, with mean survival only 28 days post implant. A significant delay ($p < 0.05$) in tumor re-growth was observed in both treatment groups. The animals that received a dosing regimen of 3 x 2.5mCi had a mean survival time of 75 days post implant and the animals treated with 4 x 5.0mCi had a mean survival of 101 days post implant. In both dosing regimens all animals ultimately showed latent re-growth of tumor mass.

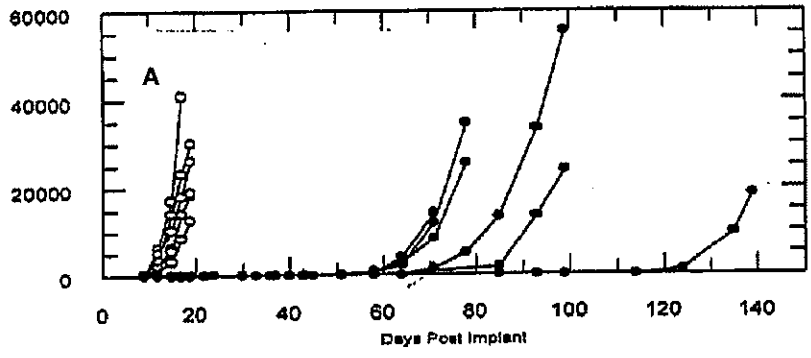

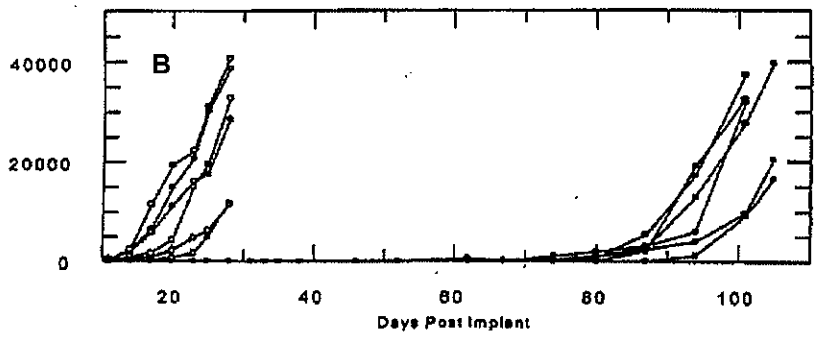

Figure 6: Tumor volumes following ^{177}Lu-Y^{3}-DOTA-octreotate radiotherapy of AR42-J flank tumor bearing Lewis rats. Panel **A**: 3 x 2.5mCi doses at 14 day intervals; Panel **B**: 4 x 5.0mCi doses at 14 day intervals. Symbols (o) = Tumor implanted untreated control animals, (.) = Tumor implanted animals with treatments as indicated. Calculated mean survival of untreated control animals was **A**. 28 days (±) 4 , **B**: 29 days (±) 3, and treated animals was **A**: 75 days (±) 9 and **B** 101 days (±) 11

Liver Metastases Model: Animals in both the treated and untreated groups were sacrificed at 34 days post injection of AR42-J cells. At that time there was a noticeable decline in general health of the untreated animals. These animals exhibited signs of morbidity marked by extreme lethargy, poor grooming and significant weight loss. In contrast, the treated animals maintained a healthy appearance and normal levels of activity throughout the time span of the study, and continued to gain weight up to the time of sacrifice. Figure 7 is a comparative photograph of the excised livers from the treated and untreated animals. There is a very clear difference in the number of metastases and extent of overall tumor involvement in the untreated animals versus the treated group that exhibited virtually no signs of tumor involvement. The mean liver weight in grams for the untreated control group was significantly higher compared to the treatment group (18.9g vs. 9.9g). The numerical score, on a range from 0 to 5+, for tumor metastases and overall hepatic involvement for the untreated group was significantly higher ($p<0.01$)

with a score of 3.90 vs. only 0.19 for the treatment group based on the visual inspection by four independent investigators (data not shown).

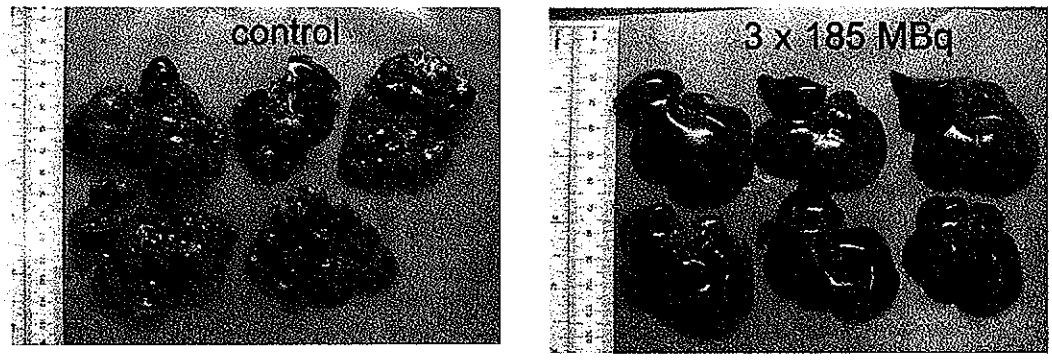

Figure 7: Photograph of excised livers from untreated (control) and treated (3 x 185 mBq) Lewis rats injected with 2.5 x 10^6 AR42-J cells directly into portal vein. Treatment group received 3 x 5.0mCi (185mBq) of ^{177}Lu-DOTA-Tyr^3-octreotate at 7, 14, and 28 days post injection of cells. Livers excised after 34 days.

DISCUSSION

The studies presented here establish the AR42-J flank and liver metastases models in Lewis rats as novel *in vivo* systems for the evaluation of sst_2 receptor targeted radiotherapeutic agents. The models described in this study represent two relatively simple and reproducible *in vivo* tumor lines that require no significant increase in expense or maintenance requirements for the research facility. The flank model was thoroughly validated for the expression of sst_2 receptor using ^{177}Lu-DOTA-Tyr^3-octreotate as the targeting radiolabeled peptide complex in biodistribution, blocking and radiotherapy studies. The liver metastases model was developed to further test the radiotherapeutic efficacy of this agent to treat small tumors that may mimic a metastatic condition in a clinical setting. Both sets of studies confirmed the utility of both models for radiotherapy, and the data from the flank model suggest that it represents a more radio-resistant neuroendocrine tumor line *in vivo*, compared to the

CA20948 flank model that has been more commonly used to evaluate potential radiotherapeutic agents. Both models are novel in that the Lewis rat is the animal used to host the AR42-J pancreatic tumor line compared to the athymic nude or SCID mouse which has conventionally been used as the animal host for this cell line *in vivo*. The use of pre-weaned Lewis rats to establish the model suggests that the immune system of these animals is not sufficiently mature to reject the quasi-murine tissue implant resulting in a discreet tumor mass. As a result, the maturing immune systems of older animals of 8-10 weeks of age are able to recognize the implants as foreign, and reject the tissue before it becomes an established tumor mass.

The flank model bearing the AR42-J tumor line was validated for the expression of sst_2 receptors by the high uptake and retention of ^{177}Lu-DOTA-Tyr^3-octreotate in a series of biodistribution and blocking studies [11, 12]. Uptake in the sst_2 positive tissue of the tumor, pancreas and adrenal glands was higher than reported for other octreotide and octreotate derivatives [7, 9]. Uptake and retention in the non-somatostatin expressing tissues of the blood, liver, muscle, spleen and heart was very low, and not apparent on the scintigraphs. As previously mentioned, the only non-somatostatin expressing tissue to show any significant uptake was the kidney. This is quite expected as the metabolism for this class of peptides is well documented [18]. The octapeptide is metabolized to ^{177}Lu-DOTA-(D)-Phe^1, and this species is readily trapped in the renal tubules of the kidneys. It has been demonstrated, however, that significant (50%) reduction in kidney retention can be achieved by the use of amino acid i.v. infusion [19-21]. The pancreas is a sst_2 receptor positive tissue, in which potentially undesirable high uptake of the radiotherapeutic agent was observed. However, additional studies in humans need to be undertaken to determine if the high pancreatic uptake in this animal model will

also be found in humans. Results with ^{125}I-sst$_{28}$ suggest that normal human pancreatic tissue does not bind this analogue, and that only weak expression of sst receptor mRNA has been found in normal pancreas [22, 23].

In a competition study using cold peptide, an 85% reduction in sst$_2$ receptor activity was observed, confirming the high sst$_2$ expression in this tumor model. Coupled with the low non-target tissue retention, high urinary clearance and low fecal clearance, this model was used to evaluate the therapeutic potential of ^{177}Lu-DOTA-Tyr^3-octreotate. Rats bearing the flank tumor model treated with either 3 x 2.5mCi or 4 x 5.0mCi per animal at 14 day intervals all showed a significant delay in tumor growth compared to untreated control animals. The mean survival time for the low dose animals was 75 days post implant, and 100 days post implant for the high dose group. Separate untreated control groups had a mean survival of only 28 days post implant. All treated animals ultimately showed re-growth of tumor mass, however. This observation is in contrast to the therapeutic efficacy of ^{177}Lu-DOTA-Tyr^3-octreotate reported by several investigators employing the CA20948 Lewis rat model. Erion et al. reported a complete remission of tumor growth in animals treated with 3 x 5.0mCi after a period of 16 months [11]. De Jong et al. reported a similar finding of complete remission of tumor growth with the same dose regimen for 150 days post implant, at which time the animals were sacrificed for histology purposes [12]. The data from the present study suggests that the AR42-J tumor line in Lewis rats is less sensitive to radiation therapy than the CA20948 tumor model, and may therefore represent a new and useful animal model for more radio-resistant neuroendocrine tumors.

The liver model employing young (4 week old) male Lewis rats injected directly with AR42-J cells into the portal vein was developed to mimic a metastatic model of tumor growth. This model, generated with CA20948 tumor cells, was previously shown to be sst_2 positive and has been used to demonstrate the radiotherapeutic potential of several octreotide and octreotate derivatives chelated with In-111 and Y-90 [15]. In the present study animals treated with 3 x 5.0mCi of ^{177}Lu-DOTA-Tyr^3-octreotate at 7, 14 and 28 intervals post injection of cells showed a pronounced therapeutic effect compared to untreated control animals. By 34 days post injection all of the untreated animals exhibited overt signs of morbidity, which included extreme lethargy, poor grooming and significant weight loss. Upon excision, the livers indicated extensive (~80%) tumor involvement of that tissue. Conversely, the treated animals showed no signs of morbidity up to the time of sacrifice, and upon excision their livers were virtually devoid of tumor involvement (<2%). Mean weight in grams of the untreated animal livers was almost twice the mean weight of the treated animal livers (18.9g vs. 9.9g). These data are in agreement with the CA20948 liver model of de Jong and Breeman, which was previously shown to be useful model for mimicking small metastases to evaluate radiotherapeutic agents for sst_2 positive tumors [15].

CONCLUSION

The increased interest in and successful demonstration of sst_2 receptor targeted radiotherapy is predicated on the judicious selection and combination of animal tumor models and radionuclides. This search has encompassed the evaluation of a number of beta and Auger emitting isotopes chelated to octreotide and octreotate derivatives primarily using the CA20948 tumor bearing Lewis rat as the model of choice [1, 6, 7, 9, 10, 12, 13, 16, 24-26]. Up to this point use of AR42-J tumor bearing animals models has been restricted to either athymic nude or SCID mice, which require more

elaborate and expensive housing requirements due to their compromised immune systems. The development of a simple and reproducible rat model would offer significant advantages over these models from a cost and ease of implementation strategy. The model systems described were validated for sst_2 receptor positive expression using ^{177}Lu-DOTA-Tyr^3-octreotate as the agent to test radiotherapeutic efficacy. In both animal models significant reduction in tumor growth was observed compared to untreated control animals, and the lack of a complete cure in this AR42-J flank model suggests that this model is more radio-resistant compared to the CA20948 Lewis rat model.

REFERENCES

1. Anderson CJ, Jones LA, Bass LA, Sherman EL, McCarthy DW, Cutler PD, Lanahan MV, Cristel ME, Lewis JS, Schwarz SW. Radiotherapy, toxicity and dosimetry of copper-64-TETA-octreotide in tumor-bearing rats. *J Nucl Med* 1998; 39:1944-1951.

2. Smith-Jones PM, Stolz B, Albert R, Knecht H. and Bruns C. Synthesis, biodistribution and renal handling of various chelate-somatostatin conjugates with metabolizable linking groups. *Nucl Med Biol* 1997; 24:761-769.

3. Stimmel JB, Kull FC. Samarium-153 and lutetium-177 chelation properties of selected macrocyclic and acyclic ligands. *Nucl Med Biol* 1998; 25:117-125.

4. Zamora PO, Gulhke S, Bender H, Diekmann D, Rhodes BA, Biersack HJ, Knapp F. F. Jr. Experimental radiotherapy of receptor-positive human prostate adenocarcinoma with ^{188}Re-RC-160, a directly-radiolabeled somatostatin analogue. *Int J Cancer* 1996; 65:214-220.

5. Reubi J-C, Schar JC, Waser B, Wenger S, Heppeler A, Schmitt JS, Mäcke HR. Affinity profiles for human somatostatin receptor subtypes SST-1-SST-5 of somatostatin radiotracers selected for scintigraphic and radiotherapeutic use. *Eur J Nucl Med* 2000; 27:273-282.

6. Anderson CJ, Pajeau TS, Edwards WB, Sherman EL, Rogers BE, Welch M. J. *In vitro* and *in vivo* evaluation of copper-64-octreotide conjugates. *J Nucl Med* 1995; 36:2315-2325.

7. Bugaj JE, Erion JL, Johnson MA, Schmidt, MA, Srinivasan, A. Radiotherapeutic efficacy of ^{153}Sm-CMDTPA-Tyr^3-octreotate in a rat tumor model, *Nuc Med Biol* 2001; 28:327-334.

8. De Jong M, Bakker WH, Krenning EP, Breeman WA, van der Pluijm ME, Bernard BF, Visser TJ, Jermann E, Behe M, Powell P, Mäcke HR. Yttrium-90 and indium-111 labelling, receptor binding and biodistribution of [DOTA^0,D-Phe^1,Tyr^3]octreotide, a promising somatostatin analogue for radionuclide therapy. *Eur J Nucl Med* 1997; 24:368-371.

9. De Jong M, Breeman WA, Bakker WH, Kooij PM, Bernard BF, Hofland LJ, Visser TJ, Srinivasan A, Schmidt MA, Erion JL, Bugaj JE, Mäcke HR, Krenning E. P. Comparison of ^{111}In-labeled somatostatin analogues for tumor scintigraphy and radionuclide therapy. *Cancer Res* 1998; 58:437-441.

10. Zamora PO, Bender H, Gulhke S, Marek MJ, Knapp RR, Rhodes BA, Biersack HJ. Pre-clinical experience with Re-188-RC-160, a radiolabeled somatostatin analog for use in peptide-targeted radiotherapy. *Anticancer Res* 1997; 17:1803-1808.

11. Erion JL, Srinivasan A, Schmidt MA, Wilhelm RR, Bugaj JE. Radiolabeled ligand-octreotate conjugates: evaluation of potential diagnostic and therapeutic radiopharmaceutical agents targeted to somatostatin receptors. *J Nucl Med* 1997; 38(supp):813.

12. De Jong M, Breeman WA, Bernard BF, Bakker WH, Scharr M, van Gameren A, Bugaj JE, Erion JL, Schmidt M, Srinivasan A, Krenning, E.P. [^{177}Lu-DOTA^{0},Tyr^{3}]Octreotate for somatostatin receptor-targeted radionuclide therapy. *Int J Cancer* 2001; 12:355-361.

13. Stolz B, Weckbecker G, Smith-Jones PM, Albert R, Raulf F, Bruns C. The somatostatin receptor-targeted radiotherapeutic [^{90}Y-DOTA-DPhe^{1},Tyr^{3}]octreotide (^{90}Y-SMT 487) eradicates experimental rat pancreatic CA20948 tumors. *Eur J Nucl Med* 1998; 25:668-674.

14. Longnecker DS, Lilja HS, French J, Kuhlmann E, Noll W. Transplantation of azaserine-induced carcinomas of pancreas in rats. *Cancer Lett* 1979; 4:197-202.

15. De Jong M, Breeman WA, Bernard BF, Kooij PM, Slooter GD, van Eijck CH, Kwekkeboom DJ, Valkema R, Mäcke HR, Krenning E. P. Therapy of neuroendocrine tumors with radiolabeled somatostatin-analogues. *Q J Nucl Med* 1999; 43:356-366.

16. Dietrich, Jean-Bernard. AR42-J Cells: A model to study polypeptide hormone receptors, *Bioscience Reports* 1996; 4:273-288.

17. Reubi J-C, Kvols L. Somatostatin receptors in human renal cell carcinomas. *Cancer Res* 1992; 52:6074-6078.

18. Akizawa Arano Y, Uezono T, Ono M, Fujioka Y, Uehara T, Yokoyama A, Akaji K, Kiso Y, Koizumi M, Saji H. Renal metabolism of ^{111}In-DTPA-DPhe^{1}-octreotide *in vivo. Bioconjugate Chem* 1998; 9:662-670.

19. Behr TM, Sharkey RM, Juweid ME, Blumenthal RD, Dunn RM, Griffiths GL, Bair H J, Wolf FG, Becker WS, Goldenberg DM. Reduction of the renal uptake of radiolabeled antibody fragments by cationic amino acids and their derivatives. *Cancer Res* 1995; 55:3825-3834.

20. Bernard BF, Krenning EP, Breeman WA, Rolleman EJ, Bakker WH, Visser TJ, Mäcke H, de Jong M. D-Lysine Reduction of Indium-111 Octreotide and Yttrium-90 Octreotide Renal Uptake, *J Nucl Med* 1996; 38:1929-1933.

21. De Jong M, Rollermann EJ, Bernard BF, Visser TJ, Bakker WH, Breeman WA, Krenning EP. Inhibition of renal uptake of indium-111-DTPA-octreotide *in vivo. J Nucl Med* 1996; 37:1388-1392.

22. Buscail L, Delesque N, Esteve J-P. Stimulation of Tyrosine Phosphatase and Inhibition of Cell Proliferation by Somatostatin Analogues: Mediation by Human Somatostatin Receptor Subtypes SSTR1 and SSTR2, *Proc Natl Acad Sci USA* 1994; 91:2315-2319.

23. Tang C, Biemond I, Verspaget HW. Offerhaus GJ, Lamers CB. Expression of Somatostatin Receptors in Human Pancreatic Tumor, *Pancreas* 1998; 17:80-84.
24. Lewis JS, Srinivasan A, Schmidt MA, Anderson CJ. *In vitro* and in vivo evaluation of ^{64}Cu-TETA-tyr^{3}-octreotate. A new somatostatin analog with improved target tissue uptake. *Nucl Med Biol* 1999; 26:267-273.

25. Breeman WA, van Hagen PM, Kwekkeboom DJ, Visser TJ, Krenning EP. Somatostatin receptor scintigraphy using [^{111}In-DTPA^{0}]RC-160 in humans: a comparison with [^{111}In-DTPA^{0}]octreotide. *Eur J Nucl Med* 1998; 25:182-186.

26. De Jong M, Breeman WA, Bernard BF, Rolleman EJ, Hofland LJ, Visser TJ, Setyono-Han B, Bakker WH, van der Pluijm ME, Krenning EP. Evaluation *in vitro* and in rats of ^{161}Tb-DTPA-octreotide, a somatostatin analogue with potential for intraoperative scanning and radiotherapy. *Eur J Nucl Med* 1995; 22:608-616.

CHAPTER 6

EFFECT OF VARYING SPECIFIC ACTIVITY ON THE BIODISTRIBUTION OF RADIOLABELED Tyr^3-OCTREOTATE IN TUMOR BEARING ANIMALS

Joseph E. Bugaj, Jack L. Erion, Michelle A. Schmidt, Ananth Srinivasan, Eric P. Krenning, Lori K. Chinen and Marion de Jong

ABSTRACT

The increased acceptance of somatostatin (sst_2) receptor scintigraphy with ^{111}In-DTPA-octreotide (OctreoScan), has now led to radiotherapy studies in early human use trials. Octreotide, when radiolabeled with In-111 using either DTPA or DOTA as the chelator, has demonstrated a bell shaped curve effect on sst_2 positive tissues in both animal models and humans. The derivative, Tyr^3-octreotate, which has demonstrated superior uptake, retention and internalization properties in sst_2 positive tissues compared to octreotide, was therefore evaluated in the CA20948 tumor bearing Lewis rat model after radiolabeling with In-111 (DTPA) and Lu-177 (DOTA) over a wide range of specific activity levels. In contrast to octreotide, no bell curve effect was observed in any sst_2 positive tissues when the agent was labeled with In-111, and when labeled with Lu-177 the only sst_2 positive organ showing this type of effect was the pancreas. Tumor uptake was largely unaffected until very low (2.5Ci/mmol) specific activity levels were reached, suggesting that a wider window of peptide to metal ratio with octreotate is possible when radiolabeling with Lu-177 for radiotherapy. Therefore, greater flexibility in peptide mass at radiolabeling exists for this agent in comparison to radiolabeled octreotide, and that very low specific activity preparations (10-100Ci/mmol) will still result in significant tumor localization. The superior biological properties and the lack of a bell curve effect on the tumor tissue support the contention that Tyr^3-octreotate is the peptide of choice when considering somatostatin receptor targeted radiotherapy.

INTRODUCTION

Scintigraphy of somatostatin positive tumors was made possible with the advent of ^{111}In-DTPA-octreotide (OctreoScan), which was introduced to the clinic in 1989 (Krenning et al., 1992; Krenning et al., 1993; Kwekkeboom et al., 1997; Kwekkeboom et al., 2000; Lamberts et al., 1991; Valkema et al., 1997). Evaluation of this compound at varying specific activity preparations in rats resulted in the unexpected biodistribution of the agent producing a bell shaped curve effect on the pancreas, pituitary and adrenal glands (Breeman et al., 1995). This effect was confirmed in human subjects bearing sst_2 positive tumors, where reduced localization of the agent was observed when the specific activity of the radiolabeled peptide injected exceeded 1600Ci/mmol (Kooij et al., 1998). This observation was contrary to the expected paradigm that receptor scintigraphy would be best performed at the highest specific activity obtainable at the time of radiolabeling (Breeman et al., 1995; de Jong et al., 1999B). This premise is predicated on the saturation effect of cold peptide on available sst_2 receptors, and implies that maximum receptor uptake would be observed at the lowest amount of peptide injected, i.e. the highest specific activity preparation injected, into the patient. The first chemical modification of octreotide (Phe^1-Phe^3) introduced a substitution of tyrosine at the third amino acid position (Phe^1->Tyr^3). This modification resulted in improved biological characteristics of the peptide including higher sst_2 receptor uptake and retention and increased sst_2 internalization over the original sequence (de Jong et al., 1997; Hofland et al., 1995). This new analogue has also been derivatized with the DOTA ligand (Figure 1) to allow for labeling with the radionuclides In-111 and Y-90 at therapeutic levels (de Jong et al., 1997; Otte et al., 1997; Otte et al., 1999). These two radionuclides offer the possibility of radiotherapy utilizing the high-energy beta particle emission from Y-90 or the Auger electron emissions of In-111 (Andersson et al., 1996; de Jong et al.,

1999A; Duncan et al., 1993). The ^{111}In-DOTA analogue was further evaluated in tumor bearing rats and also demonstrated a similar bell curve effect, indicating that maximum uptake, especially at the tumor site, was not achieved at the highest specific activity tested (de Jong et al., 1999B). This observation (in rats) suggests that the success of radionuclide therapy with Tyr^3-octreotide could be compromised if the ideal peptide to metal ratio is not achieved at the time of radiolabeling. A second implication is that the results of the radiotherapy could be quite variable if the specific activity of the therapeutic preparation is not carefully regulated.

The recent discovery of Tyr^3-octreotate, in which the C-terminal threonine has been retained as the native carboxylic acid as opposed to modification to the alcohol form, threonineol, has demonstrated superior uptake and retention in sst_2 positive tissues in several animal models (Bugaj et al., 2001; Bugaj et al., 2002; de Jong et al., 1998; de Jong et al., 2001; Erion et al., 1997). The agent has also demonstrated improved biological characteristics including increased sst_2 internalization, faster blood clearance and reduced kidney retention. This molecule has been derivatized with the metal chelator, DOTA, using standard solid-phase peptide synthesis methods enabling the facile radiolabeling with Lu-177 (Figure 1). Therapy studies in tumor bearing Lewis rats (CA20948 and AR42-J) have shown that this compound is a potent radiotherapeutic agent resulting in complete remission of tumor growth in the CA20948 Lewis model, and significant suppression of tumor growth in the AR42-J animal model (Bugaj et al., 2002; de Jong et al., 2001; Erion et al., 1997). The radiotherapeutic potential observed with ^{177}Lu-DOTA-Tyr^3-octreotate in these animal models suggests that this compound would be a promising candidate molecule for targeted radiotherapy of sst_2 positive tumors in humans. As the human and animal data with octreotide indicate a mass dependent uptake resulting in an optimum

peptide dose to achieve maximum sst_2 receptor uptake, we investigated the effect of varying the specific activity of Tyr^3-octreotate. We evaluated this agent radiolabeled with both ^{111}In-DTPA and ^{177}Lu-DOTA (Figure 1) over a wide range of specific activity levels in CA20948 tumor bearing Lewis rats to determine if a mass dependent peptide to metal ratio exists for either of these two derivatives on sst_2 receptor positive tissues.

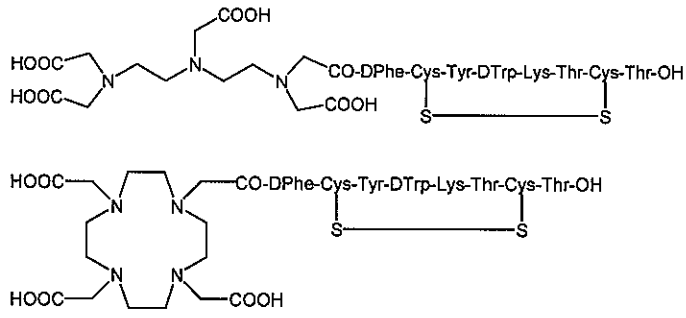

Figure 1: Structures of DTPA-Tyr^3-Octreotate and DOTA-Tyr^3-Octreotate

MATERIAL AND METHODS

Radiochemistry

The preparation of both ^{111}In-DTPA-Tyr^3-octreotate and ^{177}Lu-DOTA-Tyr^3-octreotate has been described previously in detail (de Jong et al., 1998; Erion et al., 1997). The In-111 was supplied by Mallinckrodt Inc. at a specific activity of 10,000Ci/mmol, and the Lu-177 was supplied by MURR at a specific activity of ~3000Ci/mmol. For these labeling studies the highest specific activity preparations were prepared first, and the corresponding lower specific activity preparations prepared by dilution with cold Tyr^3-octreotate to the desired specific activity. The labeling reactions were performed at room temperature for the In-111 preparation and at 80^0 C for the Lu-177 preparation. The reactions were carried out in 50mM NaOAC, 25mM NaAscorbate at a pH of 5.5.

Radiochemical yields (>99.5%) and radiochemical purities (>98%) were determined by reverse phase chromatography on an Alltech Adsorboshere C-18 column using acetonitrile/0.1%TFA gradient (20% to 95% ACN) over a 25 minute time span at 1.0ml/minute. Animal doses were prepared to deliver a constant quantity of radioactivity (25μCi ± 1μCi) per injection. The specific activity levels in Ci/mmol for the evaluation of ^{111}In-DTPA-Tyr^3-octreotate were 5600, 1400, 375, 175, 91, 35, 7.1, 1.4 and 0.10, and the specific activity levels in Ci/mmol for the evaluation of ^{177}Lu-DOTA-Tyr^3-octreotate were 2500, 700, 90, 9.0, 2.5, 1.0, 0.25 and 0.10 (Table 1).

Table 1: Specific Activity Study in CA20948 Tumor Bearing Lewis Rats

^{111}In-DTPA-Y^3-Octreotate		^{177}Lu-DOTA-Y^3-Octreotate	
SA Ci/mmol	∝g Peptide/Rat	SA Ci/mmol	μgPeptide/Rat
5600	0.006	2500	0.014
1432	0.023	657	0.049
375	0.090	88	0.370
175	0.200	9.0	3.60
91	0.380	2.5	14.4
35	1.00	1.0	35.9
7.1	5.00	0.24	144
1.4	25.0	0.10	359
0.10	358		

Animal Tumor Model

All animal studies were conducted in compliance with the Mallinckrodt Inc. Animal Welfare Committee requirements. Male Lewis rats (120-140 g) were purchased from Harlan (Indianapolis, IN). The somatostatin subtype-2 (sst_2) receptor positive acinar tumor line, CA20948, was maintained by serial passage in Lewis rats (Bugaj et al., 2001; Bugaj et al., 2002; de Jong et al., 1997; de Jong et al., 1998). Tumor tissue was implanted into the left flank area of the recipient animals, and after approximately 10-12 days tumor volumes were adequate for use in the biodistribution studies.

Tissue Distribution Studies

Biodistribution studies were carried out in male Lewis rats bearing CA20948 flank tumors (10-12 days post implant). Anesthetized (Halothane) animals received a dose of 25µl containing a constant amount of 25µCi (±1µCi) of either In-111 or Lu-177 of the radiolabeled Tyr^3-octreotate. The animals were sacrificed at three hours post injection (n = 3/group) by cervical dislocation. The selected tissues were removed, weighed and radioactivity measured in a Packard Cobra gamma-scintillation counter.

Gamma scintigraphy was performed using a Picker 300 SX gamma camera interfaced to a dedicated Odyssey Imaging Processor. The images were obtained with a large field of view camera fitted with a medium energy collimator, and the peak energies were centered at 171 and 245 keV for In-111. No scintigraphy was performed on the animals injected with the ^{177}Lu-DOTA-Tyr^3-octreotate. All rats were imaged in the prone position (Figure 5).

RESULTS

Table 2 and Figure 2A present the tissue distribution of ^{111}In-DTPA-Tyr^3-octreotate in CA20948 tumor bearing Lewis rats 3 hours post injection at the different specific activities evaluated. The data are expressed as percent injected dose per gram of tissue (% ID/gram). The non-somatostatin receptor expressing tissues of the blood, liver, muscle and spleen are virtually unaffected by the variance in the specific activities evaluated. Uptake in the sst_2 positive tissues of the pancreas and tumor remained relatively constant from 5600Ci/mmol to 35Ci/mmol. From 7.1Ci/mmol down to 0.10Ci/mmol there was a significant decrease in uptake until >95% saturation was achieved at the lowest specific activity evaluated. The other sst_2

receptor positive tissue, the adrenal glands, indicated a similar pattern of uptake but with greater variability compared to the pancreas or tumor values.

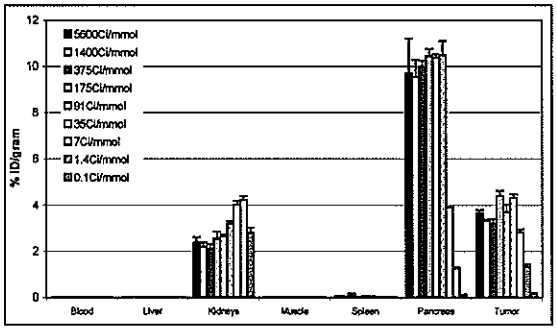

Figure 2A: Biodistribution of ^{111}In-DTPA-Tyr^3-Octreotate in CA20948 tumor beraing Lewis rats.

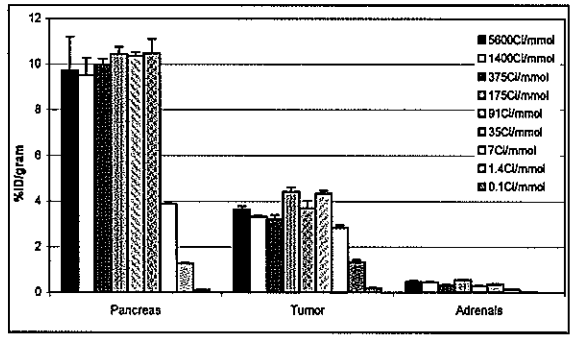

Figure 3A: Biodistribution of ^{111}In-DTPA-Tyr^3-Octreotate in three sst_2 positive tissues of the pancreas, tumor and adrenals.

None of the sst_2 positive tissues evaluated indicated a distinct bell shaped curve effect as a function of specific activity as reported for either the DTPA or DOTA derivative of octreotide. The kidneys indicated an increase in non-specific uptake of the agent as the specific activity decreased in response to elevated circulating levels of cold peptide. Figure 3A represents the uptake for the three different sst_2 receptor positive tissues as a function of decreasing specific activity. The lack of a bell curve effect on any of these tissues is readily apparent, especially for the tumor, which shows only a slight variance in uptake until the specific activity reaches the low level of 1.4Ci/mmol. Figure 4A further depicts the same tissues graphed as a log function of increasing specific activity. Both the pancreas and tumor show no significant difference in uptake from 35Ci/mmol to the maximum specific activity evaluated at 5600Ci/mmol. The adrenal uptake also shows no difference in uptake beginning at 35Ci/mmol, with the exception of a spike in uptake at 175Ci/mmol, which is

statistically significant ($p<0.05$) compared to the other data points. With this lone exception, the adrenal uptake follows a similar pattern observed for the pancreas and tumor tissues.

Figure 5 shows the images of the rats injected with 25μCi of ^{111}In-DTPA-Tyr^3-octreotate at the difference specific activities listed. The images show intense uptake of the label in the tumor and pancreas tissues from 5600Ci/mmol down to 35Ci/mmol. Kidney uptake is obscured by the pancreatic uptake at specific activities form 5600Ci/mmol to 35Ci/mmol, at which time the diminished pancreatic uptake allows for clear visualization of the kidney structure. Both tumor and pancreas uptake diminish noticeably beginning at 7.0Ci/mmol and decreases until saturation at 0.1Ci/mmol. Animals injected with ^{177}Lu-DOTA-Tyr^3-octreotate were not imaged.

Table 2: Biodistribution of ^{111}In-DTPA-Tyr^3-Octreotate at Varying SA in Ci/mmol (% ID/gram)

Tissue	5600	1400	375	175	90
Blood	0.016±0.002	0.014±0.002	0.019±0.002	0.011±0.001	0.016±0.002
Liver	0.025±0.002	0.025±0.003	0.025±0.001	0.024±0.002	0.027±0.001
Kidneys	2.370±0.242	2.203±0.172	2.113±0.194	2.535±0.313	2.644±0.090
Muscle	0.007±0.001	0.006±0.000	0.006±0.000	0.006±0.000	0.007±0.000
Spleen	0.048±0.014	0.037±0.007	0.132±0.034	0.033±0.003	0.044±0.016
Pancreas	9.725±1.471	9.531±0.737	9.977±0.253	10.45±0.325	10.37±0.157
Adrenals	0.470±0.039	0.438±0.040	0.314±0.053	0.540±0.036	0.280±0.045
Tumor	3.650±0.137	3.332±0.053	3.217±0.185	4.413±0.201	3.700±0.321

Tissue	35	7.0	1.4	0.10
Blood	0.011±0.001	0.009±0.000	0.009±0.001	0.017±0.003
Liver	0.028±0.001	0.027±0.001	0.034±0.002	0.028±0.003
Kidneys	3.191±0.112	4.003±0.186	4.219±0.172	2.796±0.223
Muscle	0.007±0.001	0.007±0.000	0.007±0.000	0.007±0.001
Spleen	0.038±0.010	0.021±0.000	0.022±0.003	0.022±0.003
Pancreas	10.47±0.615	3.884±0.023	1.262±0.046	0.114±0.016
Adrenals	0.358±0.026	0.136±0.004	0.041±0.002	0.002±0.000
Tumor	4.333±0.131	2.835±0.122	1.323±0.109	0.181±0.022

Table 3 and Figure 2B represent the tissue distribution of ^{177}Lu-DOTA-Tyr^3-octreotate in CA20948 tumor bearing Lewis rats 3 hours post injection at the different specific activities noted. The data are normalized as percent injected dose per gram of tissue. As observed with the ^{111}In-DTPA analogue, the non-somatostatin tissues of the blood, liver, muscle and spleen were unaffected by the difference in the specific activity, and none of these tissues indicated any significant accumulation of the agent. The sst_2 positive tissues of the tumor and adrenal glands showed a constant uptake of the agent from 2500Ci/mmol to 100Ci/mmol. From 10Ci/mmol down to 0.10Ci/mmol there was a steady decrease in uptake as a function of decreasing specific activity until >95% saturation of that tissue was reached at the lowest level evaluated.

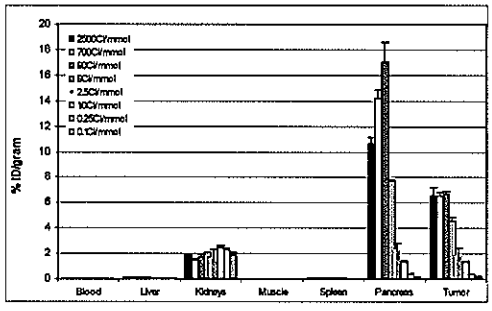

Figure 2B: Biodistribution of ^{177}Lu-DOTA-Tyr^3-octreotate in tumor bearing Lewis rats at specific activities outlined in text.

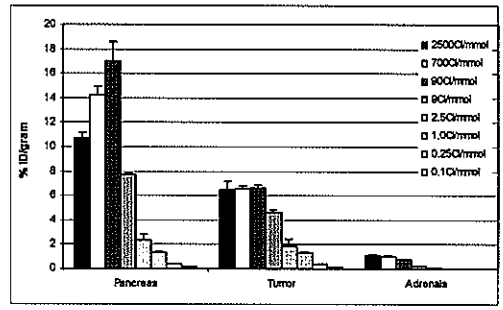

Figure 3B: Biodistribution of ^{177}Lu-DOTA-Tyr^3-octreotate in three sst_2 positive tissues of the pancreas, tumor and adrenals.

Table 3: Biodistribution of ^{177}Lu-DOTA-Y^3-Octreotate at Varying SA in Ci/mmol (% ID/gram)

Tissue	2500	700	90	9.0
Blood	0.007±0.001	0.008±0.000	0.008±0.001	0.007±0.000
Liver	0.110±0.210	0.107±0.008	0.146±0.021	0.117±0.024
Kidneys	1.778±0.088	1.496±0.046	1.744±0.183	2.057±0.050
Muscle	0.005±0.001	0.005±0.000	0.005±0.000	0.004±0.001
Spleen	0.074±0.003	0.077±0.012	0.067±0.015	0.064±0.009
Pancreas	10.69±0.514	14.20±0.707	16.99±1.614	7.752±0.065
Adrenals	1.120±0.087	1.043±0.034	0.757±0.023	0.216±0.004
Tumor	6.511±0.695	6.570±0.249	6.678±0.229	4.069±0.203

Tissue	2.5	1.0	0.25	0.10
Blood	0.008±0.001	0.006±0.000	0.007±0.001	0.005±0.001
Liver	0.111±0.003	0.089±0.002	0.086±0.006	0.067±0.013
Kidneys	2.319±0.140	2.418±0.167	2.278±0.069	1.824±0.260
Muscle	0.005±0.001	0.004±0.000	0.004±0.000	0.003±0.001
Spleen	0.078±0.030	0.039±0.004	0.034±0.001	0.030±0.006
Pancreas	2.793±0.187	1.319±0.099	0.391±0.019	0.156±0.003
Adrenals	0.081±0.001	0.036±0.000	0.012±0.001	0.004±0.000
Tumor	2.428±0.087	1.340±0.053	0.370±0.020	0.180±0.012

For these two tissues no evidence of a bell curve effect was noted. The pancreas was the only sst_2 positive tissue that exhibited a bell curve effect observed with Tyr^3-octreotate. Highest uptake was observed at 100Ci/mmol ($p<0.05$). The uptake steadily increased from 2500Ci/mmol (10.7% ID/g) with maximum uptake at 100Ci/mmol (17.0% ID/g), then declining proportionately from 10Ci/mmol to >95% saturation at 0.10Ci/mmol. Figures 3B and 4B represent the uptake of ^{177}Lu-DOTA-Tyr^3-Octreotate in the sst_2 positive tissues as depicted previously for the In-111 DTPA analogue. Figure 3B indicates that the uptake in the tumor and adrenals remains very constant from 2500Ci/mmol to 100Ci/mmol, after which a steady decline to >95% saturation is achieved at 0.10Ci/mmol. The graph also indicates the only sst_2 positive tissue, the pancreas, to show a bell curve effect observed in this study. Maximum uptake for this organ is reached at 100Ci/mmol (17%ID/gram), then declines to >95% saturation at 0.10Ci/mmol. Figure 4B graphically represents the data as a log function of increasing specific activity, clearly showing the constant uptake for both the adrenals and tumor beginning at 100Ci/mmol through 2500Ci/mmol. The bell curve effect noted for the pancreas is readily observed in this format at 100Ci/mmol.

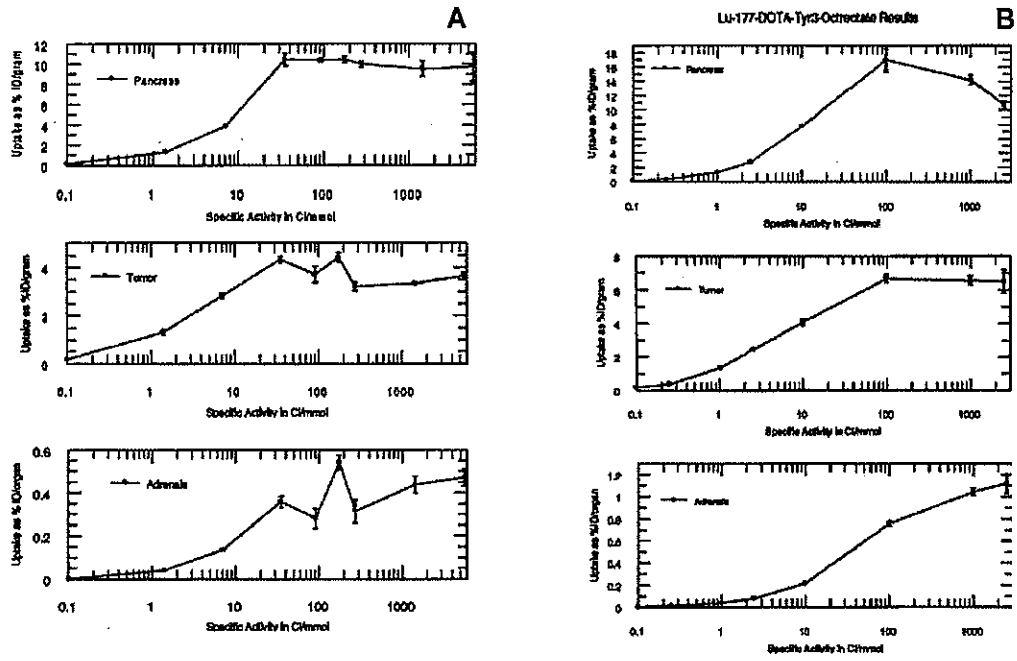

Figure 4: Uptake of ^{111}In-DTPA-Y^3-Octreotate and ^{177}Lu-DOTA-Y^3-Octreotate in sst$_2$ positive tissues of the pancreas, tumor and adrenals, as a log function of increasing specific activity in Ci/mmol. Panel **A**: ^{111}In-DTPA-Y^3-Octreotate; Panel **B**: ^{177}Lu-DOTA-Y^3-Octreotate.

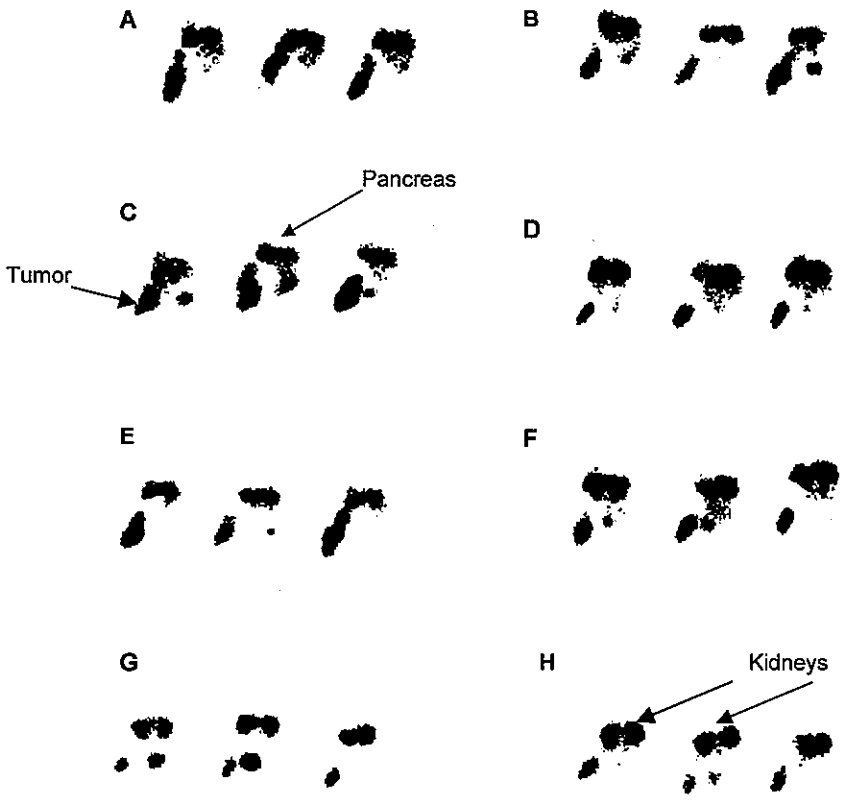

Figure 5:

Scintigraphs of injected rats with 25µCi of ^{111}In-DTPA-Tyr^3-octreotate at different specific activities.

A: 5600Ci/mmol, **B**: 1400Ci/mmol, **C**:375Ci/mmol, **D**: 175Ci/mmol, **E**: 90Ci/mmol, **F**: 35Ci/mmol, **G**: 7.0Ci/mmol, **H**: 1.4Ci/mmol

DISCUSSION

Successful therapy of sst_2 positive tumors using radiolabeled peptides will be highly dependent upon maximizing uptake and retention of these agents at the tumor sites. Treatment of neuroendocrine tumors has been reported using Tyr^3-octreotide radiolabeled with either In-111 or Y-90 (de Jong et al., 1999A; Kwekkeboom et al., 2000; Otte et al., 1997; Otte et al., 1999). To date objective responses have been observed with the In-111 chelate after injection of up to 3.0 Ci of activity per patient (Valkema et al., 2002). Treatment with the ^{90}Y-DOTA analogue has also resulted in >20% objective response in terms of partial or complete response to radiotherapy (Chinol et al., 2002). The ^{90}Y-DOTA-octreotide studies do require the infusion of amino acids to renal toxicity associated with Y-90.

The recent discovery of ^{177}Lu-DOTA-Tyr^3-octreotate as a radiotherapeutic agent has demonstrated superior therapeutic potential in several animal models compared to radiolabeled octreotide (de Jong et al., 2001; Erion et al., 1997). This peptide has shown to have greater uptake and retention in sst_2 positive tumors, and improved biological properties including faster blood clearance and reduced renal uptake (de Jong et al., 1998; Erion et al., 1997). The radionuclide Lu-177 has improved properties over Y-90, Re-188, In-111 and Sm-153. The low β^- emission (497 keV_{emax}), longer $t_{1/2}$ (6.7 d) and high radiospecific activity (>3000Ci/mmol) make this radionuclide an ideal candidate for radionuclide therapy. Additionally, Lu-177 possesses a low energy gamma emission (11%, 208 keV) that is very suitable for scintigraphy and allows for a convenient tracer emission for performing dosimetry calculations (Erion et al., 1997). Since it is a reactor product this radionuclide

presents additional advantages with regard to cost, scalability and availability over radioisotopes produced by other methods.

The studies presented here demonstrate that sst_2 receptor uptake at the tumor site is not affected by a large variance in specific activity when Tyr^3-octreotate is radiolabeled with either In-111 (DTPA) or Lu-177 (DOTA). This represents a distinct advantage over octreotide derivatives, which require optimization of the specific activity in order to maximize tumor uptake (Breeman et al., 1995; Breeman et al., 1996; Breeman et al., 1997; de Jong et al., 1999B). Therefore, in animal studies, the success of receptor-targeted radiotherapy with octreotide requires stricter manipulation of the radiolabeling conditions in order to achieve maximum therapeutic effect of the agent. Tyr^3-octreotate is not as limited by these parameters, and as the rat tumor model indicates, even very low specific activity preparations (10-100Ci/mmol) will result in significantly higher uptake and internalization of the complex compared to octreotide. Optimization of the specific activity at the time of initial radiolabeling is not necessary for the octreotate derivatives, and therefore, the likelihood of successful radiotherapy is increased with this peptide. When radiolabeled with In-111, DTPA-Tyr^3-octreotate showed no evidence of a bell curve effect on the sst_2 positive tissues of the pancreas, adrenal glands or the tumor. When radiolabeled with Lu-177 (DOTA) only the pancreas demonstrated this type of effect as observed with octreotide. It is hypothesized that the increased internalization rate for octreotate compared to octreotide results in a more uniform uptake of the peptide by the receptors thereby negating any influence of peptide mass at the receptor site. The effect of specific activity at the receptor site would be more pronounced with a peptide with a slower internalization rate, compared to peptides that internalize very rapidly (Andersson et al., 1996; Hofland et al., 1995). Precedent for this hypothesis

exists from the observations of Breeman in that the specific activity effect on sst_2 positive tissues is less pronounced for Tyr^3-octreotide than for Phe^3-octreotide (de Jong et al., 1999B). In this case greater affinity for the sst_2 receptor and an increased internalization rate of the Tyr^3 derivative are cited as the primary contributing factors for the difference between the two derivatives.

The lone exception to the lack of a bell curve effect with octreotate was observed with ^{177}Lu-DOTA complex on the pancreas. Here it can be argued that other factors such as increased sst_2 receptor density and receptor clustering specifically for the pancreas can contribute to this difference in uptake as a function of peptide mass present (de Jong et al., 1999B). There is also the possibility that the difference can be attributed in part to the lutetium metal compared to indium incorporated in the chelate. Effect on uptake at the sst_2 receptor sites as a function of the metal chelate has been reported by Reubi et al., in which the binding affinity of different octreotide and octreotate ligands varied considerably as a result of structural modifications, chelate substitution and metal replacement (Reubi et al., 2000).

Conclusion

The success of consistent and effective radiotherapy in humans would be best achieved if tumor uptake of the labeled complex is largely unaffected by specific activity. If maximum tumor uptake is highly dependent on the peptide mass effect at the time of radiolabeling, large variance in the resulting specific activity of the preparations could result in sub-optimal tumor uptake, thereby limiting the desired radiotherapeutic index (Kooij et al., 1998). Derivatives of octreotide radiolabeled with In-111 (DTPA or DOTA) have demonstrated this limiting effect on tumor uptake in both rats and humans, and therefore, additional control at the initial time of

preparation carefully regulating the final specific activity is required (Breeman et al., 1995; Breeman et al., 1996; de Jong et al., 1999B). In contrast, when radiolabeled with either In-111 or Lu-177 Tyr^3-octreotate demonstrates essentially no bell curve effect on these tissues until near receptor saturation levels (~1.0Ci/mmol). Even at low specific activity preparations of ~100-10Ci/mmol, the studies presented here show that significant tumor uptake is achieved, and that this uptake is largely unaffected at specific activity levels from 10Ci/mmol to 2500-5600Ci/mmol, depending upon the radionuclide used. These data suggest that consistent and more successful radiotherapy would be predicted from the use of Tyr^3-octreotate as the radiolabeled peptide in targeting the sst_2 receptors on neuroendocrine tumors.

REFERENCES

1. Andersson, P., Forssell-Aronsson, E., Johanson, V., Wangberg, B., Nilsson, O., Fjalling, M. and Ahlman, H., Internalization of Indium-111 into Human Neuroendocrine Tumor Cells after Incubation with Indium-111-DTPA-D-Phe1-Octreotide, *J Nucl Med*, 37, 2002-2006, (1996)

2. Breeman, W.A., Kwekkeboom, D.J., Kooij, P.P. Bakker, W.H., Hofland, L.J., Visser, T.J., Ensing, G.J., Lamberts, W.J., and Krenning, E.P., Effects of Dose and Specific Activity on Tissue Distribution of Indium-111-Pentreotide in Rats, *J Nucl Med*, 36, 623-627, (1995)

3. Breeman, W.A., Bakker, W.H., de Jong, M., Hofland, L.J., Kwekkeboom, D.J., Kooij, P.P., Visser, T.J., and Krenning, E.P., Studies on radiolabeled somatostatin analogues in rats and patients, *Q J Nucl Med*, 40, 209-220, (1996)

4. Breeman, W.A, de Jong, M., Bernard, B.F., Bakker, W.H., Rolleman, E.J., Kwekkeboom, D.J., Visser, T.J., and Krenning, E.P., Effects of Ligand Priming and Multiple-Dose Injection on Tissue Uptake of ^{111}In-Pentetreotide in Rats, *Nucl Med Biol*, 24, 749-753, (1997)

5. Bugaj, J. E., Erion, J.L., Johnson, M.A., Schmidt, M.A., and Srinivasan, A., Radiotherapeutic Efficacy of ^{153}Sm-CMDTPA-Tyr^3-Octreotate in a Rat Tumor Model, *Nucl Med Biol*, 28, 327-334, (2001)

6. Bugaj, J.E., Erion, J.L., Johnson, M.A., and de Jong, M., Radiotherapeutic Efficacy of ^{177}Lu-DOTA-Tyr^3-Octreotate in Novel Rat Tumor Models, *Submitted: EJ Nucl Med*, (2002)

7. Chinol, M., Bodei, L., Cremonesi, M. and Paganelli, G., Receptor Mediated Radiotherapy with ^{90}Y-DOTA-(D)Phe^1-Tyr^3-octreotide: The Experience of the European Institute of Oncology Group, *Seminars in Nucl Med*, 2, 141-147, (2002)

8. De Jong, M., Bakker, W.H., Krenning, E.P., Breeman, W.A., van der Pluijm, M.E., Bernard, B.F., Visser, T.J., Jermann, E., Behe, M., Powell, P., and Macke, H.R., Yttrium-90 and indium-111 labelling, receptor binding and biodistribution of [DOTA^0,D-Phe^1,Tyr^3]octreotide, a promising somatostatin analogue for radionuclide therapy, *E J Nucl Med*, 24, 368-371, (1997)

9. De Jong, M., Breeman, W.A., Bakker, W.H., Kooij, P.P., Bernard, B.F., Hofland, L.J., Visser, T.J., Srinivasan, A., Schmidt, M.A., Erion, J.L., Bugaj, J.E., Macke, H.R. and Krenning, E.P., Comparison of ^{111}In-labeled Somatostatin Analogues for Tumor Scintigraphy and Radionuclide Therapy, *Cancer Research*, 58, 437-441, (1998)

10. De Jong, M., Breeman, W.A., Bernard, B.F., Kooij, P.P., Slooter, G.D., Van Eijck, C.H., Kwekkeboom, D.J., Valkema, R., Macke, H.R., and Krenning, E.P., Therapy of neuroendocrine tumors with radiolabeled somatostatin-analogues, Q *J Nucl Med*, 43, 356-366, (1999A)

11. De Jong, M., Breeman, W.A., Bernard, B.F., van Gameren, A., de Bruin, Elisa, Bakker, W.H., van der Pluijm, M.E., Visser, T.J., Macke, H.R., and Krenning, E.P., Tumor uptake of the radiolabelled somatostatin analogue [DOTA^0,Tyr^3]octreotide is dependent on the peptide amount, *E J Nucl* Med, 26, 693-698, (1999B)

12. De Jong, M., Breeman, W.A., Bernard, H.F., Bakker, W.H., Schaar, M., van Gameren, A., Bugaj, Erion, J., J., Schmidt, M., Srinivasan, A., and Krenning, E.P., [^{177}Lu-DOTA^0,Tyr^3]Octreotate for Somatostatin Receptor-Targeted Radionuclide Therapy, *I J Cancer*, 92,628-633 (2001)

13. Duncan, J.R, and Welch, M.J., Intracellular Metabolism of Indium-111-DTPA-Labeled Receptor Targeted Proteins, *J Nucl Med*, 34, 1728-1738, (1993)

14. Erion, J.L., Srinivasan, A., Schmidt, M.A., Wilhelm, R.R., and Bugaj, J.E., Radiolabeled ligand-octreotate conjugates: evaluation of potential diagnostic and therapeutic radiopharmaceutical agents targeted to somatostatin receptors, *J Nucl Med*, 38(supp), 813, (1997)

15. Hofland, L.J., van Koetsveld, P.M., Waaijers, m., Zuyderwijk, J., Breeman, W.A., and Lamberts, W.J., Internalization of the Radioiodinated Somatostatin Analog [^{125}I-Tyr^3]Octreotide by Mouse and Human Pituitary Tumor Cells: Increase by Unlabeled Octreotide, *Endocrinology*, 136, 3698-3706, (1995)

16. Krenning, E.P., Bakker, W.H., Kooij, P.P., Breeman, W.A., Oei, H.Y., de Jong, M., Reubi, J-C., Visser, T.J., Bruns, C., ., Kwekkeboom, D.J., Reijs, A.E., van Hagen, P.M., Koper, J.W., and Lamberts, W.J., Somatostatin Receptor Scintigraphy with Indium-111-DTPA-D-Phe^1-Octreotide in Man: Metabolism, Dosimetry and Comparison with ^{123}Iodine-Tyr^3-Octreotide, *J Nucl Med*, 33, 652-658, (1992)

17. Krenning, E.P., Kwekkeboom, D.J., Bakker, W.H., Breeman, W.A., Kooij, P.P. Oei, H.Y., van Hagen, P.M., Postema, P.T., de Jong, M., Reubi, J-C., Visser, T.J., Reijs, A.E., Hofland, L.J., Koper, J.W. and Lamberts, S.J., Somatostatin receptor scintigraphy with [^{111}In-DTPA-D-Phe^1]-and [^{123}I-Tyr^3]-Octreotide: the Rotterdam experience with more than 1000patients, *E J Nucl Med*, 20, 716-731, (1993)

18. Kooij, P.P., Kwekkeboom, D.J., Breeman, W.A., Reijs, A.E., Bakker, W.H., Lamberts, S.W., Visser, T.J., and Krenning, E.P., The Effects of [I-111-DTPA-D-Phe^1]-Octreotide In Humans, *J Nucl Med*, 38, 226P(supp), (1998)

19. Kwekkeboom, D.J., and Krenning, E.P., Radiolabeled somatostatin analog scintigraphy in oncology and immune diseases:an overview, *Eur Radiol*, 7, 1103-1109, (1997)

20. Kwekkeboom, D.J., Krenning, E.P., and de Jong, M., Peptide Receptor Imaging and Therapy, *J Nucl Med*, 41, 1704-1713, (2000)

21. Lamberts, W.J., Krenning, E.P., and Reubi, J-C., The Role of Somatostatin and Its Analogs in the Diagnosis and Treatment of Tumors, *Endocrine Reviews*, 12, 450-482, (1991)

22. Otte, A., Jermann, E., Behe, M., Goetze, M., Bucher, H.C., Roser, H.W., Heppeler, A., Mueller-Brand, J., and Macke, H.R., DOTATOC: a powerful new tool for receptor-mediated radionuclide therapy, *E J Nucl Med*, 24, 792-795, (1997)

23. Otte, A., Hermann, R., Heppeler, A., Behe, M., Jermann, E., Powell, P., Macke, H.R. and Mueller, J., Yttrium-90 DOTATOC: first clinical results, *E J Nucl Med*, 26, 1439-1447, (1999)

24. Reubi, J-C., Schar, J-C., Waser, B., Wenger, S., Heppeler, A., Schmitt, J.S., and Macke, H.R., Affinity profiles of human somatostatin receptor subtypes SST1-SST5 of somatostatin radiotracers selected for scintigraphic and radiotherapeutic use, *E J Nucl Med*, 27, 273-282, (2000)

25. Valkema, R., Steens, J., Cleton, F.J., and Pauwels, E.K., The diagnostic utility of somatostatin receptor scintigraphy in oncology, *J Cancer Res Clin Oncology*, 122, 513-532, (1996)

26. Valkema, R., de Jong, M., Bakker, W.H., Breeman, W.A., Kooij, P.P., Lugtenburg, P.J., de Jong, F.H., Christansen, A., Kam, B., de Herder, W.W., Stridsberg, M., Lindemans, J., ensing, G. and Krenning, E.P., Phase I Study of Peptide Receptor Radionuclide Therapy with [^{111}In-DTPA^{0}]Octreotide: The Rotterdam Experience, *Seminars in Nucl Med*, 2, 110-122 (2002)

CHAPTER 7

TRANSFECTION OF THE RAT TUMOR LINE MAT-B WITH THE $hsst_2$ RECEPTOR FOR THE EVALUATION OF RADIOLABELED SOMATOSTATIN ANALOGUES

Joseph E. Bugaj, Jack L. Erion, Michael A. Johnson, H. Bert Bernard, Eric P. Krenning and Marion de Jong

ABSTRACT

Somatostatin (sst) receptors are expressed on a number of human tumors of neuroendocrine origin. These include pancreatic (neuroendocrine), gliomas, astrocytomas and certain lymphomas. Currently, five somatostatin subtypes (sst_{1-5}) have been identified and cloned. Development of somatostatin subtype specific radiopharmaceuticals would be an important advancement for diagnostic and therapeutic agents that target these specific subtypes. The expression of the different subtypes in tumor bearing animal models would contribute significantly to the pre-clinical development of these agents.

A DNA fragment coding for the human somatostatin subtype-2 receptor ($hsst_2$) was ligated into an expression vector designed to express the gene in either bacterial or mammalian cells (pcDNA3.1). The plasmid construct ($pchSSTR_2$) was transformed into *E. coli* and a single bacterial colony containing the plasmid was isolated. The plasmid was further isolated from a large-scale bacterial culture, purified and then transferred into the Chinese hamster ovary (CHO-K1) mammalian cell line. Clones were selected using G418 drug selective pressure techniques, and were shown to be positive for the uptake of the somatostatin analogue ^{111}In-DTPA-Octreotide. The plasmid was then transfected into the mammalian cell line, Mat-B, a rat mammary adenocarcinoma. Following selective drug pressure (G418), a single clone (Mat-B/$hsst_2$d) was isolated and shown to express a high level of $hsst_2$ receptors in a cell-binding assay. Mat-B cells transfected with the $pchSSTR_2$ clone and wild type Mat-B cells (negative control cells) were injected into female Fischer 344 rats. Eight days post injection tumor growth was noted in all animals. Animals that received the sst_2 positive clone demonstrated a >50 fold increase in the uptake of ^{111}In-DTPA-Tyr^3-octreotate compared to the animals injected with the wild type Mat-B cells.

Radiotherapy was performed on animals expressing the positive clone (Mat-B/hsst$_2$d) by treatment with ^{177}Lu-DOTA-Tyr^3-octreotate. Animals that received a therapeutic dosing regimen of 2 x 5.0mCi of ^{177}Lu-DOTA-Tyr^3-octreotate at 5 day intervals indicated a reduced growth rate of the tumor volume ($p < 0.05$). Tumor growth was significantly delayed in the treated animals compared to untreated controls. This novel *in vivo* sst$_2$ expression system demonstrates that tumor-bearing animals that are normally negative for the expression of a given receptor can be made to express foreign receptors in high number. These genetically modified tumor lines can be induced in suitable rodent animal models for the pre-clinical evaluation of potentially new diagnostic and therapeutic radiopharmaceuticals.

INTRODUCTION

The somatostatin receptor (sst) is a member of a family of proteins known as G-coupled protein receptors. Currently, five different subtypes (sst$_{1-5}$) have been identified on human tumors, and all 5 subtypes have been cloned, sequenced and expressed in different mammalian cell lines (Breeman et al., 1996; de Jong et al., 1999; Boerman et al., 2000). The somatostatin subtype-2 receptor (sst$_2$) is the most characterized of the 5 subtypes. The introduction of OctreoScan as a diagnostic agent targeted to this receptor in 1994 has led to a number of other analogues that target this subtype (Krenning et al., 1993; Krenning et al., 1994). A number of other somatostatin analogues have since been evaluated in several tumor bearing animal models as potential diagnostic and therapeutic agents targeted to neuroendocrine tumors. These agents now include chelation with a variety of beta emitting radionuclides (Y-90, Re-188, Sm-153 and Lu-177) that are used to ablate tumors that express this subtype. The nanomolar affinity of these analogues for the sst$_2$ receptor have led to impressive pre-clinical therapy results in animal models bearing CA20948

and AR42-J tumor cells (Zamora et al., 1997; Stolz et al., 1998; de Jong et al., 1998, de Jong et.al, 1999; Erion et al., 1999; Bugaj et al., 2002).

Native somatostatin (sst_{28}) is a peptide hormone whose main function is the inhibition of secretion of other hormones including insulin, glucagon and gastrin, and also acts as a neurotransmitter in the brain (Brezeau et al.,1982; Breeman et al., 1996; Boerman et al., 2000). The truncated form of sst_{28} somatostatin-14 (sst_{14}) is produced by degradation of native somatostatin, and its natural inhibitory effect on hormone production led to the development of this peptide as a potential therapeutic agent for neuroendocrine tumors including pituitary adenomas and gastroenteropancreatic origin (Fishman et al., 1993; Breeman et al., 1996). Both sst_{28} and sst_{14} demonstrate high affinity (1-6nm) for all five receptor subtypes. However, both forms of the peptide are highly unstable to serum proteases *in vivo* ($t_{1/2}$ ~3 minutes) which limited their clinical applications severely. As a result, an eight amino acid derivative, octreotide, was developed that is more resistant to enzymatic degradation *in vivo*. This octapeptide was shown to have high affinity for sst_2 (0.4nm), and sst_5 (7nm), and to a lesser degree sst_3 (35nm). *In vivo* blocking studies using cold peptide confirmed that the compound is sst_2 receptor specific. It does not bind to either sst_1 or sst_4 (>1000nm). The peptide was derivatized with the chelate DTPA, and labeled with the radionuclide In-111, resulting in the agent OctreoScan, that is now widely accepted as the gold standard for scintigraphy of sst_2 positive tumors in humans (Breeman et al., 1996; Krenning et al., 1993; Krenning et al., 1994; Reubi et al., 2000). Since then, a number of octreotide derivatives radiolabeled with Tc-99m and In-111 for scintigraphy, and more recently with the beta particle emitting radionuclides Y-90, Sm-153, Re-188, Cu-64 and Lu-177 for radiotherapeutic applications of sst_2 positive tumors have been proposed (Anderson et al., 1996;

Anderson et al., 1998; Lister-James 1996; Zamora et al., 1997; de Jong et al., 1999; de Jong et al., 2001; Erion et al., 1999; Bugaj et al., 2002).

Presently, the evaluation of novel compounds (Lanreotide and Vapreotide) for binding to the various somatostatin subtypes has largely been limited to the determination of IC_{50} values on CHO-K1 cells for expression of sst_1 and sst_5, and for the expression of sst_2, sst_3, sst_4 on CCL39 cells (Virgoloni et al., 1998; Smith-Jones et al., 1999; Virgolini et al., 2000). Recently the *in vivo* imaging of gene expression of sst_2 through the use of a radiolabeled peptide that binds directly to a reporter receptor expressed in tumor target tissues has been published. This approach uses the adenoviral vector, Ad5, which encodes the human sst_2 receptor ($hsst_2$). The vector (Ad5-CMVhSSTr2) is injected directly into A427 tumor bearing athymic nude mice, which is normally negative for $hsst_2$ expression. Following i.v. injection of ^{99m}Tc-P829, a somatostatin avid peptide, a 5-10 fold increase in accumulation of the radiotracer in the tumors directly injected with the $hsst_2$ positive vector (Ad5-CMVhSSTr2) over tissues injected with the control vector alone (Ad5) was observed (Zinn et al., 2000). This system is limited, however, in that the expression vector must be directly inoculated into the tumor, and does not reflect the expression of a receptor by tumor tissue under natural conditions. It also does not limit the localization of the vector to the target tissue, but allows for the potential release and subsequent localization of the expression vector in non-target tissue. An improvement in this delivery system involves the same tumor line and vector systems, but the vector encoding the sst_2 receptor is regionally (intraperitoneal) injected into the host animal and then preferentially localizes in the tumor after 48 hours. The same system for *in vivo* imaging of the tumor with ^{99m}Tc-P829 or ^{111}In-DTPA-octreotide is utilized (Rogers et al., 1999). Both of these systems are useful for

the imaging of gene expression and could be used for monitoring the location and level of transferred gene expression.

Useful to the research laboratory would be *in vivo* tumor bearing rat models that can be genetically modified to naturally express the other somatostatin receptor subtypes in sufficient number to evaluate novel radiopharmaceuticals that target these receptor subtypes. This technique would limit the receptor expression to the target tissue (tumor) and not be expressed elsewhere *in vivo*. This concept can be further broadened to include tumor lines that do not naturally express target receptors to express virtually any receptor of interest, i.e. prostate, bombesin, VIP, EGF etc. If the host tumor cells could be genetically modified through the insertion of a stable transfection of the gene encoding for the desired receptor, this technique would produce rodent models that could be used to evaluate a wider variety of novel diagnostic and therapeutic radiopharmaceuticals. The choice of genetically modifying rat tumor lines allows for the easy propagation of the tumors in animals that require relatively simple maintenance compared to athymic nude or SCID mice that require sterile barrier facilities for survival.

We therefore chose to genetically modify the Mat-B tumor line, a rodent mammary adenocarcinoma that does not naturally express sst_2 with a plasmid that encodes the human ($hsst_2$) receptor, pchSSTR$_2$. We then evaluated this transfected tumor line first for the expression of the $hsst_2$ subtype using ^{111}In-DTPA-Tyr^3-octreotate as the diagnostic marker, and then subsequently treated animals bearing the modified tumor line with ^{177}Lu-DOTA-Tyr^3-octreotate to demonstrate the radiotherapeutic potential of the model.

MATERIALS AND METHODS

Lambda $hsst_2$ DNA Preparation

A lambda phagemid containing a 1.3KbBamH-1/Xba-1-fragment encoding the $hsst_2$ was purchased from ATCC. This fragment was ligated into the EcoRV site of the plasmid pcDNA3.1 (Invitrogen) using standard molecular biology techniques. The resulting plasmid was labeled pcDNA3.1

Transfection and Selection of Mammalian Cells

The pcDNA3.1 plasmid/$hsst_2$ construct was first transfected into Chinese hamster ovary (CHO-K1) cells (ATCC). A sample of the pcDNA3.1/$hsst_2$ plasmid DNA was linearized following digestion with the restriction enzyme BglII. CHO-K1 cells were propagated in 6-well plates to 75% confluence. The cells were transfected with pcDNA3.1 plasmid/$hsst_2$ using Lipofectamine Plus transfection solution (Invitrogen) according to manufactures instructions. The cells were then trypsinized, and transferred to 24 well plates. Colonies were selected using growth media containing Gentisin (G418) as a selective marker. Sixteen drug resistant colonies were isolated. All 16 colonies were then subjected to a receptor-binding assay containing ^{111}In-DTPA-octreotide as the radioactive trace, and increasing concentrations of Tyr^3-octreotide as the cold competitor. The cells were counted in a Cobra scintillation counter (Packard Instruments), and the presence of $hsst_2$ receptor expression was confirmed in all 16 colonies, with one colony (CKO-F) showing 2X binding affinity compared to the other cells.

The same transfection procedure of the pcDNA3.1/$hsst_2$ construct described for the CHO-K1 cells was performed in the rat mammary adenocarcinoma cell line, Mat-B. Following selection from G418-containing media, a receptor-binding assay of the

colonies resulted in a single genetically modified Mat-B cell line clone identified as Mat-B/hsst$_2$d.

Receptor Binding Assays

Receptor binding assays on the CHO/hsst$_2$ and Mat-B/hsst$_2$d receptor positive cells were performed using ^{111}In-DTPA-Tyr^3-octreotate as the radioactive trace and Try^3-octreotide as the cold competitor. Briefly, cells were cultured in 24-well dishes to 80% confluence. After washing with PBS, binding buffer containing radioactive trace and increasing amounts of competitor (Tyr^3-octreotide) was added to each well and incubated at RT for 2 hours. The cells were then aspirated and washed to remove unbound label. Cells were counted in a gamma counter (Packard Cobra counter) and the IC_{50} values were calculated using a four-parameter curve fitting routine using the program GraFit (Erithacus, UK).

Internalization Assays

Internalization and cell uptake assays were performed using ^{177}Lu-DOTA-Tyr^3-octreotate, ^{125}I-Tyr^3-octreotide and ^{125}I-DOTA-Tyr^3-octreotate as radiolabeled peptides, and Tyr^3-octreotide as the cold competitor. Subconfluent cell cultures were transferred to six-well plates 24 hour before start of the assay. Cells were washed twice with 2 mL phosphate buffered saline (PBS) at 37°C. Incubation was started by addition of 1.0 mL incubation medium (RPMI 1640 (Gibco), supplemented with 20 mM Hepes (Sigma) and 1% bovine serum albumin (Sigma) containing 40 kBq of radioligand. Cells were incubated for 60 minutes at 37°C. Receptor specificity for ^{125}I-Tyr^3-octreotide and,^{125}I-DOTA-Tyr^3-octreotate, was determined by incubating the cells with 1 nM radiolabeled peptide and with an excess of Tyr^3-octreotide (1 μM).

Internalization studies of ^{177}Lu-DOTA-Tyr^3-octreotate were conducted in cells incubated from 1 to 1000 nM excess of Tyr^3-octreotide.

Internalization was quenched by removing medium from the cells and washing twice with 2.0 mL ice cold PBS. To discriminate between internalized and non-internalized (surface-bound) peptide, intact cells were incubated 10 minutes RT with 1.0 mL 20 mM sodium acetate (pH 5.0) in PBS. The cells were next solubilized with 1.0 mL NaOH (0.1 M). Internalized and surface-bound radioactivity was determined by measuring the different fractions in an LKB-1282-Compugamma system and expressed as a percentage of the applied dose per mg cellular protein. Protein was determined using a commercially available kit (BioRad, The Netherlands). Data are presented as the mean ± SD for triplicate incubations.

Tumor Model

All animal studies were conducted in compliance with the Mallinckrodt Inc. Animal Welfare Committee requirements. The Mat-B/hsst$_2$d cells were harvested from T-75 flasks and diluted in PBS at 5.0 x 10^6 cells/ml. Female Fischer 344 rats weighing approximately 120 grams were first anesthetized with Halothane gas, and then injected subcutaneously in the left flank area with 500µl of cell suspension. Palpable masses were present after 7 days post injection of cells. The animals used in the biodistribution studies were at 10 days post injection when the tumor masses were approximately 2.0grams. For the radiotherapy studies, animals were treated after 7 days post injection of cells when the tumor masses were ~300mm^3 in volume.

Radiochemistry

The synthesis of both the DTPA-Tyr^3-octreotate and the DOTA-Tyr^3-octreotate has been previously described in detail (de Jong et al., 1998; Erion et al., 1999). For use in the biodistribution studies, the In-111 was obtained from Mallinckrodt at 10,000Ci/mmol. Labeling of the DTPA-Tyr^3-octreotate was performed at room temperature for 15 minutes in 30mM NaOAc, 15mM ascorbate at a pH of 5.5 using 0.10μg of peptide with 500μCi of In-111 per reaction. The peptide was labeled to a specific activity of 1000Ci/mmol. Radiochemical yield (>99%) and radiochemical purity (>98%) were determined by reverse phase chromatography on a Vydac C-18 column using acetonitrile/0.01% TFA gradient (5% to 70% ACN) over a 20 minute time span at 1.0ml/min. The retention time of the labeled peptide was 12.38min.

For the radiotherapy study, the Lu-177 was obtained from MURR at 3000Ci/mmol. Labeling of the DOTA-Tyr^3-octreotate was performed at 80°C in 30mM NaOAc, 15mM ascorbate for 15 minutes at a pH of 5.5 using 0.10μg of peptide with 50mCi of Lu-177 per reaction. The peptide was labeled to a specific activity of ~700Ci/mmol. Radiochemical yield (>99%) and radiochemical purity (>98%) were determined by reverse phase chromatography on a Vydac C-18 column using acetonitrile/0.01% TFA gradient (5% to 70% ACN) over a 20 minute time span at 1.0ml/min. The retention time of the labeled peptide was 12.45min.

Tissue Distribution Studies

A biodistribution study in Fischer 344 rats bearing the Mat-B/hsst$_2$d tumor line, and in control rats bearing the wild type Mat-B cell line. This was done to establish that the resulting tumors from the Mat-B/hsst$_2$d cell line were somatostatin positive by scintigraphy, and that the wild type tumors were not sst$_2$ positive. Anesthetized

(Halothane) animals received 25µl (25µCi) of ^{111}In-DTPA-Tyr^3-octreotate via the jugular vein. The rats were divided into two groups (n = 3 per group) and sacrificed at 3 hours post injection by cervical dislocation. Scintigraphic images were obtained using a Picker 300SX gamma camera interfaced to a dedicated Odyssey image processor. A large field of view camera using a general-purpose medium energy collimator with the peak energy centered at 171 and 245 keV for In-111 was used to collect the images for 100K counts. Selected tissues were removed for radioassay, weighed and counted in a Packard Cobra gamma scintillation counter.

A full biodistribution was then conducted on animals bearing the Mat-B/hsst$_2$d cell line. Anesthetized (Halothane) animals received 25µl (25µCi) of ^{111}In-DTPA-Tyr^3-octreotate via the jugular vein. The rats were divided into two groups (n = 3 per group) and sacrificed at 1, 4 and 24 hours post injection by cervical dislocation. Urine and feces was collected at the 24-hour time point to determine the route of excretion of the agent, and to determine overall recovery of the injected trace. Scintigraphic images were obtained as noted previously. Tissues and organs of interest were removed for radioassay, weighed and counted in a Packard Cobra gamma scintillation counter.

Radiotherapy

A radiotherapy study was conducted on animals bearing the Mat-B/hsst$_2$d tumor. The study was performed on animals at 7 days post injection of cells when the tumors were ~300mm^3 at the onset of the study. Animals (n =8 per group) were randomly divided into two study groups and treated animals received two doses of 5.0mCi of ^{177}Lu-DOTA-Tyr^3-octreotate at via the jugular vein 5 days between doses. The control group (n = 8) received no treatment. Animals were weighed and tumor volumes on all

animals were measured with calipers every three days until the conclusion of the study.

RESULTS

Receptor Binding Assay

Figure 1 shows the binding of ^{111}In-DTPA-Tyr^3-octreotate to three transfected CHO cell lines and the CHO-WT negative control cell line. Binding of the trace to the CHO-F subclone was twice that of the two other CHO sst+ subclones, CHO-A and CHO-B. The CHO-WT cell line showed no affinity for the radioactive trace. Using this method, the data from the modified cell lines allowed for the selection of the plasmid clone from the CHO-F sst+ cell line for subsequent transfection into Mat-B cells. The IC_{50} values were also determined for the CHO/hsst$_2$ and Mat-B/hsst$_2$d cells were 3.5nm and 4.0nm respectively (data not shown). We have used this type of assay with CA20948 membrane preparations to screen a number of somatostatin analogues. The values for these two lines are very similar for other somatostatin analogues on the pancreatic acinar CA20948 tumor line that expresses high levels of sst$_2$ receptor (Bugaj et al. 2001). The low nanomolar affinity for ^{111}In-DTPA-Tyr^3-octreotate in these two cell lines confirms the high level of expression of the hsst$_2$ receptor in these two lines *in vitro*.

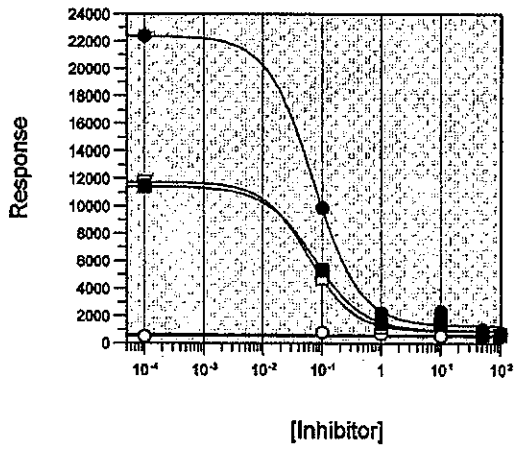

Figure 1: Competitive binding curve of ^{111}In-DTPA-Tyr^3-octreotate to different CHO cell lines in the presence of increasing concentration of cold peptide. Filled circles (●) = CHO-F(sst+); open circles (O) = CHO-WT(sst-) cells; open squares (□) = CHO-A (sst+)cells; filled squares (■) = CHO-B (sst+). Plasmid clone for subsequent Mat-B transfection selected from CHO-F(sst+) cell line.

Internalization Assays

Binding and internalization of radioiodinated Tyr^3-octreotide and ^{125}I-DOTA-Tyr^3-octreotate was studied in three somatostatin positive cell lines and a negative control cell line. Rat pancreatic cells CA20948, CHO/hsst$_2$ cells and Mat-B/hsst$_2$d cells are all SSTR positive, while the ARO cell line is SSTR negative.

Figures 2A shows that internalization ^{125}I-Tyr^3-octreotide in the somatostatin positive cell lines was receptor specific. Internalization decreased significantly in the presence of 1 μM Tyr^3-octreotide compared to 1nM concentration. There was no internalization in the somatostatin receptor negative ARO cell line even at 1nM. Internalization in the cell lines evaluated was essentially the same, however the Mat-Bd (sst +) cell line demonstrated the highest internalization in % bound /mg protein (%B/mg) compared to the other two sst+ cell lines.

Figure 2B shows that internalization ^{125}I-DOTA-Tyr^3-octreotate in the receptor sst_2 positive cell lines was receptor specific. Internalization decreased significantly in the presence of 1 μM Tyr^3-octreotide. There was no internalization in the receptor sst_2 negative ARO cell line even at 1nM. Internalization of, ^{125}I- DOTA-Tyr^3-octreotate was significantly higher than the internalization of ^{125}I-Tyr^3-octreotide (Figure 2A). The Mat-B sst(+) cell line had the highest internalization in %B/mg protein at 77%, followed by the CA20948 cells. The uptake of ^{125}I- DOTA-Tyr^3-octreotate demonstrated a similar internalization profile in these three cell lines as observed with ^{125}I-Tyr^3-octreotide, with the exception of significantly greater internalization rates.

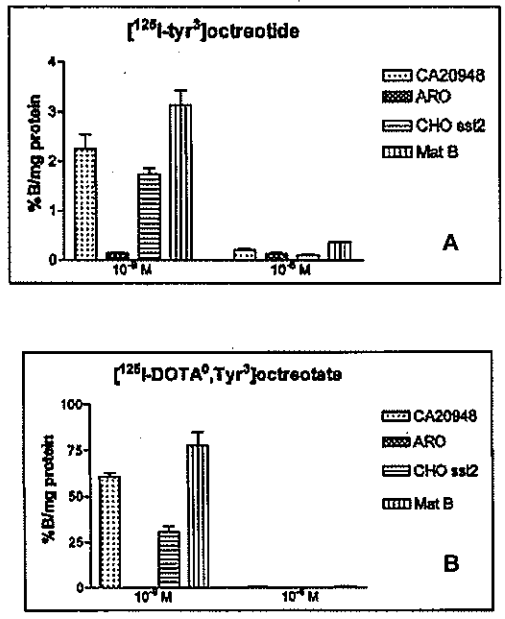

Figure 2: Internalization of different octreotate derivatives in sst_2 positive cell linesin vitro. **A**: ^{125}I-Tyr^3-octreotide at 60 minutes in CA20948 (sst+), Mat-B/hsst_2 (sst+) and ARO (sst-). Internalization expressed as %Bound/mg protein at two different concentrations. **B**: ^{125}I-Tyr^3-octreotate at 60 minutes in the same cell lines.

Figure 2C shows the internalization ^{177}Lu-DOTA-Tyr^3-octreotate in the different receptor sst_2 positive cell lines is receptor specific. Internalization decreased proportionately in the presence of an increasing concentration of cold Tyr^3-octreotide. High rate of internalization were observed at concentrations between 1-50nM, and evidence of receptor saturation occurring between 500-1000nM excess peptide for all three cell lines evaluated.

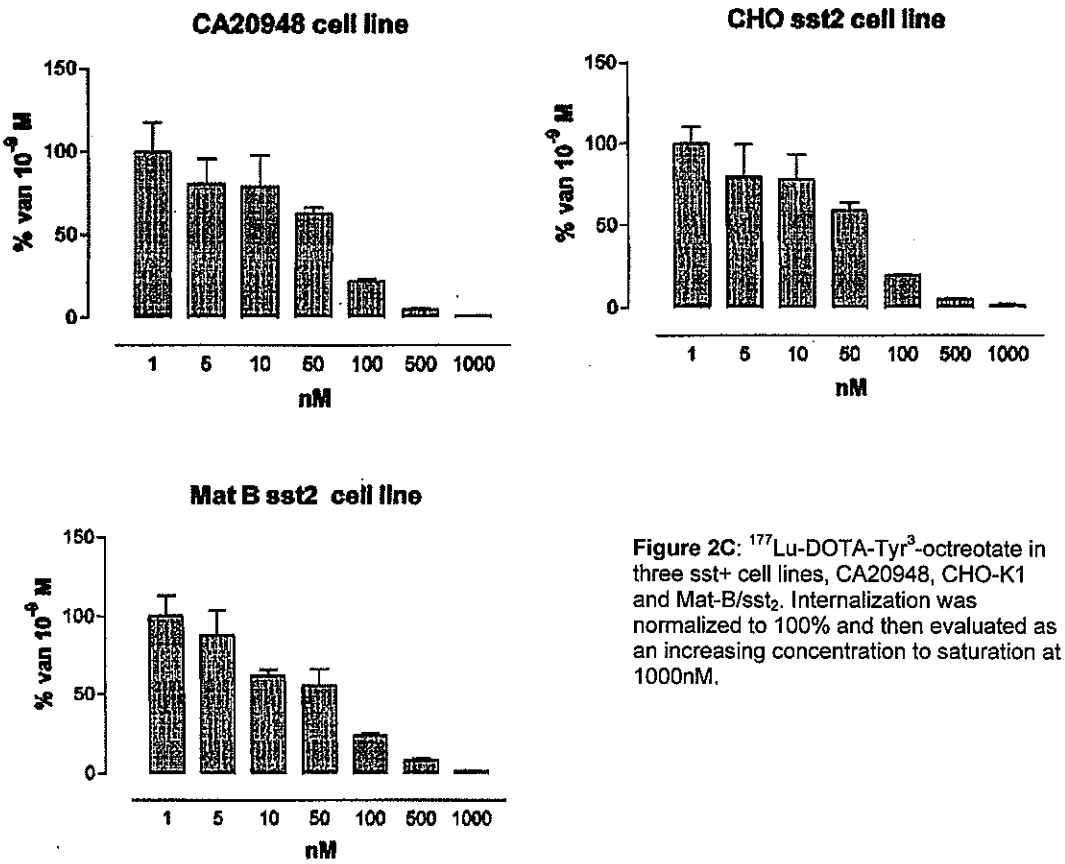

Figure 2C: ^{177}Lu-DOTA-Tyr^3-octreotate in three sst+ cell lines, CA20948, CHO-K1 and Mat-B/sst_2. Internalization was normalized to 100% and then evaluated as an increasing concentration to saturation at 1000nM.

Table 1. Biodistribution of ^{111}In-DTPA-Y^3-Octreotate in Selected Tissues from Mat-B WT and $hsst_2$ Tumor Bearing Rats 3 Hours Post Injection (Percent Injected Dose / gram ± SE)

Tissue	Mat-B WT	Mat-B $hsst_2$
Blood	0.020±0.002	0.019±0.001
Muscle	0.012±0.001	0.010±0.001
Kidneys	3.906±0.239	3.963±0.234
Tumor	0.037±0.007	2.002±0.290

Tissue Distribution Studies

The initial biodistribution study was performed to establish that the Mat-B/hsst$_2$d tumors expressed the hsst$_2$ receptor in sufficient density to be visualized by scintigraphy and quantitated after injection with ^{111}In-DTPA-Tyr^3-octreotate. The study was also conducted to confirm that wild type Mat-B tumors grown in the same animal model do not express the sst$_2$ receptor. Table 1 and Figure 2 shows that the uptake of the radiotracer in the Mat-B/hsst$_2$d tumor bearing animals was 2.00% ID/gram versus only 0.038% ID/gram for the wild type, which represents a >50 fold increase in uptake for the cell line encoding the hsst$_2$ receptor. The uptake in the other sst$_2$ positive organ of the pancreas was high in both groups of animals. Uptake in the non-somatostatin expressing tissues of the blood, muscle and kidneys was also equivalent for both groups. The comparative scintigraph (Figure 5) shows the strong localization of the radiotracer in the animals bearing the Mat-B/hsst$_2$d tumors (left flank) compared to the lack of detection of the tracer in the flanks of the animals bearing the wild type Mat-B tumors.

Table 2. Biodistribution of ^{111}In-DTPA-Y^3-Octreotate in Mat-B hsst$_2$ Tumor Bearing Rats (Percent Injected Dose / gram ± SE)

Tissue	1 hour	4 hours	24 hours
Blood	0.049±0.011	0.018±0.004	0.007±0.001
Liver	0.048±0.008	0.038±0.008	0.028±0.002
Kidneys	2.759±0.648	4.678±1.377	2.961±0.069
Muscle	0.010±0.002	0.006±0.001	0.005±0.000
Spleen	0.048±0.006	0.036±0.005	0.053±0.023
Heart	0.040±0.009	0.024±0.003	0.014±0.001
Pancreas	11.85±1.626	10.92±0.912	6.491±0.601
Sm. Intes.	1.623±0.340	1.241±0.085	0.682±0.115
Stomach	1.468±0.333	1.967±0.769	1.002±0.269
Bone	0.176±0.026	0.132±0.017	0.170±0.008
Tumor	2.101±0.270	2.203±0.330	0.683±0.031

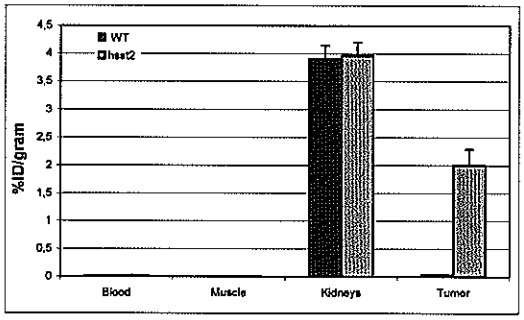

Figure 3: Biodistribution of ^{111}In-DTPA-Tyr^3-octreotate in Fischer 344 rats bearing Mat-B (WT) and Mat-B/hsst$_2$ tumors. Selected tissues (blood, muscle, kidneys and tumor) removed at 3 hours post injection with 25μCi of radiolabel.

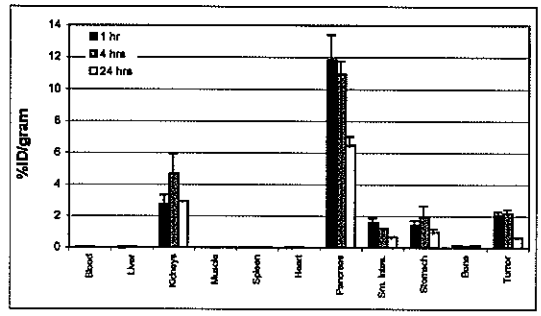

Figure 4: Biodistribution of ^{111}In-DTPA-Tyr^3-octreotate in Fischer 344 rats bearing Mat-B/hsst$_2$ tumors. Tissues were removed at 1, 4 and 24 hours post injection with 25μCi of radiolabel.

The full biodistribution study (Tables 2 and 3; Figure 4) shows the distribution over a 24-hour time frame for the uptake and retention of ^{111}In-DTPA-Tyr^3-octreotate in Fischer 344 rats bearing Mat-B/hsst$_2$d tumors. At 1, 4 and 24 hours post injection tumor uptake was 2.10%, 2.20% and 0.68% ID/gram. Uptake in the other two sst$_2$ positive organs, the pancreas and the adrenal glands was high and consistent with this agent. The other non-somatostatin expressing tissues including blood, liver, muscle and spleen and heart were all low. Kidney retention was consistent at the three time points at ~3.0% ID/gram of tissue. Uptake for the agent is higher in this somatostatin receptor negative organ due to the known metabolism of this octapeptide to the first amino acid (^{111}In-DTPA-**D**-Phe^1), which becomes trapped in the renal tubules. Urinary clearance was relatively high at 56% at 24 hours, and fecal excretion low at 9.8% at the same time point.

Figure 5 shows the scintigraphs of tumor bearing animals (A) Mat-B (WT) and (B) MatB/hsst$_2$. The Mat-B (WT) show no localization of the radiolabeled peptide at the tumor site, while there is a strong signal for the animals bearing the MatB/hsst$_2$ tumor.

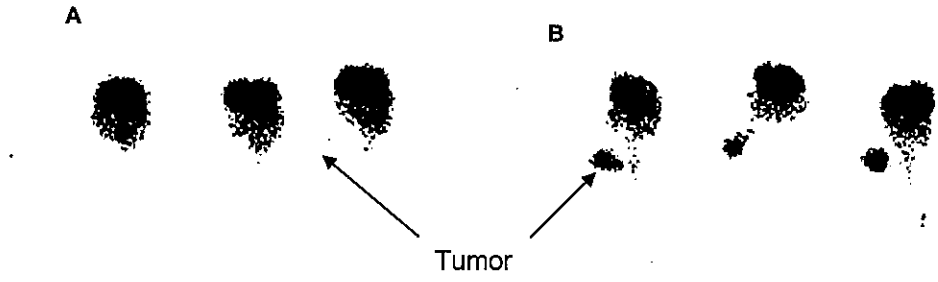

Figure 5: Scintigraphs of animals bearing the Mat-B (WT) tumor and the Mat-B/hsst$_2$ tumor in the left flank area. Animals were injected with 25µCi of ^{111}In-DTPA-Tyr^3-octreotate and imaged 3 hours post injection. **A**: Mat-B (WT) tumor bearing rats, **B**: Mat-B/hsst$_2$ tumor bearing rats. Tumor location denoted by arrows.

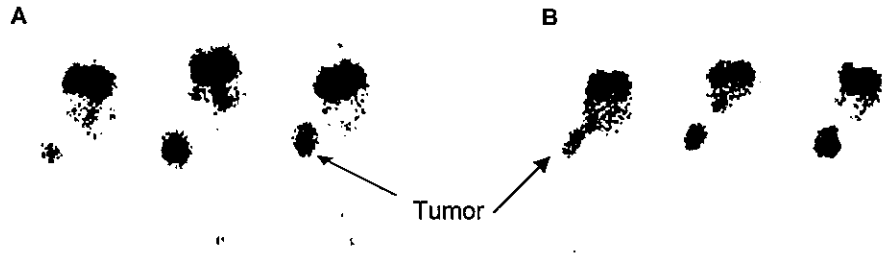

Figure 6: Scintigraphs of animals bearing Mat-B/hsst$_2$ tumors in left flank injected with either ^{111}In-DTPA-Tyr^3-octreotate or ^{177}Lu-DOTA-Tyr^3-octreotate and imaged at 3 hours post injection. **A**: Animals injected with 25µCi of ^{111}In-DTPA-Tyr^3-octreotate; **B**: animals injected with 250µCi of ^{177}Lu-DOTA-Tyr^3-octreotate. Tumor location noted with arrows.

Table 3. Biodistribution of ^{111}In-DTPA-Y^3-Octreotate in Mat-B hsst$_2$ Tumor Bearing Rats (Percent Injected Dose / organ ± SE)

Tissue	1 hour	4 hours	24 hours
Blood	0.340±0.079	0.126±0.028	0.051±0.005
Liver	0.282±0.047	0.207±0.027	0.192±0.016
Kidneys	3.338±0.794	3.781±0.626	3.660±0.046
Muscle	0.659±0.149	0.360±0.059	0.318±0.008
Spleen	0.024±0.003	0.020±0.003	0.034±0.015
Heart	0.021±0.005	0.013±0.001	0.006±0.001
Pancreas	8.175±1.112	6.269±0.542	3.949±0.304
Adrenals	0.724±0.119	0.843±0.143	0.661±0.044
Stomach	3.010±0.411	3.320±0.535	1.534±0.047
Bone	1.428±0.210	1.069±0.174	1.378±0.053
Tumor	4.263±0.599	6.600±1.118	3.432±0.520
Urine			55.74±3.099
Feces			9.785±1.327
Total Excreted			65.52±4.32
Total Recovered			80.74±4.98

Demonstration of the localization of ^{177}Lu-DOTA-Tyr^3-octreotate in Mat-B/hsst$_2$ animals is demonstrated in Figure 6. At three hours post injection comparable scintigraphs between the 111-In or Lu-177 analogues were obtained, and indicated high and equivalent uptake of both radionuclides in this tumor model.

Radiotherapy

Figure 7 shows the survival curve and tumor volumes for animals at 7 days post injection of cells. In this study the average tumor volume at the start of the study was ~300mm^3 for all animals. The curve compares animals treated with 2 x 5.0mCi of ^{177}Lu-DOTA-Tyr^3-octreotate at 5 day intervals compared to untreated control animals. In this study all animals were sacrificed at 17 days post injection of cells. The mean tumor volume for the treated group was 15,600mm^3 versus 28,000mm^3 ($p < 0.05$) for the untreated control group. As can be seen from the figure, tumor growth was very rapid in the control group and delayed in the treatment group. However, all animals showed evidence of increasing tumor growth, and by 17 days post injection all untreated animals were sacrificed.

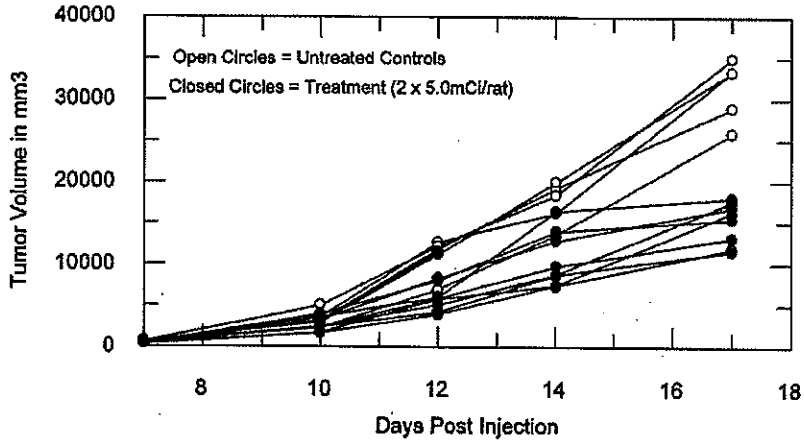

Figure 7: Tumor growth curves in therapy study for animals bearing Mat-B/hsst$_2$ tumors. Tumor volumes (mm^3) in untreated animals (open circles) and animal treated with 2 x 5.0mCi ^{177}Lu-DOTA-Tyr^3-octreotate at 5 day intervals (filled circles) All animals were sacrificed at 17 days post inoculation of cells (See text for details).

DISCUSSION

The objectives of this study were (1) to construct a plasmid encoding for the $hsst_2$, and (2) induce the expression of the sst_2 gene in mammalian cell lines normally negative for expression of that receptor. The transfected cell lines demonstrated a high level of expression of the $hsst_2$ gene by receptor-binding and internalization assays. Additionally, the development of an $hsst_2$ positive rodent mammary tumor line (Mat-B), a line that is normally negative for the expression of $hsst_2$, was genetically modified by a transfection technique to express the $hsst_2$ gene. This tumor line was implanted into Fischer 344 rats, and the *in vivo* imaging and radiotherapeutic potential of this novel animal model was demonstrated using ^{111}In-DTPA-Tyr^3-octreotate and ^{177}Lu-DOTA-Tyr^3-octreotate.

The current interest in imaging and treating tumors expressing the sst_2 receptor is the best example of a receptor-targeted approach using a variety of radionuclides. To date, imaging of sst_2 is conducted using Tc-99m and In-111 labeled peptides, and the list of potential therapeutic radionuclides includes Y-90, Cu-64, Re-188, Sm-153 and Lu-177 (Lister-James 1996; Anderson et al., 1998; Stolz et al., 1998; de Jong et al., 1998; Zamora et al., 1998; Erion et al., 1999; Bugaj et al., 2002; de Jong et al., 2001). For each of these radionuclides there are reports of pre-clinical studies that support the radiotherapeutic potential for each radionuclide. The animal model used frequently in pre-clinical studies to evaluate sst_2 avid peptides is primarily the CA20948 tumor bearing Lewis rat. This tumor line grows quite readily in this animal and the expression of the sst_2 receptor is high (Stolz et al., 1998). A number of investigators have utilized this model in radiotherapy studies using Y-90, Lu-177, Re-188 and In-111 labelled peptides. However, for peptides that target other receptors such as VIP, CCK, EGF and bombesin, the current approach is limited to the use of

human xenografts in athymic nude or SCID mouse models. These models require a sterile barrier for the maintenance and handling of the animals, and results in more cumbersome and expensive housing requirements. Therefore, a more standard tumor bearing rat model that expresses the target receptor(s) of interest would significantly increase the ease and efficiency of with which novel peptides could be evaluated at the pre-clinical stage of development. Novel peptides that target the other sst receptors (sst_1, sst_3 and sst_4) require the transfection of cells with the receptor genes, but no tumor bearing animal models expressing these receptors have been developed thus far. Compounds such as Vapreotide and Lanreotide are first evaluated in cell expression systems followed by direct early human use (EHU) studies without any pre-clinical testing in animal models.

One solution to this situation has been presented in the form of adenoviral vector expression systems for the sst_2 receptor in non-sst expressing tumor lines in athymic nude mice (Zinn et al., 2000; Rogers et al., 1999). However, these models are more appropriately designed for the *in vivo* evaluation of gene expression and gene location, as opposed to animal models that can be readily used to evaluate novel peptides at the pre-clinical stage. Although, the efficacy of potential sst_2 imaging and radiotherapeutic peptides using this system has been reported, currently this method is still limited to the use of athymic nude mice which require a sterile barrier for housing and handling of the animals.

A second solution to this problem was addressed whereby pre-weaned Lewis rats were implanted with solid AR42-J tumor material for the expression of sst_2, CCK, bombesin, and VIP, in a stable rat model (Bugaj et al., 2002). This model was validated by a series blocking and radiotherapy studies for the expression of sst_2 and

bombesin receptors, however, this model is limited in the natural expression of the receptors of that particular tumor line. As yet, rat tumor lines expressing receptors such as sst_1, sst_3, sst_4 etc., are not readily available.

The work presented here demonstrates that a rat mammary tumor line, Mat-B, can be transfected with the gene encoding the human sst_2 receptor ($hsst_2$), and that this model can be utilized for the evaluation of sst_2 avid peptides for both scintigraphic and radiotherapeutic applications. This tumor line is normally negative for the expression of sst_2, but through a series of transfection techniques was genetically modified to express $hsst_2$ at high levels. The model was validated using ^{111}In-DTPA-Tyr^3-octreotate for scintigraphy and radiotherapy studies using ^{177}Lu-DOTA-Tyr^3-octreotate were performed. The results indicated a 50-fold increase in uptake of the radiolabel over wild type (WT) Mat-B tumor bearing rats. Uptake and retention of ^{177}Lu-DOTA-Tyr^3-octreotate in the animals bearing the Mat-B/$hsst_2$ tumor was high at ~2.0% ID/gram from 1-4 hours post injection. The therapy study showed a delayed growth pattern for the animals treated with 2 x 5.0mCi of ^{177}Lu-DOTA-Tyr^3-octreotate compared to untreated control animals.

The logical extension of this work would be for the development of rat tumor models that express virtually any receptor of interest. The list would include such receptors as sst_1, sst_3 and sst_4, all of which have been sub-cloned and expressed in other mammalian cell lines. Utilizing a similar sequence of transfection protocols, it should be possible to genetically modify a variety of tumor lines to express these receptors of interest, and subsequently establish rat models for the expression of these target receptors. These models would further evaluate novel peptides that target these receptors for identifying new imaging and radiotherapeutic peptides at the pre-clinical

level, thereby facilitating the selection of new agents that enter EHU trials. This approach would also obviate the need for athymic nude and SCID mouse models, which are substantially more expensive and difficult to maintain in a laboratory setting.

REFERENCES

1. Anderson, C. J., Pajeau, T. S., Edwards, W. B., Sherman, E. L., Rogers, B. E. and Welch, M. J. (1995) In Vitro and In Vivo Evaluation of Copper-64-Octreotide Conjugates, *J Nucl Med*, 36, 2315-2325.

2. Anderson, C. J., Jones, L. A., Bass, L. A., Sherman, E. L., McCarthy, D. W., Cutler, P. D., Lanahan, M. V., Cristel, M. E., Lewis, J. S. and Schwarz, S. W. (1998) Radiotherapy, Toxicity and Dosimetry of Copper-64-TETA-Octreotide in Tumor-Bearing Rats, *J Nucl Med,* 39, 1944-1951.

3. Boerman, O.C., Oyen, W.J., and Corstens, F.H., (2000) Radio-Labeled Receptor-Binding Peptides: A New Class of Radiopharmaceuticals, *Seminars in Nuclear Medicine*, 195-208.

4. Brazeau, P. (1986) Somatostatin: A Peptide with Unexpected Physiologic Activities, *Am J Med*, 81 (supp. 6B) 8-13.
Breeman, W. A., Bakker, W. H., de Jong M., Hofland, L. J., Kewkkeboom, D. J, Kooij, P. P., Visser, T. J. and Krenning, E. P. (1996) Studies on Radiolabeled Somatostatin Analogues in Rats and Patients, *Q J Nucl Med*, 40, 209-220.

5. Bugaj, J. E., Erion, J. L., Johnson, M. A., Schmidt, M. A. and Srinivasan, A. (2001) Radiotherapeutic Efficacy of ^{153}Sm-CMDTPA-Tyr^3-Octreotate in Tumor-Bearing Rats, *Nucl Med Biol*, 28, 327-334.

6. Bugaj, J. E., Erion, J. L., Johnson, M. A. and de Jong, M. (2002) Radiotherapeutic Efficacy of ^{177}Lu-DOTA-Tyr^3-Octreotate in Novel Rat Tumor Animal Model Systems, *E J Nucl Med (Submitted).*

7. De Jong, M., Breeman, W. A., Bakker, W. H., Kooij, P. P., Bernard, B. F., Hofland, L. J., Visser, T. J., Srinivasan, A., Schmidt, M. A., Erion, J. L., Bugaj, J. E., Macke, H. R. and Krenning, E. P. (1998) Comparison of ^{111}In-Labeled Somatostatin Analogues for Tumor Scintigraphy and Radionuclide Therapy, *Cancer Research*, 58, 437-441.

8. De Jong, M., Breeman, W. A., Bernard, H. F., Kooij, P. P., Slooter, G. D., Van Eijck, C. H., Kwekkeboom, D. J., Valkema, R., Macke, H. R. and Krenning, E. P. (1999) Therapy of Neuroendocrine Tumors with Radiolabeled Somatostatin-Analogues, *Q J Nucl Med*, 43, 356-366.

9. De Jong, M., Breeman, W. A., Bernard, H. F., Bakker, W. H., Schaar, M., van Gameren, A., Bugaj, J. E., Erion, J. L., Schmidt, M. A., Srinivasan, A. and Krenning, E. P. (2001) [^{177}Lu-DOTA^0, Tyr^3] Octreotate for Somatostatin Receptor-Targeted Radionuclide Therapy, *Int. J Cancer*, 92, 628-633.

10. Erion, J. L., Bugaj, J. E., Schmidt, M. A. and Srinivasan, A. (2001) Long Term Survival of Tumor-Bearing Rats Treated with ^{177}Lu-DOTA-Tyr^3-Octreotate, *Cancer Research*, (Submitted).

11. Fischman, A.J., Babich, J.W., and Strauss, H.W., (1993) A Ticket to Ride: Radiopharaceuticals, *J Nucl Med*, 34, 2253-2263.

12. Krenning, E.P., Kwekkeboom, D.J., Bakker, W.H., Breeman, W.A., Kooij, P.P., Oei, H.Y., van Hagen, M., Postema, P.T., de Jong, M., Reubi, J-C., Visser, T.J., Reijs, A.E., Hofland, L.J., Koper, J.W., and Lamberts, S.W., (1993) Somatostatin receptor scintigraphy with [^{111}In-DTPA-D-Phe^{1}]- and [^{123}I-Tyr^{3}]- octreotide: the Rotterdam experience with more than 1000 patients, *E J Nucl Med*, 20, 716-731.

13. Krenning, E. P., Kooij, P. P., Bakker, W. H., Breeman, W. A., Postema, P. T., Kwekkwboom, D. J., Oei, H. Y., de Jong, M., Visser, T. J., Reijs, A. E., and Lamberts, S. W. (1994) Radiotherapy with a Radiolabelled Somatostatin Analogue, [^{111}In-DTPA-D-Phe^{1}]Octreotide, *Ann NY Acad Sci*, 733, 496-506.

14. Lister-James, J., (1996) Small peptides radiolabeled with ^{99m}Tc, *Q J Nucl Med*, 40, 221-233.

15. Reubi, J-C., Schaer, J.C., Waser, B. and Mengod, G., (1994) Expression and localization of somatostatin receptor SSTR1, SSTR2 and SSTR3 messenger RNAs in primary human tumors using in situ hybridization, *Cancer Research*, 54, 3455-3459.

16. Reubi, J-C., Schar, J-C., Waser, B., Wenger, S., Heppeler, A., Schmitt, J. S., and Macke, H. R. (2000) Affinity Profiles for Human Somatostatin Receptor Subtypes SST1-SST5 of Somatostatin Radiotracers Selected for Scintigraphic and Radiotherapeutic Use, *E J Nucl Med*, 27, 273-282.

17. Rogers, B.E., McLean, S.F., Kirkman, R.L., Olsen, C.C., Bright, S.J., Myracle, A.D., Mayo, M.S., Curiel, D.T., and Buchsbaum, D.J., (1999) *In Vivo* Localization of [^{111}In]-DTPA-D-Phe^{1}-Octreotide to Human Ovarian Tumor Xenografts Induced to Express the Somatostatin Receptor Subtype 2 Using an Adenoviral Vector, *Clinical Cancer Research*, 5, 383-393.

18. Smith-Jones, P.M., Bischof, C., Leimer, M., Gludovacz, D., Angelberger, P., Pangerl, T., Peck-Radosavljevic, M., Hamilton, G., Kaserer, K., Kifler, A., Schlagbauer-Wadl, H., Traub, T., and Virgolini, I., (1999) DOTA-Lanreotide: A Novel Somatostatin Analog for Tumor Diagnosis and Therapy, *Endocrinology*, 40, 5136-5148.

19. Stolz, B., Weckbecker, G., Smith-Jones, P. M., Albert, R., Raulf, F. and Bruns, C. (1998) The Somatostatin Receptor-Targeted Radiotherapeutic [^{90}Y-DOTA-(D)Phe^{1},Tyr^{3}]Octreotide (^{90}Y-SMT 487) Eradicates Experimental Rat Pancreatic CA20948 Tumours, *E J Nucl Med*, 25, 668-674.

20. Virgolini, I., Traub, T., Leimer, M., Novotony, C., Pangerl, T., Ofluoglu, S., Halvadjieva, E., Smith-Jones, P.M., Flores, J., Li, S., Angelberger, P., Havlik, E., Andreae, F., Raderer, M., Kutaran, A., Neiderle, B., and Dudczak, R., (2000) New radiopharmaceuticals for receptor scintigraphy and radionuclide therapy, *Q J Nucl Med*, 44, 50-58.

21. Virgolini, I, Leimer, M., Handmaker, H., Lastoria, S., Bischof, C., Muto, P., Pangerl, T., Gludovacz, D., Peck-Radosavljevic, M., Lister-James, J., Hamilton, G., Kaserer, K., Valent, P., and Dean, R., (1998) Somatostatin Receptor Subtype Specificity and *in Vivo* Binding of a Novel Tumor tracer, 99mTc-P829, *Cancer Research*, 58, 1850-1859.

22. Zamora, P.O., Bender, H., Gulhke, S., Marek, M.J., Knapp, F.F., Rhodes B.A., and Biersack, H.J., (1997) Pre-Clinical Experience with Re-188-RC-160, a Radiolabeled Somatostatin Analog for Use in Peptide-Targeted Radiotherapy, *Anticancer Research*, 17, 1803-1808.

23. Zinn, K.R., Buchsbaum, D.J., Chaudhuri, T.R., Mountz, J.M., Grizzle, W.E., and Rogers, B.E., (1999) Noninvasive Monitoring of Gene Therapy Using a Reporter Receptor Imaged with a High-Affinity Peptide Radiolabeled with ^{99m}Tc or ^{188}Re, *J Nucl Med*, 41, 887-895.

CHAPTER 8A

TOXICITY AND DOSIMETRY OF ^{177}LU-DOTA-Y^{3}-OCTREOTATE IN A RAT MODEL

International Journal of Cancer, 94, 873-877, (2001)

TOXICITY AND DOSIMETRY OF ^{177}LU-DOTA-Y3-OCTREOTATE IN A RAT MODEL

Jason S. LEWIS[1], Mu WANG[1], Richard LAFOREST[1], Fan WANG[1], Jack L. ERION[2], Joseph E. BUGAJ[2], Ananth SRINIVASAN[2] and Carolyn J. ANDERSON[1]*

[1]*Mallinckrodt Institute of Radiology, Washington University School of Medicine, St. Louis, MO, USA*
[2]*Mallinckrodt Inc., Hazelwood, MO, USA*

Radiolabeled somatostatin analogs have demonstrated effectiveness for targeted radiotherapy of somatostatin receptor-positive tumors in both tumor-bearing rodent models and humans. A radionuclide of interest for cancer therapy is reactor-produced ^{177}Lu ($t_{1/2}$ = 6.64 d; β^- [100%]). The high therapeutic efficacy of the somatostatin analog ^{177}Lu-DOTA-Tyr^3-octreotate (DOTA-Y3-TATE, where DOTA is 1,4,7,10-tetraazacyclododecane-1,4,7,10-tetraacetic acid) was previously demonstrated in a tumor-bearing rat model (Erion et al., J. Nucl. Med. 1999;40:223P; de Jong et al., Int. J. Cancer, 2001; 92:628–633). In the current study, the toxicity and dosimetry of ^{177}Lu-DOTA-Y3-TATE were determined in both normal and tumor-bearing rats. Doses of ^{177}Lu-DOTA-Y3-TATE ranging from 0 to 123 mCi/kg were administered to rats and complete blood counts (CBCs) and blood chemistries were analyzed out to 6 weeks. No overt signs of toxicity were observed with ^{177}Lu-DOTA-Y3-TATE (i.e., lethargy, weight loss, scruffy coat or diarrhea) at any of the dose levels. Blood chemistries and CBCs were normal except for the white blood cell counts, which showed a dose-dependent decrease. The maximum tolerated dose was not reached at 123 mCi/kg. The biodistribution of ^{177}Lu-DOTA-Y3-TATE was determined in CA20948 rat pancreatic tumor-bearing rats, and the data were used to estimate human absorbed doses to normal tissues. The dose-limiting organ was determined to be the pancreas, followed by the adrenal glands. The absorbed dose to the rat CA20948 tumor was estimated to be 336 rad/mCi (91 mGy/MBq). These data demonstrate that ^{177}Lu-DOTA-Y3-TATE is an effective targeted radiotherapy agent at levels that show minimal toxicity in this rat model.

Key words: *targeted radiotherapy; lutetium-177; somatostatin; neuroendocrine cancer*

The use of radiolabeled ligands that bind to somatostatin receptors (SSTRs) as targeted radiotherapy agents in humans is increasing.[1–5] Preliminary results of clinical trials with ^{111}In-DTPA-OC, a diagnostic radiopharmaceutical approved by the United States Food and Drug Administration, have demonstrated evidence of tumor response to treatment.[1,6] Reported responses include stable disease, but no significant tumor regressions or remissions. ^{90}Y-DOTA-Tyr^3-octreotide (^{90}Y-DOTA-Y3-OC or ^{90}Y-DOTATOC or SMT487) is currently in clinical trials, with favorable results demonstrating significant tumor regressions.[2–4] Preliminary data with ^{177}Lu-DOTA-tyrosine3-octreotate (^{177}Lu-DOTA-Y3-TATE) are presented in a recently published abstract and suggest a range of responses from tumor shrinkage (8/26) to stable disease (14/26) to partial remission (1/26) to tumor progression (3/26).[5]

The progress with somatostatin receptor ligands is very exciting; however, some questions remain to be answered. One issue is whether ^{90}Y is the best radionuclide for targeted radiotherapy of all tumor types and sizes.[7] Yttrium-90 has a mean β-energy of 0.9 MeV with a maximum energy of 2.27 MeV and a maximum particle range of about 11 mm in tissue, making it an appropriate radionuclide for larger tumor burdens. A potential problem with ^{90}Y is that the high-energy β^- may also be the cause of the observed renal toxicity in humans treated with high doses of ^{90}Y-DOTATOC. This raises the question of whether or not other radionuclides with lower β^- energies may have utility for smaller tumors or micrometastatic disease.

An alternative radionuclide for targeted radiotherapy is ^{177}Lu ($t_{1/2}$ = 6.65 d),[8] which decays by lower energy β^- emissions (0.498 MeV [78.6%], 0.176 MeV [12.2%] and 0.385 [9.1%]).[9] Lutetium-177 is produced at the University of Missouri Research Reactor (MURR) by the ^{176}Lu(n,γ)^{177}Lu reaction.[10] In patients with ovarian cancer, the ^{177}Lu-labeled monoclonal antibody (Mab) CC49 showed considerable efficacy at controlling micrometastatic disease.[11] The groups at the University of Rotterdam and Mallinckrodt, Inc. have evaluated ^{177}Lu-labeled somatostatin analogs in a tumor-bearing rat model and demonstrated impressive therapeutic efficacy.[12,13] Here we present data on the toxicity of ^{177}Lu-DOTA-tyrosine^3-octreotate (^{177}Lu-DOTA-Y3-TATE; Fig. 1) in normal Lewis rats, as well as the estimated human absorbed doses of ^{177}Lu-DOTA-Y3-TATE to normal tissues and the dose to a rat tumor.

MATERIAL AND METHODS

General

All chemicals, unless otherwise stated, were purchased from Aldrich (Milwaukee, WI). Lutetium-177 was obtained from the University of Missouri Research Reactor in a specific activity of 20 Ci/mg.[10] All solutions were prepared using ultrapure water (18 MΩ cm resistivity). Radio-thin layer chromatography (radio-TLC) detection was accomplished using a BIOSCAN (Washington, DC) System 200 Imaging Scanner. Radioactive samples were counted on a Beckman (Fullerton, CA) 8000-γ-counter.

Preparation of ^{177}Lu-DOTA-Y3-TATE

DOTA-Y3-TATE was synthesized as previously described.[14] DOTA-Y3-TATE was labeled with $^{177}LuCl_3$ (0.05 M HCl) in 30 mM NaOAc/25 mM sodium ascorbate, pH 5.0, for 25 min at 80°C. Radiochemical purity was determined by radio-TLC with C18 plates developed in 70:30 MeOH:10% NH_4OAc (^{177}Lu-DOTA-Y3-TATE, R_f = 0.8; ^{177}Lu-acetate, R_f = 0). Radiochemical purity of ^{177}Lu-DOTA-Y3-TATE in all studies was >98%.

Abbreviations: DOTA, 1,4,7,10-tetraazacyclododecane-*N,N',N'',N'''*-tetraacetic acid; DTPA, diethylenetriaminepentaacetic acid; OC, octreotide; SSTR, somatostatin receptors; TATE, octreotate; TETA, 1,4,8,11-tetraazacyclotetradecane-*N,N',N'',N'''*-tetraacetic acid; Y3, tyrosine-3.

Grant sponsor: National Cancer Institute; Grant number: CA64475; Grant sponsor: Biotechnology Research Development Corporation; Grant sponsor: University of Missouri Research Reactor under the Department of Energy's Reactor Sharing Support Program; Grant number: DE-FG07-01ID14146.

*Correspondence to: Mallinckrodt Institute of Radiology, Washington University School of Medicine, 510 South Kingshighway Blvd., Campus Box 8225, St. Louis, MO 63110, USA. Fax: +314-362-9940.
E-mail: andersoncj@mir.wustl.edu

Received 6 April 2001; Revised 6 June 2001; Accepted 13 July 2001

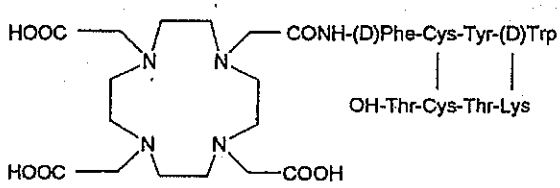

FIGURE 1 – Structure of DOTA-Y3-TATE.

Animal studies

All animal experiments were conducted in compliance with the Guidelines for the Care and Use of Research Animals established by Washington University's Animal Studies Committee. The rat pancreatic tumor CA20948[15] was obtained from the Tumor Bank at Biomeasure (Hopkinton, MA). Adult male Lewis rats (190–240 g) were purchased from Charles River (Wilmington, MA). The CA20948 tumor was maintained by serial passage in animals. In rat experiments, male Lewis rats were injected with a 1 mm^3 section of CA20948 tumor 10 days prior to treatment as previously described.[16]

Toxicity study

Doses of ^{177}Lu-DOTA-Y3-TATE (specific activity 0.89 mCi/μg) ranging from 0 to 130 mCi/kg in 5 toxicity groups (0–4.4, 16.3–18.2, 36.7–40.5, 64.7–71.2 and 102.2–122.6 mCi/kg; n = 6 in each group) were administered i.v. via the tail vein to normal rats. Toxicity was monitored by weight loss and gross physical appearance, as well as changes in hematologic, liver and kidney function compared with control rats (n = 6). In each group, anesthetized rats were weighed, and blood was removed by cardiac puncture before and during the experimental period. Toxicity analyses were performed by the Diagnostic Services Laboratory in the Department of Comparative Medicine at Washington University School of Medicine. The hematology analysis included white blood cell counts (WBCs), red blood cell counts (RBCs), platelet counts and measurement of hemoglobin, hematocrit and differential WBCs. Liver and kidney analysis included alanine aminotransferase (ALT), blood urea nitrogen (BUN) and creatinine. Gross necropsy examination of the respiratory, digestive, musculoskeletal, urinary and genital systems as well as the brain, thymus, spleen, lymph nodes, adrenals, pituitary and eye was performed on 2 animals from the highest dose group at the experimental endpoint of 38 days post injection. Histopathologic examination of the liver, kidney, pancreas and adrenal gland was also performed.

Rat dosimetry

The absorbed doses of ^{177}Lu-DOTA-Y3-TATE were obtained for normal tissues and a rat tumor using biodistribution data in CA20948 tumor-bearing rats, according to previously described methods.[16–19] ^{177}Lu-DOTA-Y3-TATE (40 μCi [1.3 MBq]; 0.67 μg) was injected i.v., and the rats bearing 0.5–3.5 g tumors were euthanized by Metofane overdose and cervical dislocation at 1, 3, 6, 14, 24, 48, 72, 96 and 168 hr (each group, n = 5) post injection. The rats in the 72 hr group were housed in metabolism cages to determine the percent injected dose (% ID) excreted in urine and feces at 1, 3, 18, 24, 48 and 72 hr.

Twenty-three organs and tissues (blood, lung, liver, spleen, kidney, bladder, muscle, fat, heart, brain, pituitary, bone, marrow [from femur], testes, prostate, adrenals, pancreas, thymus, tumor, stomach, small intestine, upper large intestine and lower large intestine) were harvested, and time-activity curves were generated for each of them. Additionally, the % ID/g and %ID/organ for each tissue were calculated. (Tables of % ID/g and %ID/organ with standard deviations for 23 tissues and 8 time points for ^{177}Lu-DOTA-Y3-TATE are available.) Uptake in the intestinal tract was assumed to be due to fecal matter and not to receptor-specific uptake of the radiolabeled peptide. The cumulative activity (μCi/hr or kBq/hr) for each organ was determined by analytically integrating a mathematical function fitted by the least-square method on the data. This function was chosen to be a combination of exponentials.

Human absorbed dose estimates were calculated using measured residence times and the MIRD S-value for ^{177}Lu calculated with values supplied as supplementary information by the author of MIRDOSE 3.0.[20] The absorbed dose to the bladder was calculated assuming no voiding, and the dose to the kidney was calculated assuming homogenous distribution of the activity throughout the organ, a potential limitation of the MIRDOSE model. Tumor dosimetry was calculated taking into account all radiation emissions from ^{177}Lu, and the S-value for the tumor was calculated for a spherical tumor of unit density filled uniformly with activity. This approach assumed that tumors of similar size in different animals had similar uptake characteristics, and the resulting absorbed dose was the average of the doses absorbed by the individual tumors.

After reactor production, the ^{177}Lu contains 2 impurities, a small amount of ^{176m}Lu ($t_{1/2}$ = 3.64 hr) and 0.02% of ^{177m}Lu ($t_{1/2}$ = 160.4 days). Due to the short half-life of ^{176m}Lu and the delivery time for the isotope, its contribution to the absorbed dose estimates was not considered. The 0.02% presence of ^{177m}Lu, a value recently confirmed and published by the NIST,[8] was considered, but the dose contribution of this contaminant was not included in our dosimetry calculations. It was assumed that this small impurity would only alter the absorbed dose estimates to the second decimal place and was easily within the reported standard deviations of the estimated absorbed doses.

Statistical analysis

To determine statistical significance in the biodistribution studies, a Student's t-test was performed with $p < 0.05$ being considered significantly different.

RESULTS

Toxicity study

The average weight of the treated rats increased similarly to that of the control animals, and they maintained a healthy physical appearance (with no sign of scruffy coat or diarrhea) over the experimental period. Throughout the examination period there were no significant changes in platelet counts, hemoglobin, hematocrit and differential WBCs (Table I). Levels of BUN, creatinine and ALT remained at baseline values, showing no overt liver and kidney toxicities. The hematology analysis values for the highest dose group (102.2–122.6 mCi/kg) are presented in Table I. WBC changes followed a dose-response pattern after administration (Fig. 2). In the lowest dose group (0–4.4 mCi/kg) there were no significant changes in WBCs over the experimental period (day −4, 11.95 ± 4.51 × 10^3/mm^3; day 2, 14.0 ± 4.38 × 10^3/mm^3; day 6, 12.8 ± 2.64 × 10^3/mm^3; day 15, 11.8 ± 1.64 × 10^3/mm^3; day 22, 11.4 ± 0.60 × 10^3/mm^3; $p > 0.1$). The 3 intermediate groups exhibited a transient depression in WBCs at 6 days (16.3–18.2 mCi/kg, 11.3 ± 2.43 × 10^3/mm^3; 36.7–40.5 mCi/kg, 8.9 ± 1.15 × 10^3/mm^3; 64.7–71.2 mCi/kg, 5.83 ± 1.34 × 10^3/mm^3; $p < 0.001$), but all recovered to baseline (day −4, 11.95 ± 4.51 × 10^3/mm^3) levels by day 22. The 102.2–122.6 mCi/kg dose group showed the greatest neutropenic response; however, the WBCs recovered to baseline levels by day 35 (day −4, 14.15 ± 2.98 × 10^3/mm^3; day 2, 8.4 ± 4.41 × 10^3/mm^3; day 6, 3.9 ± 1.8 × 10^3/mm^3; day 15, 5.6 ± 2.47 × 10^3/mm^3; day 22, 8.2 ± 2.00 × 10^3/mm^3; day 28, 10.5 ± 1.99 × 10^3/mm^3; day 35, 11.4 ± 1.58 × 10^3/mm^3; $p < 0.001$). In the gross necropsy and histopathologic examinations of selected tissues, there were no apparent lesions, showing the lack of gross or histologic signs of toxicity.

TABLE I – CHANGES IN HEMATOLOGIC, LIVER AND KIDNEY FUNCTION IN RATS TREATED WITH 102–122.6 mCi/kg ($n = 6$) OF ^{177}Lu-DOTA-Y3-TATE COMPARED WITH CONTROL RATS[1]

Days after injection	RBC 10^6/mm^3	Platelets 10^3/mm^3	ALT U/L	Creatinine mg/dL	BUN mg/dL
	7.9 ± 0.46	774.8 ± 154.9	45.0 ± 25.0	0.5 ± 0.2	9.0 ± 2.1
2	8.1 ± 0.95	886.7 ± 492.8	60.3 ± 9.0	0.7 ± 0.1	10.7 ± 2.3
6	8.8 ± 0.76	1050.2 ± 392.76	58.2 ± 6.8	0.6 ± 0.1	14.2 ± 2.2
15	8.7 ± 0.88	654.8 ± 122.4	51.8 ± 9.8	0.5 ± 0.1	16.4 ± 3.5
22	8.1 ± 0.40	757.3 ± 108.0	44.5 ± 11.7	0.4 ± 0.0	15.1 ± 1.5
28	8.4 ± 0.33	909.2 ± 130.3	54.7 ± 17.3	0.5 ± 0.1	13.3 ± 1.5
35	9.3 ± 0.24	840.3 ± 142.9	68.0 ± 11.8	0.5 ± 0.2	17.3 ± 0.5

[1]RBC, red blood cells; ALT, alanine aminotransferase; BUN, blood urea nitrogen.

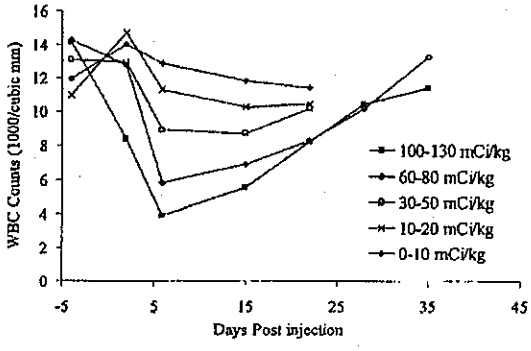

FIGURE 2 – White blood cell (WBC) counts (10^3/mm^3) in rats after administration of ^{177}Lu-DOTA-Y3-TATE in doses ranging from 0 to 123 mCi/kg. Error bars not shown for clarity.

Dosimetry

Human absorbed doses to normal organs from ^{177}Lu-DOTA-Y3-TATE were estimated from biodistribution data in CA20948 tumor-bearing rats. Biodistributions were performed at 1, 3, 6, 14, 24, 48, 72, 96 and 168 hr post injection, with the harvesting of 23 organs and tissues, a summary of which is shown in Table II. The rats for the 72 hr time point were housed in metabolism cages to determine %ID excreted in urine and feces at 1, 3, 18, 24, 48 and 72 hr (Table III). Total activity excreted in the urine by 72 hr was 68.74 ± 2.37%, and the total fecal excretion was 15.84 ± 3.11%. The human absorbed dose estimates to normal organs are presented in Table IV. The primary and secondary critical organs are the pancreas (11.12 ± 2.07 rad/mCi; 3.01 ± 0.56 mGy/MBq) and the adrenals (5.67 ± 0.86 rad/mCi; 1.53 ± 0.23 mGy/MBq), both somatostatin receptor-rich tissues. Primary excretion via the renal system resulted in an absorbed dose to the kidneys of 2.48 ± 0.17 rad/mCi (0.67 ± 0.05 mGy/MBq). In the CA20948 rat tumor, the average absorbed dose to the tumor was calculated to be 336 rad/mCi (91 mGy/MBq) for a single injection of ^{177}Lu-DOTA-Y3-TATE.

DISCUSSION

There have been several reports in recent years on targeted radiotherapy studies in tumor-bearing rodent models with radiolabeled somatostatin analogs labeled with ^{90}Y[21,22] and with alternative radionuclides such as ^{64}Cu,[16,19] ^{111}In,[1,6,23,24] ^{153}Sm,[25] ^{161}Tb,[26] ^{188}Re[27] and ^{177}Lu.[12,13] It has been demonstrated that with somatostatin-based peptides, changing the C-terminus from an alcohol (OC) to a carboxylic acid (TATE) increases uptake of these peptides in receptor-rich tissues.[18,23,28] This can result in a higher dose to the tumor, while not dramatically affecting the absorbed doses to normal tissue.[18] As a consequence, the most recent developments in the use of radiolabeled somatostatin analogs have focused on the use of the TATE derivative.[12,13,19,25]

The radiotherapy data obtained in rats with ^{177}Lu-labeled somatostatin analogs has been particularly impressive.[12,13] With ^{177}Lu-DOTA-Y3-TATE, the administration of 3 × 5 mCi over a 7-day period to tumor-bearing rats bearing 14-day-old CA20948 tumors resulted in a >95% decrease in tumor volume, with 66% of the animals remaining tumor-free 200 days after treatment.[13] In the same study, a single 5 mCi administration of ^{177}Lu-DOTA-Y3-TATE in rats bearing 14-day-old CA20948 tumors resulted in tumor regression to <5% of the original tumor volume by day 14. In this group of rats >50% of the animals showed no palpable tumor mass and exhibited long-term survival of over 5 months. A multiple dose regimen of ^{177}Lu-DOTA-Y3-TATE (3 × 5 mCi at 30-day intervals) resulted in similar regression responses but with a greater percentage of animals surviving long term. De Jong *et al.*[12] observed a 100% cure rate in rats bearing small CA20948 tumors (<1 cm^3) after administering either 2 doses of 7.5 mCi ^{177}Lu-DOTA-Y3-TATE or a single dose of 15 mCi. In the same study using larger tumors (>1 cm^3), 40 and 50% cure rates were achieved in the groups that received 1 or 2 7.5 mCi injections of ^{177}Lu-DOTA-Y3-TATE, respectively. These data prompted the current study examining the maximum tolerated dose (MTD) levels and human absorbed dose estimates for ^{177}Lu-DOTA-Y3-TATE.

In the largest dose group examined in our study (102.2–122.6 mCi/kg), no abnormalities were found with regard to animal behavior (movement, sleeping, eating, posture) over the first 48 hr after injection. Moreover, the treated rats gained weight throughout the experiment and at no time had any overt physical signs of toxicity, such as lethargy, scruffy coat, >10% weight loss or diarrhea. Transient decreases in WBC levels were noted, but by day 35 after the first treatment the WBC counts returned to baseline values. Although not fully comprehensive, these toxicity data are encouraging since the MTD was not achieved, and it is apparent that larger quantities of radioactivity can probably be administered safely. It is particularly notable that in the same CA20948 tumor model a 100% cure rate was found with ^{177}Lu-DOTA-Y3-TATE by administering either 2 doses of 7.5 mCi or a single dose of 15 mCi.[12] The doses used in the toxicity study (102.2–122.6 mCi/kg) correspond to an administration of 22.9–24.4 mCi per animal, which are over 50–60% higher than doses administered in the successful therapy studies by de Jong *et al.* In addition, previous studies have demonstrated minimal toxicity of the unlabeled peptide DOTA-Y3-TATE at levels far in excess of those that would be used in humans.[12]

Previous studies have demonstrated the usefulness of using rat biodistribution in predicting human absorbed dose estimates. A preliminary evaluation of the absorbed doses in normal organs with ^{64}Cu-TETA-OC performed by averaging positron emission tomography (PET) data from 5 patients demonstrated that the urinary bladder was the dose-limiting organ, which was predicted from human absorbed dose measurements estimated from rat biodistribution and baboon PET imaging data.[16,29] In the current study, the human absorbed estimates extrapolated from the biodistribution of ^{177}Lu-DOTA-Y3-TATE in rats showed that the primary and secondary critical organs were the pancreas (11.12 ± 2.07 rad/mCi; 3.01 ± 0.56 mGy/MBq) and

TABLE II – BIODISTRIBUTION AT 1, 3, 6, 24, 72 AND 168 HOURS OF ^{177}Lu-DOTA-Y3-TATE[1] IN SELECTED ORGANS

Organ	1 hr	3 hr	6 hr	24 hr	72 hr	168 hr
Blood	2.03 ± 0.42	0.31 ± 0.10	0.05 ± 0.05	0.03 ± 0.01	0.03 ± 0.00	0.01 ± 0.00
Lung	0.14 ± 0.01	0.08 ± 0.01	0.05 ± 0.00	0.04 ± 0.00	0.03 ± 0.01	0.02 ± 0.00
Liver	0.55 ± 0.23	0.34 ± 0.06	0.30 ± 0.03	0.28 ± 0.04	0.26 ± 0.08	0.18 ± 0.03
Spleen	0.02 ± 0.00	0.02 ± 0.00	0.01 ± 0.00	0.01 ± 0.00	0.01 ± 0.01	0.01 ± 0.00
Kidney	1.92 ± 0.11	1.93 ± 0.11	1.63 ± 0.06	1.71 ± 0.13	1.55 ± 0.09	0.94 ± 0.05
Muscle	1.25 ± 0.25	0.27 ± 0.03	0.08 ± 0.05	0.12 ± 0.01	0.09 ± 0.02	0.07 ± 0.02
Heart	0.04 ± 0.00	0.01 ± 0.00	0.01 ± 0.00	0.00 ± 0.00	0.00 ± 0.00	0.00 ± 0.00
Pituitary	0.03 ± 0.01	0.05 ± 0.01	0.04 ± 0.00	0.04 ± 0.01	0.03 ± 0.00	0.03 ± 0.01
Bone	11.96 ± 0.96	9.28 ± 1.34	5.47 ± 3.08	6.70 ± 0.75	5.03 ± 0.52	4.20 ± 0.19
Adrenal	0.31 ± 0.06	0.31 ± 0.09	0.30 ± 0.02	0.21 ± 0.03	0.14 ± 0.02	0.11 ± 0.02
Small intestine	0.89 ± 0.44	0.93 ± 0.48	0.73 ± 0.19	0.33 ± 0.06	0.19 ± 0.04	0.15 ± 0.05
Upper large intestine	0.77 ± 0.14	1.32 ± 0.47	2.70 ± 0.76	0.47 ± 0.12	0.16 ± 0.03	0.13 ± 0.01
Lower large intestine	2.87 ± 0.46	2.82 ± 0.27	4.89 ± 1.94	3.04 ± 0.65	0.87 ± 0.16	0.68 ± 0.21
Pancreas	10.49 ± 1.91	9.20 ± 1.42	6.43 ± 2.76	2.25 ± 0.32	1.80 ± 0.36	1.07 ± 0.10
Tumor	3.92 ± 3.84	5.92 ± 3.00	5.97 ± 4.04	6.13 ± 2.84	2.86 ± 1.77	0.65 ± 0.35

Data for 15 of 23 organs are given as % injected dose (ID) per organ ± SD (n = 5).–[1]The %ID/g data are available as supplementary information. Data for 14, 48 and 96 hr are not shown.

TABLE III – EXCRETION OF ^{177}Lu-DOTA-Y3-TATE IN CA20948 TUMOR-BEARING LEWIS RATS (N = 5) AT SELECTED TIME POINTS

	% Injected dose ± SD				
	1 hr	1–3 hr	3–24 hr	24–48 hr	1–72 hr total
Urine	20.91 ± 18.56	15.46 ± 19.15	26.13 ± 17.95	2.54 ± 0.64	68.74 ± 2.37
Feces	0.004 ± 0.012	0.004	6.12 ± 1.79	3.17 ± 0.94	15.84 ± 3.11

TABLE IV – HUMAN ABSORBED DOSE ESTIMATES OF ^{177}Lu-DOTA-Y3-TATE OBTAINED IN CA20948-BEARING RATS

Organ	Rad/mCi ± SD	mGy/MBq ± SD
Adrenals	5.670 ± 0.86	1.533 ± 0.233
Lower large intestine	3.289 ± 1.17	0.889 ± 0.316
Small intestine	0.172 ± 0.06	0.047 ± 0.015
Stomach	0.461 ± 0.09	0.125 ± 0.023
Upper large intestine	0.440 ± 0.10	0.119 ± 0.028
Heart wall	0.042 ± 0.01	0.011 ± 0.002
Kidneys	2.477 ± 0.17	0.670 ± 0.047
Liver	0.086 ± 0.02	0.023 ± 0.005
Lungs	0.029 ± 0.01	0.008 ± 0.002
Muscle	0.038 ± 0.01	0.010 ± 0.004
Pancreas	11.12 ± 2.07	3.006 ± 0.561
Red marrow	0.360 ± 0.05	0.097 ± 0.014
Bone surfaces	1.926 ± 0.23	0.521 ± 0.061
Spleen	0.074 ± 0.02	0.020 ± 0.004
Bladder wall	1.322 ± 0.16	0.357 ± 0.042
Total body	0.116 ± 0.03	0.031 ± 0.007

the adrenals (5.67 ± 0.86 rad/mCi; 1.53 ± 0.23 mGy/MBq), both somatostatin receptor-rich tissues. It was further demonstrated that the primary excretion route was via the renal system, which resulted in an absorbed dose to the kidneys of 2.48 ± 0.17 rad/mCi (0.67 ± 0.05 mGy/MBq). It should be noted that the kidney uptake of ^{177}Lu-DOTA-Y3-TATE can be significantly reduced by 40% by the coinjection of 400 mg/kg D-lysine.[12] The transient depression in WBCs may also be indicative of the dose delivered to the bone marrow causing toxicity. A multiple dose regimen might significantly reduce the absorbed doses to nontarget organs by allowing the delivery of a consistent amount of tolerable radiation over an extended period to the tumor, while allowing intermittent recovery of nontarget tissues. It is also important to note that hepatobiliary and renal clearance of many radiopharmaceuticals,[30] as well as receptor concentrations and subtype expression,[31] vary widely from rodents to humans and that primate and actual human doses may be improved over dose estimates from animal models. With this in mind, in humans the primary and secondary tissue may not be the pancreas and the adrenals.

In the de Jong *et al.*[12] study, a single 15 mCi dose of ^{177}Lu-DOTA-Y3-TATE resulted in a 100% cure in 200–300 g rats bearing small tumors, which would suggest a dose of over 2 Ci of ^{177}Lu-DOTA-Y3-TATE for clinical therapy trials in humans. In the ongoing clinical trials the patients are scheduled to receive a maximum cumulative dose of only 600–800 mCi.[5] In these human trials, 26 patients with progressive disease were given 300 mCi of ^{177}Lu-DOTA-Y3-TATE with amino acid infusion to reduce the kidney dose.[5] Of the 26 patients, 31% experienced nausea, 9% vomiting and 11% mild abdominal discomfort. Additionally, of the 26 patients, 5 presented with mild leukocytopenia, 3 with mild thrombocytopenia and 10 with mild anemia. At the time of presentation none of the patients had received their maximum cumulative dose of 600–800 mCi and had shown a range of responses from tumor shrinkage (8/26) to stable disease (14/26) to partial remission (1/26) to tumor progression (3/26).

The absorbed dose to the CA20948 tumor from ^{177}Lu-DOTA-Y3-TATE calculated from the rat biodistribution was 336.46 ± 203 rad/mCi (90.94 ± 54.9 mGy/MBq); a similar value of 96 mGy/MBq was reported by de Jong *et al.*[12] This value is higher than that calculated for ^{64}Cu-DOTA-Y3-TATE (33.2 rad/mCi) but is considerably lower than that calculated for ^{90}Y-DOTA-Y3-TATE (1753 rad/mCi).[18] Comparing the estimated absorbed doses for ^{177}Lu-DOTA-Y3-TATE with ^{64}Cu-DOTA-Y3-TATE, the dose imparted to the kidney was ~5 times higher (2.48 ± 0.17 *vs.* 0.48 ± 0.16 rad/mCi) but imparted ~10-fold more dose (336 rad/mCi vs 33.24 rad/mCi) to the CA20948 tumor. When comparing the absorbed dose to the kidney between ^{177}Lu-DOTA-Y3-TATE and ^{90}Y-DOTA-Y3-TATE, the dose imparted to the kidney was ~3 times lower (2.48 ± 0.17 *vs.* 7.29 ± 1.22 rad/mCi), with a ~5-fold reduction in dose (336 rad/mCi *vs.* 1753 rad/mCi) to the CA20948 tumor. These data suggest that although ^{177}Lu-DOTA-Y3-TATE appears to have distinct advantages over ^{64}Cu-DOTA-Y3-TATE, ^{177}Lu-DOTA-Y3-TATE and ^{90}Y-DOTA-Y3-TATE may be more comparable with respect to their tumor and normal tissue toxicity.

Doses of ^{177}Lu-DOTA-Y3-TATE ranging from 0 to 123 mCi/kg were administered to normal rats and complete blood counts (CBCs) and blood chemistries were analyzed out to 6 weeks. No overt signs of toxicity were observed with ^{177}Lu-DOTA-Y3-TATE at any of the dose levels. We further estimated human absorbed radiation doses to normal tissues and the absorbed dose to the rat CA20948 tumor for ^{177}Lu-DOTA-Y3-TATE, for which

the adrenals and pancreas were determined to be the dose-limiting organs. Since previous studies have demonstrated that ^{177}Lu-DOTA-Y3-TATE is effective in causing tumor regression of CA20948 tumors in rats, these toxicity and dosimetry data suggest that ^{177}Lu-DOTA-Y3-TATE may be an effective targeted radiotherapy agent at levels that show minimal toxicity in humans. These data, in conjunction with the human trial data,[5] further suggest that this radiopharmaceutical may be at least as effective as the ^{90}Y-labeled somatostatin analogs currently in use.

ACKNOWLEDGEMENTS

We thank Dr. M.A. Schmidt (Mallinckrodt, Inc.) for providing DOTA-Y3-TATE and DOTA-Y3-OC, as well as M.M. Morris, L. Jones and J. Wang for technical support. This work was supported by grants from the National Cancer Institute (CA64475 to C.J.A.) and the Biotechnology Research Development Corporation (to C.J.A.). Lutetium-177 was supplied by the University of Missouri Research Reactor (to J.S.L.) under the Department of Energy's Reactor Sharing Support Program (DE-FG07-01ID14146).

REFERENCES

1. Krenning EP, Kooij PP, Bakker WH, et al. Radiotherapy with a radiolabeled somatostatin analogue, [^{111}In-DTPA-D-Phe^1]-octreotide. A case history. Ann NY Acad Sci 1994; 733:496–506.
2. Otte A, Herrmann R, Heppeler A, et al. Yttrium-90 DOTATOC: first clinical results. Eur J Nucl Med 1999;26:1439–47.
3. Otte A, Mueller-Brand J, Goetze M, et al. Yttrium-90-DOTA-octreotide treatment of somatostatin receptor positive tumors. J Nucl Med 1998;39:70P.
4. Pagenelli G, Zoboli S, Cremonesi M, et al. Receptor-mediated radiotherapy with ^{90}Y-DOTA-D-Phe^1-Tyr^3-octreotide. Eur J Nucl Med 2001;28:426–34.
5. Kwekkeboom DJ, Kam BL, Bakker WH, et al. Treatment with [^{177}Lu-DOTA^0,Tyr^3]octreotate in patients with somatostatin receptor positive tumors: Preliminary results. J Nucl Med 2001;452:37P.
6. Fjälling M, Andersson P, Forssell-Aronsson E, et al. Systemic radionuclide therapy using Indium-111-DTPA-D-Phe^1-octreotide in midgut carcinoid syndrome. J Nucl Med 1996;37:1519–21.
7. O'Donoghue JA, Bardies M, Wheldon TE. Relationships between tumor size and curability for uniformly targeted therapy with beta-emitting radionuclides. J Nucl Med 1995;36:1902–9.
8. Zimmerman BE, Unterweger MP, Brodack JW. The standardization of ^{177}Lu by 4πβ liquid scintillation spectrometry with ^{3}H-standard efficiency tracing. Appl Radiat Isotopes 2001;54:623–31.
9. Chu SYU, Ekstrom LP, Firestone RB. The Lund/LBNL nuclear data search. LBNL isotopes project 1999; Version 2.0.
10. Ehrhardt GJ, Ketring AR, Ayers LM. Reactor-produced radionuclides at the University of Missouri Research Reactor. Appl Radiat Isotopes 1998;49:295–7.
11. Alverez RD, Partridge EE, Khazaeli MB, et al. Intraperitoneal radioimmunotherapy of ovarian cancer with ^{177}Lu-CC49: a phase I/II study. Gynecol Oncol 1997;65:94–101.
12. de Jong M, Breeman WAP, Bernard HF, et al. [^{177}Lu-DOTA^0,Tyr^3]octreotate for somatostatin receptor-targeted radionuclide therapy. Int J Cancer 2001;92:628–33.
13. Erion JL, Bugaj JE, Schmidt MA, et al. High radiotherapy efficacy of [Lu-177]-DOTA-Y^3-octreotate in a rat tumor model. J Nucl Med 1999;40:223P.
14. Lewis JS, Srinivasan A, Schmidt MA, et al. In vitro and in vivo evaluation of ^{64}Cu-TETA-Tyr^3-Octreotate. A new somatostatin analog with improved target tissue uptake. Nucl Med Biol 1999;26:267–73.
15. Longnecker DS, Lilja HS, French J, et al. Transplantation of azaserine-induced carcinomas of pancreas in rats. Cancer Lett 1979;7:197–202.
16. Anderson CJ, Jones LA, Bass LA, et al. Radiotherapy, toxicity and dosimetry of copper-64-TETA-octreotide in tumor bearing rats. J Nucl Med 1998;39:1944–51.
17. Lewis JS, Buettner TL, Connett JM, et al. Cu-64-diacetyl-bis(N^4-methylthiosemicarbazone): an agent for radiotherapy. Proc Natl Acad Sci USA 2001;89:1206–11.
18. Lewis JS, Laforest R, Lewis MR, et al. Comparative dosimetry of copper-64 and yttrium-90-labeled somatostatin analogs in a tumor-bearing rat model. Cancer Biotherapy Radiopharm 2000;15:593–604.
19. Lewis JS, Lewis MR, Cutler PD, et al. Radiotherapy and dosimetry of ^{64}Cu-TETA-Tyr^3-octreotate in a somatostatin receptor-positive, tumor bearing rat model. Clin Cancer Res 1999;5:3608–16.
20. Stabin M. MIRDOSE: personal computer software for internal dose assessment in nuclear medicine. J Nucl Med 1996;37:538–46.
21. Stolz B, Weckbecker G, Smith-Jones PM, et al. The somatostatin receptor-targeted radiotherapeutic [^{90}Y-DOTA-DPhe^1, Tyr^3]octreotide (^{90}Y-SMT 487) eradicates experimental rat pancreatic CA20948 tumours. Eur J Nucl Med 1998;25:668–74.
22. Stolz B, Smith-Jones P, Weckbecker G, et al. Radiotherapy with Yttrium-90 labeled DOTA-Tyr^3-octreotide in tumor bearing rodents. J Nucl Med 1997;38:18P.
23. de Jong M, Bakker WH, Breeman WAP, et al. Preclinical comparison of [DTPA^0]octreotide, [DTPA^0,Tyr^3]-octreotide and [DOTA^0,Tyr^3]-octreotide as carriers for somatostatin receptor-targeted scintigraphy and radionuclide therapy. Int J Cancer 1998;75:406–11.
24. de Jong M, Breeman WAP, Bakker WH, et al. Comparison of ^{111}In-labeled somatostatin analogues for tumor scintigraphy and radionuclide therapy. Cancer Res 1998;58:437–41.
25. Bugaj JE, Erion JL, Johnson MA, et al. Radiotherapeutic efficacy of ^{153}Sm-CMDTPA-Tyr^3-octreotate in tumor-bearing rats. Nucl Med Biol 2001;28:327–34.
26. de Jong M, Breeman WAP, Bernard BF, et al. Evaluation *in vitro* and in rats of ^{161}Tb-DTPA-octreotide, a somatostatin analogue with potential for intraoperative scanning and radiotherapy. Eur J Nucl Med 1995;22:608–16.
27. Zamora PO, Gulhke S, Bender H, et al. Experimental radiotherapy of receptor-positive human prostate adenocarcinoma with ^{188}Re-RC-160, a directly-radiolabeled somatostatin analogue. Int J Cancer 1996; 65:214–20.
28. Lewis JS, Lewis MR, Srinivasan A, et al. Comparison of four ^{64}Cu-labeled somatostatin analogues *in vitro* and in a tumor-bearing rat model: evaluation of new derivatives for positron emission tomography imaging and targeted radiotherapy. J Med Chem 1999;42:1341–7.
29. Anderson CJ, Dehdashti F, Cutler PD, et al. ^{64}Cu-TETA-octreotide as a PET imaging agent for patients with neuroendocrine tumors. J Nucl Med 2001;42:213–21.
30. Fritzberg AR, Bloedow DC. Animal models in the study of hepatobiliary radiotracers. In: Lambrecht RM, Eckelman WC, eds. Animal models in radiotracer design. New York: Springer-Verlag, 1983. 179–209.
31. Bruns C, Raulf F, Hoyer D, et al. Binding properties of somatostatin receptor subtypes. Metabolism 1996;45:17–20.

CHAPTER 8B

LONG TERM TOXICITY of ^{177}Lu-DOTA-Tyr^{3}-OCTREOTATE IN TUMOR BEARING ANIMALS

Joseph E. Bugaj , Marion de Jong, Eric P. Krenning and Jack L. Erion

ABSTRACT

The past several years have witnessed an increase in the number of somatostatin analogues evaluated for radiotherapeutic efficacy in tumor bearing animal models and early human studies. A growing number of potential radionuclides chelated to these analogues include Y-90, Re-188, Cu-64, In-111, Sm-153 and Lu-177. All of these radionuclides have demonstrated varying degrees of therapeutic efficacy in tumor bearing animal models with Y-90, In-111 and Lu-177 advancing to early human clinical studies. Preliminary toxicology studies in rats have largely focused on acute toxic effects, but as yet no long term toxicology study (>12 months post treatment) has been reported. The current study describes the long-term toxicology of ^{177}Lu-DOTA-Tyr^3-octreotate in CA20948 tumor bearing rats that have survived 14-18 months post treatment. Of the16 rats examined after different treatment regimens with ^{177}Lu-DOTA-Tyr^3-octreotate, 13 animals (81%) indicated evidence of renal neoplasm and were classified as renal cell carcinoma. Pancreatic carcinoma was found in 40% of the treated animals (4/10) examined histologically. Somatostatin receptor negative tissues of the spleen and liver were all negative for pathology. In contrast, normal control animals of the same age at the time of sacrifice indicated no evidence of neoplasia in any of the target or non-target tissues examined. This is the first study evaluating the long-term radiotoxicity of ^{177}Lu-DOTA-Y^3-Octreotate in rodents, with the primary focus on delayed renal toxicity.

INTRODUCTION

Targeted radiotherapy using somatostatin analogues has progressed from early efficacy studies in animal models to objective responses in human clinical trials. A variety of somatostatin analogues radiolabeled with Re-188, Cu-64, In-111, Sm-153, Y-90 and Lu-177 have all demonstrated varying degrees of efficacy in animal

models, and the latter two isotopes have progressed to early human use trials with promising results (3, 4, 8, 9, 13, 14, 15, 17, 22, 23). Of the different agents evaluated, the chelate ^{177}Lu-DOTA-Tyr^3-octreotate (Figure 1) has demonstrated the most pronounced therapeutic effect in tumor bearing rat models. Because of the well documented mechanism for the in vivo breakdown of this class of peptides, the kidney is the primary organ of toxicity in these types of studies (1, 2, 7). Though the dose to the kidneys can be reduced by 40-50% using amino acid infusion, the kidneys require close monitoring by dosimetry to reduce potential chronic renal toxicity (4, 5, 7).

A growing number of somatostatin analogues chelated to a variety of radionuclides have been evaluated in tumor models. These radionuclides range in energy from low to very high β^- emissions. Other radionuclides that have demonstrated varying degrees of therapeutic efficacy include Cu-64 (0.564MeV), Sm-153 (0.65MeV) and In-111 (Auger). Of these radionuclides, two that have demonstrated the most promising results in tumor bearing rat models are Y-90 and Lu-177 (12, 14, 15-17). These two isotopes differ greatly in their physiochemical characteristics. Y-90 is a high-energy β^- emitter, 2.2MeV, with a relatively short t $_{½}$ of 60 hours, while Lu-177 emits a β^- particle of only 0.497 MeV with a long t $_{½}$ of 6.7 days. Lu-177 also emits a low abundance of a 0.208MeV gamma emission that is very suitable for scintigraphy and for use in dosimetry calculations (16, 17).

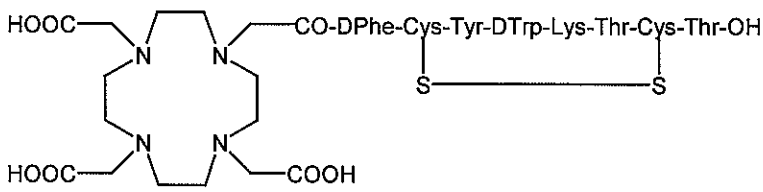

Figure 1: Structure of DOTA-Tyr^3-octreotate

When evaluated in the CA20948 tumor bearing Lewis rat model, ^{90}Y-DOTA-Tyr^3-Octreotide showed a complete ablation of the tumor in 5 of 7 (71%) animals treated with a single dose of 2.5mCi/rat (21). No marked impairment of the animal's health was observed during the eight month observation period, but no histology data on the kidneys was or has since been reported. In contrast, rats bearing the same tumor line treated with 3 x 5.0mCi of ^{177}Lu-DOTA-Tyr^3-octreotate at 30 day intervals demonstrated complete tumor ablation in 100% of the animals for a period of up to 16 months post treatment. Additionally, a lower dosing regimen of this agent (3 x 2.5mCi/rat at 30 day intervals) resulted in complete tumor remission in 75% of rats treated at 18 months post treatment (16, 17).

In this study we report on the long-term toxicity of ^{177}Lu-DOTA-Tyr^3-octreotate in CA20948 tumor bearing Lewis rats. Animals were first treated with the agent using either a single dose of 5.0 mCi/rat or multiple doses of 3 x 2.5mCi or 3 x 5.0mCi at 30 day intervals. At the time of death selected tissues were evaluated by histology for evidence of toxicity after the animals had reached or exceeded 14 months post treatment.

MATERIALS AND METHODS

Radiochemistry

$^{177}LuCl_3$ in 0.05N HCl was obtained from MURR (Colombia, MO) at a specific activity of 3000Ci/mmol. DOTA-Tyr^3-octreotate was synthetized as previously described (15-17). The ligand was radiolabeled with $^{177}LuCl_3$ in 30mM NaOAc/25mM ascorbate, pH 5.0 for 15 minutes at 80 C. Radiochemical purity was determined by reverse phase HPLC on a Nova Pac C-18 column using a 15 minute linear gradient of 0% to 70%

ACN/25mM triethylamine, pH 6.0. The labeled peptide eluted at 12.47 minutes (Solvent A = 5% ACN/25mM triethylamine, pH 6.0).

Animal Tumor Model

All animal studies were conducted in compliance with the Mallinckrodt Inc. Animal Welfare Committee requirements. Male Lewis rats (120-140 g) were purchased from Harlan (Indianapolis, IN). The somatostatin subtype-2 (sst_2) receptor positive pancreatic acinar tumor line, CA20948, was maintained by serial passage into Lewis rats (3, 9, 15). Tumor tissue was implanted into the left flank of the animal, and after approximately seven days tumor masses were palpable and were then used in the radiotherapy studies.

Radiotherapy Studies

CA20948 tumor tissue was implanted into the left flank of Lewis rats as described above. At 7 days post implant, animals were randomly divided into study groups. The presence of tumor mass was confirmed by palpation. For each treatment group a set of negative control animals (n = 6) was maintained. Negative control animals were implanted with tumor material but received no therapeutic treatment. Treated animals received dosing regimens of ^{177}Lu-DOTA-Tyr^3-octreotate were as follows: (1) single dose of 5.0mCi, (2) three doses of 2.5mCi/rat at 30 day intervals (n = 8) or (3) three doses of 5.0 mCi/rat at 30 day intervals (n = 8). Tumor volume measurements were performed on a weekly basis and calculated using the formula for an ellipsoid ($v = \pi/6[l \cdot w \cdot h]$) (17).

HISTOLOGY

Tissues were taken from two separate groups of animals of the same approximate age. Tumor bearing animals that underwent treatment with the radiolabeled peptide,

and a second control group of animals that were housed and maintained for a period of 18 months but were neither implanted with tumor material, nor received any dose of radiolabeled peptide. This control group was created to allow for the possibility of age related pathology for comparison to the tissues from the treatment groups approximating the time of sacrifice. The tissues were trimmed and processed by standard techniques for embedding in paraffin. Two sections were taken from most of the tissue samples. The blocks were sectioned with a rotary mictotome set at a thickness of four micrometers. After sectioning, the sections were deparaffinized and stained with hematoxylin and eosin. Representative lesions were photographed using an Olympus BHS Photomicroscope and a 35mm Fujichrome Provia 100 F film. Digitized photos were captured with a Polaroid Sprint Scan 35 film scanner.

RESULTS

Radiotherapy Studies

Figure 2 shows the survival curves for the untreated control group versus the two treatment regimens. Tumor bearing negative control animals that received no treatment were sacrificed after approximately 35 days due to excessive tumor growth. Only fifty percent of the animals that received the single dose of 5.0mCi/rat survived to 3 months post treatment. Animals receiving 3 doses of 2.5 mCi/rat at 30 day intervals resulted in a long-term survival of 50% of the animals living 21 months post treatment. The high dose group that received 3 doses of 5.0mCi/rat at the same interval all survived past 14 months post treatment, and all animals were tumor free at the time of sacrifice or death. By 18 months all animals from this group had died.

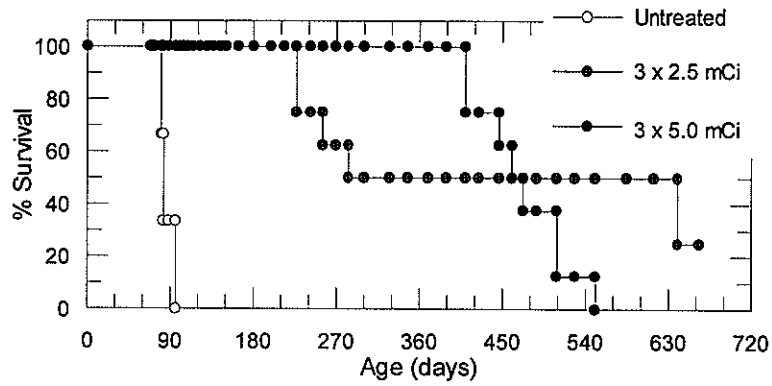

Figure 2: Survival graph of rats treated with ^{177}Lu-DOTA-Tyr^3-octreotate. Open circles = untreated animals., shaded circles = 3 x 2.5mCi dose regimen; filled circles = 3 x 5.0mCi dose regimen. Doses were administered at 30 day intervals.

Histology

Tumor bearing rats that had undergone treatment with ^{177}Lu-DOTA-Tyr^3-octreotate survived from 16-22 months post treatment. Untreated control animals that were maintained for the 18 month survival period were sacrificed at that time to mimic the age of the treated groups at the time of death to ascertain any age related pathology for the tissues evaluated. A total of 16 treated animals and 6 untreated control animals (18 months of age) were analyzed post mortem for evidence of pathology. The kidneys were the primary focus of this evaluation. Additionally, pancreas (n= 10), spleen (n = 12) and liver (n =16) tissues were also removed from most of these animals. From the untreated control animals the kidneys, pancreas, liver, and spleen were removed and analyzed. Table 1 shows the overall results of the histological findings.

Table 1: Histology Results from Tissue Samples of Rats Treated with Different Regimens of ^{177}Lu-DOTA-Y^3-Octreotate

(Positive Histology/Number of Samples Examined)

Regimen	Kidney	Spleen	Pancreas	Liver
1 x 5.0mCi	1/3	0/3	2/2	0/3
3 x 2.5mCi	5/6	0/5	2/4	0/6
3 x 5.0mCi	7/7	0/5	2/5	0/7

The negative control animals that had been housed for the 18 month survival period were sacrificed at that time, and the kidneys, liver, spleen and pancreas tissues removed and analyzed for pathology. In all six animals no evidence of any abnormal pathology in any of the tissues was observed. Typically, the kidneys (Figure 3) from these animals exhibited evidence of glomerular nephritis and glomerular sclerosis, chronic nephritis, tubular ectasia and tubular proteinosis. All of the renal changes are typical of those observed in chronic rat nephropathy. Islet cell hyperplasia was commonly found in the pancreas samples from this group. No significant pathology was noted from any animal for either the spleen or liver tissues.

Figure 3: High power photomicrograph of kidney from negative control animal (18 months old). The glomeruli are relatively normal in appearance, with minimal degree of multifocal glomerular sclerosis, typical changes observed in chronic rat nephropathy.

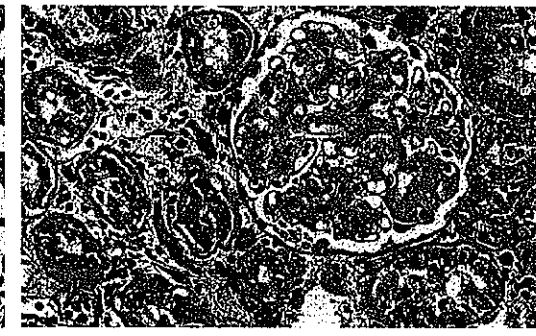

Figure 4: High power photomicrograph of kidney from treated rat with 3 x 5.0mCi of ^{177}Lu-DOTA-Tyr^3-octreotate at 30 day intervals. Glomerulus has marked multifocal fibrosis, and the glomerulersclerosis is characterized by multiple areas of hypocellualrity, thickening of capilliary loops and eosinophilic material. Contrast to glomeruli in Figure 3.

Of the 16 treated animals 13 (81%) showed evidence of renal carcinoma or urothelial neoplasm that appeared to arise from the tubular epithelia. Figure 4 is a high power photomicrograph of kidney tissue from an animal treated with 3 x 5.0mCi of ^{177}Lu-DOTA-Tyr^3-octreotate.

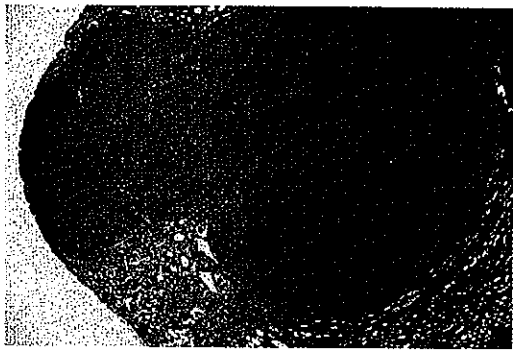

Figure 5: Low power photomicrograph of kidney indicating large neoplasm replacing most of renal parenchyma. Mass was diagnosed as renal cell carcinoma. Rat was treated with 3 x 5.0mCi of ^{177}Lu-DOTA-Tyr^3-octreotate at 30 day intervals.

Figure 6: Medium power photomicrograph of renal hilus from animal treated with 3 x 2.5mCi of ^{177}Lu-DOTA-Tyr^3-octreotate at 30 day intervals. Urothelial neoplasm is shown surrounding ureter and infiltrating muscle wall.

The glomerulus shows marked fibrosis, hypocellularity and thickening of capillary loops. Figure 5 is a photo of a rat kidney indicating large neoplasm of renal parenchyma. Rat was treated with 3 x 5.0mCi of ^{177}Lu-DOTA-Tyr^3-octreotate. In Figure 7, a medium power photomicrograph shows the renal cell carcinoma characterized by marked karyomegaly and nuclear pleomorphism. A urothelial neoplasm is shown in Figure 6. In this medium power photomicrograph of the renal hilus, the neoplasm is shown surrounding the ureter and infiltrating the muscle wall. Rat received 3 x 2.5mCi of ^{177}Lu-DOTA-Tyr^3-octreotate. The remaining three kidney samples showed evidence of karyomegaly of the tubular epithelia cells suggesting pre-neoplastic lesions (Figure 8). There was a greater than expected severity of

chronic renal disease that has been attributed to treatment with the radiolabeled peptide.

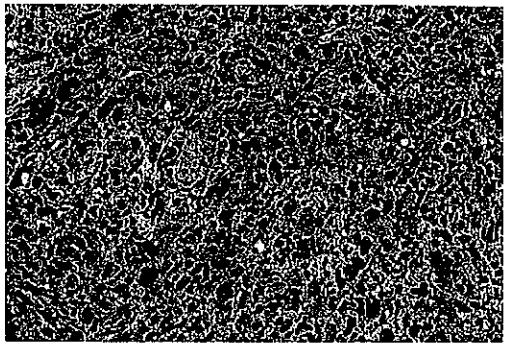

Figure 7: Medium power photomicrograph of renal cell carcinoma characterized by marked karyomegaly and nuclear pleomorphisim. Rat was treated with 3 x 2.5mCi of ^{177}Lu-DOTA-Tyr^3-octreotate at 30 day intervals.

Figure 8: High power photomicrograph of renal glomerulus marked by hyperplasia and karyomegaly of cells lining glomerular space. Animal treated with 3 x 2.5mCi of ^{177}Lu-DOTA-Tyr^3-octreotate at 30 day intervals.

The pancreas samples from the treated animals indicated a 50% incidence of cancer with 40% as islet cell carcinoma and one pancreatic adenoma. The two-sst_2 receptor negative tissues of the spleen and liver showed no evidence of underlying pathology in any tissues analyzed from the treated groups.

DISCUSSION

The increased number of targeted radiotherapeutic peptides in rodent models and early human studies for the ablation of neuroendocrine tumors has involved a variety of somatostatin analogues radiolabeled with beta particle and Auger emitting radionuclides. It has been previously demonstrated with somatostatin-based peptides that changing the C-terminus from an alcohol to the native carboxylic acid

significantly increases the uptake and retention in sst_2 positive tissues without affecting uptake in normal non-target tissue (9, 13, 15, 19). However, inherent in this general class of peptides, is the in vivo metabolic degredation of the peptide to truncated molecules composed of the chelate and the first few amino acids (D-Phe^1). As a result these small peptide fragments are readily reabsorbed in the renal tubules, resulting in high non-specific uptake and retention in the kidneys (1, 2). Internalization of the radiolabeled fragments occurs through receptor mediated endocytosis, become trapped in the lysosomes of the proximal tubules, and delivers a localized radiation dose to the tubules (7). This non-specific retention accounts for the high kidney dose observed for these peptides, and the use of beta emitting isotopes make the kidneys the primary organ for radiotoxicity. Of the radionuclides evaluated in animal models thus far, the isotope Lu-177 has demonstrated the most pronounced therapeutic effect when chelated to DOTA-Y^3-Octreotate (15-17). Complete ablation of CA20948 tumors was observed from 16-22 months post implant after 3 doses of 2.5mCi or 5.0mCi of that agent. Previously, only the Y-90 octreotide derivative showed complete ablation of the same tumor line in vivo, with long-term survival of the animal reported to eight months post injection. In that particular study no histological evaluation of the kidneys was reported (21). Recently, the observation of end stage renal disease after treatment with ^{90}Y-DOTATOC was published (10). In this study, the renal effects were observed 15 months post administration of the agent, and the authors suggest that the delayed renal insufficiency was due to a low cumulative dose of the radiotherapeutic. As a result, more cautious dosing regimens to avoid renal toxicity were encouraged.

The studies presented here focus on the long-term toxicity of the agent ^{177}Lu-DOTA-Y^{3}-Octreotate, with primary attention to kidney toxicity. To date several acute toxicity studies have been performed. Doses of 100mCi/kg of DOTA-Y^{3}-Octreotate and 10mCi/kg of ^{90}Y- DOTA-Y^{3}-Octreotide indicated that no abnormalities were observed in any tissues, and the only observed toxicity was a transient drop in the WBC level which returned to normal after 30 days (20, 21). These reports suggest that elevated doses of the agents can be safely administered, especially when amino acid infusion is included in the regimen to reduce kidney toxicity. However, this study suggest that the radiotoxic effects observed with Lu-177, and likely for other β^- emitters, are not readily observable until the animals survive approximately one-year post injection. As a result, the real effect is chronic renal toxicity, and the acute studies are not predictive of the actual toxicity of the agent. Since no previous therapy studies in animal models went beyond a period of 8 months, this represents the first toxicity study that demonstrates long-term renal toxicity of an administered radiotherapeutic. As previously indicated, no untreated tumor bearing animals survived beyond 40 days post inoculation. The long-term survival observed in the treated animals from this study would equate to a significantly increased life span in humans. Additionally, in this study no attempt to block non-specific kidney retention using amino acid infusion was attempted. A number of studies in several laboratories support a 50% reduction in kidney uptake effected using amino acid infusion, there by reducing significantly the potential toxic effects of this radiotherapeutic. This technique is currently in place in the early human use studies evaluating the therapeutic efficacy of Y-90-Octreotide and Lu-177-Octreotate (5, 6, 10, 11). The importance of protecting the kidneys of all patients undergoing radiotherapy is further emphasized in the Cybulla reference (10).

The last two years has seen an increase in the use of Lu-177 as a therapeutic radionuclide (15-17, 20). Impressive pre-clinical studies in tumor bearing animal models using ^{177}Lu-DOTA-Y^{3}-Octreotate, has led to the evaluation of this agent in the clinical setting, and preliminary data in an early human trial support the efficacy observed in the rodent model (18). As a result, the long term toxicity of this agent is currently unknown, even though acute toxicity studies in animals report no toxicity of the agent, renal or otherwise, even at dose of >100mCi/kg. This study expands on the acute toxicity studies for this agent, and represents the first report of long term toxicity in an animal model using this agent as a radiotherapeutic.

Though these studies suggest that any radiotoxicity associated with this agent will be a chronic event, the administration of amino acids will reduce this effect and is a viable alternative in expanding the therapeutic window for this agent. Long-term studies in rodents using such infusion techniques are warranted to more fully assess the chronic renal toxicity under a clinical setting.

REFERENCES

1. Akizawa Arano Y., Uezono T., Ono M., Fujioka Y., Uehara T., Yokoyama A., Akaji K., Kiso Y., Koizumi M. and Saji H. (1998) Renal metabolism of ^{111}In-DTPA-DPhe^{1}-octreotide *in vivo*. *Bioconjugate Chem.* 9, 662-670.

2. Akizawa Hiromichi, Arano Yasushi, Mifune Masaki, Iwado Akimasa, Saito Yutaka, Mukai Takahiro, Uehera Tomoya, Ono Masahiro, Fujioka Yasushi, Ogawa Kazuma, Kiso Yoshiaki and Saji Hideo. (2001) Effects of molecular charges on renal uptake of 111In-DTPA-conjugated peptides. *Nucl Med & Bio*, 28, 761-768.

3. Anderson C. J., Pajeau T. S., Edwards W. B., Sherman E. L., Rogers B. E. and Welch M. J. (1995) *In vitro* and *in vivo* evaluation of copper-64-octreotide conjugates. *J. Nucl. Med.* 36, 2315-2325.

4. Anderson C. J., Jones L. A., Bass L. A., Sherman E. L., McCarthy D. W., Cutler P. D., Lanahan M. V., Cristel M. E., Lewis J. S. and Schwarz S. W. (1998) Radiotherapy, toxicity and dosimetry of copper-64-TETA-octreotide in tumor-bearing rats. *J. Nucl. Med.* 39, 1944-1951.

5. Behr T. M., Sharkey R. M., Juweid M. E., Blumenthal R. D., Dunn R. M., Griffiths G. L., Bair H. J., Wolf F. G., Becker W. S. and Goldenberg D. M. (1995) Reduction of the renal uptake of radiolabeled antibody fragments by cationic amino acids and their derivatives. *Cancer Res.* 55, 3825-3834.

6. Bernard B. F., Krenning E. P., Breeman W. A., Rolleman E. J., Bakker W. H., Visser T. J., Macke H. And de Jong M. (1996) D-Lysine Reduction of Indium-111 Octreotide and Yttrium-90 Octreotide Renal Uptake, *J Nucl Med*, 38, 1929-1933.

7. Boerman O.C., Oyen W.J.G., and Corstens F.H.M. (2001) Between the Scylla and Charybdis of peptide radionuclide therapy: hitting the tumor and saving the kidney, *Eur J Nucl Med*, 28, 1447-1449.

8. Breeman W. A., van Hagen P. M., Kwekkeboom D. J., Visser T. J. and Krenning E. P. (1998) Somatostatin receptor scintigraphy using [^{111}In-DTPA^{0}]RC-160 in humans: a comparison with [^{111}In-DTPA^{0}]octreotide. *Eur J Nucl. Med*, 25, 182-186.

9. Bugaj, J.E., Erion, J.L., Johnson, M.A., Schmidt, M.A., and Srinivasan, A. (2001) Radiotherapeutic efficacy of ^{153}Sm-CMDTPA-Tyr^{3}-octreotate in a rat tumor model, *Nuc Med Biol.,* 28, 327-334.

10. Cybulla M., Weiner S. and Otte A. (2001) End-stage renal disease after treatment with ^{90}Y-DOTATOC, *Eur J Nucl Med*, 28, 1552-1554.

11. De Jong M., Rolleman E. J., Bernard B. F., Visser T. J., Bakker W. H., Breeman W. A. and Krenning E. P. (1995) Inhibition of Renal Uptake of Indium-111-DTPA-Octreotide in Vivo, *J Nucl Med* 37, 1388-1392.

12. De Jong M., Bakker W. H., Krenning E. P., Breeman W. A., van der Pluijm M. E., Bernard B. F., Visser T. J., Jermann E., Behe M., Powell P. and Macke H. R. (1997) Yttrium-90 and indium-111 labelling, receptor binding and biodistribution of [DOTA^0,D-Phe^1,Tyr^3]octreotide, a promising somatostatin analogue for radionuclide therapy. *Eur J Nucl Med.* 24, 368-371.

13. De Jong M., Breeman W. A., Bakker W. H., Kooij P. M., Bernard B. F., Hofland L. J., Visser T. J., Srinivasan A., Schmidt M. A., Erion J. L., Bugaj J. E., Macke H. R. and Krenning E. P. (1998) Comparison of ^{111}In-labeled somatostatin analogues for tumor scintigraphy and radionuclide therapy. *Cancer Res.* 58, 437-441.

14. De Jong M., Breeman W. A., Bernard B. F., Kooij P. M., Slooter G. D., van Eijck C. H., Kwekkeboom D. J., Valkema R., Macke H. R. and Krenning E. P. (1999) Therapy of neuroendocrine tumors with radiolabeled somatostatin-analogues. *Q J Nucl Med* 43, 356-366.

15. De Jong M., Breeman W. A., Bernard B. F., Bakker, W.H., Scharr, M., van Gameren, A., Bugaj, J.E., Erion, J.L., Schmidt, M., Srinivasan, A., and Krenning, E.P. (2001) [^{177}Lu-DOTA^0,Tyr^3]Octreotate for somatostatin receptor-targeted radionuclide therapy. *Int J Cancer* 92, 628-633.

16. Erion J. L., Srinivasan A., Schmidt M. A., Wilhelm R. R. and Bugaj J. E. (1997) Radiolabeled ligand-octreotate conjugates: evaluation of potential diagnostic and therapeutic radiopharmaceutical agents targeted to somatostatin receptors. *J Nucl Med* 38 (supp), 813.

17. Erion J.L., Bugaj J.E., Schmidt M.A., and Srinivasan A. (2002) Long Term Survival of Tumor-Implanted Lewis Rats Treated with ^{177}Lu-DOTA^0,Tyr^3 Octreotate, To Be Published

18. Kwekkwboom D.J., Baker W.H., Kooij P.M., Konijenberg M.W., Srinivasan A., Erion J.L., Schmidt M.A., Bugaj J.E., de Jong M., and Krenning E.P. (2001) ^{177}Lu-DOTA^0,Tyr^3]Octreotate: comparison with [^{111}In-DTPA^0]octreotide in patients, *Eur J. Nucl Med*, 28, 1319-1325.

19. Lewis J. S., Srinivasan A., Schmidt M. A. and Anderson C. J. (1999) *In vitro* and in vivo evaluation of ^{64}Cu-TETA-tyr^3-octreotate. A new somatostatin analog with improved target tissue uptake. *Nucl Med Biol* 26, 267-273.

20. Lewis J.S., Wang W., Laforest R., Wang F., Erion J.L., Bugaj J.E., Srinivasan A., and Anderson C.J. (2001) Toxicity and Dosimetry of ^{177}Lu-DOTA-Tyr^3 Octreotate in a Rat Model, *Int. J. Cancer*, 94, 873-877.

21. Stolz B., Weckbecker G., Smith-Jones P. M., Albert R., Raulf F. and Bruns C. (1998) The somatostatin receptor-targeted radiotherapeutic [^{90}Y-DOTA-DPhe^1,Tyr^3]octreotide (^{90}Y-SMT 487) eradicates experimental rat pancreatic CA20948 tumors. *Eur J Nucl Med.* 25, 668-674.

22. Zamora P. O., Gulhke S., Bender H., Diekmann D., Rhodes B. A., Biersack H. J. and Knapp F. F. Jr. (1996) Experimental radiotherapy of receptor-positive human

prostate adenocarcinoma with ^{188}Re-RC-160, a directly-radiolabeled somatostatin analogue. *Int J Cancer*, 65, 214-220.

23. Zamora P. O., Bender H., Gulhke S., Marek M. J., Knapp R. R., Rhodes B. A. and Biersack H. J. (1997) Pre-clinical experience with Re-188-RC-160, a radiolabeled somatostatin analog for use in peptide-targeted radiotherapy. *Anticancer Res.*, 17, 1803-1808.

CHAPTER 9

NOVEL FLUORESCENT CONTRAST AGENTS FOR OPTICAL IMAGING OF IN VIVO TUMORS BASED ON A RECEPTOR-TARGETED DYE PEPTIDE CONJUGATE PLATFORM

Journal of Biomedical Optics, 6, 327-334, (2001)

Novel fluorescent contrast agents for optical imaging of *in vivo* tumors based on a receptor-targeted dye-peptide conjugate platform

Joseph E. Bugaj
Samuel Achilefu
Richard B. Dorshow
Raghavan Rajagopalan
Mallinckrodt Inc.
P.O. Box 5840
St. Louis, Missouri 63134-0840

Abstract. We have designed, synthesized, and evaluated the efficacy of novel dye-peptide conjugates that are receptor specific. Contrary to the traditional approach of conjugating dyes to large proteins and antibodies, we used small peptide-dye conjugates that target over-expressed receptors on tumors. Despite the fact that the peptide and the dye probe have similar molecular mass, our results demonstrate that the affinity of the peptide for its receptor and the dye fluorescence properties are both retained. The use of small peptides has several advantages over large biomolecules, including ease of synthesis of a variety of compounds for potential combinatorial screening of new targets, reproducibility of high purity compounds, diffusiveness to solid tumors, and the ability to incorporate a variety of functional groups that modify the pharmacokinetics of the peptide-dye conjugates. The efficacy of these new fluorescent optical contrast agents was evaluated *in vivo* in well-characterized rat tumor lines expressing somatostatin (sst_2) and bombesin receptors. A simple continuous wave optical imaging system was employed. The resulting optical images clearly show that successful specific tumor targeting was achieved. Thus, we have demonstrated that small peptide-dye conjugates are effective as contrast agents for optical imaging of tumors.
 [DOI: 10.1117/1.1352746]

Keywords: peptide-dye conjugates; targeting agents; optical contrast agents; tumor detection; near infrared dyes; fluorescence; indocyanine green; receptors.

Paper CARD-03 received Aug. 1, 2000; revised manuscript received Dec. 13, 2000; accepted for publication Dec. 13, 2000.

1 Introduction

Interest in the early detection of tumors has increased recently as a result of the increasing number of deaths caused by cancer.[1] Common methods for cancer diagnosis rely on the physical detection of a palpable tumor mass or the use of different forms of roentgenography, scintigraphy, ultrasound and magnetic resonance imaging techniques for tissue imaging.[2,3] In both cases, the presence of a significant tumor mass is necessary for reliable diagnosis, at which stage patient prognosis may have already been compromised. Recently, optical imaging has been proposed as an alternative tumor detection method with great potential in clinical diagnosis.[4–8] Among other advantages over conventional modalities, the optical approach uses neither ionizing radiation nor radioactive materials, and a wealth of information can be extracted from light-tissue interaction in the electromagnetic region of interest.[9–16]

As in traditional imaging techniques, optical contrast agents designed to enhance the differentiation of normal from abnormal tissues *in vivo* would result in an increased sensitivity and specificity for tumor detection.[17] The ideal properties for optical contrast agents include biocompatibility, high molar absorptivity and fluorescent quantum yield. Furthermore, compounds which absorb or emit in the near infrared (NIR) region of the electromagnetic spectrum are also desirable due to the enhanced tissue penetration of light in this wavelength range.[18,19]

Localization of dyes in tumors can be mediated by several factors, including leaky vasculature and high metabolic activity in proliferating cells.[20] However, tumor targeting by such nonspecific mechanisms may not differentiate inflammation from benign or malignant tumors. In addition, nonspecific contrast agents initially distribute to several organs, hence, require a prolonged waiting period to clear from normal tissues.

Advances in tumor biology have shown that many tumors over-express specific receptors that could be used to differentiate them from normal cells.[20,21] Therefore, ligands for such receptors can be used as drug delivery vehicles to enhance tumor specificity.[22,23] Studies by scintigraphic imaging have demonstrated the feasibility of targeting tumor receptors with antibodies and other large biomolecules.[24,25] Adaptation of this approach to optical imaging has been described.[26,27] However, such large molecules are preferentially taken up by the liver and can elicit adverse immunogenic reactions in humans.[28] Some have very long blood residence times, which prolongs the period required for improved tumor-to-

Address all correspondence to Richard B. Dorshow. Tel: 314-719-4550; E-mail: dorshow@mallaps.org

1083-3668/2001/$15.00 © 2001 SPIE

background ratio.[29] For solid tumors, which rely on the diffusion of biomarkers from the vasculature, penetration of large dye bioconjugates is not favorable due to the net positive pressure within the tumor.[30] Hence, a better method to specifically deliver optical probes to tumors is highly desirable.

Recent studies in nuclear medicine have demonstrated that attachment of chelating agents to small molecular peptides can be used to target tumors without loss of receptor affinity of the peptides[31] (see Figure 1). This approach has several advantages with respect to either the use of nonspecific agents or the conjugation of probes to large biomolecules. Such advantages include enhanced localization in tumors, rapid clearance from blood, and the possibility of synthesizing a combinatorial library of peptides for rapid identification of bioactive products.[20] Our goal in this study was to replace the radiolabeled chelate component of the peptides used in scintigraphy with fluorescent dyes while preserving the receptor affinity of the peptide and the fluorescence of the dye. To this end, we designed and synthesized novel dye-peptide conjugates that are receptor specific.

The efficacy of these new fluorescent contrast agents (sometimes referred to in the literature as "molecular beacons," or "designer fluorophores") was evaluated *in vivo* in two well-characterized rat tumor models using a simple continuous wave fluorescence imaging apparatus. These models were chosen because both cell lines have been used extensively in nuclear medicine as *in vitro* cell binding assay systems and for *in vivo* tissue biodistribution studies. Several laboratories currently use the CA20948 rat tumor model for *in vivo* evaluation of novel sst_2 specific compounds. The AR42-J cell line is known to express multiple receptors, and this line has been widely used in cell binding assays and *in vivo* biodistribution studies in severe combined immunodeficient (SCID) and athymic nude mice. Therefore, both animal models serve as appropriate *in vivo* systems to demonstrate and establish the concept of receptor-mediateduptake and retention of novel fluorescent dye-peptide conjugates expressed on cell surface tumor lines *in vivo*.

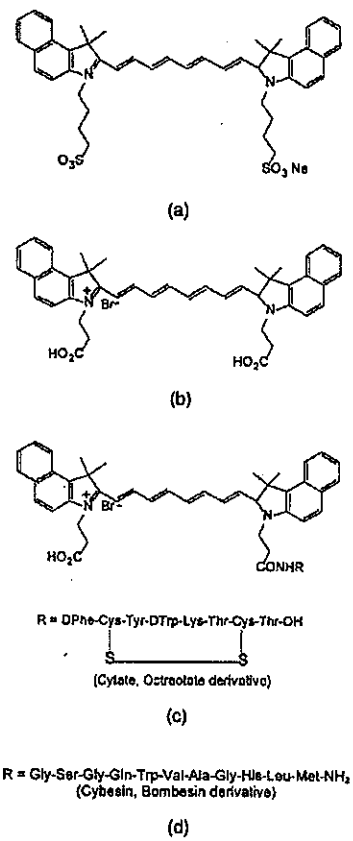

Fig. 2 Structure of (a) the dye ICG, (b) the dye cypate, (c) the peptide-dye conjugate cytate, and (d) the peptide-dye conjugate cybesin.

2 Materials and Methods

2.1 Indocyanine Green

Indocyanine green (ICG) was obtained from Sigma (St. Louis, MO), and was used without further purification.

The structure of ICG is schematically shown in Figure 2(a).

2.2 Synthesis of Bispropylcarboxymethylindocyanine Dye (Cypate)

A mixture of 1,1,2-trimethyl-[1H]-benz[e]indole (9.1 g, 43.58 mmole) and 3-bromopropanoic acid (10.0 g, 65.37 mmoles) in 1,2-dichlorobenzene (40 mL) was heated at 110°C for 12 h. The solution was cooled to room temperature and the residue obtained was filtered and washed with a mixture of acetonitrile:diethyl ether (1:1). The solid obtained was dried under vacuum to give 10 g (64%) of light brown powder. A portion of this solid (6.0 g; 16.56 mmole) was added to a mixture of glutaconaldehyde dianil monohydrochloride (2.36 g, 8.28 mmoles) and sodium acetate trihydrate (2.93 g, 21.53 mmoles) in ethanol (150 mL) and the resulting heterogeneous mixture was heated at reflux for 90 min. After evaporating the solvent, the residue was washed with HCl (2M, 4×40 mL) and the green paste obtained was lyophilized in water:acetonitrile (3:2) to give 2 g of dark green flakes. Cypate was obtained in greater than 99% purity as established by ^{1}H-nuclear magnetic resonance (NMR) and liquid chromatography-mass spectrometry (LC-MS).

The structure of cypate is schematically shown in Figure 2(b).

2.3 Synthesis of the Cypate-Octreotate Peptide Conjugate (Cytate)

The octapeptide was prepared by an automated fluorenylmethyloxycarbonyl (Fmoc) solid phase peptide synthesis[32] using a commercial peptide synthesizer from Applied Biosystems (Model 432A SYNERGY Peptide Synthesizer). The first peptide cartridge contained Wang resin pre-loaded with Fmoc-Thr on a 25 μmole scale. Subsequent cartridges containing Fmoc-protected amino acids were sequentially attached to the resin-bound amino acid. The peptide was synthesized from the C→N terminal using 2-(1H-benzotriazol-1-yl)-1,1,3,3-tetramethyluronium hexafluorophosphate (HBTU)/

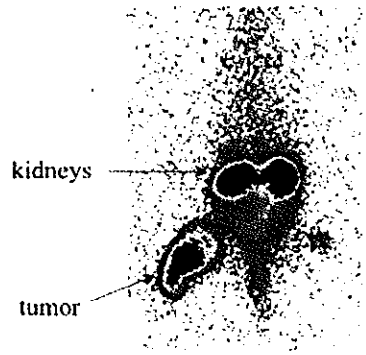

Fig. 1 Scintigraph of a somatostatin sst_2 receptor-rich CA20948 tumor bearing Lewis rat at 24 h postadministration of the radiolabeled peptide conjugate ^{111}In-DTPA-Y^3-Octreotate. Specific retention of this radiolabeled tracer is observed in the sst_2 positive tumor (left flank area), with nonspecific uptake observed in the kidneys. This gamma scintigraph was measured using Picker 300SX gamma camera interfaced to a dedicated Odyssey Image processor. The image was obtained with a large field of view camera fitted with a medium energy collimator, with the peak energies centered at 171 and 245 keV for In-111.

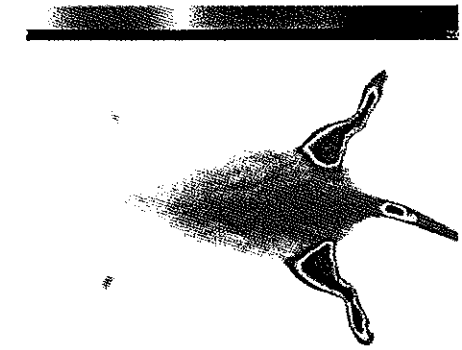

(a)

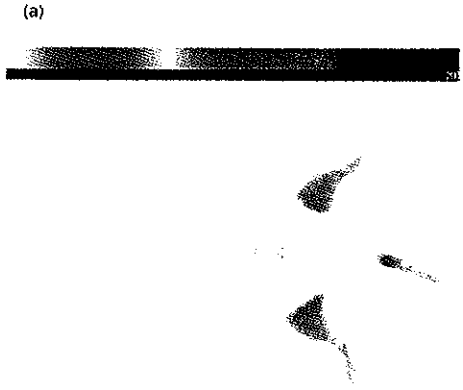

(b)

Fig. 5 Time sequence fluorescent images of ICG in a normal (nontumor bearing) rat at (a) 1 min postadministration, and (b) 60 min postadministration. A 0.5 mL bolus intravenous administration of an aqueous solution of ICG (at 5.4 μM concentration) was dosed. Rat was in prone position.

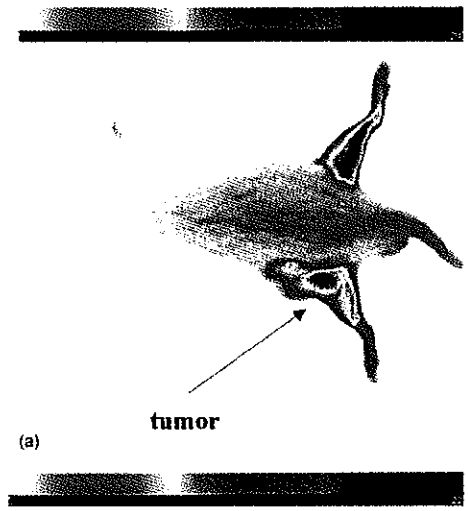

(a)

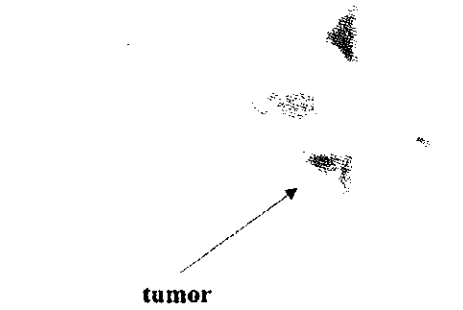

(b)

Fig. 6 Time sequence fluorescent images of ICG in a CA20948 tumor-bearing rat at (a) 1 min postadministration, and (b) 60 min postadministration. A 0.5 mL bolus intravenous administration of an aqueous solution of ICG (at 5.4 μM concentration) was dosed. Rat was in prone position.

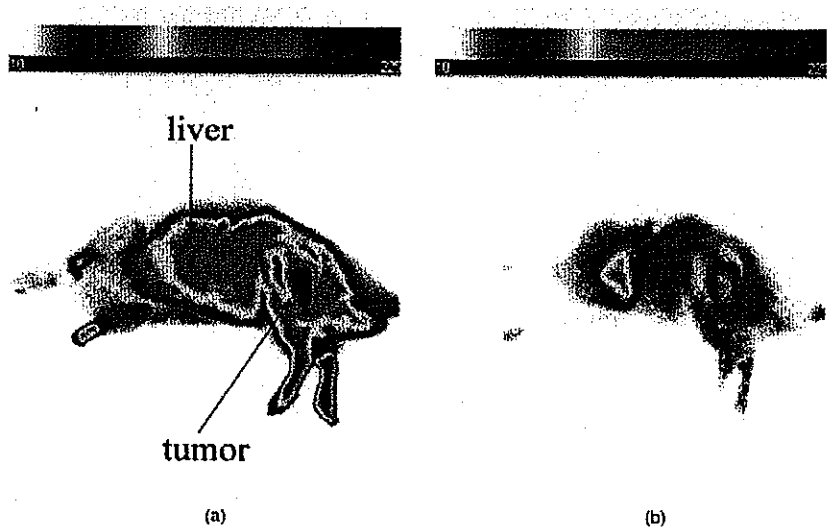

Fig. 7 Time sequence fluorescent images of cypate in a CA20948 tumor-bearing rat at (a) 1 min postadministration, and (b) 60 min postadministration. A 0.5 mL bolus intravenous administration of an aqueous solution of cypate (at 5.2 μM concentration) was dosed. Rat was positioned on its side.

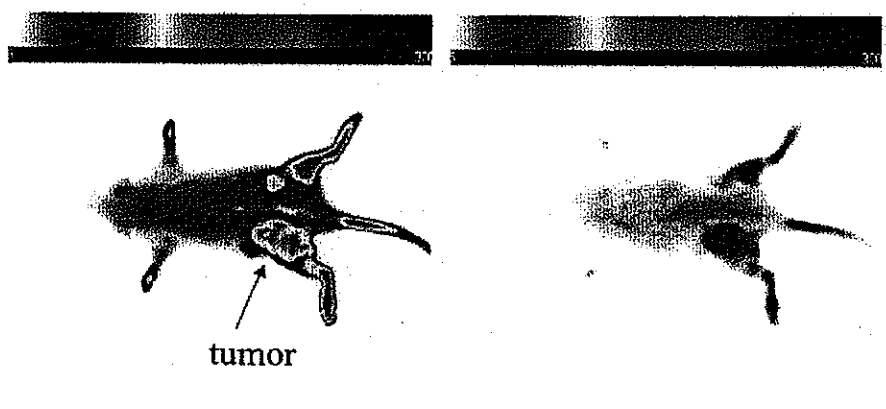

Fig. 8 Time sequence fluorescent images of ICG in an AR42-J tumor-bearing rat at (a) 1 min postadministration, and (b) 60 min postadministration. A 0.5 mL bolus intravenous administration of an aqueous solution of ICG (at 5.4 μM concentration) was dosed. Rat was in prone position.

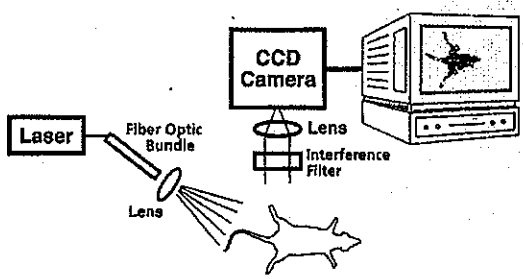

Fig. 3 Schematic of the *in vivo* imaging apparatus.

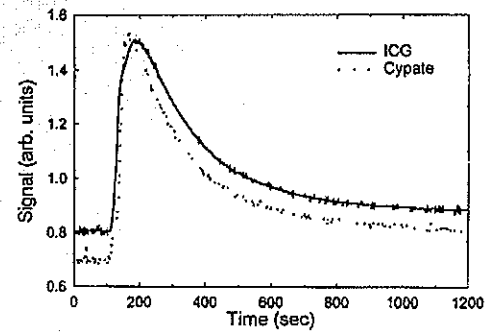

Fig. 4 *In vivo* fluorescence time dependence measured at the ear of rats with normal liver function after a 0.5 mL bolus intravenous administration of an aqueous solution of ICG (at 5.4 μM concentration), or an aqueous solution of cypate (at 5.2 μM concentration).

N-hydroxybenzotriazole as coupling reagent. After the synthesis was complete, the thiol group was cyclized with thallium trifluoroacetate.

While still on solid support, the last N-terminal Fmoc group (Phe) was removed and the resin-bound peptide was added to pre-activated cypate (53 mg, 75 mmole; pre-activated with HBTU in dimethyl sulfoxide (DMSO) for 30 min). After 3 h, the peptide was cleaved from the resin and the side chain protecting groups were removed with a mixture of 85% trifluoroacetic acid, 7.5% water, and 7.5% thioanisole. The peptide-dye conjugate was precipitated with cold *t*-butyl methyl ether and lyophilized in acetonitrile:water (2:3) mixture. The crude product was purified by high performance liquid chromatography (HPLC) to give cytate in 99% HPLC purity.

The structure of cytate is schematically shown in Figure 2(c).

2.4 Synthesis of the Cypate-Bombesin Peptide Analogue Conjugate (Cybesin)

Cybesin was prepared by the same procedure described for cytate except that cyclization with thallium trifluoroacetate was not needed. Side-chain deprotection and cleavage of the peptide from the resin was carried out with 50 μL each of ethanedithiol, thioanisole and water, and 850 μL of trifluoroacetic acid. HPLC purity was established at greater than 99.5%.

The structure of cybesin is schematically shown in Figure 2(d).

2.5 Tumor Lines

Two distinct tumor lines were employed in these studies.

2.5.1 *Pancreatic Acinar Carcinoma (CA20948) Tumor*

Male Lewis rats (120–140 g) were implanted with the pancreatic acinar tumor by serial implantation of solid material from a donor animal to a recipient animal. This transplantable tumor line has previously been shown to express somatostatin (sst_2) receptors, and has been widely used in *in vitro* and *in vivo* receptor binding assays.[33–35] The number of binding sites has been determined at 489 fmol/mg protein.[36] Briefly, a tumor is excised aseptically from a donor animal, rinsed with sterile saline and placed in a petri dish containing Gibco media 199. From this tissue, an off-white solid material was obtained, which was further cut into smaller (~2×2 mm) pieces before placing it in a second petri dish containing media 199. A single tumor piece was then placed into the bevel of a cancer implant needle. The recipient animals were anesthetized with halothane gas, and the left flank prepared by swabbing with povidone solution followed by cleansing with 70% isopropanol. The trocar containing the tumor material was inserted subcutaneously and then advanced to the center of the hind leg region. The material was released using the obdurator, followed by removal of the implant needle. Palpable tumor masses are evident approximately nine days postimplant, and between 13 and 15 days postimplant the tumor masses reach 2–2.5 g at which time they are used in the imaging studies described below. This tumor line has been maintained *in vivo* by serial implantation for more than 120 generations with no change in receptor expression.

2.5.2 *Pancreatic Acinar Carcinoma (AR42-J) Tumor*

This cell line is derived from exocrine rat pancreatic acinar carcinoma. It can be grown in continuous culture or maintained *in vivo* in athymic nude mice, SCID mice or in Lewis rats. This cell line is particularly attractive for *in vitro* receptor assays as it is known to express a variety of hormone receptors including cholecystokinin, epidermal growth factor, pituitary adenylate cyclase activating peptide, somatostatin (sst_2) and bombesin.[37]

In this model, male Lewis rats were implanted with solid tumor material in a similar manner as described for the CA20948 rat model. Palpable masses were present seven days postimplant and imaging studies were conducted on animals at 10–12 days postimplant when the mass had achieved ~2–2.5 g. This tumor line has been maintained *in vivo* for more than 20 generations without change in receptor expression.

2.6 Animal Preparation and Dose Administration Procedure

All studies were conducted in compliance with the Mallinckrodt Animal Welfare Committee's requirements for the care

and use of laboratory animals in research. The animals were anesthetized with rat cocktail (xylazine; ketamine; acepromazine 1.5: 1.5: 0.5) at 0.8 mL/kg via intraperitoneal injection. The area of the tumor (left flank) was shaved to expose the tumor and surrounding surface area, as was the contralateral flank which served as the control. A 21 gauge butterfly infusion set equipped with a stopcock and two syringes containing heparinized saline was placed into the lateral tail vein of the rat. Patency of the vein was checked prior to administration of the agent via the butterfly apparatus.

2.7 Imaging Apparatus and Procedure

A simple noninvasive *in vivo* continuous wave fluorescence imaging apparatus was employed to assess the efficacy of contrast agents developed for tumor detection in animal models. A schematic of this apparatus is shown in Figure 3. Light from a LaserMax Inc. laser diode of nominal wavelength 780 nm and nominal power of 40 mW was launched into a fiberoptic bundle. A defocusing lens in position after the bundle expanded the beam such that most of the rat was illuminated. The laser power at the output of the bundle was approximately one half of the input power.

The detector was a Princeton Instruments model RTE/ charge coupled device (CCD)-1317-K/2 CCD camera with a Rodenstock 10 mm F2 lens (stock No. 542.032.002.20) attached. An 830 nm interference lens (CVI Laser Corp. part No. F10-830-4-2) was mounted in front of the CCD input lens such that only emitted fluorescent light from the contrast agent was imaged. Images were acquired and processed using WinView software from Princeton Instruments.

An image of the animal was taken pre-administration of contrast agent. Subsequently, images were typically taken at 0.5, 1, 2, 5, 10, 20, 30, 45, 60, and 90 min postadministration of the agent, all performed with the rat in a stationary position. Data analysis consisted of subtracting (pixel by pixel) the pre-administration image from the postadministration images, and displaying the false color results. An approximate 24 h time point was also imaged, however the subtraction of the original background was not performed since the animal had been removed from the sample area and returned at this later time.

3 Results

3.1 Clearance of Dyes in Nontumored (Normal) Animals

3.1.1 *Clearance Monitoring*

Cypate dye, as well as ICG for comparison, was administered to nontumor bearing rats in order to ascertain its intrinsic blood clearance rate before conjugation to the respective peptides. The apparatus which monitors clearance of a fluorescent agent from the bloodstream has been described extensively elsewhere, as have the results employing ICG.[13,38] A typical clearance curve for cypate (from a sampling of $n=3$) is shown in Figure 4, along with a typical result for ICG (from a sampling of $n=6$) using the same methodology. Cypate has essentially the same rapid and complete clearance profile as ICG. ICG is well known to be cleared from the vasculature by the liver, with more than 90% eliminated within 15 min.[39]

3.1.2 *Imaging*

Time sequence images pre- and postadministration of a 0.5 mL aqueous solution of ICG (at 5.4 μM concentration) were obtained with the optical imager shown in Figure 3. The entire rat fluoresced at 30 s postadministration (which was the earliest time point image taken), had the highest intensity at about 1 min postadministration, and was subsequently followed by a rapid loss of fluorescence with time. A small amount of residual fluorescence was seen after 1 h postadministration, in accordance with previous studies involving ICG clearance monitoring.[13] Typical images from an $n=4$ study are shown in Figure 5 at 1 and 60 min post dye administration.

Time sequence images pre- and postadministration of 0.5 mL aqueous solution of cypate of concentration 0.5 mg/mL were also obtained (images not shown). Once again, the entire rat again fluoresced at 30 s postadministration, had the highest intensity at about 1 min postadministration, and was subsequently followed by a rapid loss of fluorescence with time. A small amount of residual fluorescence was seen after 1 h postadministration. Thus, cypate blood clearance is very similar to that of ICG, in accordance with the nonimaging clearance monitoring study described above.

3.2 Clearance and Uptake of Dyes in CA20948 Tumor-Bearing Animals

ICG, and its derivatized analog cypate, were administered to CA20948 tumor bearing rats in order to ascertain tumor uptake and retention of each dye independent of conjugation to the targeting peptide.

3.2.1 *ICG*

Time sequence images pre- and postadministration of a 0.5 mL aqueous solution of ICG (at 5.4 μM concentration) were obtained, and typical images from an $n=4$ study at 1 and 60 min postadministration are displayed in Figure 6. The entire rat fluoresced at 30 s postadministration, reached the highest intensity at approximately 1 min postadministration, and was subsequently followed by a rapid loss of fluorescence. The tumor also fluoresced at 30 s postadministration, reached the highest intensity at approximately 1 min postadministration, and was subsequently followed by a rapid loss of fluorescence. Thus, ICG does not bind to, does not leak into, nor localize in this somatostatin receptor-rich tumor tissue. A small amount of total body residual fluorescence is seen after 1 h postadministration, in accordance with the results from normal rats.

3.2.2 *Cypate*

Time sequence images pre- and postadministration of 0.5 mL aqueous solution of cypate (at 5.2 μM concentration) were obtained, and typical images from an $n=4$ study at 1 and 60 min postadministration are displayed in Figure 7. The entire rat fluoresced at 30 s postadministration, reached the highest intensity at approximately 1 min postadministration, and was subsequently followed by a rapid loss of fluorescence. The tumor also fluoresced at 30 s postadministration, reached the highest intensity at approximately 1 min postadministration, and was subsequently followed by a rapid loss of fluorescence. Thus, cypate also does not bind to, does not leak into,

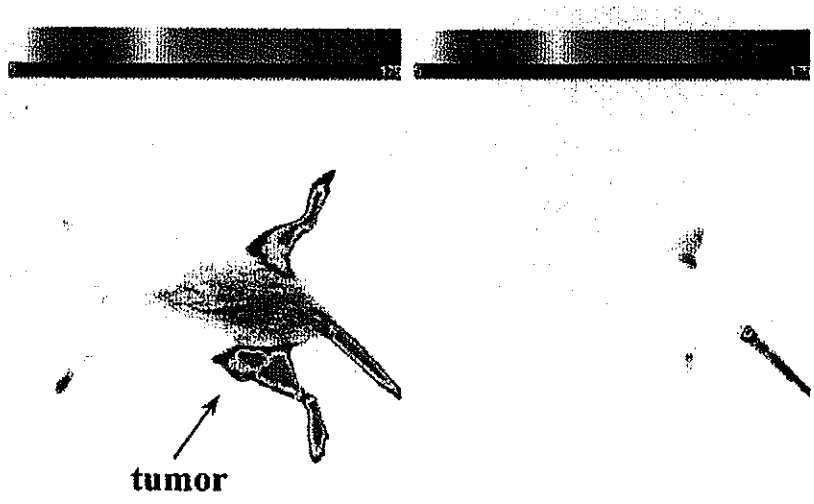

(a) (b)

Fig. 9 Time sequence fluorescent images of cypate in an AR42-J tumor-bearing rat at (a) 1 min postadministration, and (b) 60 min postadministration. A 0.5 mL bolus intravenous administration of an aqueous solution of cypate (at 5.2 μM concentration) was dosed. Rat was in prone position.

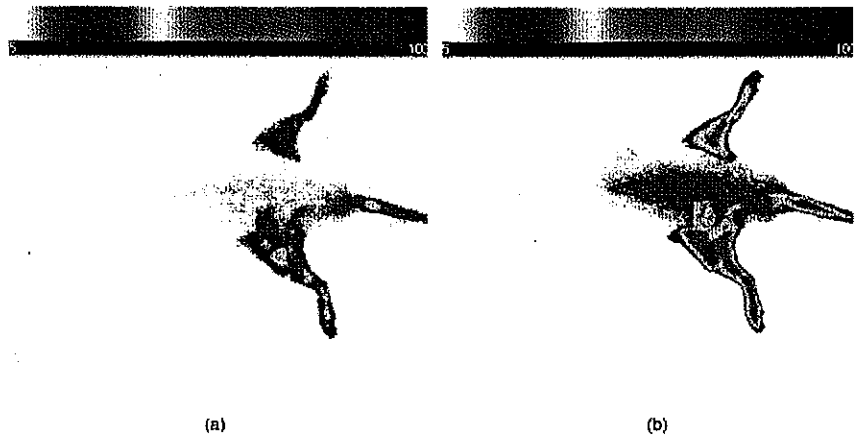

(a) (b)

Fig. 10 Time sequence fluorescent images of cytate in a CA20948 tumor-bearing rat (a) 1 min postadministration, and (b) at 45 min postadministration. A 0.5 mL bolus intravenous administration of an aqueous solution of cytate (at 6.0 μM concentration) was dosed. Rat was in prone position.

Fig. 11 Fluorescent image of cytate in a CA20948 tumor bearing rat at 27 h postadministration. Cytate is well localized in the tumor.

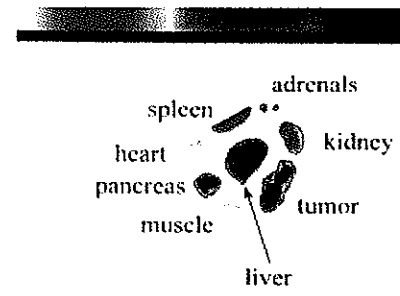

Fig. 12 *Ex-vivo* tissues and organs from a CA20948 tumor bearing rat at 27 h postadministration.

(a) (b)

Fig. 13 Time sequence fluorescent images of cybesin in an AR42-J tumor bearing rat (a) 1 min postadministration, and (b) at 60 min postadministration. A 0.5 mL bolus intravenous administration of an aqueous solution of cybesin (at 6.0 μM concentration) was dosed. Rat was in prone position.

Fig. 14 Fluorescent image of cybesin in an AR42-J tumor bearing rat at 22 h postadministration. Cybesin is localized in the tumor.

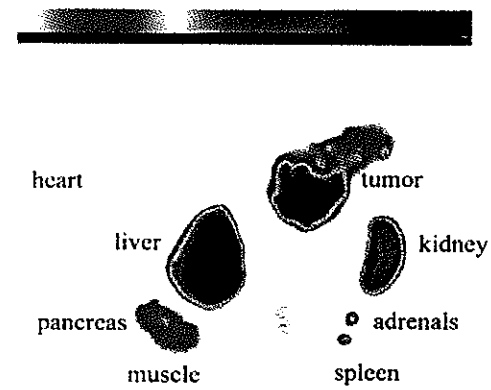

Fig. 15 *Ex-vivo* tissues and organs from an AR42-J tumor-bearing rat at 22 h postadministration.

nor localize in this somatostatin receptor-rich tumor tissue. A small amount of total body residual fluorescence is seen after 1 h postadministration, in accordance with the results from normal rats.

3.3 Clearance and Uptake of Dyes in AR42-J Tumor-Bearing Animals

3.3.1 *ICG*

Time sequence images pre- and postadministration of a 0.5 mL aqueous solution of ICG (at 5.4 μM concentration) were obtained, and typical images from a $n=2$ study at 1 and 60 min postadministration are displayed in Figure 8. The entire rat fluoresced at 30 s postadministration (which was the earliest time point image taken), achieved the highest intensity near 1 min postadministration, which then dissipated rapidly. The tumor also fluoresced at 30 s postadministration, achieved the highest intensity near 1 min postadministration, then dissipated rapidly. Thus, ICG does not bind to, does not leak into, nor localize in this bombesin receptor-rich tumor tissue. A small amount of total body residual fluorescence was seen after 1 h postadministration, in accordance with the results from normal rats.

3.3.2 *Cypate*

Time sequence images pre- and postadministration of a 0.5 mL aqueous solution of cypate (at 5.2 μM concentration) were obtained, and typical images from a $n=2$ study at 1 and 60 min postadministration are displayed in Figure 9. The entire rat fluoresced at 30 s postadministration (which was the earliest time point image taken), had the highest intensity near 1 min postadministration, then faded rapidly. The tumor also fluoresced at 30 s postadministration, had the highest intensity near 1 min postadministration, then faded rapidly. Thus, cypate also does not bind to, does not leak into, nor localize in this bombesin receptor-rich tumor. A small amount of total body residual fluorescence is seen after 1 h postadministration, in accord with the results from normal rats.

3.4 Uptake of the Dye-Peptide Conjugates in Tumor-Bearing Animals

Fluorescence serial time sequence images of the tumor bearing rats were typically followed for 90 min postadministration. The rats were returned to their cages, and then subsequently re-imaged at approximately 24 h postadministration. After this image, the rat was sacrificed, and the internal organs were imaged *ex vivo* to observe the biodistribution of the fluorescence.

3.4.1 *Cytate in CA20948 Tumor-Bearing Animals*

Time sequence images pre- and postadministration of a 0.5 mL aqueous solution of cytate (at 6.0 μM concentration) were obtained. Typical early time point images from a $n=6$ study at 1 and 45 min postadministration are displayed in Figure 10. The fluorescence at 1 min postadministration is evident, although not as intense as with the cypate dye alone. Accumulation of the fluorescent conjugate in the tumor was clearly evident at 45 min postadministration.

Table 1 Ratio of tumor to normal tissue (T/NT).

Normal tissue	CA20948 T/NT	AR42-J T/NT
Muscle	20	25
Heart	17	25
Kidney	5	3
Spleen	5	14
Adrenals	2	7
Liver	2	1
Pancreas	1	9

A typical image from the above study obtained at approximately 24 h postadministration is shown in Figure 11. Preferential localization and retention of the dye-peptide conjugate in the tumor was readily observed. At this time point, the vast majority of this compound had been eliminated from all other tissues, with only a residual fluorescence still observed within the rat.

A fluorescence map of several *ex vivo* organs and tissues from the above study is shown in Figure 12. The somatostatin receptor-rich tissues of the tumor, pancreas and the adrenal glands, indicate specific localization of the fluorescent label. Residual uptake of compound in the liver, due presumably to the dye component, was evident. A rough estimate of the average pixel intensity within a tissue was employed to construct the tumor-to-normal tissue ratios listed in Table 1 for this CA20948 tumor line. Average values from a $n=3$ sampling are given.

3.4.2 *Cybesin in AR42-J Tumor-Bearing Animals*

Time sequence images pre- and postadministration of a 0.5 mL aqueous solution of cybesin (at 6.0 μM concentration) were obtained. Typical early time point images from a $n=3$ study at 1 and 60 min postadministration are displayed in Figure 13. The fluorescence at 1 min postadministration pervades the entire body of the rat. Accumulation of fluorescence at the tumor site on the left flank is evident as early as 1 min postadministration. The position of this particular tumor apparently inhibits free capillary flow in the left leg, and some of the compound is trapped there for a prolonged time. At 60 min postadministration the difference between the tumored left flank and the contralateral nontumored flank is easily distinguishable.

Figure 14 is an image of the 22 h time point postadministration. Localization and retention of the dye-peptide conjugate in the tumor is readily observed. The compound has mainly been eliminated from all other tissues, although a

small residual fluorescence is still seen to emanate from the remainder of the rat. The agent previously trapped in the left leg has been eliminated.

A fluorescence map of several *ex vivo* organs and tissues is shown in Figure 15. The bombesin receptor-rich tumor is highly fluorescent with respect to the muscle and heart tissues, which are barely distinguishable from the background. Uptake of the compound by the liver, due presumably to the dye component, was observed. The two bombesin positive tissues, pancreas and tumor, indicate receptor mediated specific uptake and retention. Again, a rough estimate of the average pixel intensity within a tissue was employed to construct the tumor-to-normal tissue ratios listed in Table 1 for this AR42-J tumor line. Average values from a $n=3$ sampling are given.

4 Discussion

ICG is well known to be cleared from the vasculature by the liver, with subsequent excretion through the large intestine. The rapid rate of clearance is illustrated by two different experiments in Figures 4 and 5.

Figures 6 and 8 definitively show that ICG is neither tumor selective for the pancreatic acinar tumor line CA20948 nor the pancreatic acinar tumor line AR42-J. Coupled with our previously published observation that ICG does accumulate in the DSL6/A rat pancreatic tumor model, and in the Dunning R3327H prostate tumor model[40,41] (both presumably due to a leaky vasculature system in the tumor), we conclude that there is no specific mechanism of action for this dye to localize in tumors. Although previous reports in the literature suggest a mechanism of active preferential uptake of ICG in tumors,[42] our findings based on repeated experiments in several tumor lines demonstrate that ICG uptake in tumors is not a universal phenomenon. Therefore, use of ICG for tumor differentiation may be expected to result in many false positives and false negatives, and thus its use would not be reliable for general clinical prognosis in tumor detection.

Figures 7 and 9 definitively show that cypate is not tumor selective for either rat pancreatic acinar tumor lines CA20948 or AR42-J. Thus, the dye alone (not conjugated to the peptide) does not accumulate in tumor tissue. This observation is the negative control for our hypothesis that only the dye-peptide conjugates are receptor specific, and the dye alone (either ICG or cypate) is not. The CA20948 tumor is known to over express the sst_2 receptor. Fortunately, several somatostatin peptide analogues have been demonstrated by gamma scintigraphy to target the sst_2 receptor.[43] Indeed, a commercial nuclear medicine diagnostic product based on targeting the somatostatin tumor receptor, OctreoScan®, is currently used for the detection of neuroendocrine tumors.[31] Thus, a logical step would be the conjugation of dyes to biomarkers that have high affinity for this receptor. However, the active targeting component of this imaging agent is a small eight-amino acid peptide, and it was not known whether the attachment of a large dye molecule to an analogue of this peptide would decrease the affinity of the peptide for the receptor. In addition, the transformation of cyanine dyes, such as ICG, for peptide conjugation is difficult, generally requiring harsh reaction conditions which may contribute to the attenuation of both dye and peptide properties.

Consequently, we evaluated the feasibility of using small peptide-dye conjugates in tumor detection by optical imaging. This approach required the synthesis of functionalizable dyes for the attachment of the peptides. We developed a method to conjugate the dyes to peptides by standard solid phase synthesis, a process that is quite amenable to automated synthesis. Control samples of aqueous solution of cytate continue to retain their high fluorescence intensity even after 18 months of storage at room temperature on an open shelf.

Figures 10 and 11 illustrate the accumulation of cytate *in vivo* in the CA20948 rat tumor and the clearance of the compound from the nontarget tissues. The quality of the optical image at 27 h is very similar to that of a scintigraph employing a radiolabeled peptide analog.[44] Comparison of Figure 11 with Figure 7 leads to the conclusion that the receptor targeting moiety of cytate retains affinity for the receptor, and the dye retains its fluorescence. Thus, the images confirm that cytate is a receptor-specific targeted fluorescent contrast agent.

Figure 12 graphically depicts the biodistribution of cytate in several organs and tissues. The tumor-to-muscle ratio, given in Table 1, is approximately an order of magnitude greater than the porphyrin compounds currently employed in photodynamic therapy.[45,46] Thus, cytate is a receptor targeted fluorescent contrast agent with a high tumor-to-muscle tissue biodistribution.

The corresponding ratios for the pancreas and adrenals are also rather low, as those two organs naturally express the sst_2 receptor and therefore, like the tumor, indicate a greater uptake and retention of the dye-peptide conjugate. In addition, the peptide is metabolized to smaller amino acid fragments *in vivo*, which are retained within the lysosomal compartment of the renal cells. This metabolic breakdown of the peptide[47] results in the persistent localization of the dye-peptide conjugate in the kidneys, and hence the low tumor-to-kidney tissue ratio. Last, the low tumor-to-liver tissue ratio is presumably due to the well-known preferential uptake of the dye by the liver.

Ex vivo inspection and further dissection of the tumor tissue revealed that the fluorescence, and hence dye-peptide conjugate, was localized in the viable regions. Necrotic regions of the tumor were essentially devoid of fluorescence. This result is in contrast to the recently reported finding that serum protein-dye compounds yield fluorescence signatures that were "mainly localized in the necrotic regions of the tumors."[48]

Figures 13 and 14 illustrate the accumulation of cybesin *in vivo* in the AR42-J rat tumor and the clearance of the compound from the nontarget tissues. The quality of the optical image at 22 h is very similar to that of a scintigraph employing the radiolabeled peptide analog.[44] Comparison of Figure 14 with Figure 9 leads to the conclusion that the receptor targeting moiety of cybesin retains affinity for the receptor, and the dye retains its fluorescence. Thus, the images confirm that cybesin is a receptor-specific targeted fluorescent contrast agent.

Figure 15 graphically depicts the biodistribution of cybesin in several organs and tissues. The tumor-to-muscle ratio, given in Table 1, is also approximately an order of magnitude greater than the porphyrin compounds currently employed in photodynamic therapy.[45,46] Thus cybesin is a receptor-targeted

fluorescent contrast agent with a high tumor-to-muscle tissue biodistribution.

The bombesin receptors on the pancreas, and to a lesser extent on the adrenal glands, are naturally expressed in a lower density with respect to the somatostatin receptors. Thus, this accounts for the higher tumor-to-normal tissue ratio for these two organs in the AR42-J tumor line than in the CA20948 tumor line. The kidney retention is not believed to be the result of specific uptake, but most likely is the result of *in vivo* metabolism of the parent peptide into smaller fragments that persist within the renal cell lysosomes, as reported in the literature.[47] Again, the low tumor-to-liver tissue ratio is presumably due to the well-known preferential uptake of the dye by the liver.

Furthermore, *ex vivo* inspection and further dissection of this tumor tissue revealed that the fluorescence, and hence dye-peptide conjugate, was also localized in the viable regions.

5 Summary

Our results indicate that small peptide-dye conjugates can be efficacious as fluorescent contrast agents for *in vivo* tumor detection by optical imaging, analogous to what has been demonstrated in nuclear medicine. Both the newly synthesized cytate and cybesin compounds preferentially localized for over 24 h in tumors known to over-express somatostatin and bombesin receptors, respectively, whereas the dye moiety devoid of the receptor targeting peptide was not retained in these two tumor model lines.

The tumor-to-muscle fluorescence ratio is approximately an order of magnitude greater in the tumor targeting dye-peptide conjugates reported herein with respect to typical porphyrin-type compounds reported in the literature.[46] The images reported herein of fluorescent-glowing tumors provide an unambiguous demonstration of tumor targeting, without resorting to extensive pharmacokinetic data analysis as employed for agents with low targeting efficacy.[49,50]

A functionalizable carbocyanine dye, with similar photophysical properties and pharmacokinetics as ICG was synthesized. Conjugation of this dye to biomolecules was readily achieved without loss of the relevant photophysical properties for deep tissue penetration of light.

The novel synthetic schemes employed yielded compounds of purity on the order of 99% or greater. Thus, ambiguity in the results due to contaminants was eliminated. In addition, new techniques in the art of solid state peptide synthesis were needed and developed in order to attain these levels of purity in the conjugates.

The large signals obtained using targeted exogenous contrast agents allowed the use of a simple continuous wave imaging apparatus, with vendor supplied imaging software employed for the measurement and for the output. Neither exotic instrumentation nor extensive data analysis and manipulation with rigorous computer algorithms were needed.

Acknowledgments

The authors wish to thank R. R. Wilhelm and H. Jimenez for their contributions.

References

1. R. T. Greenlee, T. Murray, S. Bolden, and P. A. Wingo, "Cancer statistics, 2000," *CA Cancer J. Clin.* **50**, 7–33 (2000).
2. D. D. Shaw, "Contrast media: Directions for the 1990s," *Invest. Radiol.* **28**, S138–S139 (1993).
3. M. L. Giger and C. A. Pelizzari, "Advances in tumor imaging," *Sci. Am.* **275**, 110–112 (1996).
4. D. A. Benaron and D. K. Stevenson, "Optical time-of-flight and absorbance imaging of biologic media," *Science* **259**, 1463–1466 (1993).
5. R. F. Potter (Series Editor), *Medical Optical Tomography: Functional Imaging and Monitoring*, SPIE Optical Engineering Press, Bellingham (1993).
6. G. J. Tearney, M. E. Brezinski, B. E. Bouma, S. A. Boppart, C. Pitris, J. F. Southern, and J. G. Fujimoto, "*In vivo* endoscopic optical biopsy with optical coherence tomography," *Science* **276**, 2037–2039 (1997).
7. B. J. Tromberg, O. Coquoz, J. B. Fishkin, T. Pham, E. R. Anderson, J. Butler, M. Cahn, J. D. Gross, V. Venugopalan, and D. Pham, "Non-invasive measurements of breast tissue optical properties using frequency-domain photon migration," *Philos. Trans. R. Soc. London, Ser. B* **352**, 661–668 (1997).
8. S. Fantini, S. A. Walker, M. A. Franceschini, M. Kaschke, P. M. Schlag, and K. T. Moesta, "Assessment of the size, position, and optical properties of breast tumors *in vivo* by non-invasive optical methods," *Appl. Opt.* **37**, 1982–1989 (1998).
9. U. Dirnagl, A. Villringer, and K. M. Einhaupl, Eds., *Optical Imaging of Brain Function and Metabolism*, Plenum, New York (1993).
10. A. J. Welch and M. J. C. van Gemert, Eds., *Optical-Thermal Response of Laser-Irradiated Tissue*, Plenum, New York (1995).
11. C. H. Contag, S. D. Spilman, P. R. Contag, M. Oshiro, B. Eames, P. Dennery, D. K. Stevenson, and D. A. Benaron, "Visualizing gene expression in living mammals using a bioluminescent reporter," *Photochem. Photobiol.* **66**, 523–531 (1997).
12. J. C. Hebden and D. T. Delpy, "Diagnostic imaging with light," *Br. J. Radiol.* **70**, S206–S214 (1997).
13. R. B. Dorshow, J. E. Bugaj, B. D. Burleigh, J. R. Duncan, M. A. Johnson, and W. B. Jones, "Noninvasive fluorescence detection of hepatic and renal function," *J. Biomed. Opt.* **3**, 340–345 (1998).
14. B. Chance, E. Anday, S. Nioka, S. Zhou, L. Hong, K. Worden, C. Li, T. Murray, Y. Ovetsky, D. Pidikiti, and R. Thomas, "A novel method for fast imaging of brain function, non-invasively, with light," *Opt. Express* **2**, 411–423 (1998).
15. G. A. Wagnieres, W. M. Star, and B. C. Wilson, "*In vivo* fluorescence spectroscopy and imaging for oncological applications," *Photochem. Photobiol.* **68**, 603–632 (1998).
16. B. R. Masters, "Early development of optical low-coherence reflectometry and some recent biomedical applications," *J. Biomed. Opt.* **4**, 236–247 (1999).
17. V. M. Runge, "Contrast media research," *Invest. Radiol.* **34**, 785–790 (1999).
18. O. O. Abugo, R. Nair, and J. R. Lakowicz, "Fluorescence properties of rhodamine 800 in whole blood and plasma," *Anal. Biochem.* **279**, 142–150 (2000).
19. A. Yodh and B. Chance, "Spectroscopy and imaging with diffusing light," *Phys. Today* **48**, 34–40 (1995).
20. S. J. Goldsmith, "Receptor imaging: Competitive or complementary to antibody imaging?," *Seminars in Nucl. Med.* **27**, 85–93 (1997).
21. T. Reisine and G. I. Bell, "Molecular biology of somatostatin receptors," *Endocrine Rev.* **16**, 427–442 (1995).
22. S. D. Konda, M. Aref, M. Brechbiel, and E. C. Wiener, "Development of a tumor-targeting MR contrast agent using the high affinity folate receptor: Work in progress," *Invest. Radiol.* **35**, 50–57 (2000).
23. E. Unger, P. Metzger III, E. Krupinski, M. Bakker, R. Hulett, D. Gabaeff, J. Mills, D. Ihnat, and T. McCreery, "The use of a thrombus-specific ultrasound contrast agent to detect thrombus in arteriovenous fistulae," *Invest. Radiol.* **35**, 86–89 (2000).
24. D. J. Buchsbaum, "Experimental tumor targeting with radiolabeled ligands," *Cancer (N.Y.)* **80**, 2371–2377 (1997).
25. T. M. Behr, S. Gratz, P. M. Markus, R. M. Dunn, M. Hufner, A. Schauer, M. Fischer, D. L. Muntz, H. Becker, and W. Becker, "Anti-carcinoembryonic antigen antibodies versus somatostatin analogs in the detection of metastatic medullary thyroid carcinoma," *Cancer (N.Y.)* **80**, 2436–2457 (1997).
26. B. Ballou, G. W. Fisher, A. S. Waggoner, D. L. Farkas, J. M.

Reiland, R. Jaffe, R. B. Mujumdar, and T. R. Hakala, "Tumor labeling *in vivo* using cyanine-conjugated monoclonal antibodies," *Cancer Immunol. Immunother* **41**, 257–263 (1995).
27. R. Weissleder, C.-H. Tung, U. Mahmood, and A. Bogdanov, Jr., "*In vivo* imaging of tumors with protease-activated near-infrared fluorescent probes," *Nat. Biotechnol.* **17**, 375–378 (1999).
28. A. C. Guyton and J. E. Hall, *Textbook of Medical Physiology*, Saunders, Philadelphia (1996).
29. K. Licha, A. Becker, F. Kratz, and W. Semmler, "New contrast agents for optical imaging: Acid-cleavable conjugates of cyanine dyes with biomolecules," *Proc. SPIE* **3600**, 29–35 (1999).
30. R. K. Jain, "Barriers to drug delivery in solid tumors," *Sci. Am.* **271**, 58–65 (1994).
31. D. J. Kwekkeboom, E. P. Krenning, G. S. Kho, W. A. P. Breeman, and P. M. Van Hagen, "Somatostatin receptor imaging in patients with sarcoidosis," *Eur. J. Nucl. Med.* **25**, 1284–1292 (1998).
32. E. Atherton, *Fluorenylmethoxycarbonyl-polyamide solid phase peptide synthesis: General principles and development*, Information Press, Oxford (1989).
33. J.-C. Reubi, U. Horrisberger, C. E. Essed, J. Jeekel, J. G. Klijn, and S. W. Lamberts, "Absence of somatostatin receptors in human exocrine pancreatic adenocarcinomas," *Gastroenterology* **95**, 760–763 (1988).
34. C. J. Anderson, L. A. Jones, L. A. Buss, E. L. C. Sherman, D. W. McCarthy, P. D. Cutler, M. V. Lanahan, M. E. Cristel, J. S. Lewis, and S. W. Schwarz, "Radiotherapy, toxicity and dosimetry of copper-64-TETA-octreotide in tumor-bearing rats," *J. Nucl. Med.* **39**, 1944–1951 (1998).
35. M. De Jong, W. A. P. Breeman, B. F. Bernard, E. J. Rolleman, L. J. Hofland, T. J. Visser, B. Setyono-Han, W. H. Bakker, M. E. van der Pluijm, and E. P. Krenning, "Evaluation *in vitro* and in rats of ^{161}Tb-DTPA-octreotide, a somatostatin analogue with potential for intraoperative scanning and radiotherapy," *Eur. J. Nucl. Med.* **22**, 608–616 (1995).
36. B. Stolz, G. Weckbecker, P. M. Smith-Jones, R. Albert, F. Raulf, and C. Bruns, "The somatostatin receptor-targeted radiotherapeutic [^{90}YDOTA-DPhe^1,Tyr^3]octreotide (^{90}Y-SMT 487) eradicates experimental rat pancreatic CA 20948 tumors," *Eur. J. Nucl. Med.* **25**, 668–674 (1998).
37. J.-B. Deitrich, "AR4-2J cells: A model to study polypeptide hormone receptors," *Biosci. Rep.* **16**, 273–288 (1996).
38. R. B. Dorshow, J. E. Bugaj, S. Achilefu, R. Rajagopalan, and A. H. Combs, "Monitoring physiological function by detection of exogenous contrast agents," *Proc. SPIE* **3599**, 2–8 (1999).
39. G. Paumgartner, P. Probst, R. Kraines, and C. M. Leevy, "Kinetics of indocyanine green removal from the blood," *Ann. N.Y. Acad. Sci.* **170**, 134–147 (1970).
40. S. Achilefu, R. B. Dorshow, J. E. Bugaj, and R. Rajagopalan, "Novel receptor-targeted fluorescent contrast agents for *in vivo* tumor imaging," *Invest. Radiol.* **35**, 479–485 (2000).
41. S. Achilefu, R. B. Dorshow, J. E. Bugaj, and R. Rajagopalan, "Tumor specific fluorescent contrast agents," *Proc. SPIE* **3917**, 80–86 (2000).
42. J. S. Reynolds, T. L. Troy, R. H. Mayer, A. B. Thompson, D. J. Waters, K. K. Cornell, P. S. Snyder, and E. M. Sevick-Muraca, "Imaging of spontaneous canine mammary tumors using fluorescent contrast agents," *Photochem. Photobiol.* **70**, 87–94 (1999).
43. W. H. Bakker, E. P. Krenning, W. A. P. Breeman, J. W. Koper, P. P. Kooij, J.-C. Reubi, J. G. Klijn, T. J. Visser, R. Docter, and S. W. Lamberts, "Receptor scintigraphy with a radioiodinated somatostatin analogue: Radiolabeling, purification, biological activity, and *in vivo* application in animals," *J. Nucl. Med.* **31**, 1501–1509 (1990).
44. M. de Jong, W. A. P. Breeman, W. H. Bakker, P. P. M. Kooij, B. F. Bernard, L. J. Hofland, T. J. Visser, A. Srinivasan, M. A. Schmidt, J. L. Erion, J. E. Bugaj, H. R. Macke, and E. P. Krenning, "Comparison of ^{111}In-labeled somatostatin analogues for tumor scintigraphy and radionuclide therapy," *Cancer Res.* **58**, 437–441 (1998).
45. M. Yeng, E. Baranov, P. Jiang, F.-X. Sun, X.-M. Li, L. Li, S. Hasegawa, M. Bouvet, M. Al-Tuwaijri, T. Chishima, H. Shimada, A. R. Moossa, S. Penman, and R. M. Hoffman, "Whole-body optical imaging of green fluorescent protein-expressing tumors and metastases," *Proc. Natl. Acad. Sci. U.S.A.* **97**, 1206–1211 (2000).
46. J. F. Evensen, S. Sommer, J. Moan, and T. Christensen, "Tumor-localizing and photosensitizing properties of the main components of hematoporphyrin derivative," *Cancer Res.* **44**, 482–486 (1984).
47. H. Akizawa, Y. Arano, T. Uezono, M. Ono, Y. Fujioka, T. Uehara, A. Yokoyama, K. Akaji, Y. Kiso, M. Koizumi, and H. Saji, "Renal metabolism of ^{111}In-DTPA-D-Phe-Octreotide *in vivo*," *Bioconjugate Chem.* **9**, 662–670 (1998).
48. A. Becker, B. Riefke, B. Ebert, U. Sukowski, H. Rinneberg, W. Semmler, and K. Licha, "Macromolecular contrast agents for optical imaging of tumors: Comparison of indotricarbocyanine-labeled human serum albumin and transferrin," *Photochem. Photobiol.* **72**, 234–241 (2000).
49. J. T. H. M. van den Akker, O. C. Speelman, H. J. van Staveren, A. L. Moore, T. A. Moore, D. Gust, W. M. Star, and H. J. C. M. Sterenborg, "Localisation and accumulation of a new carotenoporphyrin in two primary tumour models," *J. Photochem. Photobiol., B* **54**, 108–115 (2000).
50. M. Gurfinkel, A. B. Thompson, W. Ralston, T. L. Troy, A. L. Moore, T. A. Moore, J. D. Gust, D. Tatman, J. S. Reynolds, B. Muggenburg, K. Nikula, R. Pandey, R. H. Mayer, D. J. Hawrysz, and E. M. Sevick-Muraca, "Pharmacokinetics of ICG and HPPH-car for the detection of normal and tumor tissue using fluorescence, near-infrared reflectance imaging: A case study," *Photochem. Photobiol.* **72**, 94–102 (2000).

Summary and Conclusions

Summary and Conclusions

In the years since the discovery of the somatostatin receptor and the subcloning of the five subtypes, there has been a large number of investigations into the development of imaging agents and therapeutic approaches targeting this well characterized receptor. The seminal work of Krenning, Lamberts and co-workers in the late 1980's was the first to establish the feasibility of receptor scintigraphy using a radiolabeled peptide as the targeting moiety. In 1994 ^{111}In-DTPA-octreotide (OctreoScan) received FDA approval as the first product of its kind, and to this day remains the „Gold Standard" in somatostatin receptor scintigraphy. Krenning et al. then continued in this area by introducing PRRT using the radionuclides In-111 (Auger) and Y-90 (Beta) for radiotherapy of this receptor.

A major improvement in the core pharmacophore (Chapter II) occurred with the replacement of the C-terminal threonineol with the native carboxylic acid threonine. The modified alcohol was introduced to increase the serum $t_{1/2}$, with the expectations that the native form would clear too rapidly from the blood to be an effective pharmacophore. This seemingly subtle change resulted in superior uptake and internalization properties of the radiolabel in sst_2 positive tissues in tumor bearing animals compared to OctreoScan. The new molecule was named Octreotate. This improved uptake, and more importantly, internalization of the compound led to the fisrt evaluation of a medium energy beta emitting radionuclide, samarium-153, for radiotherapy in an animal model. When chelated to CMDTPA-octreotate, this agent demonstrated significant supression of tumor growth in the CA20948 rat model compared to untreated control animals (Chapter III). However, it was determined that

this radionuclide suffers from two inherent drawbacks: (a) low specific activity at <700Ci/mmol and (b) a short half life of only 46.3 hours.

To circumvent these deficiencies while keeping the chemistry essentially unchanged, the radionuclide Lu-177 was then evaluated. This radionuclide is availabe at a significantly greater specific activity of >3000Ci/mmol and has a $t_{1/2}$ of 6.7 days. Additionally, Lu-177 also possesses an 11% abundance of a 208keV gamma ray suitable for scintigraphy and dosimetry calculations. Chelation of this radionuclide to DOTA-octreotate (Chapter IV) was performed, and the agent ^{177}Lu-DOTA-Y^{3}-octreotate was then evaluated in a series of biodistribution and radiotherapy studies in CA20948 tumor bearing rats. Animals treated with 3 x 5.0mCi administered at 30 day intervals resulted in complete ablation of the tumors, and the animals survived up to 18 months post inoculation. Efficacy of this radiotherapeutic was expanded into two novel SSTR positive tumor bearing rat models in Chapter V. In these models the rat acinar pancreatic cell line, AR42-J, which has been traditionally cultured in vivo in athymic or SCID mouse models, was established in normal Lewis rats in the flank model and in a metastatic model for liver metatsases. These newly developed models used pre-weaned animals for inoculation of tumor cells, allowing for growth and serial implantation of the tumor line in vivo in successive generations of Lewis rats. These models obviated the need for athymic or SCID mice that require more stringent barrier and housing requirements due to the reduced immune systems of both mouse models. The therapeutic efficacy of ^{177}Lu-DOTA-Y^{3}-octreotate was evaluated in both novel rat models. Significant supression of tumor growth in the flank model was observed compared to negative control animals, and in the liver model three treatments of 5.0mCi of ^{177}Lu-DOTA-Y^{3}-octreotate resulted in virtual elimination of liver metastases. There was re-growth of tumor masses noted in the

flank model after 85 days suggesting that this new model may represent a more radioresistant neuroendocrine tumor line compared to CA20948.

Breeman had previously observed that the uptake and retention of octreotide in sst_2 positive tissues of the pancreas and adrenals exhibited a bell shape curve effect with respect to the injected specific activity of the preparation. This observation was contrary to the paradigm that maximum uptake should result form the highest specific activity injected. This effect is important especially with regard to radiotherapy applications in order to maximize tumor uptake of the therapeutic peptide. Experiments were conducted testing the bell curve effect for octreotate labeled with both In-111 and Lu-177 (Chapter VI). In the CA20948 tumor model no bell curve effect was noted with either form of octreotate with the lone exception of the pancreas when the agent was labeled with Lu-177. More importantly, these studies showed that tumor uptake was virtually unaffected over a very wide range of specific activity (10-5700Ci/mmol), and that receptor saturation at the tumor site does not occur until the specific activity was reduced to ~1.5Ci/mmol. Thus, the biodistribution of this molecule is very different from octreotide, and as a radiotherapeutic would be expected to deliver a significantly higher dose to the target tissue over a wide range of labeling conditions.

Further animal model development for somatostatin expressing tumor lines is described in Chapter VII. Currently a pre-clinical limitation exists for the evaluation of other somatostatin specific subtypes, most notably sst_1, sst_3 and sst_4. This chapter describes the development of an $hsst_2$ posivtive tumor bearing rat model in a mammary tumor line (Mat-B) normally negative for sst_2 expression. This tumor line was made to express high density of the $hsst_2$ receptor through transfection of a

plasmid encoding for that specific receptor. In this model the uptake and retention of ^{177}Lu-DOTA-Y^{3}-octreotate was determined to be >50 times the uptake for the wild type tumor line. Scintigraphic images confirmed the expression of the receptor and that expression was confined to only the tumor mass. Preliminary radiotherapy experiments also demonstrated a significant delay in tumor growth using ^{177}Lu-DOTA-Y^{3}-octreotate compared to untreated control animals. The availability of the five subclones makes it possible to use this approach in creating subtype specific models of sst expression in vivo. Additionally, it is believed that this technology could also enable the expression of non-somatostatin receptors such as VIP, CCK or bombesin possible in order to evaluate peptides that specifically target these receptors.

The issues of acute and chronic toxicity of ^{177}Lu-DOTA-Y^{3}-octreotate were investigated in Chapter VIII. Rats were first injected with up to 100mCi/kg and evaluated for dosimetry and acute toxicology. The data show that the uptake of the agent is significantly higher in the tumor site and lower in the kidneys compared to ^{90}Y-octreotide, and represents a safer agent for radiotherapy as a result. In these studies no acute toxicity was observed except for a transient drop in WBC values and a loss in body weight that recovered to normal values after 4 weeks. However, the question of chronic renal toxicity was addressed in the long term surviving animals from the radiotherapy studies from Chapter IV. Though these animals showed complete ablation of tumor mass, mortality of the animals began to occur at ~ 12 months post inoculation. Though virtually all animals were found to be tumor free at necropsy, there was a high prevalence of renal carcinoma (80%) and a predisposition to karyomegaly in other animals suggesting a pre-neoplastic condition. The prevalence of renal cell carcinoma was most pronounced in the high dose

regimen, but even at lower doses renal carcinoma was the main cause of death, and the high degree of renal carcinoma was likely the result of the targeting agent. These results, must be taken into context however, as in these radiotherapy studies no attempt to block renal uptake of the peptide using amino acid infusion was attempted. It is well know that anino acid infusion will reduce renal uptake by approximately 50% and that in these studies the administered doses do not reflect an optimal therapy scenario employing a radiolabeled peptide such as ^{177}Lu-DOTA-Y^{3}-octreotate.

In the final studies (Chapter IX) the extension of this peptide into an optically active molecule for fluoresence imaging of sst_2 positive tumors was explored. Using a modified indocyanine green conjugated to octreotate (Cytate) it was shown that this agent has high affinity for the CA20948 and AR42-J tumor lines in vivo, and were the first studies that showed imaging of tumors in vivo using a simple CCD camera apparatus with excitation at 780nm and emission at 820nm is possible. The chemistry was expanded to a bombesin specific flurophore with similiar imaging results (Appendix III). These experiments lay the ground work for the logical extension of this approach to photodynamic therapy (PDT) using optically modified peptides to moieties that would liberate singlet oxygen upon excitation instead of fluoresence as shown in this initial work. The improvement over conventional PDT agents such as Photophrin IX or 5-ALA is that a highly receptor specific peptide like Cytate would deliver a greater therapeutic dose to the target tissue, and also reduce the toxictiy associated with non-specific porphyrin like agents.

In the appendices the articles authored by Kwekkeboom reduce the concept of using a low energy beta emitting radionuclide to clinical practice with ^{177}Lu-DOTA-Y^{3}-octreotate. These two studies confirm the pre-clinical hypothesis and data from this

thesis that a low energy beta emitter like Lu-177 can have significant therapeutic potential. The current use of this agent has been considered to be most promising by the physicians of record, and that the use of ^{177}Lu-DOTA-Y^{3}-octreotate is clinically superior to ^{90}Y-DOTA-Y^{3}-octreotate for radiotherapy of neuroendocrine tumors.

SAMENVATTING EN CONCLUSIES

Samenvatting en Conclusies

Sinds de ontdekking van de somatostatinereceptor en het subkloneren van de vijf somatostatinereceptor-subtypes is er veel research gestart met betrekking tot de ontwikkeling van radiofarmaca voor imaging en therapie via deze goed gekarakteriseerde receptor. Het werk van Krenning, Lamberts en medewerkers eind jaren 80 van de vorige eeuw liet als eerste zien dat receptorscintigrafie met behulp van een radioactief gelabeld peptide mogelijk is. In 1994 ontving ^{111}In-DTPA-octreotide (OctreoScan) goedkeuring van de FDA en tot vandaag is het de "Gouden Standaard" voor somatostatine-receptor-scintigrafie. Krenning et al. continueerden met de introductie van peptide-receptor-radionuclide-therapie (PRRT) via de somatostatine receptor met behulp van de radionucliden In-111 (Auger) en Y-90 (Beta) for radiotherapie.

Een belangrijke verbetering in de uitgangsstof octreotide (Hoofdstuk 2) ontstond door de vervanging van het C-terminale threonineol door het natieve threonine. De gemodificeerde alcohol threonineol was indertijd geintroduceerd om de serumhalfwaardetijd te verlengen, de verwachting was dat de natieve vorm te snel uit het bloed geklaard zou worden om effectief te kunnen zijn.

De ogenschijnlijk subtiele vervanging van threonineol door threonine resulteerde echter in superieure opname- en internalizatie-eigenschappen ten opzichte van OctreoScan in somatostatinereceptor (met name subtype 2(sst_2)-positieve organen en tumoren in tumordragende ratten. Het nieuwe molecuul kreeg de naam octreotate. De verbeterde opname en, belangrijker nog, internalizatie van deze stof leidde tot het onderzoek naar de mogelijkheden van radiotherapie in een diermodel met behulp van een beta-emitter met gemiddelde energie, samarium-153, gekoppeld

aan octreotate via de chelator CMDTPA. Deze stof kon significante suppressie van tumorgroei in het CA20948-rattentumormodel bewerkstelligen in vergelijking met die in onbehandelde controledieren (Hoofdstuk III). Samarium-153 had echter 2 nadelen: (a) lage specifieke activiteit <700Ci/mmol en (b) een korte halfwaardetijd van slechts 46.3 uren.

Om deze problemen op te lossen zonder de chemie van het molecuul in belangrijke mate aan te moeten passen, werd het radionuclide Lu-177 onderzocht. Dit radionuclide is beschikbaar met een veel hogere specifieke activiteit (>3000Ci/mmol) en heeft een halfwaardetijd van 6.7 dagen. Lu-177 zend naast betadeeltjes ook 208keV gammastraling uit, die zeer geschikt is voor scintigrafie en dosimetriebepalingen. Dit radionuclide werd gelabeld aan DOTA-octreotate (Hoofdstuk IV) en het radiofarmacon ^{177}Lu-DOTA-Y^{3}-octreotate werd onderzocht in biodistributie- en therapiestudies in CA20948-tumordragende ratten. In dieren behandeld met 3 x 5.0mCi (30 dagen interval) werd complete ablatie van de tumoren gevonden en de dieren leefden tot tenminste18 maanden na tumorinoculatie. De efficientie van het radiofarmacon werd getest in twee nieuwe sst_2-positieve tumormodellen in ratten (Hoofdstuk 5). In deze modellen de rattenpancreascellijn AR42J , die tot dan alleen gebruikt werd in athymische of SCID-muizen, werd geintroduceerd in normale Lewis ratten in een flanktumormodel en in een metastasenmodel voor levermetastasen. Deze nieuwe modellen maken gebruik van zeer jonge ratten, waardoor tumorgroei en seriele implantatie in meerdere generaties Lewis-ratten mogelijk werd. Hierdoor was het gebruik van athymische of SCID-muizen, waarbij hogere eisen gesteld moeten worden aan huisvesting vanwege hun verminderde immuunsysteem, voor deze studies niet meer nodig. De therapeutische werkzaamheid van ^{177}Lu-DOTA-Y^{3}-octreotate werd onderzocht in beide

rattenmodellen (flanktumor- en levermetastasenmodel). Significante tumorgroeisupressie werd gezien in het flankmodel in vergelijking met controledieren en in het levermodel resulteerden drie behandelingen 5.0mCi ^{177}Lu-DOTA-Y^{3}-octreotate in zichtbare eliminatie van levermetastasen. Hergroei van tumor werd gezien in het flankmodel na 85 dagen, hetgeen suggereert dat dit nieuwe tumormodel meer radioresistent is dan de CA20948-cellijn.

Eerdere studies hadden getoond dat de opname en retentie van octreotide-analoga in sst_2-positieve weefsels, zoals de the pancreas en bijnieren, een bellshapecurve vertonen als ze uitgezet worden tegen afnemende specifieke activiteit. Deze observatie was onverwacht, het paradigma was dat de maximum opname gevonden zou worden bij de hoogste specifieke activiteit. Dit effect is belangrijk met betrekking tot radiotherapie, omdat daar gestreefd moet worden naar de maximale opname van het therapeutische peptide in de tumor. Experimenten zijn daarom uitgevoerd om de bellshape van octreotate gelabeled met In-111 and Lu-177 te onderzoeken (Hoofdstuk VI). In het CA20948-tumormodel werd geen echte bellshapecurve gevonden voor octreotate, met uitzondering van opname in de pancreas na labeling van het peptide met Lu-177. In feite lieten de experimenten zien dat de tumoropname betrekkelijk hoog bleef over een grote range van specifieke activiteiten (10-5700Ci/mmol) en dat volledige receptorsaturatie van de tumor pas gevonden werd bij ~1.5Ci/mmol. Dus is de biodistributie van dit molecuul anders dan die van octreotide en als radiotherapeuticum zal het een hogere dosis leveren op de tumoren over een grotere range van labelingscondities.

Een ander diermodel voor sst_2-positieve tumorcellijnen is beschreven in Hoofdstuk VII. Dit hoofdstuk beschrijft de ontwikkeling van een $hsst_2$- positief rattentumormodel,

de borsttumorcellijn Mat-B die normaal sst_2-negatief is. Deze tumorcellijn is getransfecteerd met een plamide dat codeert voor deze receptor waardoor in hoge densiteit $hsst_2$ tot expressie komt. In dit model werd gevonden dat de opname en retentie van ^{177}Lu-DOTA-Y^3-octreotate >50 keer de opname in de wildtype tumorcellijn was. Scintigrafie bevestigde de expressie van de receptor, de expressie werd alleen gevonden in de tumor. Eerste radiotherapie-experimenten met ^{177}Lu-DOTA-Y^3-octreotate lieten een significante vertraging in tumorgroei zien in vergelijking met onbehandelde controledieren. De beschikbaarheid van 5 subclones maakt het mogelijk deze benadering te gebruiken om subtypespecifieke modellen wat betreft sst-expressie in vivo te maken. Deze techniek kan ook de expressie van niet-somatostatinereceptoren, zoals voor VIP, CCK of bombesine, mogelijk maken om peptiden te evalueren die specifiek aan deze receptoren binden.

Acute en chronische toxiciteit van ^{177}Lu-DOTA-Y^3-octreotate worden beschreven in Hoofdstuk VIII. Ratten werden geinjecteerd met oplopende doses to 100mCi/kg en geevalueerd voor dosimetrie en acute toxiciteit. De data laten zien dat de opname van deze stof in de tumor significant hoger is dan die van ^{90}Y-octreotide, terwijl de nieropname lager is, het is dus een veiliger stof voor radiotherapie. In deze studies werd geen acute toxiciteit geobserveerd, behalve een tijdelijke vermindering van WBC-waarden en gewichtsverlies die weer normaliseerden na vier weken. De chronische renale toxiciteit werd onderzocht in een lange overlevingsstudie na therapie in tumordragende ratten, zoals beschreven in Hoofdstuk IV. In deze dieren werd volledige verdwijning van de tumor gevonden, mortaliteit trad op ongeveer 12 maanden na inoculatie. Hoewel eigenlijk alle dieren CA20948-tumorvrij bleken bij necropsie, werd er een hoge prevalentie niercarcinoma gevonden (80%) en karyomegalie in andere dieren suggereerde een pre-neoplastische conditie. De

prevalentie van niercarcinoma was het hoogst in de dieren die de hoogste dosis hadden ontvangen, maar ook bij lagere doses was het de meest voorkomende doodsoorzaak en een hoog percentage van de gevonden carcinomen werd waarschijnlijk veroorzaakt door het ^{177}Lu-DOTA-Y^{3}-octreotate. Deze resutaten moeten wel gezien worden in hun contekst, in deze radiotherapiestudies is geen reductie van nieropname bewerkstelligd door aminozuren. Het is bekend dat deze aminozuren de nieropname met ongeveer 50% verminderen en de studies zoals uitgevoerd reflecteren dus geen optimaal therapiescenario voor een radioactief gelabeled peptide zoals ^{177}Lu-DOTA-Y^{3}-octreotate.

In the laatste beschreven studies (Hoofdstuk 9) is de extentie van dit molecuul tot een optisch actieve stof voor fluoresentie-imaging van sst_2-positieve tumoren onderzocht. Met behulp van een gemodificeerd indocyanine-groen geconjugeerd aan octreotate (Cytate) werd getoond dat dit stofje een hoge affiniteit heeft voor CA20948 en AR42J tumoren in vivo, dit waren de eerste studies die toonden dat imaging van tumoren in vivo mogelijk is met behulp van een eenvoudige CCD-camera met excitatie bij 780nm en emissie bij 820nm. De chemie werd uitgebreid met een fluorescerend bombesin met vergelijkbare imaging-resultaten (Appendix III). Deze experimenten leggen de basis voor de logische extentie van deze benadering tot fotodynamische therapie (PDT) met optisch gemodificeerde peptiden die zuurstofradicalen uitzenden na excitatie, in plaats van fluorescentie. Het voordeel ten opzichte van conventionele PDT stoffen, zoals Photophrin IX or 5-ALA, is dat een hoog receptorspecifiek peptide zoals Cytate een grotere therapeutische dosis levert op de doelorganen, terwijl de toxiciteit die geassocieerd is met niet-specifieke stoffen gereduceerd wordt.

In de appendices wordt getoond dat het concept van een laag-energetische beta-emitter voor radiotherapie ook in de klinische praktijk toegepast kan worden. Deze twee artikelen bevestigen de preklinische hypothese en data dat een radionuclide als Lu-177 significant therapeutisch potentieel kan hebben. Het huidige gebruik in de kliniek toont dat deze stof zeer veelbelovend is en klinisch superieure resultaten geeft bij radiotherapie van neuroendocriene tumoren ten opzichte van ^{90}Y-DOTA-Y^3-octreotide.

Appendix I

NOVEL RECEPTOR-TARGETED FLUORESCENT CONTRAST AGENTS FOR IN VIVO TUMOR IMAGING

Investigative Radiology, 35, 479-485, (2000)

Novel Receptor-Targeted Fluorescent Contrast Agents for In Vivo Tumor Imaging

SAMUEL ACHILEFU, PHD,* RICHARD B. DORSHOW, PHD,† JOSEPH E. BUGAJ, MS,* AND RAGHAVAN RAJAGOPALAN, PHD†

Achilefu S, Dorshow RB, Bugaj JE, Rajagopalan R. Novel receptor-targeted fluorescent contrast agents for in vivo tumor imaging. Invest Radiol 2000;35:479–485.

RATIONALE AND OBJECTIVES. **To evaluate the efficacy of a novel tumor receptor-specific small-peptide–near-infrared dye conjugate for tumor detection by optical imaging.**

METHODS. **A novel, near-infrared dye-peptide conjugate was synthesized and evaluated for tumor-targeting efficacy in a well-characterized rat tumor model (CA20948) known to express receptors for the chosen peptide. A simple continuous-wave optical imaging system, consisting of a near-infrared laser diode, a cooled CCD camera, and an interference filter, was used in this study.**

RESULTS. **Tumor retention of two non–tumor-specific dyes, indocyanine green and its derivatized analogue, bis-propanoic acid cyanine dye (cypate), was negligible. In contrast, the receptor-specific peptide-cypate conjugate (cytate) was retained in the CA20948 tumor, with an excellent tumor-to-normal-tissue ratio in the six rats examined.**

CONCLUSIONS. **Optical detection of tumors with a receptor-targeted fluorescent contrast agent has been demonstrated. This result represents a new direction in cancer diagnosis and patient management.**

KEY WORDS. **Optical imaging; contrast agents; tumor targeting; dye-peptide conjugates.**

INTEREST IN THE early detection of tumors has increased recently as a result of the increasing number of deaths caused by cancer.[1] Common methods for cancer diagnosis rely on the physical detection of a palpable tumor mass or the use of different forms of roentgenography, scintigraphy, ultrasound, and MR imaging techniques for tissue imaging.[2,3] In both cases, the presence of a significant tumor mass is necessary for reliable diagnosis, at which stage patient prognosis may have already been compromised. Recently, optical imaging has been proposed as an alternative tumor detection method with great potential in clinical diagnosis.[4–8] Among other advantages over conventional modalities, the optical approach uses neither ionizing radiation nor radioactive materials, and a wealth of information can be extracted from light-tissue interaction in the electromagnetic region of interest.[9–16]

As with traditional imaging techniques, contrast agents enhance the differentiation of normal from abnormal tissues in vivo.[17] The ideal properties for optical contrast agents include biocompatibility, high molar absorptivity, and high fluorescent quantum yield. Furthermore, several studies have established that compounds which absorb or emit in the near-infrared region are highly desirable. This wavelength range constitutes a transparent window in the human body in which autofluorescence and absorption of light by endogenous chromophores are minimized.[18] A combination of these properties would enhance the sensitivity of any detection system and also provide deeper tissue penetration of light. For example, the large molar absorptivity (250,000 cm^{-1} at 780 nm) of indocyanine green (ICG, Fig. 1A) affords a unique opportunity for the detection of a small tumor volume.[19]

Localization of dyes in tumors can be mediated by several factors, including "leaky" vasculature and high metabolic activity in proliferating cells.[20] However, tumor targeting by such nonspecific mechanisms may not differentiate inflammation from benign or malignant tumors. In addition, nonspecific contrast agents initially distribute to several organs, and hence, require a prolonged waiting period to clear from normal tissues.

From *Discovery Research and †Imaging R&D, Mallinckrodt Inc., St. Louis, Missouri.

Reprint requests: Samuel Achilefu, PHD, Mallinckrodt, Inc., 675 McDonnell Blvd., St. Louis, MO 63042; e-mail: Samuel.achilefu@mkg.com

Received March 29, 2000, and accepted for publication, after revision, May 11, 2000.

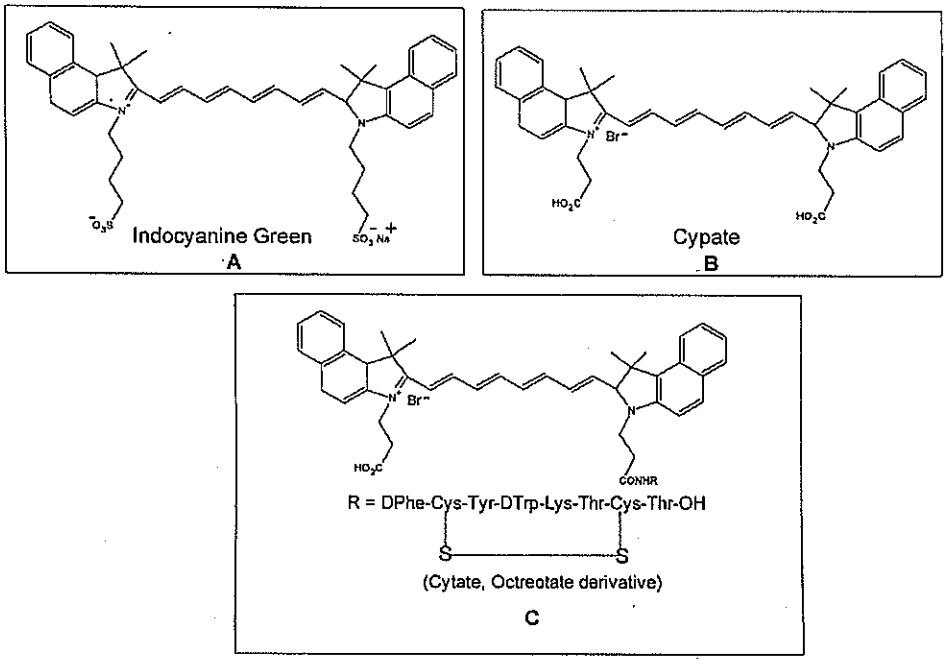

Figure 1. Molecular structure of indocyanine green (A), cypate (B), and cytate (C).

Fortunately, many tumors are known to overexpress specific receptors that could be used to differentiate them from normal cells.[20,21] Therefore, ligands for such receptors can be used as drug delivery vehicles to enhance tumor specificity.[22,23] Studies by scintigraphic imaging have demonstrated the feasibility of targeting tumor receptors with antibodies and other large biomolecules.[24,25] Adaptation of this approach to optical imaging has been described.[26,27] However, such large molecules are preferentially taken up by the liver and can elicit adverse immunogenic reactions in humans.[28] Some have very long blood residence times, which prolong the period required for improved tumor-to-background ratio.[29] For solid tumors, which rely on the diffusion of biomarkers from the vasculature, penetration of large dye bioconjugates is not favorable owing to the net positive pressure within the tumor.[30] Hence, a better method to specifically deliver optical probes to tumors is highly desirable.

Recent studies in nuclear medicine have demonstrated that attachment of chelating agents to small molecular peptides can be used to target tumors without loss of receptor affinity of the peptides.[31] This approach has several advantages with respect to either the use of nonspecific agents or the conjugation of probes to large biomolecules. Such advantages include enhanced localization in tumors, rapid clearance from the blood, and the possibility of synthesizing a combinatorial "library" of peptides for rapid identification of bioactive products.[20] Our goal in this study was to replace the radiolabeled chelate component of the peptides used in scintigraphy with fluorescent dyes while preserving the receptor affinity of the peptide and the fluorescence of the dye. To this end, we designed and synthesized a novel dye-peptide conjugate that is receptor specific and evaluated the efficacy of this new fluorescent contrast agent in rat tumor lines by using a simple, continuous-wave fluorescence imaging apparatus.

Materials and Methods

Contrast Agents

Commercially available ICG dye (Fig. 1A) was used without further purification. Bispropylcarboxymethylindocyanine dye (cypate, Fig. 1B) was prepared by the reaction of a mixture of 1,1,2-trimethyl-[*1H*]-benz[e]indole and 3-bromopropanoic acid in 1,2-dichlorobenzene. Reaction of the brown solid precipitate obtained with glutaconaldehyde dianil monohydrochloride (Pfaltz & Bauer, Waterbury, CT) in ethanol gave a green solution. Evaporation of the solvent, followed by purification of the crude product by high-performance liquid chromatography (HPLC) and lyophili-

zation of the isolated compound, gave cypate as dark green flakes in >99.5% HPLC purity.

The somatostatin receptor–specific peptide octreotate was prepared by standard 9-fluorenylmethoxycarbonyl solid-phase synthesis,[32] and the two cysteine residues per molecule were cyclized into a disulfide bond on solid support with thallium trifluoroacetate to give the cyclic peptide. Reaction of cypate with the peptide on solid support and subsequent peptide cleavage from the resin with trifluoroacetic acid gave a crude product that was purified by HPLC to give the desired dye-peptide compound, cytate, in 99.5% HPLC purity (Fig. 1C).

Animal Protocols

All studies were conducted in compliance with the Mallinckrodt Animal Welfare Committee's requirements for the care and use of laboratory animals in research. Pancreatic ductal adenocarcinoma (DSL6/A) tumors were induced in male Lewis rats in the left flank area by the introduction of material from a solid (donor) implant, and the tumors were palpable in approximately 14 days. This tumor line is not somatostatin subtype 2 (sst_2) receptor–positive.

Prostatic carcinoma (Dunning R3327-H) tumors were induced in young male Copenhagen rats in the left flank area from a solid implant. These tumors grow very slowly, and palpable masses were present 4 to 5 months after implant. This tumor line is also not sst_2 receptor–positive.

Rat pancreatic acinar carcinomas (CA20948) expressing the sst_2 receptor were induced by solid-implant technique in the left flank area, and palpable masses were detected 9 days after implant. This tumor line has been widely used for sst_2 receptor–positive assays, and the number of binding sites for somatostatin is 489 fmol/mg.[33]

The animals were anesthetized with a rat cocktail (xylazine/ketamine/acepromazine 1.5:1.5:0.5, v/v/v; obtained from Butler Co., Columbus, OH; Fort Dodge Animal Health, Fort Dodge, IA; and Fermenta Animal Health Co., Kansas City, MO, respectively) at 0.8 mL/kg via intraperitoneal injection. The area of the tumor (left flank) was shaved to expose the tumor and surrounding surface area. A 21-gauge butterfly infusion set equipped with a stopcock and two syringes containing heparinized saline was placed into the lateral tail vein of the rat. Patency of the vein was checked before administration of the ICG, cypate, or cytate dyes via the butterfly apparatus. Each animal received 0.5 mL of aqueous solution of ICG (5.4 μmol/L), cypate (5.0 μmol/L), or cytate (6.0 μmol/L).

Imaging Apparatus and Procedure

A noninvasive in vivo fluorescence imaging apparatus was used to assess the efficacy of contrast agents developed for tumor detection in animal models. A LaserMax laser diode (LaserMax Inc., Rochester, NY) of nominal wavelength 780 nm and nominal power of 40 mW was used. The detector was a Princeton Instruments (Trenton, NJ) model RTE/CCD-1317-K/2 CCD camera with a Rodenstock 10-mm f2 lens (stock No. 542.032.002.20; Rodenstock, Rockford, IL) attached. An 830-nm interference filter (CVI Laser Corp., Albuquerque, NM; part No. F10-830-4-2) was mounted in front of the CCD input lens such that only emitted fluorescent light from the contrast agent was detected. Typically, an image of the animal was taken before injection of a contrast agent. This image was subsequently subtracted (pixel by pixel) from the postadministration images. However, the background subtraction was never done once the animal had been removed from the sample area and returned at a later time for images taken several hours after administration. The images shown in Figures 3, 4, and 6 were obtained by this procedure. ICG was evaluated in four separate CA20948 tumor–bearing Lewis rats, and for comparison, the cytate dye was evaluated in six separate CA20948 tumor–bearing Lewis rats. The cypate dye was evaluated in three separate tumor-bearing animals. Measurement of the blood clearance profile of ICG and cypate (Fig. 5) was carried out as described previously.[13] Retention of ICG (Fig. 2, $n = 4$) and cytate (Fig. 7, $n = 4$) in selected tissues was assessed by imaging excised tissues from sacrificed rats at a specified time.

Results

The false-color image of fluorescence intensity measured at 2 and 30 minutes after bolus injection of a 0.5-mL aqueous solution of ICG (5.4 μmol/L) in three different tumor lines is shown in Figure 2. All tumors were about 2 g in size. Nonspecific retention of the dye is noted in the DSL6/A and Dunning R3327-H tumor lines 30 minutes after administration. Rapid clearance of ICG from the CA20948 tumor line indicated no nonspecific retention.

Time-sequence fluorescent images of ICG in a normal rat are shown in Figure 3. Rapid localization of the dye in the liver was observed, which is consistent with the known hepatobiliary excretion of ICG.[34,35] Similar experiments with cypate gave identical results to ICG. Figure 4 shows the time-sequence fluorescent images of ICG in a CA20948 tumor–bearing rat. Localization of the dye in the liver and the left flank tumor was evident as early as 1 minute after administration; however, almost total clearance from the tumor was apparent by 60 minutes after administration. Thus, ICG is not retained in this tumor in vivo.

The in vivo fluorescence time dependence in a rat with normal liver function measured at the ear after bolus intravenous administration of aqueous solutions of ICG and cypate is shown in Figure 5, with the use of instrumentation described elsewhere.[13] The newly synthesized dye cypate was cleared from the vasculature with essentially the same blood clearance profile as ICG.

The time-sequence fluorescent images of cytate in a CA20948 tumor–bearing rat is shown in Figure 6. Delineation of the tumor from normal tissue was easily observed at 90 minutes after administration. Thus, cytate retained both the fluorescent properties of the dye and the targeting properties of the peptide in vivo. Localization of cytate in

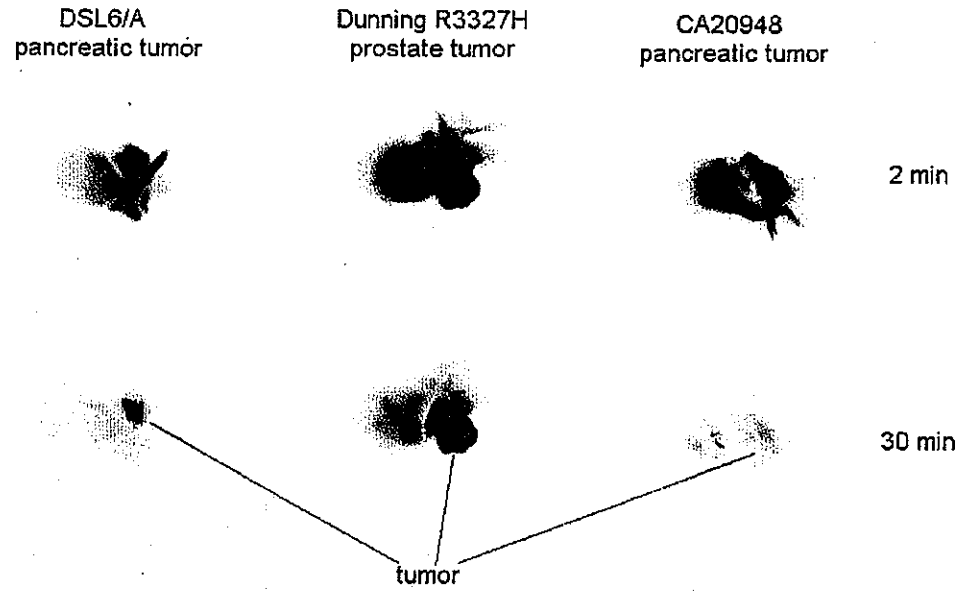

Figure 2. False-color image of fluorescence intensity measured at 2 and 30 minutes after bolus injection of a 0.5-mL aqueous solution of indocyanine green (5.4 μmol/L) in three different tumor lines in vivo. Images are constrained to the tumor and a small surrounding area of the left flank of rats.

tissues of a tumor-bearing rat 24 hours after administration is shown in Figure 7. The tumor, adrenals, and pancreas, which are sst2 receptor–positive tissues, had significant uptake of the dye-peptide conjugate. The relative ratio of tumor to normal tissue fluorescent intensity, calculated from the average camera pixel intensities of individual organs in Figure 7, is shown in Table 1.

Discussion

Clinical studies have established that ICG, which absorbs in the near-infrared region, is biocompatible, excreted primarily by the hepatobiliary system,[34,35] and localizes in certain tumors by a nonspecific mechanism.[36] Thus, to identify a good model for the evaluation of

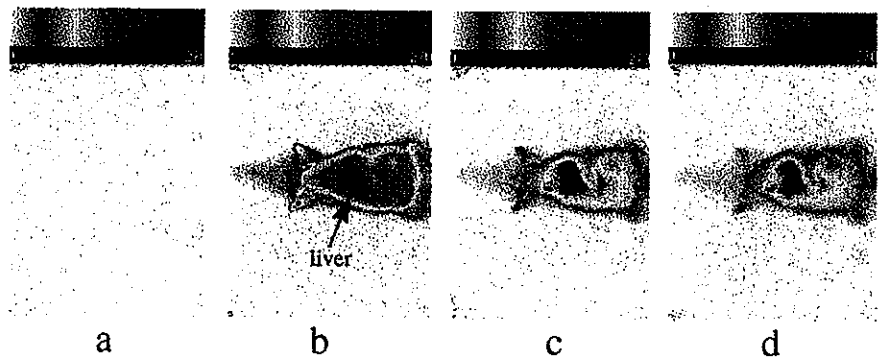

Figure 3. Time-sequence fluorescence images (n = 4) of indocyanine green in a normal rat before administration (a), 1 minute after administration (b), 10 minutes after administration (c), and 60 minutes after administration (d). For each image, the rat was placed in a supine position.

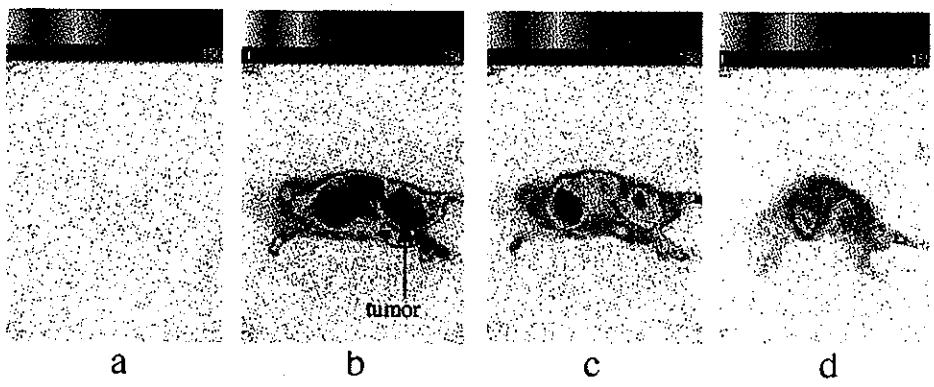

Figure 4. Time-sequence fluorescence images (n = 4) of indocyanine green in a CA20948 tumor–bearing rat before administration (a), 1 minute after administration (b), 10 minutes after administration (c), and 60 minutes after administration (d). For each image, the rat was placed lying on its side to optimally expose the flank.

targeting tumor receptors with dye-peptide conjugates, we screened three tumor models with ICG (Fig. 2). ICG localized in two (DSL6/A and R3327-H) of the three tumor lines examined. However, it has only transient retention in the CA20948 tumor line, which is known to overexpress the sst_2 receptor.[37] A biodistribution study of ICG in various organs from normal and CA20948 tumor–bearing rats 60 minutes after administration confirmed that the known mechanism of ICG excretion through the liver was not altered by the tumor (Figs. 3 and 4).

Fortunately, the literature abounds with many short-chain somatostatin analogues that efficiently target sst_2 receptors. The US Food and Drug Administration has approved one such product, OctreoScan (Mallinckrodt, Inc., St. Louis, MO), for the imaging of neuroendocrine tumors by scintigraphy.[20] A logical approach would therefore involve the conjugation of dyes to peptides that have high affinity for this receptor. However, unlike contrast agents in scintigraphy, in which the probe is a smaller component of the peptide, near-infrared dyes have comparable molecular weights to the peptides. Hence, the conjugate could impair the ability of the tumor receptors to recognize the peptide. For this reason, several researchers have generally opted to use other approaches for tumor targeting, such as large biomolecule-dye conjugate systems.[27,29]

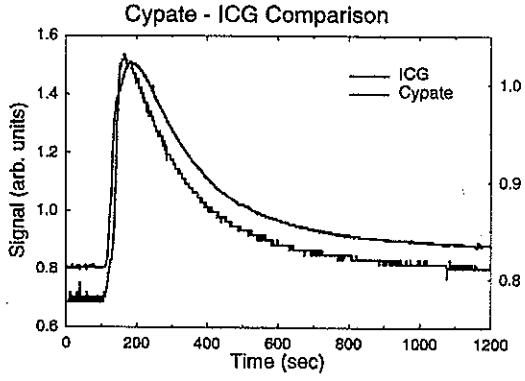

Figure 5. In vivo fluorescence time dependence in a rat with normal liver function measured at the ear after a 0.5-mL bolus of aqueous solutions of indocyanine green (ICG, 5.4 μmol/L, n = 6) or cypate (5.2 μmol/L, n = 3) was administered intravenously.

Indocyanine green, which is approved for human use by the US Food and Drug Administration, is practically inert to conditions for the incorporation of peptides and proteins, and hence, must be derivatized for such use. Thus, we sought to synthesize biocompatible dyes that have similar photophysical and blood clearance characteristics as ICG. Results of these studies identified the propanoic acid derivative of indolenium cyanine dye (cypate) as a good candidate for this work. Both cypate and ICG have similar photophysical properties and blood clearance profiles (see Fig. 5). Experiments with cypate in both normal and CA20948 tumor–bearing rats (n = 3) yielded results identical to ICG, in that cypate was taken up by the liver within 60 minutes after administration (similar to Fig. 3), and tumor washout was virtually complete by 60 minutes after administration (similar to Fig. 4). Consequently, both ICG and cypate were useful negative controls in the CA20948 tumor–targeting study.

The small peptide-dye compound investigated (cytate, Fig. 1C) was a synthesized conjugate of cypate dye and the octreotate peptide. Administration of this conjugate

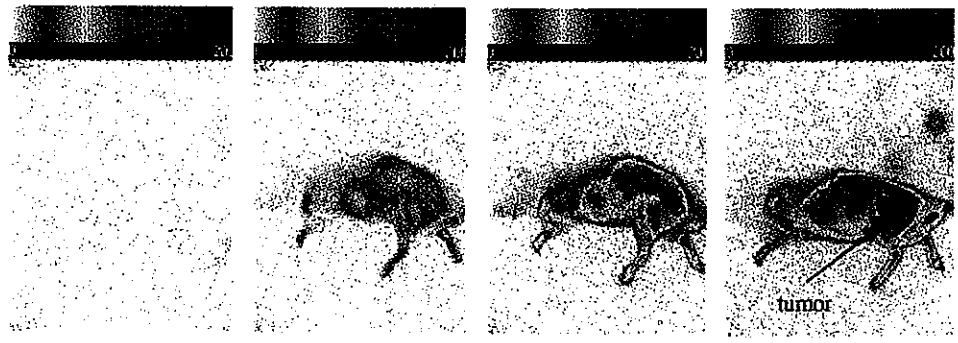

Figure 6. Time-sequence fluorescence images (n = 6) of cytate in a CA20948 tumor–bearing rat before administration (a), 1 minute after administration (b), 10 minutes after administration (c), and 90 minutes after administration (d). A 0.5-mL bolus of an aqueous solution of cytate (6.0 μmol/L) was given intravenously. For each image, the rat was placed lying on its side to optimally expose the flank.

into tumor-bearing rats (n = 6) produced fluorescence at the tumor site within 10 minutes after administration, and at 90 minutes, the tumor was unequivocally observable (Fig. 6). This observation is in sharp contrast to the results obtained with large biomolecule-dye conjugates, for which postinjection times of 24 to 36 hours may be needed to obtain a reasonable tumor-to-background ratio.[27,29] Biodistribution studies showed that cytate also localized in tissues (pancreas and the adrenal glands) that are known to express the somatostatin receptor[38] (Fig. 7). Nonspecific uptake by the kidneys and the liver, which constitute the primary routes of excreting the nonconjugated peptide and dye, respectively, was also observed.

Previous studies have shown that subtle differences (tumor-to-tissue ratios <2) between a tumor and normal tissue can be detected in vivo.[15] The specificity of the new dye-peptide conjugate cytate enhanced this ratio tremendously (Table 1), resulting in improved enhancement in the diagnostic capability of optical imaging assays. In addition, the ease of tumor detection with such products as cytate may lead to the use of cheaper and less-sophisticated optical instruments for tumor imaging and detection. Furthermore, delineation of kidney morphology was readily observed. This finding demonstrates the potential of the optical modality, in the presence of a contrast agent, to provide detailed anatomic information not readily available with other techniques.

The use of small peptides has several advantages over large biomolecules, including ease of synthesis of a variety of compounds for potential combinatorial screening of new targets, reproducibility of high-purity compounds, diffusivity to solid tumors, and the ability to incorporate a variety of functional groups that modify the pharmacokinetics of the peptide-dye conjugates. During this study, we developed a method to prepare dye-peptide conjugates by solid-phase synthesis, a process that is amenable to automated synthesis. We have demonstrated, for the

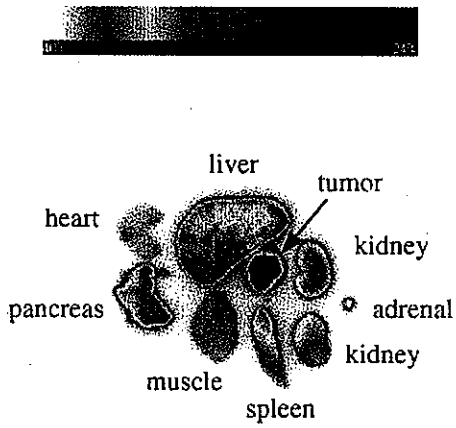

Figure 7. Localization of cytate in tissues of a CA20948 tumor–bearing rat 24 hours after administration.

TABLE 1. Ratio of Tumor to Normal Tissues (T/NT) Fluorescent Intensity

Tissue	T/NT
Heart	10
Muscle	7
Kidney	5
Liver	2

Note: The data were obtained by taking the relative fluorescence intensity averages for each organ 24 hours after administration in six CA20948 tumor–bearing rats.

first time, that small peptide-dye conjugates are effective in tumor detection by optical imaging. Cytate specifically binds to CA20948 tumor, which is known to overexpress the sst_2 receptor, whereas dyes devoid of the receptor-targeting component were not retained in this tumor. The concept of using tumor-targeted, small molecular probes for optical imaging is not limited to dye-peptide conjugates but could be extended to other small, bioactive molecules.

Acknowledgments

The authors wish to thank R. Randy Wilhelm (mass spectrometry), Michelle A. Schmidt (peptide chemistry), and Hermo Jimenez (dye chemistry) for their various contributions.

References

1. Greenlee RT, Murray T, Bolden S, Wingo PA. Cancer statistics, 2000. CA Cancer J Clin 2000;50:7–33.
2. Shaw DD. Contrast media: Directions for the 1990s. Invest Radiol 1993;28:S138–S139.
3. Giger ML, Pelizzari CA. Advances in tumor imaging. Sci Am 1996; 275:110–112.
4. Benaron DA, Stevenson DK. Optical time-of-flight and absorbance imaging of biologic media. Science 1993;259:1463–1466.
5. Mutter G, Chance B, Alfano R, et al, eds. Medical optical tomography: Functional imaging and monitoring. Bellingham, WA: SPIE Optical Engineering Press; 1993.
6. Tearney GJ, Brezinski ME, Bouma BE, et al. In vivo endoscopic optical biopsy with optical coherence tomography. Science 1997; 276:2037–2039.
7. Tromberg BJ, Coquoz O, Fishkin JB, et al. Non-invasive measurements of breast tissue optical properties using frequency-domain photon migration. Philos Trans R Soc Lond B Biol Sci 1997;352: 661–668.
8. Fantini S, Walker SA, Franceschini MA, et al. Assessment of the size, position, and optical properties of breast tumors in vivo by noninvasive optical methods. Appl Opt 1998;37:1982–1989.
9. Dirnagl U, Villringer A, Einhaupl KM, eds. Optical imaging of brain function and metabolism. New York, NY: Plenum Press; 1993.
10. Welch AJ, van Gemert MJC, eds. Optical-thermal response of laser-irradiated tissue. New York, NY: Plenum Press; 1995.
11. Contag CH, Spilman SD, Contag PR, et al. Visualizing gene expression in living mammals using a bioluminescent reporter. Photochem Photobiol 1997;66:523–531.
12. Hebden JC, Delpy DT. Diagnostic imaging with light. Br J Radiol 1997;70:S206–S214.
13. Dorshow RB, Bugaj JE, Burleigh DB, et al. Noninvasive fluorescence detection of hepatic and renal function. J Biomed Opt 1998;3:340–345.
14. Chance B, Anday E, Nioka S, et al. A novel method for fast imaging of brain function, non-invasively, with light. Opt Express 1998;2: 411–423.
15. Wagnieres GA, Star WM, Wilson BC. In vivo fluorescence spectroscopy and imaging for oncological applications. Photochem Photobiol 1998;68:603–632.
16. Masters BR. Early development of optical low-coherence reflectometry and some recent biomedical applications. J Biomed Opt 1999; 4:236–247.
17. Runge VM. Contrast media research. Invest Radiol 1999;34:785–790.
18. Abugo OO, Nair R, Lakowicz J. Fluorescence properties of rhodamine 800 in whole blood and plasma. Anal Biochem 2000;279:142–150.
19. Zhao S, Huang S, Xie S, et al. Optical imaging of breast tumor by using dual wavelength amplitude cancellation system (phased array). Biomed Opt Spectrosc Diagn Tech Dig 1998;163–165.
20. Goldsmith SJ. Receptor imaging: Competitive or complementary to antibody imaging? Semin Nucl Med 1997;27:85–93.
21. Reisine T, Bell GI. Molecular biology of somatostatin receptors. Endocr Rev 1995;16:427–442.
22. Konda SD, Aref M, Brechbiel M, Wiener EC. Development of a tumor-targeting MR contrast agent using the high affinity folate receptor: Work in progress. Invest Radiol 2000;35:50–57.
23. Unger E, Metzger P 3rd, Krupinski E, et al. The use of a thrombus-specific ultrasound contrast agent to detect thrombus in arteriovenous fistulae. Invest Radiol 2000;35:86–89.
24. Buchsbaum DJ. Experimental tumor targeting with radiolabeled ligands. Cancer 1997;80:2371–2377.
25. Behr TM, Gratz S, Markus PM, et al. Anti-carcinoembryonic antigen antibodies versus somatostatin analogs in the detection of metastatic medullary thyroid carcinoma. Cancer 1997;80:2436–2457.
26. Ballou B, Fisher GW, Waggoner AS, et al. Tumor labeling in vivo using cyanine-conjugated monoclonal antibodies. Cancer Immunol Immunother 1995;41:257–263.
27. Weissleder R, Tung CH, Mahmood U, et al. In vivo imaging of tumors with protease-activated near-infrared fluorescent probes. Nat Biotech 1999;17:375–378.
28. Guyton AC, Hall JE. Textbook of medical physiology. Philadelphia, PA: W. B. Saunders Co.: 1996.
29. Licha K, Becker A, Kratz F, et al. New contrast agents for optical imaging: Acid-cleavable conjugates of cyanine dyes with biomolecules. Proc SPIE 1999;3600:29–35.
30. Jain RK. Barriers to drug delivery in solid tumors. Sci Am 1994;271: 58–65.
31. Kwekkeboom DJ, Krenning EP, Kho GS, et al. Somatostatin receptor imaging in patients with sarcoidosis. Eur J Nucl Med 1998;25: 1284–1292.
32. Atherton E. Fluorenylmethoxycarbonyl-polyamide: Solid phase peptide synthesis. Oxford, UK: Information Press; 1989.
33. Stolz B, Weckbecker G, Smith-Jones P, et al. The somatostatin receptor-targeted radiotherapeutic [^{90}Y-DOTA-DPhe^1-Tyr^3]octreotide (^{90}Y-SMT 487) eradicates experimental rat pancreatic CA 20948 tumors. Eur J Nucl Med 1998;25:668–674.
34. Caesar J, Shaldon S, Chiandussi L, et al. The use of indocyanine green in the measurement of hepatic blood flow and as a test of hepatic function. Clin Sci 1961;21:43–57.
35. Paumgartner G, Probst P, Kraines R, Leevy CM. Kinetics of indocyanine green removal from blood. Ann N Y Acad Sci 1970;170:134–147.
36. Li X, Beauvoit B, White R, et al. Tumor localization using fluorescence of indocyanine green (ICG) in rat models. Proc SPIE 1995; 2389:789–797.
37. Bakker WH, Krenning EP, Breeman WAP, et al. Receptor scintigraphy with a radioiodinated somatostatin analogue: Radiolabeling, purification, biological activity, and in vivo application in animals. J Nucl Med 1990;31:1501–1509.
38. de Jong M, Breeman WAP, Bakker WH, et al. Comparison of ^{111}In-labeled somatostatin analogues for tumor scintigraphy and radionuclide therapy. Cancer Res 1998;58:437–441.

Appendix II

[^{177}Lu-DOTA^{0};Tyr^{3}] Octreotate: Comparison with [^{111}In-DTPA^{0}] Octreotide in Patients

European Journal of Nuclear Medicine, 28, 1319-1325, (2001)

[^{177}Lu-DOTA^{0},Tyr^{3}]octreotate: comparison with [^{111}In-DTPA^{0}]octreotide in patients

Dik J. Kwekkeboom[1], Willem H. Bakker[1], Peter P. M. Kooij[1], Mark W. Konijnenberg[3], Ananth Srinivasan[4], Jack L. Erion[4], Michelle A. Schmidt[4], Joe L. Bugaj[4], Marion de Jong[1], Eric P. Krenning[1,2]

[1] Department of Nuclear Medicine, University Hospital Rotterdam, Dr Molewaterplein 40, 3015 GD Rotterdam, the Netherlands
[2] Department of Internal Medicine, University Hospital Rotterdam, the Netherlands
[3] Mallinckrodt Medical, Petten, the Netherlands
[4] Mallinckrodt Medical, St. Louis, Missouri, USA

Received 26 February and in revised form 24 April 2001 / Published online: 4 July 2001

Abstract. The somatostatin analogue [DOTA^{0},Tyr^{3}]octreotate has a nine-fold higher affinity for the somatostatin receptor subtype 2 as compared with [DOTA^{0}, Tyr^{3}]octreotide. Also, labelled with the beta- and gamma-emitting radionuclide lutetium-177, this compound has been shown to have a very favourable impact on tumour regression and animal survival in a rat model. Because of these reported advantages over the analogues currently used for somatostatin receptor-mediated radiotherapy, we decided to compare [^{177}Lu-DOTA^{0},Tyr^{3}]octreotate (^{177}Lu-octreotate) with [^{111}In-DTPA^{0}]octreotide (^{111}In-octreotide) in six patients with somatostatin receptor-positive tumours. Plasma radioactivity after ^{177}Lu-octreotate expressed as a percentage of the injected dose was comparable with that after ^{111}In-octreotide. Urinary excretion of radioactivity was significantly lower than after ^{111}In-octreotide, averaging 64% after 24 h. The uptake after 24 h, expressed as a percentage of the injected dose of ^{177}Lu-octreotate, was comparable to that after ^{111}In-octreotide for kidneys, spleen and liver, but was three- to fourfold higher for four of five tumours. The spleen and kidneys received the highest absorbed doses. The doses to the kidneys were reduced by a mean of 47% after co-infusion of amino acids. It is concluded that in comparison with the radionuclide-coupled somatostatin analogues that are currently available for somatostatin receptor-mediated radiotherapy, ^{177}Lu-octreotate potentially represents an important improvement. Higher absorbed doses can be achieved to most tumours, with about equal doses to potentially dose-limiting organs; furthermore, the lower tissue penetration range of ^{177}Lu as compared with ^{90}Y may be especially important for small tumours.

Dik J. Kwekkeboom (✉)
Department of Nuclear Medicine, University Hospital Rotterdam, Dr Molewaterplein 40, 3015 GD Rotterdam, The Netherlands
e-mail: djkwekkeboom@hotmail.com
Tel.: +31-10-4635963, Fax: +31-10-4635997

Keywords: Somatostatin – Somatostatin receptor imaging – Octreotate – Peptide receptor radiotherapy

Eur J Nucl Med (2001) 28:1319–1325
DOI 10.1007/s002590100574

Introduction

Somatostatin receptor imaging with [^{111}In-DTPA^{0}]octreotide (Octreoscan) is nowadays recognised to be an important, if not the primary imaging technique for the localisation and staging of neuroendocrine tumours.

In patients with progressive, metastasised neuroendocrine tumours, radionuclide therapy with high doses of [^{111}In-DTPA^{0}]octreotide is performed with encouraging results [1, 2, 3, 4]. However, ^{111}In-coupled peptides are not ideal for peptide receptor radiotherapy (PRRT) because of the small particle range and the resultant short tissue penetration. Therefore, another radiolabelled somatostatin analogue, [^{90}Y-DOTA^{0},Tyr^{3}]octreotide, was developed. A preliminary study by Otte et al. [5] showed favourable results of [^{90}Y-DOTA^{0},Tyr^{3}]octreotide treatment in five patients with neuroendocrine tumours. Also, a recent analysis of the results of this treatment in a multicentre trial in 22 end-stage patients with progressive disease showed a partial tumour response in two, a minor response in three and stable disease in ten [6]. Paganelli et al. [7] have also reported favourable preliminary results regarding tumour growth with this ^{90}Y-labelled compound.

Recently, it was reported that compared with [DTPA^{0}, Tyr^{3}]octreotide, [DTPA^{0},Tyr^{3}]octreotate (in which the C-terminal threoninol is replaced with threonine) showed improved binding to somatostatin receptor-positive tissues in animal experiments [8]. Also, its DOTA-coupled counterpart, [DOTA^{0},Tyr^{3}]octreotate, labelled with the

beta- and gamma-emitting radionuclide lutetium-177, was reported to have a very successful impact on tumour regression and animal survival in a rat model [9]. Reubi et al. [10] reported a ninefold increase in affinity for the somatostatin receptor subtype 2 for [DOTA^0,Tyr^3]octreotate as compared with [DOTA^0,Tyr^3]octreotide, and a six- to sevenfold increase in affinity for their yttrium-loaded counterparts.

Because of these reported advantages over both somatostatin analogues currently used for PRRT, we decided to study [DOTA^0,Tyr^3]octreotate in patients with somatostatin receptor-positive tumours. It was complexed with ^{177}Lu because this radionuclide, apart from intermediate beta energy, also emits gammas suitable for scintigraphy and subsequent dosimetry.

Materials and methods

Patients

[^{177}Lu-DOTA^0,Tyr^3]octreotate (^{177}Lu-octreotate) was administered in six patients (four women and two men, aged 15–76 years). In five of them, somatostatin receptor imaging with [^{111}In-DTPA^0]octreotide (^{111}In-octreotide), performed during the 3 months preceding ^{177}Lu-octreotate scintigraphy, was available. None of the patients used somatostatin analogues.

One patient had medullary thyroid carcinoma (MTC), one had non-Hodgkin lymphoma (NHL), one had a gastroenteropancreatic (GEP) tumour, one had acsthesioneuroblastoma, one had a remnant of a Hürthle cell carcinoma of the thyroid, and one had papillary thyroid carcinoma.

All patients gave written informed consent to participation in the study, which was approved by the medical ethical committee of the hospital.

Methods

[DOTA^0,Tyr^3]Octreotate was obtained from Mallinckrodt (St Louis, Mo., USA). Kits were prepared consisting of 120 μg [DOTA^0,Tyr^3]octreotate, 37.8 mg sodium ascorbate and 7.5 mg gentisic acid in 300 μl 0.05 *M* HCl. Kits were stored at –20°C until use. $^{177}LuCl_3$ was obtained from Missouri University Research Reactor (MURR; University of Missouri, Mo., USA). $^{177}LuCl_3$ was diluted in 0.05 *M* HCl to a concentration of 11.1 GBq/ml, and 2,220 MBq $^{177}LuCl_3$ was added to each kit. The mixture was heated for 30 min at 80°C. The labeling yield was checked using instant thin-layer chromatography (ITLC-SG, Gelman, Ann Arbor, Mich., USA) with 0.1 *M* Na citrate, pH 5.0, as solvent. The labelled peptide migrated from the origin till Rf=0.67, while the free radionuclide migrated with the solvent front (Rf=1).

The radiochemical purity was determined by high-performance liquid chromatography (HPLC) according to the following procedure. Column: Symmetry C_{18} 4.6×250 mm, 5 μm (Waters, Milford, Mass., USA). Flow: 1 ml/min. Solvent A: methanol; solvent B: 0.06 *M* sodium acetate pH 5.5. From *t*=0 to 6.5 min 100% B; from *t*=6.5 to 7.0 min from 100% B to 50% B; from *t*=7.0 to 27 min from 50% B to 40% B; from *t*=27 min to 27.2 min from 40% B to 100% A; from *t*=27.2 min to 32 min: 100% A.

The labeling yield always exceeded 98% and the radiochemical purity was higher than 88%. The injected dose was 1,850 MBq (range 1,847–1,874 MBq); the injected mass of [DOTA^0,Tyr^3]octreotate was 90–100 μg.

^{111}In-octreotide was prepared using the Octreoscan kit from Mallinckrodt Medical (Petten, the Netherlands). The injected dose was about 220 MBq, coupled to 8–9 μg [DTPA^0]octreotide.

Imaging

^{177}Lu-octreotate. The infusion volume was 80 ml and the infusion speed was 10 min. The infusion line by which the radiopharmaceutical was administered was thereafter rinsed with about 100 ml saline. Dynamic images of the upper abdomen were obtained from the time of injection up to 20 min p.i. Planar spot images of the upper abdomen and chest in five patients, and of the upper abdomen and the head and neck in the sixth patient, were obtained with a dual-head camera (Picker Prism 2000) 4 h and 1, 3, 10 and 17 days p.i. Counts from both gamma peaks (208 and 113 keV) were collected in separate windows (width 20%). The acquisition time was 15 min/view. For dosimetry, a standard with a known aliquot of the injected dose was also counted.

^{111}In-octreotide. The windows were centered over both ^{111}In photon peaks (245 and 172 keV) with a window width of 20%. Fifteen-minute spot images were obtained 24 h p.i.

Co-infusion of amino acids

In five patients the administration of the same amount and dose of ^{177}Lu-octreotate was repeated 6–9 weeks later. An infusion of amino acids (lysine 2.5%, arginine 2.5% in 1 l 0.9% NaCl; 250 ml/h) was started 30 min before the administration of the radiopharmaceutical and lasted up to 3.5 h afterwards. Via a second pump system the radiopharmaceutical was co-administered.

Measurement of radioactivity in blood and urine

Blood samples were drawn 10, 20, 40, 60 and 90 min and 2, 5 and 24 h after injection. Urine was collected at two 3-h intervals and thereafter up to 24 h after injection.

Radioactivity in blood and urine was measured with a COBRA-Packard auto-gamma counting system (Packard, Meriden, Conn., USA).

The chemical status of the radionuclide in blood and urine was analysed as a function of time by HPLC techniques (see above).

In vivo measurements

The uptake in organs and tumours was calculated as described previously [11]. Dosimetric calculations were performed using the MIRDOSE package, version 3.0.

Statistics

Analysis of variance (ANOVA) and paired *t* tests were used. *P* values <0.05 were considered significant.

Results

No side-effects or changes in ECG pattern or pulse rate were observed in any patient during the 10-min infusion

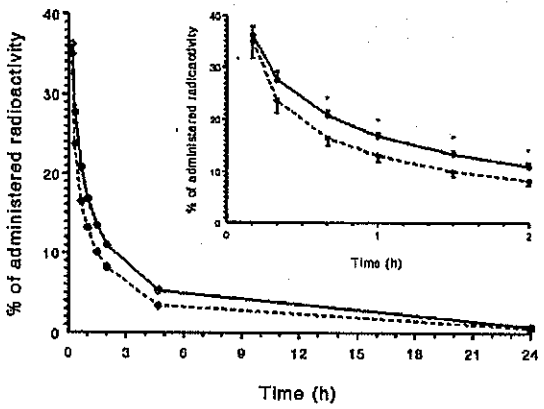

Fig. 1. Mean (±SEM) plasma radioactivity expressed as percentage of the injected dose in six patients after ^{177}Lu-octreotate (*closed dots, stippled line*), compared with that in four other patients after ^{111}In-octreotide from a previous study [12] (*open dots, solid line*). *P<0.05 vs other radiopharmaceutical at the same time point

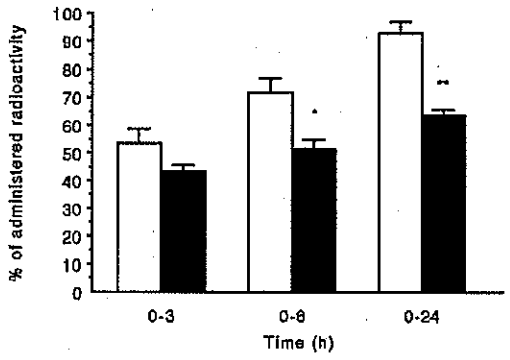

Fig. 2. Cumulative radioactivity excreted in the urine, expressed as mean (±SEM) percentage of the injected dose in four patients after ^{177}Lu-octreotate (*closed bars*), compared with that in six other patients after ^{111}In-octreotide from a previous study [12] (*open bars*). *P<0.05 and **P<0.01 vs other radiopharmaceutical during the same interval

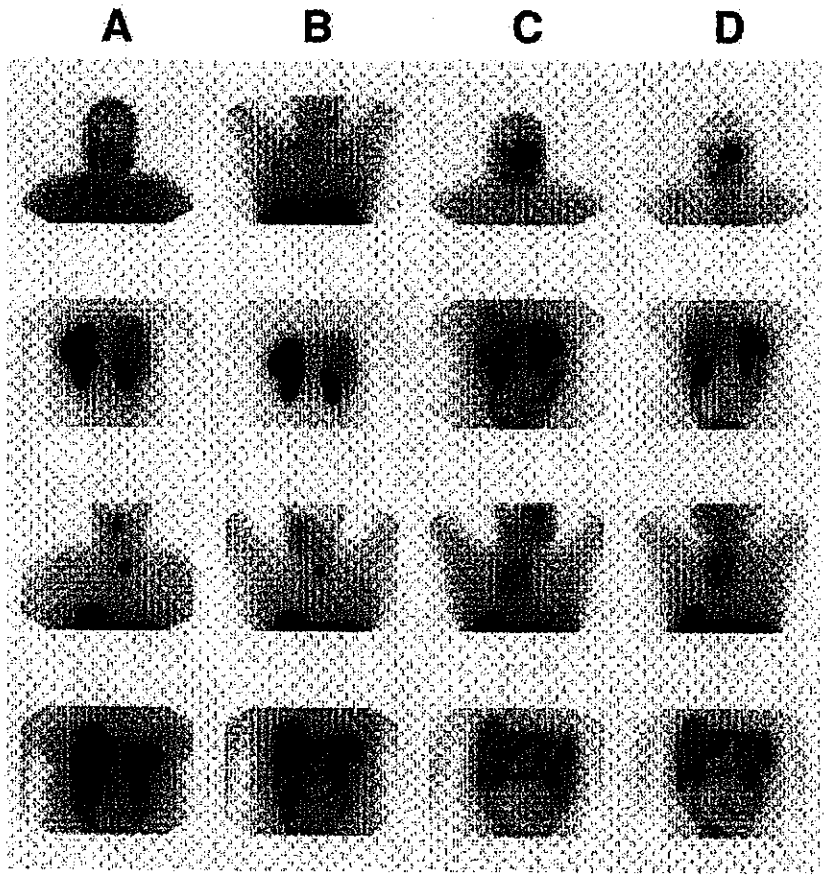

Fig. 3. Images comparing ^{177}Lu-octreotate and ^{111}In-octreotide, 24 h p.i. *Columns A and C:* ^{177}Lu-octreotate; *columns B and D:* ^{111}In-octreotide. The *first row* shows corresponding images of tumour sites in a lymphoma patient (left two images) and a patient with an aesthesioneuroblastoma of the eye with a neck metastasis (right two images); *second row:* posterior (left two images) and anterior abdominal images in the same patients. The *third row* shows corresponding images of tumours in a patient with residual Hürthle cell carcinoma (left two images) and a patient with papillary thyroid carcinoma (right two images); *fourth row:* anterior abdominal images in the same patients. Note the similar biodistribution and the clearer visualisation of the tumour sites, except in the patient with papillary thyroid carcinoma

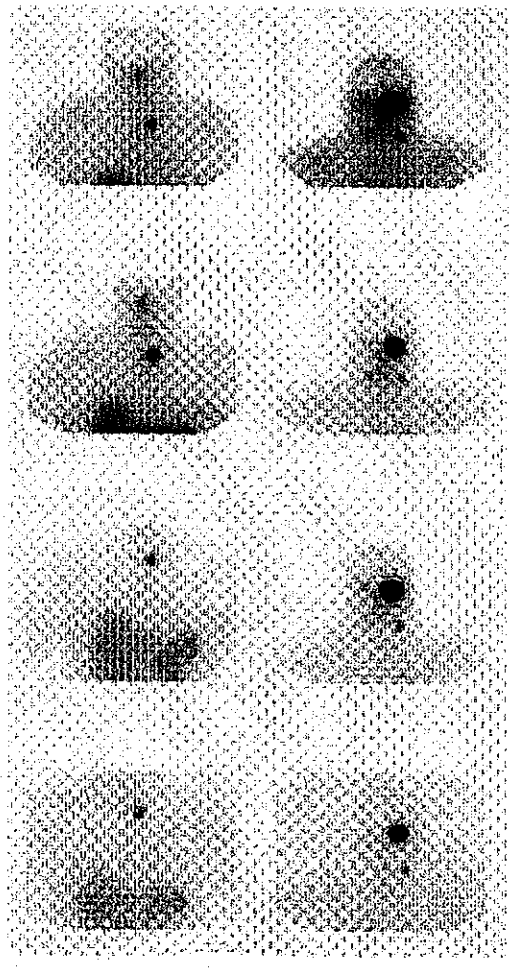

Fig. 4. Images after 4 h and 1, 3 and 17 days (*top row to lower row*) in patients with Hürthle cell carcinoma (*left column*) and aesthesioneuroblastoma (*right column*). Note the retention of radioactivity in the tumour sites

of ^{177}Lu-octreotate or up to 20 min thereafter. The distribution pattern of ^{177}Lu-octreotate was comparable to that of ^{111}In-octreotide, with rapid visualisation of the kidneys directly after injection, and with visualisation of the liver, spleen, kidneys and, in some patients, the pituitary, thyroid and tumours 4 h p.i.

Plasma radioactivity after ^{177}Lu-octreotate expressed as a percentage of the injected dose was slightly, but significantly lower compared with ^{111}In-octreotide measurements from a previous study [12]. After 24 h, however, they were comparable (Fig. 1).

HPLC analysis of plasma, taken at 1 h p.i. in two patients, demonstrated the same pattern as the original injection fluid (data not shown).

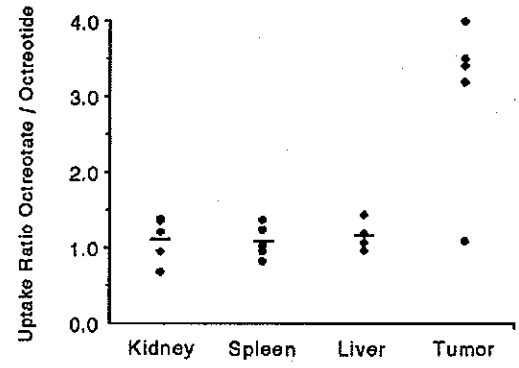

Fig. 5. Ratios of ^{177}Lu-octreotate to ^{111}In-octreotide uptake in organs and tumour sites, with uptake expressed as a percentage of the administered dose. Means are indicated. There is comparable organ uptake and higher tumour uptake after ^{177}Lu-octreotate in most tumours

Table 1. Patient organ doses in cGy (rad)/3,700 MBq (100 mCi)

Patient	Kidneys		Liver	Spleen	Bone marrow
	Without AA	With AA			
1	825	403	90	803	26
2	533	–	76	1,010	29
3	692	282	112	770	27
4	359	252	44	662	27
5	648	366	75	740	20
Mean	611	326	79	797	26

With AA: Kidney dose after amino acid co-infusion

Urinary excretion of radioactivity in the first 24 h after the injection of ^{177}Lu-octreotate is shown in Fig. 2. In comparison with ^{111}In-octreotide, the urinary excretion was significantly lower after ^{177}Lu-octreotate, averaging 64% after 24 h. Peptide-bound radioactivity in urine collected after 1 h in one patient showed the same pattern as the original injection fluid (data not shown).

The scans obtained 24 h p.i. showed the same biodistribution for ^{177}Lu-octreotate and ^{111}In-octreotide, with comparable uptake in the liver, spleen and kidneys (Fig. 3). Also, variable radioactivity was seen in the bowel and urinary bladder. The uptake in the tumours seemed higher after ^{177}Lu-octreotate, except in the patient who had papillary thyroid carcinoma (Fig. 3). At later time points, there was retention of the radioactivity in the tumours, even 17 days p.i. (Fig. 4). The calculated, background-corrected, uptake 24 h after ^{177}Lu-octreotate expressed as a percentage of the injected dose was comparable to that after ^{111}In-octreotide for kidneys, spleen and liver, but was three- to fourfold higher for four of the five tumours (Fig. 5). In the patient with papillary thyroid carcinoma, this uptake was about the same after both radiopharmaceuticals.

Table 2. Dose estimates for ^{177}Lu-octreotate, ^{111}In-octreotide and ^{90}Y-DOTA-octreotide

Target organ	Absorbed dose [cGy (rad)/3,700 MBq (100 mCi)][a]							
	^{177}Lu-octreotate	^{111}In-octreotide			^{90}Y-DOTA-octreotide			
		(1)	(2)	(3)	(4)	(5)	(6)	(7)
Kidneys[b]	610 (325)	170	190	340	2,240	1,220	1,040 (780)	(788)
Liver	80	30	25	90	100	260	120	–
Spleen	800	120	130	320	1,980	2,820	–	–
Bone marrow	26	7	11	23	–	11	26	–
Maximum cumulative dose (GBq)[c]	26.4	50.0	44.8	25.0			10.9	10.8
Maximum cumulative dose (mCi)[c]	710	1,350	1,210	680			290	290

[a] Dosimetry data reported by: (1) Krenning et al. [13]; (2) Stabin et al. [14]; (3) McCarthy et al. [15]; (4) Kwekkeboom et al. [12] (dosimetry based on [^{111}In-DOTA^0,Tyr^3]octreotide); (5) Cremonesi et al. [16] (dosimetry based on [^{111}In-DOTA^0,Tyr^3]octreotide); (6) Rosch et al. [17] (dosimetry based on [^{86}Y-DOTA^0, Tyr^3]octreotide PET studies in primates); (7) Barone et al. [18] (dosimetry based on [^{86}Y-DOTA^0,Tyr^3]octreotide PET studies in patients)

[b] Kidney doses after amino acid co-infusion are shown within parentheses

[c] Mean maximum cumulative dose based on the maximum dose to the kidneys of 23 Gy. Values for ^{177}Lu-octreotate and ^{90}Y-DOTA-octreotide are with amino acid co-infusion

Table 3. Theoretical maximum delivered tumour doses for three different radiolabelled somatostatin analogues

	Absorbed dose (Gy)		
	^{111}In-octreotide	^{90}Y-DOTA-octreotide	^{177}Lu-octreotate
Tumour 1 g	344	563	1,001
Tumour 10 g	36	69	102
Tumour uptake	0.1%	0.2%	0.4%
Maximum cumulative dose [mCi (GBq)]	1,350 (50.0)	290 (10.9)	710 (26.4)

Maximum cumulative doses are derived from Table 2. The calculations take into account the fact that the tumour uptake of [^{90}Y-DOTA,Tyr^3]octreotide is about two times higher [18], and that of ^{177}Lu-octreotate about four times higher, (present study) than the tumour uptake of ^{111}In-octreotide

Dosimetry data are listed in Table 1. The highest absorbed doses were to spleen and kidneys. In five patients, scintigraphy was repeated several weeks later, after co-infusion of amino acids (lysine 2.5%, arginine 2.5%; 250 ml/h for 4 h, starting 30 min before the administration of ^{177}Lu-octreotate). Calculated doses to the liver, spleen, bone marrow and tumours were about the same, whereas the doses to the kidneys were reduced by a mean of 47% (range 34%–59%) (Table 1).

The dose estimates after ^{177}Lu-octreotate are compared with those after ^{111}In-octreotide and [^{90}Y-DOTA,Tyr^3]octreotide in Table 2. Compared with [^{90}Y-DOTA,Tyr^3]octreotide, the dose to the spleen and kidneys was lower after ^{177}Lu-octreotate, whereas the dose to the bone marrow was comparable or higher, depending on the model that was used. Theoretical maximum tumour doses for ^{111}In-octreotide, [^{90}Y-DOTA,Tyr^3]octreotide, and ^{177}Lu-octreotate, based on a maximum kidney dose of 23 Gy, are listed in Table 3. The highest tumour doses in this model are achieved with ^{177}Lu-octreotate, especially in smaller tumours.

Discussion

The somatostatin analogue Tyr^3-octreotate, whether chelated with DTPA or DOTA, has been demonstrated to have a higher affinity than Tyr^3-octreotide for the most frequently encountered somatostatin receptor, subtype 2, both in vitro and in vivo in animal experiments [8, 9, 10]. Because the total administered therapeutic dose with radiolabelled somatostatin analogues is determined by organ dose limits, any newly developed analogues that show either a lower uptake in the dose-limiting organs (kidneys and/or bone marrow) or a higher uptake in the tumour targets, may improve such therapy. For this reason, we compared the distribution pattern and dosimetry of ^{177}Lu-octreotate with those of ^{111}In-octreotide in patients. We found the same biodistribution for the analogues on scintigrams 24 h p.i., with comparable percentage uptake in the liver, spleen and kidneys. The tumour uptake, however, was three- to fourfold higher in four of the five studied patients, implying that potentially higher doses to the tumour can be achieved with about

equal dose-limiting organ doses. The comparability of the percentage uptake in the liver and kidneys for the two analogues is most likely due to the fact that the uptake in these organs is for the most part not receptor mediated and is accounted for by excretion of the radiopharmaceutical. Our finding that the uptake in the spleen was comparable for the two analogues may indicate that a considerable part of this uptake is due to binding to a somatostatin receptor subtype other than subtype 2. Somatostatin receptor subtype 2 has been demonstrated in the red pulp of the spleen by autoradiography [19]; however, with reverse transcriptase polymerase chain reaction (RT-PCR) techniques, mRNA for receptor subtype 3 has also been demonstrated, located in the white pulp and with a much lower expression than for subtype 2 [20]. It is therefore puzzling why the scintigraphic uptake in the spleen after ^{177}Lu-octreotate is not much higher than after ^{111}In-octreotide. The presence of other somatostatin receptor subtypes may explain why, in our patient with papillary thyroid carcinoma, uptake was not higher with ^{177}Lu-octreotate than with ^{111}In-octreotide. This is in agreement with an in vitro study using RT-PCR on human thyroid carcinoma cell lines, which demonstrated a predominance of mRNA for somatostatin receptor subtypes 3 and 5, but only very low amounts of mRNA for subtype 2 [21].

We found a comparable, but slightly faster plasma disappearance for ^{177}Lu-octreotate than for ^{111}In-octreotide. More importantly, the cumulative urinary excretion after 24 h was significantly lower for ^{177}Lu-octreotate than for ^{111}In-octreotide. In another study [12], we found that the cumulative urinary excretion of [^{111}In-DOTA^0,Tyr^3]octreotide was also significantly lower than that of [^{111}In-DTPA^0]octreotide. Because this analogue has the tyrosine insertion in common with [^{177}Lu-DOTA^0,Tyr^3]octreotate, this may be the cause of the lower urinary excretion. This lower urinary excretion of ^{177}Lu-octreotate results in a significantly higher absorbed bone marrow dose, because this dose is determined by the whole-body retention (i.e. injected minus excreted radioactivity minus activity in major target organs). Because of this, both the radiation dose to the kidneys and that to the bone marrow may be dose limiting in patient therapy with ^{177}Lu-octreotate. It has previously been demonstrated that the percentage uptake by and the radiation dose to the kidneys from ^{111}In-octreotide can be lowered by the infusion of amino acids, both in animals and in patients [22, 23]. In our group of patients, we found that this is also true for ^{177}Lu-octreotate. This finding is important because applying a dose limit to the kidneys of 23 Gy, as is also applied for external beam radiation therapy, 14.0 GBq (380 mCi) would be the mean cumulative dose limit, whereas with the reduction due to amino acid infusion this limit would be 26.4 GBq (710 mCi). Barone et al. [18] compared the uptake after ^{111}In-octreotide and after [^{86}Y-DOTA^0,Tyr^3]octreotide in the tumours and kidneys of five patients. They found that the percentage uptake in tumours was about two times higher after [^{86}Y-DOTA^0,Tyr^3]octreotide, whereas it was about 1.4 times higher in the kidneys. Applying a dose limit of 23 Gy to the kidneys and accounting for amino acid co-infusion, the maximum cumulative dose of [^{90}Y-DOTA^0,Tyr^3]octreotide would be 10.8 GBq (290 mCi) (Table 2). Using ^{177}Lu-octreotate, the mean maximum cumulative dose that can be administered is 26.4 GBq (710 mCi) (Table 2). Apart from the more than double mean maximum cumulative dose that can be administered using ^{177}Lu-octreotate instead of [^{90}Y-DOTA^0,Tyr^3]octreotide, it should be considered that in this study we found a three- to fourfold higher tumour uptake with ^{177}Lu-octreotate than with ^{111}In-octreotide, whereas with [^{86}Y-DOTA^0,Tyr^3]octreotide the tumour uptake was reported to be about twofold that of ^{111}In-octreotide [18]. In a model calculation, based on the maximum cumulative dose that can be given, the tumour doses that can be achieved with ^{177}Lu-octreotate were higher than those for ^{111}In-octreotide or [^{90}Y-DOTA^0,Tyr^3]octreotide.

There are four reasons why we used ^{177}Lu and not ^{90}Y as the radionuclide to label [DOTA^0,Tyr^3]octreotate:

1. ^{177}Lu-octreotate has been reported to have a very favourable impact on tumour regression in a rat model [9].
2. Reubi et al. [10] reported comparable affinities in the low nanomolar range for non-radioactive In and Y complexed [DOTA^0,Tyr^3]octreotate, implying that the modification in the peptide, and not the change in the metal, is primarily responsible for the improved affinity.
3. With the ^{177}Lu-labelled analogue it is possible to perform dosimetry and therapy with the same compound while no PET scans with short-lived radionuclides are needed.
4. The tissue penetration range of ^{177}Lu (maximum range ≈2 mm) is more favourable than that of ^{90}Y (maximum range ≈12 mm), especially for smaller tumours from which much of the radiation dose of ^{90}Y will be lost to the surrounding tissues.

Because of the advantages that both the modified somatostatin analogue and the different radionuclide offer, we think that ^{177}Lu-octreotate represents an improvement in somatostatin receptor-mediated radiotherapy. Indeed, we have already observed improvements in complaints, decreases in serum tumour markers and CT-assessed tumour shrinkage in patients who are being treated with this new compound, although none of these patients has yet received the maximum cumulative dose.

In conclusion: In comparison with the radionuclide-coupled somatostatin analogues that are currently available for somatostatin receptor-mediated radiotherapy, ^{177}Lu-octreotate potentially represents an important improvement because of the higher absorbed doses that can be achieved to most tumours and because of the more fa-

vourable tissue penetration range, which may be especially important for small tumours.

Acknowledgements. The authors want to thank all the co-workers of the technical staff of the Department of Nuclear Medicine for their expert cooperation.

References

1. Krenning EP, Valkema R, Kooij PP, Breeman WA, Bakker WH, de Herder WW, van Eijck CH, Kwekkeboom DJ, de Jong M, Jamar F, Pauwels S. The role of radioactive somatostatin and its analogues in the control of tumor growth. *Recent Results Cancer Res* 2000; 153:1–13.
2. McCarthy KE, Woltering EA, Espenan GD, Cronin M, Maloney TJ, Anthony LB. In situ radiotherapy with ^{111}In-pentetreotide: initial observations and future directions. *Cancer J Sci Am* 1998; 4:94–102.
3. Caplin ME, Mielcarek W, Buscombe JR, Jones AL Croasdale PL, Cooper MS, Burroughs AK, Hilson AW. Toxicity of high-activity ^{111}In-octreotide therapy in patients with disseminated neuroendocrine tumours. *Nucl Med Commun* 2000; 21:97–102.
4. Meyers MO, Anthony LB, McCarthy KE, Drouant G, Maloney TJ, Espanan GD, Woltering EA. High-dose indium ^{111}In pentetreotide radiotherapy for metastatic atypical carcinoid tumor. *South Med J* 2000; 93:809–811.
5. Otte A, Herrmann R, Heppeler A, Behe M, Jermann E, Powell P, Maecke HR, Muller J. Yttrium-90 DOTATOC: first clinical results. *Eur J Nucl Med* 1999; 26:1439–1447.
6. Valkema R, Jamar F, Jonard P, Bakker WH, Norenberg J, Hadley J, Smith C, Kvols L, Pauwels S, Krenning EP. Targeted radiotherapy with ^{90}Y-DOTA-Tyr(3)-octreotide (^{90}Y-SMT487; OctreoTher): a phase I study. *J Nucl Med* 2000; 41:111P.
7. Paganelli G, Zoboli S, Cremonesi M, Macke HR, Chinol M. Receptor-mediated radionuclide therapy with ^{90}Y-DOTA-D-Phe1-Tyr3-octreotide: preliminary report in cancer patients. *Cancer Biother Radiopharm* 1999; 14:477–483.
8. de Jong M, Breeman WA, Bakker WH, Kooij PP, Bernard BF, Hofland LJ, Visser TJ, Srinivasan A, Schmidt MA, Erion JL, Bugaj JE, Macke HR, Krenning EP. Comparison of ^{111}In-labeled somatostatin analogues for tumor scintigraphy and radionuclide therapy. *Cancer Res* 1998; 58:437–441.
9. Erion JL, Bugaj JE, Schmidt MA, Wilhelm RR, Srinivasan A. High radiotherapeutic efficacy of [Lu-177]-DOTA-Y(3)-octreotate in a rat tumor model. *J Nucl Med* 1999; 40:223P.
10. Reubi JC, Schar JC, Waser B, Wenger S, Heppeler A, Schmitt JS, Macke HR. Affinity profiles for human somatostatin receptor subtypes SST1–SST5 of somatostatin radiotracers selected for scintigraphic and radiotherapeutic use. *Eur J Nucl Med* 2000; 27:273–282.
11. Bakker WH, Krenning EP, Breeman WAP, et al. In vivo use of a radioiodinated somatostatin analogue: Dynamics, metabolism, and binding to somatostatin receptor-positive tumors in man. *J Nucl Med* 1991; 32:1184–1189.
12. Kwekkeboom DJ, Kooij PPM, Bakker WH, Mäcke HR, Krenning EP. Comparison of indium-111-DOTA-octreotide and indium-111-DTPA-octreotide in the same patients: biodistribution, kinetics, organ and tumor uptake. *J Nucl Med* 1999; 40:762–767.
13. Krenning EP, Bakker WH, Kooij PPM, Breeman WAP, Oei HY, De Jong M, Reubi JC, Visser TJ, Kwekkeboom DJ, Reijs AEM, Van Hagen PM, Koper JW, Lamberts SWJ. Somatostatin receptor scintigraphy with [^{111}In-DTPA-D-Phe^1]-octreotide in man: metabolism, dosimetry and comparison with [^{123}I-Tyr^3]-octreotide. *J Nucl Med* 1992; 33:652–658.
14. Stabin MG, Kooij PPM, Bakker WH, Inoue T, Endo K, Coveney J, de Jong R, Minegishi A. Radiation dosimetry for indium-111-pentetreotide. *J Nucl Med* 1997; 38:1919–1922.
15. McCarthy KE, Woltering EA, Anthony LB. In situ radiotherapy with ^{111}In-pentetreotide. *Q J Nucl Med* 2000; 44:88–95.
16. Cremonesi M, Ferrari M, Zoboli S, Chinol M, Stabin MG, Orsi F, Maecke HR, Jermann E, Robertson C, Fiorenza M, Tosi G, Paganelli G. Biokinetics and dosimetry in patients administered with ^{111}In-DOTA-Tyr(3)-octreotide: implications for internal radiotherapy with ^{90}Y-DOTATOC. *Eur J Nucl Med* 1999; 26:877–886.
17. Rosch F, Herzog H, Stolz B, Brockmann J, Kohle M, Muhlensiepen H, Marbach P, Muller-Gartner HW. Uptake kinetics of the somatostatin receptor ligand [^{86}Y]DOTA-D-Phe1-Tyr3-octreotide ([^{86}Y]SMT487) using positron emission tomography in non-human primates and calculation of radiation doses of the ^{90}Y-labelled analogue. *Eur J Nucl Med* 1999; 26:358–366.
18. Barone R, Jamar F, Walrand S, Labar D, Carlier P, Smith C, Kvols L, Krenning EP, Pauwels S. Can ^{111}In-DTPA-octreotide (In-Oc) predict kidney and tumor exposure during treatment with ^{90}Y-SMT487 (Octreother)? *J Nucl Med* 2000; 41:110P.
19. Reubi JC, Horisberger U, Kappeler A, Laissue JA. Localization of receptors for vasoactive intestinal peptide, somatostatin, and substance P in distinct compartments of human lymphoid organs. *Blood* 1998; 92:191–197.
20. Ferone D, Pivonello R, van Hagen PM, Lichtenauer-Kaligis EGR, Zuijderwijk J, de Krijger RR, Colao A, Hofland LJ, Lamberts SWJ. Immunohistochemical localization and quantitative expression of somatostatin receptors in normal human spleen and thymus [abstract]. 5th European Congess of Endocrinology, Turin, Italy, 2001.
21. Ain KB, Taylor KD, Tofiq S, Venkataraman G. Somatostatin receptor subtype expression in human thyroid and thyroid carcinoma cell lines. *J Clin Endocrinol Metab* 1997; 82:1857–1862.
22. de Jong M, Rolleman EJ, Bernard BF, Visser TJ Bakker WH, Breeman WA, Krenning EP. Inhibition of renal uptake of indium-111-DTPA-octreotide in vivo. *J Nucl Med* 1996; 37:1388–1392.
23. Hammond PJ, Wade AF, Gwilliam ME, Peters AM Myers MJ, Gilbey SG, Bloom SR, Calam J. Amino acid infusion blocks renal tubular uptake of an indium-labelled somatostatin analogue. *Br J Cancer* 1993; 67:1437–1439.

Appendix III

SYNTHESIS, IN VITRO RECEPTOR BINDING AND IN VIVO EVALUATION OF FLUORESCEINE AND CARBOCYANINE PEPTIDE-BASED OPTICAL CONTRAST AGENTS

Journal of Medicinal Chemistry, 9, 2003-2015 (2001)

Synthesis, In Vitro Receptor Binding, and In Vivo Evaluation of Fluorescein and Carbocyanine Peptide-Based Optical Contrast Agents

Samuel Achilefu,*,† Hermo N. Jimenez,‡ Richard B. Dorshow,‡ Joseph E. Bugaj,‡ Elizabeth G. Webb,‡ R. Randy Wilhelm,‡ Raghavan Rajagopalan,‡ Jill Johler,‡ and Jack L. Erion‡

Mallinckrodt Institute of Radiology, Washington University School of Medicine, 4525 Scott Avenue, St. Louis, Missouri 63110, and Mallinckrodt Inc., 675 McDonnell Boulevard, St. Louis, Missouri 63042

Received November 8, 2001

Site-specific delivery of drugs and contrast agents to tumors protects normal tissues from the cytotoxic effects of drugs and enhances the contrast between normal and pathologic tissues. One approach to achieve selectivity is to target overexpressed receptors on the membranes of tumor cells and to visualize the tumors by a noninvasive optical imaging method. Accordingly, we conjugated fluorescein and carbocyanine dyes to somatostatin and bombesin receptor-avid peptides and examined their receptor binding affinities. We also prepared potential dual imaging probes consisting of a bioactive peptide for tumor targeting, a biocompatible dye for optical imaging, and a radioactive or paramagnetic metal chelator for scintigraphic or magnetic resonance imaging of tumors. Using these approaches, the resulting carbocyanine derivatives of somatostatin and bombesin analogues retained high binding for their respective receptors. Further evaluation of representative molecules in rats bearing somatostatin- and bombesin-positive tumors showed selective uptake of the agents by the tumor cells. Unlike carbocyanine derivatives, the receptor binding of fluorescein–somatostatin peptide conjugates was highly sensitive to the type of linker and the site of fluorescein attachment on the nonreceptor binding region of the peptide. In general, the presence of flexible linkers disrupted binding affinity, possibly due to the interaction of the linker's thiourea group with the peptide's cyclic disulfide bond. While the receptor binding affinity of the dual probes was not dependent on the type of chelating group examined, it was affected by the relative positions of fluorescein and chelator on the lysine linker. For somatostatin compounds, best results were obtained when the chelator was on the α-amino lysine linker and fluorescein was on the ϵ-amino group. In contrast, conjugation of the chelator to ϵ- and fluorescein to the α-amino lysine linker of bombesin peptides resulted in high receptor binding. These findings indicate that despite their small size, conjugation of dyes to truncated somatostatin and bombesin peptide analogues results in promising diagnostic agents that retain high receptor binding activity in vitro. The results further show that these contrast agents can selectively and specifically localize in receptor-positive tumors in rat models.

Introduction

Biomedical optical imaging is an emerging diagnostic method that uses propagating light to activate chromophores in tissues and a detector to capture the transmitted or reflected photons.[1,2] It provides distinctly new diagnostic capabilities while complementing conventional imaging modalities.[3–7] Previous studies have demonstrated the feasibility of using endogenous contrast effectors such as the ratio of oxy- and deoxyhemoglobin to detect pathologic tissues by optical imaging and spectroscopy in the visible and near-infrared (NIR) wavelengths.[1,8] This approach represents a viable, noninvasive method to monitor various diseased states, quantify pathologically relevant physiologic functions, and localize cancer. However, delineation of the spectral differences between normal and pathologic tissues based on endogenous contrast, especially at the early stages of cancer, remains difficult despite the availability of sophisticated image reconstruction algorithms.[9–15] For this reason, several studies are currently focusing on the use of exogenous optical contrast agents to improve image resolution by increasing the signal-to-noise ratio. Unlike endogenous contrast effectors, these compounds are less dependent on inter- and intraspecies variations and can furnish unique information regarding the functional status of tissues. These agents also promote rapid selective localization, improve specificity and sensitivity, and provide important histopathological information such as cell viability.

The utility of contrast agents in diagnostic procedures depends on the preferential accumulation of the molecules in target tissues. One approach to achieve this selectivity in oncology takes advantage of the overexpression of specific receptors on certain tumor cells to target various diagnostic agents to tumors.[16] Hence, a useful strategy involves conjugating a contrast agent to carriers that target the overexpressed tumor receptors to enhance specificity, as demonstrated with fluorescein– and carbocyanine–antibody conjugates.[17–24] Beside antibodies, dye conjugation to other large targeting molecules, which are occasionally coupled by secondary activation mechanisms, also enhances site-

* To whom correspondence should be addressed. Tel.: 314-362-8599. Fax: 314-747-5191. E-mail: achilefus@mir.wustl.edu.
† Washington University School of Medicine.
‡ Mallinckrodt Inc.

specific delivery of the agents.[25,26] However, targeting of tumor receptors with antibodies or large biomolecules is hampered by many factors, including low diffusion rates into tumors, rapid uptake by the liver, and the potential to elicit adverse immunogenic reactions.

On the basis of previous findings that somatostatin and bombesin receptors are up-regulated on many tumor cell membranes and that truncated peptide analogues of the native ligands effectively target these receptors, we recently demonstrated for the first time that this approach is applicable to optical imaging of tumors.[27] The bioconjugates selectively localized in somatostatin-positive tumors without loss of the probe's photophysical properties. More recently, other studies have supported this finding.[28,29] Some advantages of the peptide-based approach include enhanced localization in tumors, rapid clearance from nontarget tissues, ease of structure–activity relationship studies, and the possibility of preparing a combinatorial library of peptides for rapid identification of bioactive molecules.

Earlier reports in nuclear medicine have demonstrated that in vitro receptor binding studies with somatostatin and bombesin peptide analogues correlate with in vivo findings.[30–35] As progress in the design of novel receptor-based optical contrast agents continues, the need exists for rapid screening of these compounds by quantifying their receptor binding affinity. Accordingly, we report here the preparation and biological evaluation of novel, peptide-based receptor-specific optical contrast agents that absorb and emit radiation in the visible (fluorescein derivatives) and the NIR (carbocyanine derivatives) regions. Both fluorescein and carbocyanine dye-labeled biomolecules are widely used in optical imaging studies. Because of the rapid attenuation of light by endogenous chromophores in the visible wavelength (400–700 nm), the fluorescein derivatives are useful for imaging superficial lesions, endoscopy-accessible deep tissues, surgically exposed tissues, and delicate organs such as the prostate, where rapid attenuation of light prevents damage to sensitive organ parenchymal cells. At the NIR region between 700 and 900 nm, the low light scattering and absorption by endogenous photoactive biomolecules permit photons to penetrate several centimeters into tissue. Thus, the carbocyanine dye derivatives are particularly useful for detecting and diagnosing pathologic conditions in deep tissues.

Furthermore, optical imaging is an emerging diagnostic method and its acceptance in clinical practice requires validation of the images obtained with established imaging modalities such as scintigraphy and magnetic resonance imaging (MRI).[6,36–38] One approach to validating optical imaging involves the coregistration of the target tissue with a second modality using the same exogenous contrast molecule. To this effect, we synthesized and evaluated novel dual imaging probes comprising a receptor-avid peptide for tumor targeting, fluorescein for optical imaging, and a radioactive or paramagnetic metal chelator for scintigraphy or MRI, respectively. This method would obviate the need to administer two or more different compounds that may complicate the coregistration due to differences in the individual drug's pharmacokinetics.

Chemistry

Fluorescein Isothiocyanate (FITC) Derivatives. We prepared four groups of fluorescein-labeled peptides as shown in Tables 1–4. Previous studies have demonstrated that the truncated somatostatin and bombesin octapeptides **2** and **13** exhibit high binding to their appropriate receptors.[32,39] Consequently, we retained the basic structural framework of these peptides in all somatostatin and bombesin derivatives prepared. The peptides were synthesized on solid support by standard automated fluorenylmethyloxycarbonyl (Fmoc) solid phase synthesis.[40] Subsequent conjugation of commercially available FITC with the peptides was performed either on solid support or by solution phase synthesis, depending on the nature of the peptide.

Fluorescein derivatives of peptides devoid of multiple FITC-reactive functional groups, such as **17**, are readily prepared by solution phase reaction, while those possessing more than one FITC-reactive site on cleavage from the resin, such as **3**, are best prepared on solid phase before removing all side chain protecting groups. However, reaction of FITC with **2** to form **3** on solid support was slow and gave poor yields (<5%) of the desired isolated compound. We also observed a similar trend for all of the peptides possessing N-terminal aromatic amino acid units, and this low yield could be attributed to steric factors. Hence, we investigated the traditional solution phase reaction for the conjugation of FITC to the somatostatin peptide analogues. Initially, we prepared the octapeptide (**2**) on trityl resins, which permits cleavage of the peptide from the solid support with mild acids that leave all side chain protecting groups intact. Selective removal of the N-terminal Fmoc protecting group, followed by base-catalyzed coupling of FITC in solution, did not give the desired compound after high-performance liquid chromatography (HPLC) separation of the crude mixture. It is possible that the bulky side chain protecting groups hinder the reaction of FITC with amines under this reaction condition. Because the reactivity of FITC favors primary amines, we overcame this problem by removing all side chain protecting groups, except the K^5 ϵ-amino group that is critical for maintaining the peptide's receptor binding activity. The orthogonal protecting group was removed after conjugation of fluorescein to the N-terminal amino group (Scheme 1). This approach consistently gave the desired compounds shown in Table 1. However, we observed that the introduction of hydrophilic and lipophilic spacers to the nonreceptor binding N-terminal end of the somatostatin peptide enhanced the conjugation of FITC to the peptide on solid support.

Synthesis of the fluorescein derivatives of bombesin peptide analogues was readily accomplished by solution phase reaction since the receptor binding moiety does not contain multiple FITC-reactive functions (Table 3). Selective attachment of FITC to the α- or ϵ-amino group of lysine was accomplished by orthogonal protection of the amines with either Fmoc or 1-(4,4-dimethyl-2,6-dioxocyclohexylidene)-3-methylbutyl) (ivDde) group. Typically, the amino group for FITC attachment is protected as Fmoc to enable automatic deprotection of the amino group by standard peptide synthesis protocol. For the synthesis of homogeneous dual optical probes (**20** and **24**), both amino functions of lysine were protected with

Scheme 1

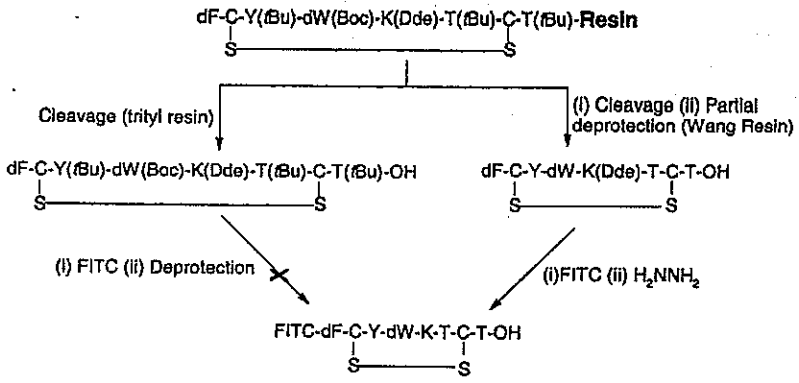

Table 1. Somatostatin Analogues and Fluorescein Derivatives

Compd	Condensed Structure[a]	IC_{50} (nM)	SE ± (nM)
1	dF-C-Y-dW-K-T-C-T-ol	0.4	0.07
2	dF-C-Y-dW-K-T-C-T-OH	0.6	0.10
3	FITC-dF-C-Y-dW-K-T-C-T-OH	9.9	2.1
4	FITC-βA-dF-C-Y-dW-K-T-C-T-OH	>1.000	NA[b]
5	FITC-G-S-G-dF-C-Y-dW-K-T-C-T-OH	285.2	NA
6	α-FITC-K-dF-C-Y-dW-K-T-C-T-OH	6.4	1.3
7	ε-FITC-K-dF-C-Y-dW-K-T-C-T-OH	187.8	NA

[a] FITC, fluorescein thiourea group; T-ol, threoninol; T-OH, threonine. [b] NA, not applicable because our assay was limited to 100 nM of the competing ligand and the stated IC_{50} value was obtained by extrapolating the data from a four parameter curve-fitting program.

Table 2. Somatostatin Analogues for Multimodality Imaging

Compd	Condensed Structure[a]	IC_{50} (nM)	SB ± (nM)
8	DTPA-dF-C-Y-dW-K-T-C-T-OH	1.9	0.2
9	(α-DTPA-ε-FITC)-K-dF-C-Y-dW-K-T-C-T-OH	10.3	1.8
10	(α-FITC-ε-DTPA)-K-dF-C-Y-dW-K-T-C-T-OH	71.3	NA
11	(α-DOTA-ε-FITC)-K-dF-C-Y-dW-K-T-C-T-OH	10.3	2.1

[a] FITC, fluorescein thiourea group.

identical groups (usually Fmoc) during peptide synthesis. Expectedly, solid and solution phase reactions of FITC with **14** and **16** gave a mixture of the bis-fluorescein derivatives (**20** and **24**) and the corresponding α- and ε-amino lysine mono-FITC analogues. Fortunately, the differences in the retention time of each compound on HPLC are sufficient to facilitate their isolation with ease. While the mono- and bis-FITC derivatives are readily distinguishable by mass spectrometry, the isomeric monoderivatives were identified by spiking each fraction of the isolated compounds with authentic samples prepared by the orthogonal protection procedure described above. Because of the simplicity of this reaction procedure and the ease of isolating each component of the reaction product, we also used this one pot synthesis approach for the preparation of all three (α-, ε-, and bis-fluorescein) derivatives.

The tandem receptor-specific dye–chelator probes prepared for potential dual optical and scintigraphic or MRI are shown in Tables 2 and 4. The availability of chelator precursors that are compatible with solid phase synthesis[41] allowed us to prepare the diethylenetriaminepentaacetic acid (DTPA) and cyclododecane-1,4,7,-10-tetraazaacetic acid (DOTA) derivatives on solid support. Thus, in all cases, we coupled orthogonally protected tri-*tert*-butyl DTPA or tri-*tert*-butyl DOTA to an α- or ε-amino group of lysine by the same automated solid phase synthesis procedure used to prepare the peptides.[41] Although direct coupling of FITC to the chelator–peptide derivatives on solid support was not successful, good results were obtained by solution phase reactions. For the somatostatin tandem probes (Table 2), the K^6 ε-amino group was protected with ivDde, the α- or ε-amino function of K^1 for coupling the chelator was protected with Fmoc, and the remaining K^1 amino group for FITC attachment was protected with a *tert*-butyloxycarbonyl (Boc) group. Cleavage of the chelator–peptide derivative from the resin also removes the Boc protection, and reaction of FITC with this free amine, followed by removal of the ivDde group, gave the desired compounds **9**–**11**. Because the bombesin peptide analogues in Table 4 lack multiple FITC-reactive groups, the synthesis of compounds **29**–**31** involves concomitant cleavage of the peptide from the resin and removal of all side chain protecting groups, followed by coupling of FITC to the peptide.

Carbocyanine Derivatives. The receptor-specific carbocyanine derivatives prepared for this study absorb and fluoresce in the NIR region and are thus useful for deep tissue imaging. Scheme 2 summarizes the procedure employed to prepare the NIR optical probes shown in Table 5. Synthesis of the carbocyanine dyes has been described elsewhere.[27,29] All other reactions, including

Table 3. Bombesin Analogues and Fluorescein Derivatives

compd	condensed structure[a]	IC_{50} (nM)	SE ± (nM)
12	pQ-Q-R-Y-G-N-Q-W-A-V-G-H-L-M-NH_2	1.1	0.2
13	Q-W-A-V-G-H-L-M-NH_2	28.3	3.7
14	K-Q-W-A-V-G-H-L-M-NH_2	10.5	3.8
15	G-S-G-Q-W-A-V-G-H-L-M-NH_2	7.6	1.3
16	K-G-S-G-Q-W-A-V-G-H-L-M-NH_2	4.8	0.6
17	FITC-Q-W-A-V-G-H-L-M-NH_2	3.2	0.4
18	α-FITC-K-Q-W-A-V-G-H-L-M-NH_2	5.8	1.4
19	ϵ-FITC-K-Q-W-A-V-G-H-L-M-NH_2	5.7	1.5
20	α,ϵ-$(FITC)_2$-K-Q-W-A-V-G-H-L-M-NH_2	9.5	1.8
21	FITC-G-S-G-Q-W-A-V-G-H-L-M-NH_2	9.2	0.3
22	α-FITC-K- G-S-G-Q-W-A-V-G-H-L-M-NH_2	15.6	4.8
23	ϵ-FITC-K-G-S-G-Q-W-A-V-G-H-L-M-NH_2	9.6	1.7
24	α,ϵ-$(FITC)_2$-K G-S-G-Q-W-A-V-G-H-L-M-NH_2	20.5	2.9

[a] FITC, fluorescein thiourea group; pQ, pyroglutamic acid.

Table 4. Bombesin Analogues for Multimodality Imaging

compd	condensed structure[a]	IC_{50} (nM)	SE ± (nM)
25	DTPA-P-Q-R-Y-G-N-Q-W-A-V-G-H-L-M-NH_2	4.7	0.3
26	α-DTPA-K-Q-W-A-V-G-H-L-M-NH_2	410	NA
27	ϵ-DTPA-K-Q-W-A-V-G-H-L-M-NH_2	4.8	1.1
28	α,ϵ-$(DTPA)_2$-K-Q-W-A-V-G-H-L-M-NH_2	240	NA
29	α-DTPA-ϵ-FITC-K-Q-W-A-V-G-H-L-M-NH_2	276	NA
30	α-FITC-ϵ-DTPA-K-Q-W-A-V-G-H-L-M-NH_2	20	11.7[b]
31	α-FITC-ϵ-DOTA-K-Q-W-A-V-G-H-L-M-NH_2	15	9[b]

[a] FITC, fluorescein thiourea group. [b] The shape of the competitive binding curves for these compounds does not conform to regular inhibition curve form, despite repeated experiments. Receptor binding assay was optimized for IC_{50} values between 1 and 10 nM.

Scheme 2

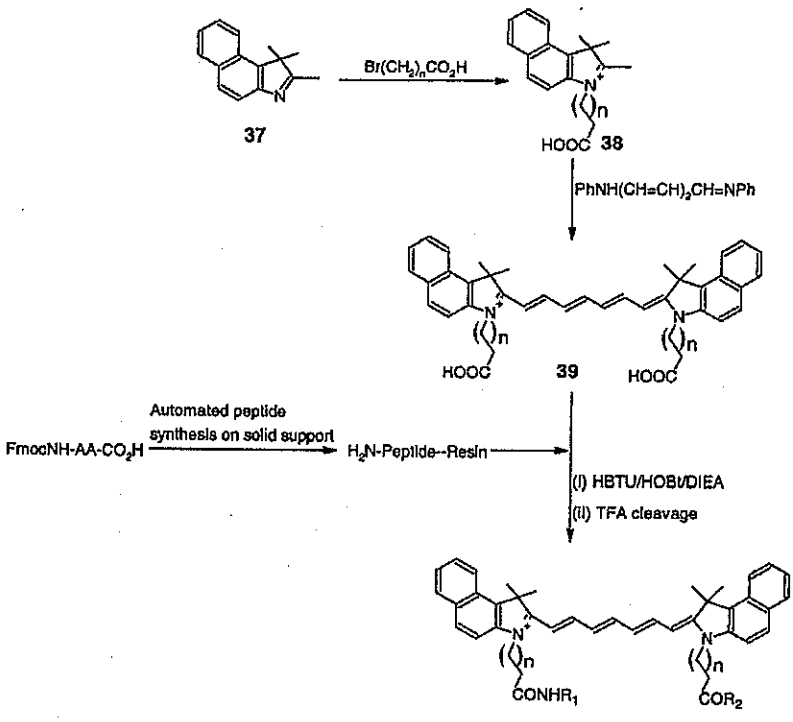

conjugation of the dye to peptides, were carried out on solid support. This approach enabled us to selectively prepare the monopeptide conjugates and a mixture of the mono and the bis-peptide derivatives, depending on the reaction conditions. Activation of carbocyanine bis-propanoic acid (**39**) with 3 equiv of a carboxyl-activating reagent and subsequent condensation to the N terminus amino group of **2** gave predominantly the monooctapeptide conjugate (**32**). A significant amount of the bis-peptide derivative can be prepared by reactivating the

Table 5. Pepde-Carbocyanine NIR Optical Contrast Agents

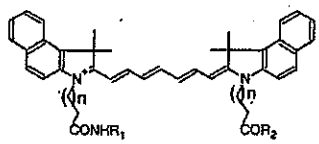

Compd	Receptor	R_1	R_2	n	IC_{50} (nM)	SE ± (nM)
32	Somatostatin	-dF-C-Y-dW-K-T-C-T-OH (S—S)	OH	1	4.6	0.7
33	Somatostatin	-dF-C-Y-dW-K-T-C-T-OH (S—S)	OH	4	5.4	1.0
34	Somatostatin	-dF-C-Y-dW-K-T-C-T-OH (S—S)	NHR_1	4	1.1	0.1
35	Somatostatin	-βA-dF-C-Y-dW-K-T-C-T-OH (S—S)	OH	1	3.4	0.4
36	Bombesin	-Q-S-G-Q-W-A-V-G-H-L-M-NH_2	OH	1	1.8	0.2

free carboxylic acid group of the monopeptide–carbocyanine dye while still on solid support and allowing the reaction to proceed for 24 h in the dark. Elongation of the *N*-alkyl group of the carbocyanine dye from ethyl (**40**, $n = 1$) to pentyl (**40**, $n = 4$) facilitated the preparation of both mono- (**33**) and bis- (**34**) peptide derivatives with 3 equiv of a carboxyl activation reagent. Isolation of these compounds by HPLC was not cumbersome due to the large difference in the elution pattern of the mono- and bis-peptide derivatives, as described in the Experimental Section.

The absorption and emission of fluorescein (λ_{max} 490 nm absorption, 530 nm emission), carbocyanine dye **39** (λ_{max} 795 absorption, 830 emission), and their respective bioconjugates in 25% aqueous dimethyl sulfoxide (DMSO) were practically the same at the submicromolar concentrations examined. At higher concentrations (100 μM), changes in photophysical properties of the dyes arise from molecular aggregation or dimerization.[42]

Biological Results and Discussion

In Vitro Studies. Results of the in vitro binding assays of fluorescein derivatives are shown in Tables 1 and 2 for somatostatin receptor using the rat pancreatic tumor cell line, CA20498, and Tables 3 and 4 for bombesin receptor using the rat pancreatic acinar cell line, AR42-J. Table 5 shows the receptor binding affinity of the carbocyanine derivatives for both somatostatin and bombesin receptors. Both tumor cell lines express somatostatin and bombesin receptors. Established somatostatin or bombesin receptor-avid peptides were used as internal standard for the receptor binding studies. To validate the assay, we assessed the binding of fluorescein disodium salt, indocyanine green, and the carbocyanine dye **39**, all of which are devoid of a receptor-avid peptide component. No binding to receptors was observed in the presence of up to 100 nM concentration of these dyes, and similar results were obtained with scrambled peptides that lack the receptor binding motif (Figure 1). The reliability of the assay protocol was also confirmed by the lack of competitive inhibition of a radiolabeled bombesin receptor-avid tracer by an otherwise somatostatin receptor-avid dye-labeled peptide.

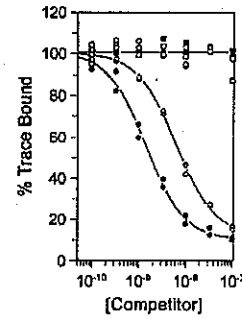

Figure 1. Inhibition of [^{111}In]-DTPA-[Y^4]-bombesin (trace) binding to AR42-J membranes using varying concentrations of control compounds and known competitors. Symbols correspond to the following compounds: ◇, DTPA-[Y4]-bombesin; ●, bombesin; ○, FITC; ■, ICG; □, cypate.

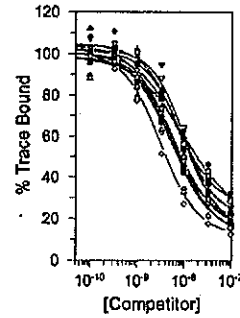

Figure 2. Inhibition of [^{111}In]-DTPA-[Y^4]-bombesin (trace) binding to AR42-J membranes using varying concentrations of the bombesin analogues listed in Table 3. Symbols corresponding to compounds or to number codes given in Table 3 are as follows: ○, DTPA-[Y^4]-bombesin; ●, 14; □, 15; ■, 16; ◇, 17; ◆, 18; △, 19; ▲, 20; ▽, 21; ▼, 22.

After we established the reliability of the binding assays, we evaluated the receptor binding affinity of the novel compounds prepared. Most of the new compounds effectively competed with the receptor binding of the appropriate reference standard (Figures 2 and 3). As shown in Table 1, direct coupling of FITC to the bioactive somatostatin octapeptide **2** to form **3** resulted in a peptide with high receptor affinity, having an IC_{50} in the nanomolar range. We further investigated the effect of linkers at the nonreceptor binding N terminus that could improve the peptide's solubility in a biological medium, modify the in vivo biodistribution, and facilitate the preparation of tandem heterogeneous diagnostic probes for combined optical and scintigraphic or magnetic resonance tumor imaging. Introduction of a nonbulky hydrophobic linker was expected to minimize the renal excretion of **2** and enhance the conjugation of FITC to peptides on solid support. However, coupling of β-alanine to **2** and subsequent conjugation of FITC to obtain **4** drastically reduced the binding affinity (IC_{50} > 1 μM). Compound **5**, which has a hydrophilic linker between FITC and **2**, improved water solubility and receptor binding as compared with **4**, albeit still orders of magnitude lower than **3**. Addition of a lysine linker to **2** provides two sites for coupling one or more probes

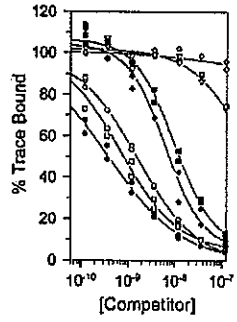

Figure 3. Inhibition of [^{111}In]-DTPA-[Y^3]-octreotate (trace) binding to CA20948 membranes using varying concentrations of the somatostatin analogues listed in Table 1. Symbols corresponding to compounds or to number codes given in Table 1 are as follows: ○, DTPA-[Y^3]-octreotate; ●, 1; □, 2; ■, 3; ◇, 4; ◆, 6; ▽, 5.

to the same molecule. Of these possible positions, conjugation of FITC to the α-amino lysine group (**6**) is preferred to the ϵ-position (**7**).

The inclusion of a lysine linker enabled us to prepare molecules that are potentially useful for diagnosis of tumors by a dual imaging system. This approach could provide distinctly new diagnostic information while complementing established imaging modalities. Because optical tomography is an emerging diagnostic method, tandem probes are also useful for cross-validation purposes. Accordingly, we coupled FITC and a chelator to the alternate amino group of the nonbinding N-terminal lysine (Table 2). We chose DTPA and DOTA as chelators because they are widely used to prepare radioactive and paramagnetic metal chelates for biomedical imaging.[41,43,44] Table 2 shows that while the relative position of the metal chelator and optical probe affect the receptor binding affinity of the peptides, the nature of the chelating group (linear DTPA or cyclic DOTA) had virtually no effect. Thus, for such dual heterogeneous imaging agents, coupling the chelator to the α-position and the optical probe to the ϵ-position of lysine resulted in conjugates that retain the receptor binding affinity of the peptide.

Similarly, we evaluated the binding affinity of several derivatives of bombesin receptor-avid peptides. Unlike somatostatin analogues, all of the bombesin peptide derivatives had high receptor affinity with measured IC_{50} values in the nanomolar range, indicating tolerance of the N terminus modifications by the peptide's pharmacophore (Table 3). However, as with the somatostatin analogues, the receptor binding affinity of the dual probes was less dependent on the nature of the chelator (**30** and **31**) but was affected by the relative position of the optical probe and the chelator (**29** and **30**). In this case, the preferred molecular design requires coupling the chelator to the ϵ-amino group and the optical probe to the nonreceptor binding α-amino lysine position.

All of the NIR-absorbing carbocyanine dye derivatives prepared, which are useful for deep tissue optical imaging, retained very high binding affinity for somatostatin and bombesin receptors (Table 5). Within the somatostatin series, increasing the dye's linker *N*-alkyl chain length from ethyl (**32**) to pentyl (**33**) or the introduction of a β-alanine spacer (**35**) did not considerably alter the receptor binding affinity of these compounds. However, comparison of **32** and **34** shows that the bis-peptide derivative **34** has about four times the receptor binding affinity of the monopeptide conjugate **32**. This difference in binding could be attributed to cooperative effect of the two peptides per dye molecule. In the case of carbocyanine–bombesin conjugate **36**, higher receptor binding affinity than the parent peptide **15** was obtained.

In Vivo Studies. Whole body imaging of rats and imaging of excised organs were accomplished by using a low-powered continuous wave laser source to excite the probe at the appropriate wavelength and monitor the distribution of the imaging agent with a charge-coupled device camera. The characteristic absorption (490 nm) and fluorescence (530 nm) of fluorescein require the use of light in the visible region for optimal localization of pathologic tissues with the aid of fluorescein-based contrast agent. Hence, fluorescein derivatives are best-suited for imaging superficial tissues because of the shallow penetration of blue light in tissues. In contrast, the absorption (780 nm) and fluorescence (830 nm) of the carbocyanine derivatives in the NIR region permit their use for optical imaging of deep tissues.

For in vivo optical imaging, we injected AR42-J (bombesin receptor-positive) or CA20948 (somatostatin receptor-positive) pancreatic tumor cells into the left flank of rats and allowed them to grow into a palpable mass. Control experiments with inactive receptor binding fluorescein disodium salt and the low-receptor affinity β-alanine-somatostatin fluorescein derivative (**4**) show that these compounds were not retained in the tumor.

A representative fluorescein-based somatostatin receptor binding peptide **3** was injected into the lateral tail vein of CA20948 tumor-bearing rats. Preferential retention of the agent in the tumor was slow and peaked at about 1 h postinjection but remained in the tumor up to 5 h later (Figure 4). On the other hand, differentiation of the tumor from normal tissue was evident 10 min postinjection of the bombesin peptide analogue **17** into AR42-J tumor-bearing rats. Although time sequence imaging showed that the preferential retention of **17** in the tumor increased gradually with time, this agent cleared from the tumor and other tissues 1 h postinjection. To account for the rapid elimination from tissues, we collected urine and excised various organs and tissue samples 2 h postinjection of **17** into AR42-J tumor-bearing rats. Optical imaging revealed that the conjugate was almost exclusively excreted by the kidneys into urine (Figure 5). Postulating that inhibition of this clearance pathway would improve tumor retention by keeping the probe in blood for a longer period, we carried out a bilateral ligation of the kidneys before injection of **17**. Our results indicate that instead of increasing the tumor retention, the probe reverted to the hepatobilliary excretion route (Figure 5). Thus, despite their favorable receptor binding values, the pharmacokinetics of compounds such as **17** may preclude their use for in vivo tumor detection.

As demonstrated by the in vitro data, the NIR conjugates have high receptor binding affinity. Prior to in vivo evaluation of representative receptor-specific

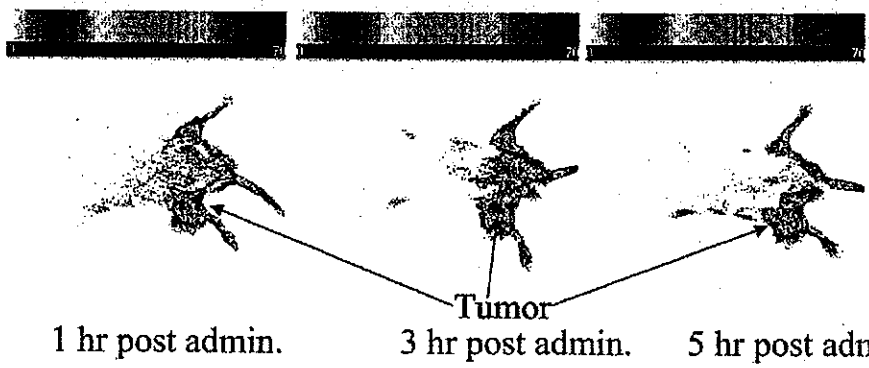

Figure 4. Time sequence localization of fluorescein–somatostatin receptor-avid optical probe 3 in a CA20948 tumor-bearing rat.

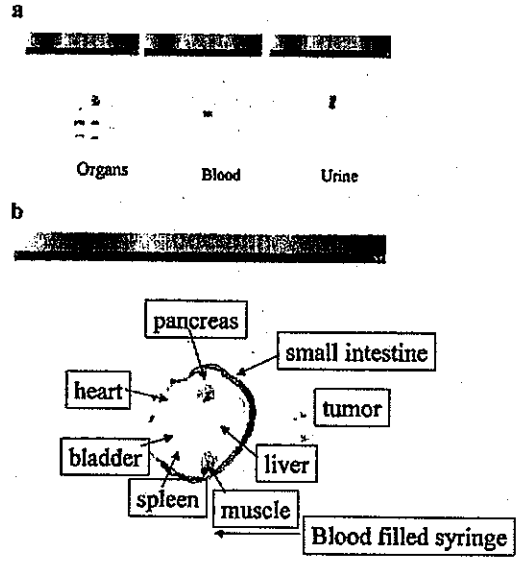

Figure 5. (a) Imaging of urine, excised organs, and tissues 2 h postinjection of **17** to Ar42-J tumor-bearing rat. The organs include liver, pancreas, kidneys, and the heart. The compound is almost exclusively excreted by the kidneys into urine. (b) Imaging of excised organs and tissues 2 h postinjection of **17** into a bilateral ligation of the kidneys of AR42-J tumor-bearing rat. The excretion route changed from renal to hepatobiliary.

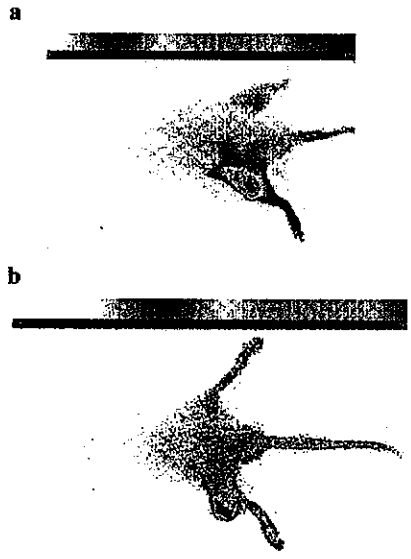

Figure 6. (a) Fluorescent image of the NIR somatostatin receptor-avid optical probe **32** in a CA20948 tumor-bearing rat at 27 h postinjection. (b) Fluorescent image of the NIR bombesin receptor-avid optical probe **36** in an AR-42-J tumor-bearing rat at 22 h postinjection.

agents, we assessed the nonspecific retention of the nonconjugated carbocyanine dye **39** in CA20948 tumor-bearing rats. Administration of **39** to tumor-bearing rats, and subsequent time sequence optical imaging, demonstrated that this dye was not retained in the tumor. Furthermore, ex vivo evaluation of excised organs 1 h postinjection showed that the compound was predominantly taken up by the liver. This lack of uptake by the tumor agrees with the observed poor specific binding of the dye to somatostatin receptor. Conversely, the high receptor binding affinity of the carbocyanine–peptide conjugates **32**, **34**, and **36** correlated with selective retention of the agents in tumors in vivo. Time sequence imaging of the whole rat revealed rapid delineation of the tumor within 30 min postinjection and showed that the compounds were retained in tumors up to 40 h later (Figure 6). The imaging of excised organ parts also confirmed the whole animal imaging results (Figure 7).

Discussion

The upregulation of somatostatin and bombesin receptors in tumors relative to normal surrounding tissues permits the preferential delivery of therapeutic and diagnostic molecules to pathologic cells without harming healthy tissues.[31,35] Previous studies with radiolabeled octapeptide analogues of native somatostatin and bombesin polypeptides demonstrated the site-specific localization of these truncated peptides in the appropriate receptor-positive tumor cells.[44,45] Findings of these studies also showed a good correlation between in vitro receptor binding affinities and selective retention of the peptide's radioactive metal complexes in tumors in vivo.

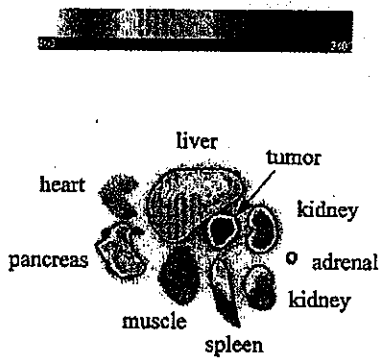

Figure 7. Localization of **32** in tissues of a CA20948 tumor-bearing rat 24 h postadministration.

Consequently, we prepared fluorescein- and carbocyanine-labeled analogues of the truncated somatostatin and bombesin peptides and evaluated their receptor binding activities.

Fluorescein Derivatives. Direct conjugation of FITC to **2** gave the octapeptide **3**, which retained the receptor binding affinity of the ligand in the nanomolar range. However, the difficulty in preparing **3** on solid support and the need to modify the biodistribution of the agent and introduce multiple probes per targeting moiety prompted us to study the effect of both hydrophilic and lipophilic linkers. Although the incorporation of β-alanine to **2** facilitated the synthesis of **4** on solid support, the resulting compound was inactive up to 1 μM. Furthermore, in vivo evaluation of **4** in CA20948 tumor-bearing rats showed no preferential retention in the tumor and was primarily excreted by the kidneys. It is possible that the flexible ethylene linker of β-alanine favored a disruptive interaction of the conjugate's thiourea moiety with the peptide's cyclic disulfide bond. Because the disulfide bond of **4** is critical for the peptide's bioactivity, any such intramolecular interaction could disrupt the receptor binding of the entire molecule. Another plausible explanation for the inactivity of **4** could result from other inhibitory interactions of the hydrophilic fluorescein with the receptor binding domain, which could be induced by the presence of nonsterically hindered flexible linkers such as an ethylene group.

Replacement of the β-alanine with a less flexible nonionic hydrophilic linker to give **5** improved receptor binding, albeit still several orders of magnitude less than **3**. However, substitution of β-alanine in **4** by lysine improved the receptor binding and also provided two possible FITC-reactive sites that influence the bioactivity of the conjugate. Thus, coupling FITC to the α-amino position of lysine gives a compound (**6**) that is several orders of magnitude more active than the ϵ-amino conjugate analogue (**7**). As expected, attachment of FITC to the flexible ϵ-amino group increased the potential of the resulting thiourea group to interact with the peptide's disulfide bond or the receptor in a similar manner as was observed with β-alanine (**4**) and GSG (**5**) linkers. However, the extent of this negative interaction appears to depend on the distance of the FITC-reactive site of the flexible linker from the peptide's disulfide bond. Thus, the receptor binding affinity increased as longer flexible lingers were used (i.e., ϵ-amino lysine > GSG > β-alanine). Interestingly, direct coupling or conjugation of FITC to a more rigid linker that minimizes interaction of the thiourea group with the peptide's disulfide bond favored high receptor binding of the fluorescein–peptide derivatives such as **3** and **6**. The negative effect of flexible linkers on ligand–receptor binding was only observed in the fluorescein conjugates of the cyclic disulfide somatostatin peptide analogues but not with the bombesin peptide analogues **21**–**23** or the hydrophobic carbocyanine analogue **35**, which retained their receptor binding activity in the presence of flexible linkers.

The influence of fluorescein and linkers on the bioactivity of bombesin peptide analogues is less pronounced relative to somatostatin derivatives (Table 3). Direct attachment of FITC to the bombesin peptide **13** to give **17** improved the receptor binding affinity of the ligand. Furthermore, incorporation of two fluorescein moieties to truncated bombesin peptides did not compromise the receptor binding affinity of the conjugates (**20** and **24**). These homogeneous multiprobe ligands could improve detection sensitivity by a net enhancement of optical signal per molecule and could be particularly useful for imaging tissues with low receptor density. Because bombesin analogues tolerate a variety of substituents at the N terminus without loss of receptor binding activity, they could serve as model bioactive molecules for multispectral optical imaging studies.

Although biomedical optical imaging is not new, recent advances in laser technology and image reconstruction techniques have reignited interest in the use of this highly sensitive and noninvasive method for diagnosing pathologic conditions.[46] Acceptance of optical tomography in clinical settings, however, requires validation of the images with conventional imaging methods such as scintigraphy or MRI. Such cross-validation studies would benefit from the use of a single molecule that is capable of providing important diagnostic information from both optical and other imaging methods. Accordingly, we prepared and evaluated the binding affinity of potential tandem imaging agents (Tables 2 and 4) and compared the result with analogous peptide–chelator conjugates that are traditionally used in nuclear medicine. For example, the DTPA–somatostatin peptide analogue **8** is extensively used in basic research and clinical studies.[47]

On the basis of the somatostatin receptor binding affinity of compounds **6** and **7** (Table 1), we expected that conjugation of FITC to the α-amino lysine and a chelator to the ϵ-amino group would give better binding molecules than vice versa. To test this hypothesis, we prepared compounds **9** and **10**. The results of binding studies using these molecules were the converse of our expectation (Table 2). Apparently, the relative position of the chelating group to fluorescein significantly influences the receptor binding of the tandem imaging agents. Thus, coupling DTPA to the α-amino group of lysine mitigates the deleterious effect of conjugating FITC to the flexible ϵ-amino lysine. In addition, changing the chelator from DTPA to DOTA did not alter this result (**10** and **11**). Because the binding affinity of the dual imaging agents was independent of the nature of

the chelating group, initial screening of the somatostatin receptor binding affinity of new dual modality compounds could be accomplished with the less expensive DTPA.

While the receptor binding affinity of various fluorescein–bombesin derivatives showed little variation, incorporation of DTPA into fluorescein-containing bombesin peptides induced a position-dependent binding activity, as was observed with the somatostatin analogues. However, unlike the DTPA–octreotate conjugates (Table 2), coupling DTPA to the ϵ-amino lysine and FITC to the α-amino group improved receptor binding rather than the converse (compare **29** and **30**, Table 4). Replacement of the linear DTPA with DOTA at the ϵ-amino group (**31**) gave a similar receptor binding value. Thus, in designing molecules for tandem fluorescein–chelator probes, the overall activity of the resultant molecule appears to rely on the relative position of the chelator on the linker than fluorescein.

Carbocyanine Derivatives. The carbocyanine derivatives prepared for this study absorb and fluoresce in the NIR region and are thus useful for deep tissue imaging. Coupling the hydrophobic carbocyanine dye **39** to somatostatin and bombesin peptides resulted in conjugates that retained high binding affinity to the appropriate receptor, despite the relatively large size of the dye component. Comparison of the fluorescein and carbocyanine analogues shows that the latter consistently had better receptor binding affinity than the former. Specifically, while the fluorescein conjugate **4** is inactive up to 1 μM, the carbocyanine analogue **35** retained high receptor binding affinity in the nanomolar range. Furthermore, comparison of the carbocyanine–bombesin derivative (**36**, Table 5) with the fluorescein analogue (**21**, Table 3) indicates that the former is about five times better than the latter.

At first glance, the small size of the peptide targeting groups used in this study would suggest that coupling the carbocyanine dye **39**, which is more than twice the molecular weight of fluorescein and constitutes over 40% of the entire conjugate's molecular weight, would interfere with receptor binding. This, however, is not the case. A variety of possible mechanisms could be postulated for the observed high receptor binding of the carbocyanine dye derivatives. It is likely that the large molecular volume of the hydrophobic NIR dye precluded it from fitting into the binding region of the receptor, thereby permitting the bioactive peptide unit to interact exclusively with the receptor. This preclusion of the large hydrophobic dye component could deter competing ligands from displacing the dye–peptide conjugate from the receptor by two possible mechanisms. On one hand, displacement of the receptor-bound peptide of the conjugate by hydrophilic competitors is inhibited by unfavorable interaction by the protruding hydrophobic dye portion. On the other hand, the favorable association of hydrophobic competitors with the dye component prevents access to the receptor binding domain occupied by the peptide component of the conjugate. Both possible mechanisms would enhance the receptor binding of the carbocyanine molecules. However, confirmation of the exact mechanism and the structural disposition of the ligand–receptor interaction would require additional studies beyond the scope of this work.

The in vitro studies also show that while the receptor binding affinity of the carbocyanine conjugates is not influenced by the length of the *N*-alkyl linker, it depends on the number of peptide conjugates per dye molecule (compare **32**–**34**, Table 5). The enhanced receptor binding of the bis-peptide derivative **34** may be attributed to cooperative interaction of the two peptides with the receptor or may be simply due to the effective doubling of the peptides concentration.

Biodistribution and Tumor Localization. The preferential accumulation of the fluorescein conjugate **3** in the somatostatin receptor-positive tumor CA20948 peaked at about 1 h postinjection and suggests active uptake of the compound by the receptor (Figure 4) because in negative control experiments using either fluorescein disodium salt or nonsomatostatin-avid dye–peptide conjugates, retention in the tumor was not observed.

Control experiments with the nonconjugated carbocyanine dye **39** and the corresponding nonsomatostatin-avid peptide conjugates neither localized in the tumor in vivo nor had detectable affinity for the somatostatin receptor in vitro. In contrast, the high receptor binding affinity of the carbocyanine derivatives was also reflected by tumor localization in vivo. Thus, injection of **32** and **34** into somatostatin receptor-positive CA20948 tumor-bearing rat and subsequent optical imaging demonstrates the site-specific localization of the agent in the tumor (Figure 6). Ex vivo imaging of excised organs and tissues shows the predominant retention of the agents in tumor tissues (Figure 7). The small uptake of the agent by the liver and the pancreas is expected because the liver is the primary excretion route of the nonconjugated carbocyanine dye while the rat pancreas possesses some somatostatin receptors. This finding affirms the reliance on the receptor binding studies for rapid evaluation and selection of tumor-specific optical contrast agents for biomedical studies. In addition to its use in tumor diagnosis, this approach is applicable to the treatment of appropriate receptor-positive tumors by a photodynamic therapy method.

In conclusion, we prepared novel optical and heterogeneous dual imaging agents for tumor diagnosis. The delivery mechanism is based on targeting overexpressed receptors on tumor cell membranes. We quantified the receptor binding affinity of all of the reported bioconjugates and showed that the in vitro data correlate positively with the in vivo selective retention of the receptor-specific probes in the appropriate receptor-positive tumor model. The fluorescein and carbocyanine dye conjugates of bombesin peptide analogues retained their receptor binding affinity in the nanomolar range. On the contrary, the receptor binding affinity of the somatostatin receptor-avid optical probes was dependent on the dye used. While the carbocyanine peptide conjugates retained high receptor binding affinity, binding of the fluorescein analogues depended on the nature of the thiourea linker. Conjugation of FITC to form thiourea with an amino group of the peptide via a flexible linker appears to destabilize the peptide's disulfide bond, which is part of the molecule's pharmacophore. Consequently, a more stable fluorescein conjugate of somatostatin peptide analogues may be prepared from fluoresceinamine, which gives an amide

bond that does not destabilize the peptide's disulfide group. Finally, the structural feature of the receptor-specific dual optical-scintigraphic imaging agents represents a new direction toward the validation of clinical data obtained from the emerging optical tomography method. These findings form the basis for future development of receptor-based optical contrast agents and could provide new approaches to the selective delivery of phototoxic agents to tumors for therapeutic interventions.

Materials and Methods

General. All reagents and solvents were obtained commercially and used without further purification. Compounds **1**, **8**, **12**–**14**, and **25** were supplied to us by our collaborator at Mallinckrodt, Inc. Purification and analysis of the dye-labeled fluorescein and carbocyanine derivatives were performed by HPLC with a tunable UV–visible detector. Analytical (flow rate = 0.5 mL/min) and semipreparative (flow rate = 10 mL/min) RP-HPLC were performed as described in the literature by using a C-18 column.[39] The gradient elution protocol ranged from a mixture of 95% A and 5% B to 30% A and 70% B in 30 min, where A is 5% MeCN in 0.1% aqueous TFA and B is 90% MeCN in 0.1% aqueous TFA. A second elution system consisting of an isocratic mixture of 60% H_2O containing 0.1% TFA, 30% MeOH, and 10% MeCN was used to confirm purity of compounds by analytical HPLC. Peak detection was at 214 nm, unless otherwise stated. Electrospray ionization mass spectrometry experiments were performed on a triple quadruple mass spectrometer. The electrospray interface was operated in positive ion mode with a spray voltage of 4.5 kV and a capillary temperature of 225 °C. Samples were introduced into the spectrometer by flow injection utilizing 70% MeCN and 30% H_2O containing 0.1% TFA. The absorption and emission spectra of the dye conjugates were performed on a Cary 500 UV–visible spectrophotometer (Varian) and QuantaMaster spectrofluorometer (Photon Technology International), respectively. High-resolution mass spectrometry (HRMS) (MALDI-TOF) analyses were performed at the Washington University School of Medicine in St. Louis, MO. The HPLC purity of all compounds used in the in vivo and in vitro studies was >99%. The dye–peptide conjugates were stable under the experimental conditions used, and no aggregation is expected at the nanomolar concentration employed in the in vitro studies.

Peptide Synthesis. All of the peptides synthesized in this study follow the procedure described below. Exceptions are noted under specific peptides. The peptides were synthesized on solid support by standard automated Fmoc procedures.[40] Rink amide and Wang resins were used for the synthesis of C-terminal amide and carboxyl peptides, respectively. Chlorotrityl resins were used for mild selective cleavage of peptides from the resin without removing the amino acids side chain protecting groups. Initial loading of each Fmoc amino acid bound resin is 25 μmol. Automatic activation of the carboxyl group with a 1:1 mixture of N-hydroxylbenzotriazole (HOBt, 2 M) and 2-(1-H benzotriazole-1-yl)-1,1,1,3-tetramethyluronium hexafluorophosphate (HBTU, 2 M) and coupling of subsequent Fmoc-protected amino acids (75 μmol) were carried out in situ. For octreotate derivatives, intramolecular cyclization of the acetamidomethyl-protected dithiol groups of cysteine was accomplished by adding thallium trifluoroacetate (23 mg, 42 μmol) in anhydrous dimethylformamide (DMF, 1 mL) and shaking the heterogeneous mixture for 2 h, followed by successive washing of the residue with water, DMF, tetrahydrofuran (THF), and DCM. Whenever applicable, incorporation of DTPA or DOTA was accomplished by placing tri-*tert*-butyl DTPA or tri-*tert*-butyl DOTA (75 μmol) in the last cartridge of amino acid rack, which is then coupled to the appropriate amino group by the same automated method used to synthesize the amino acid sequence.[41] Cleavage of the peptides from the resin and concomitant removal of the side chain protecting groups were accomplished with 85% TFA, 5% H_2O, 5% PhOH, and 5% thioanisole for 4 h at room temperature. The crude peptides were precipitated with cold *tert*-butyl methyl ether and purified by RP-HPLC using gradient elution protocol described in the general section above. All peptides and their conjugates were characterized by analytical HPLC and electrospray spectrometric (EI) analysis after lyophilization in 67% H_2O and 33% MeCN. The nonfluorescein conjugated peptides **2**, **15**, **16**, and **26**–**28** were prepared by this procedure.

DPhe-cyclo(Cys-DTyr-Trp-Lys-Thr-Cys)Thr-OH (2). ESI-MS: *m/z* 1050 $[M + H]^+$, 526 $[M + 2H]^{2+}$.

Gly-Ser-Gly-Gln-Trp-Ala-Val-Gly-His-Leu-Met-NH_2 (15). ESI-MS: *m/z* 1141 $[M + H]^+$, 571 $[M + 2H]^{2+}$.

Lys-Gly-Ser-Gly-Gln-Trp-Ala-Val-Gly-His-Leu-Met-NH_2 (16). ESI-MS: *m/z* 1270 $[M + H]^+$, 636 $[M + 2H]^{2+}$.

α-DTPA-Lys-Gln-Trp-Ala-Val-Gly-His-Leu-Met-NH_2 (26). ESI-MS: *m/z* 1444 $[M + H]^+$, 723 $[M + 2H]^{2+}$, 481 $[M + 3H]^{3+}$.

ε-DTPA-Lys-Gln-Trp-Ala-Val-Gly-His-Leu-Met-NH_2 (27). ESI-MS: *m/z* 1444 $[M + H]^+$, 723 $[M + 2H]^{2+}$, 482 $[M + 3H]^{3+}$.

α,ε-$(DTPA)_2$-Lys-Gln-Trp-Ala-Val-Gly-His-Leu-Met-NH_2 (28). ESI-MS: *m/z* 910 $[M + 2H]^{2+}$, 607 $[M + 3H]^{3+}$.

Preparation Fluorescein–Peptide Conjugates by Solid Phase Synthesis. A typical example for this procedure is represented by the synthesis of the β-alanine somatostatin derivative **4**. Preparation of the peptide **2** was carried out by standard Fmoc strategy. While still on solid support and with all side chain protecting groups intact, the intramolecular cyclization of the disulfide bond was carried out with $(CF_3CO_2)_3Tl$ in DMF followed by the removal of the N-terminal Fmoc to liberate the amino group. After the resin was washed with CH_2Cl_2 (DCM), the resin was swollen in DMF for 10 min before adding Et_3N (10 mg, 100 μmol) and commercially available FITC (14 mg, 36 μmol). The mixture was shaken for 16 h, and the resin was washed sequentially with DMF, THF, and DCM. The product was cleaved from the resin as described above, and the resulting TFA solution was poured into cold MTBE to precipitate the yellow crude material, which was lyophilized and purified using HPLC. This procedure was used to prepare the fluorescein–nonpeptide conjugate **4** and other less sterically hindered N-terminal peptide derivatives **5** and **21**–**24**. Note that the cyclization step was omitted for all bombesin derivatives. Several attempts to prepare **3** by this method were not successful.

FITC-βAla-DPhe-cyclo(Cys-DTyr-Trp-Lys-Thr-Cys)-Thr-OH (4). ESI-MS: *m/z* 1510 $[M + H]^+$, 756 $[M + 2H]^{2+}$; 5 mg; 13% overall yield of isolated compound.

Preparation Fluorescein–Peptide Conjugates by Solution Phase Synthesis. Two methods were evaluated for the preparation of the bioconjugates by solution phase reaction. In the first method, the peptide was prepared on a chlorotrityl resin as described above. This resin allowed us to cleave the peptide with mild acid (5% TFA in DCM; 2 × 30 min) without removing the side chain *t*-Boc amino and *t*-Bu carboxyl side chain protecting groups on the peptide. In a typical procedure, the octapeptide **2** was cleaved from the trityl resin after cyclization and removal of N-terminal Fmoc. The crude product was precipitated with MTBE and lyophilized. Without further purification, a mixture of the orthogonally protected peptide (5 mg, 3.5 μmol), FITC (3 mg, 7 μmol), and $NaHCO_3$ (5 mg, 60 μmol) in 2 mL of DMF was shaken vigorously for 5 h. The insoluble salt was filtered, and the filtrate was precipitated and washed with MBTE (3 × 2 mL) and centrifuged, and the supernatant was decanted before lyophilization. Mass spectrometry of the crude product did not indicate a quantifiable amount of the desired compound. Coupled with the poor yield, this procedure would require extensive workup in order to remove all protecting groups and isolate the compound. Hence, this procedure was abandoned.

The second approach, which was used to prepare a majority of the conjugates, involved simultaneous cleavage of the peptide from the resin and removal of side chain protecting groups before coupling FITC to the peptide. Synthesis of the fluorescein peptide conjugate **21** is typical for the preparation of bombesin derivatives by this approach. Briefly, the peptide was prepared by standard Fmoc procedure described above

and cleaved from the resin to obtain the undecapeptide **15**. A mixture of this peptide (10 mg, 9 μmol), FITC (10 mg, 25 μmol), and $NaHCO_3$ (10 mg, 120 μmol) in 2 mL of DMF was stirred for 12 h at room temperature and filtered into cold MTBE to give a yellow-orange precipitate. The supernatant was removed after centrifugation, and the crude product was washed with MTBE (3 × 3 mL), dried, lyophilized, and purified by preparative HPLC.

In this procedure, cleavage of the somatostatin derivatives also exposes the ε-amino group of the lysine pharmacophore (e.g., compound **2**, K^5) to reaction with FITC. Consequently, this amino group was protected with ivDde, which is not affected by the cleavage mixture. Thus, a typical procedure for the synthesis of the somatostatin derivatives begins with the incorporation of Fmoc-lysine(ε-ivDde)OH in the receptor binding lysine. After the peptide synthesis was completed, cyclization and removal of the N-terminal Fmoc group and cleavage of the peptide from the resin with TFA also removed all side chain protecting groups, except ivDde. Subsequent reactions are illustrated by the synthesis of **3**. FITC (12 mg, 28 μmol) and $NaHCO_3$ (10 mg, 120 μmol) were added to a solution of the crude peptide (prepared on a 25 μmol scale) in 2 mL of DMF and stirred for 12 h. The mixture was filtered into 8 mL of MBTE to precipitate the orange product, and analysis of the crude product by HPLC showed about 50% conversion. This product was treated with a 1 mL solution of 2% hydrazine in DMF for 20 min in order to remove the ivDde. The resulting mixture was poured into cold MBTE to precipitate the conjugate, which was lyophilized and purified by HPLC.

A similar method was used to prepare the bombesin peptide derivatives, except that the cyclization step was not required. Because the receptor binding region of bombesin peptides are devoid of lysine residue, orthogonal protection of the amino groups with ivDde was only required when a lysine linker was involved. On the basis of the FITC coupling reaction step, the isolated yield in all cases ranged from 20 to 25% of the expected yield.

FITC-DPhe-cyclo(Cys-DTyr-Trp-Lys-Thr-Cys)Thr-OH (3). ESI-MS: *m/z* 1438 $[M + H]^+$, 720 $[M + 2H]^{2+}$.

FITC-Gly-Ser-Gly-DPhe-cyclo(Cys-DTyr-Trp-Lys-Thr-Cys)Thr-OH (5). ESI-MS: *m/z* 1640 $[M + H]^+$, 821 $[M + 2H]^{2+}$.

α-FITC-Lys-DPhe-cyclo(Cys-DTyr-Trp-Lys-Thr-Cys)-Thr-OH (6). To specifically prepare this compound, the ε-amino group of both K^1 and K^6 was protected with ivDde, which remained intact after peptide cleavage from the resin with TFA. This guarantees that only the α-amino group of N-terminal lysine reacts with FITC. Subsequent removal of the ivDde protecting group was carried out with 2% hydrazine in DMF, as described above. ESI-MS: *m/z* 1567 $[M + H]^+$, 784 $[M + 2H]^{2+}$, 523 $[M + 3H]^{3+}$.

ε-FITC-Lys-DPhe-cyclo(Cys-DTyr-Trp-Lys-Thr-Cys)-Thr-OH (7). To ensure the coupling of FITC to the ε-position, the reaction was carried out as described for compound **6** above, except that the α-amino group of K^1 was protected with ivDde. ESI-MS: *m/z* 1567 $[M + H]^+$, 784 $[M + 2H]^{2+}$, 523 $[M + 3H]^{3+}$.

α-DTPA-ε-FITC-Lys-DPhe-cyclo(Cys-DTyr-Trp-Lys-Thr-Cys)Thr-OH (9). In this reaction, the ε-amino group of K^6 was protected as ivDde while Fmoc-Lys(Boc) was used for the N-terminal amino group. Thus, at the end of the peptide synthesis, tri-*tert*-butyl DTPA was directly coupled to the α-amino group of K^1 after Fmoc removal. Cleavage of the peptide from the resin with TFA also removed the Boc group, which allowed us to introduce FITC at the ε-amino position. ESI-MS: *m/z* 1942 $[M + H]^+$, 972 $[M + 2H]^{2+}$, 648 $[M + 3H]^{3+}$.

α-FITC-ε-DTPA-Lys-DPhe-cyclo(Cys-DTyr-Trp-Lys-Thr-Cys)Thr-OH (10). A similar method described for compound **9** was used except that Boc-Lys(Fmoc) was used for the N-terminal lysine. ESI-MS: *m/z* 1942 $[M + H]^+$, 972 $[M + 2H]^{2+}$, 648 $[M + 3H]^{3+}$.

α-DOTA-ε-FITC-Lys-DPhe-cyclo(Cys-DTyr-Trp-Lys-Thr-Cys)Thr-OH (11). A similar method described for compound **9** was used except that tri-*tert*-butyl DOTA instead of tri-*tert*-butyl DTPA was used as the chelating group. ESI-MS: *m/z* 1953 $[M + H]^+$, 977 $[M + 2H]^{2+}$, 652 $[M + 3H]^{3+}$.

FITC-Gln-Trp-Ala-Val-Gly-His-Leu-Met-NH_2 (17). ESI-MS: *m/z* 1330 $[M + H]^+$, 666 $[M + 2H]^{2+}$.

α-FITC-Lys-Gln-Trp-Ala-Val-Gly-His-Leu-Met-NH_2 (18). To ensure selective coupling of FITC to the α-position, Fmoc-Lys(ivDde) was used to prepare this compound by the procedure described for the synthesis of compound **6**. ESI-MS: *m/z* 1458 $[M + H]^+$, 730 $[M + 2H]^{2+}$, 487 $[M + 3H]^{3+}$.

ε-FITC-Lys-Gln-Trp-Ala-Val-Gly-His-Leu-Met-NH_2 (19). Conjugation of FITC to the ε-position was assured by using ivDde-Lys(ivDde) by the procedure described for the synthesis of compound **6**. ESI-MS: *m/z* 1458 $[M + H]^+$, 730 $[M + 2H]^{2+}$, 487 $[M + 3H]^{3+}$.

α,ε-$(FITC)_2$-Lys-Gln-Trp-Ala-Val-Gly-His-Leu-Met-NH_2 (20). ESI-MS: *m/z* 1846 $[M + H]^+$, 924 $[M + 2H]^{2+}$, 616 $[M + 3H]^{3+}$.

FITC-Gly-Ser-Gly-Gln-Trp-Ala-Val-Gly-His-Leu-Met-NH_2 (21). ESI-MS: *m/z* 1532 $[M + H]^+$, 766 $[M + 2H]^{2+}$.

α-FITC-Lys-Gly-Ser-Gly-Gln-Trp-Ala-Val-Gly-His-Leu-Met-NH_2 (22). ESI-MS: *m/z* 1659 $[M + H]^+$, 830 $[M + 2H]^{2+}$, 554 $[M + 3H]^{3+}$.

ε-FITC-Lys-Gly-Ser-Gly-Gln-Trp-Ala-Val-Gly-His-Leu-Met-NH_2 (23). ESI-MS: *m/z* 1660 $[M + H]^+$, 830 $[M + 2H]^{2+}$, 554 $[M + 3H]^{3+}$.

α,ε-$(FITC)_2$-Lys-Gly-Ser-Gly-Gln-Trp-Ala-Val-Gly-His-Leu-Met-NH_2 (24). ESI-MS: *m/z* 1025 $[M + 2H]^{2+}$, 684 $[M + 3H]^{3+}$.

α-DTPA-ε-FITC-Lys-Gln-Trp-Ala-Val-Gly-His-Leu-Met-NH_2 (29). ESI-MS: *m/z* 1833 $[M + H]^+$, 918 $[M + 2H]^{2+}$, 612 $[M + 3H]^{3+}$.

α-FITC-ε-DTPA-Lys-Gln-Trp-Ala-Val-Gly-His-Leu-Met-NH_2 (30). ESI-MS: *m/z* 1833 $[M + H]^+$, 918 $[M + 2H]^{2+}$, 612 $[M + 3H]^{3+}$.

α-FITC-ε-DOTA-Lys-Gln-Trp-Ala-Val-Gly-His-Leu-Met-NH_2 (31). ESI-MS: *m/z* 1845 $[M + H]^+$, 923 $[M + 2H]^{2+}$, 615 $[M + 3H]^{3+}$.

Synthesis of Peptide–Tricarbocyanine-*bis*-propanoic Acid Derivatives (32, 35, 36). A mixture of 1,1,2-trimethyl-[1H]-benz[e]indole **37** (9.1 g, 43.58 mmol) and 3-bromopropanoic acid (10.0 g, 65.37 mmol) in 1,2-dichlorobenzene (40 mL) was heated at 110 °C for 12 h. The solution was cooled to room temperature, and the residue obtained was filtered and washed with a mixture of acetonitrile/diethyl ether (1/1). The solid obtained was dried under vacuum to give 10 g (64%) of light brown powder. A portion of this solid (6.0 g, 16.56 mmol) was added to a mixture of glutaconaldehyde dianil monohydrochloride (2.36 g, 8.28 mmol) and sodium acetate trihydrate (2.93 g, 21.53 mmol) in 150 mL of ethanol, and the resulting heterogeneous mixture was heated at reflux for 90 min. After the solvent was evaporated, the residue was washed with 2 M aqueous HCl (4 × 40 mL) and the green paste obtained was lyophilized in water/MeCN (3/2) to give dark green flakes (2 g, 35% yield; ESI-MS: *m/z* 625.3 $[M + H]^+$.

While still on solid support, the N-terminal Fmoc group of the peptide was removed and washed with 3 mL each of DMF, MeOH, THF, and DCM in that order. The resin-bound peptide was added to preactivated carbocyanine dye **39** (53 mg, 75 mmol; activated with 80 mmol of HBTU in DMSO for 30 min). After the reaction mixture was shaken for 3 h, the resin was washed with DMF and DCM, followed by peptide cleavage and removal of side chain protecting groups with a mixture of 85% TFA, 7.5% H_2O, and 7.5% thioanisole in 4 h. The peptide–dye conjugate was precipitated from the cleavage mixture with cold MTBE and lyophilized in MeCN/H_2O (2/3) mixture. The green crude product was purified by HPLC as described in the General Section to give the cytate in 99% HPLC purity.

Tricarbocyanine-DPhe-cyclo(Cys-DTyr-Trp-Lys-Thr-Cys)Thr-OH (32). ESI-MS: *m/z* 1656 $[M + H]^+$, 829 $[M + 2H]^{2+}$.

Tricarbocyanine-βAla-DPhe-cyclo(Cys-DTyr-Trp-Lys-Thr-Cys)Thr-OH (35). ESI-MS: *m/z* 1728 $[M + H]^+$, 864 $[M + 2H]^{2+}$.

Tricarbocyanine-Gly-Ser-Gly-Gln-Trp-Ala-Val-Gly-His-Leu-Met-NH_2 (36). ESI-MS: *m/z* 1748 $[M + H]^+$, 875 $[M + 2H]^{2+}$.

Synthesis of Peptide–Tricarbocyanine-*bis*-hexanoic Acid Derivatives (33, 34). A similar procedure described above was used to prepare these compounds except that 1,1,2-trimethyl-[1H]-benz[e]indole **37** was reacted with 6-bromohexanoic acid instead of 3-bromopropanoic acid to give the intermediate 1,1,2-trimethyl-[1H]-benz[e]indole-*N*-hexanoic acid. Reaction of this intermediate (4 g, 9.89 mmol) with glutaconaldehyde dianil hydrochloride (1.4 g, 4.95 mmol) as described above gave the carbocyanine dye **39** (with hexanaoic instead of propanoic acid *N*-alkyl derivative, 1.8 g, 46% yield; ESI-MS: *m/z* 709.4 $[M + H]^+$). This dye was used to prepare the peptide conjugates **33** and **34**.

Tricarbocyanine-DPhe-cyclo(Cys-DTyr-Trp-Lys-Thr-Cys)Thr-OH (33). ESI-MS: *m/z* 1740 $[M + H]^+$, 871 $[M + 2H]^{2+}$, 581 $[M + 3H]^{3+}$.

Tricarbocyanine(DPhe-cyclo(Cys-DTyr-Trp-Lys-Thr-Cys)Thr-OH)$_2$ (34). ESI-MS: *m/z* 1387 $[M + 2H]^{2+}$, 925 $[M + 3H]^{3+}$.

In Vitro Receptor Binding Assays. Receptor binding assays were performed using membranes prepared from the rat pancreatic acinar cell lines AR42-J and CA20948 for bombesin and somatostatin receptor binding assays, respectively. Membranes were prepared by a method similar to that previously reported.[30] Assays were carried out using Millipore FC96 plates and the Millipore Multiscreen system (Bedford, MA). For bombesin derivatives, the competitive receptor binding of the tracer [^{111}In]-DTPA-[P^1,Y^4]-bombesin to AR42-J cell membranes (~50 μg/well) was determined in the presence of increasing concentration of cold competitors in buffer (50 mM Tris-HCl, pH 7.4, 5 mM $MgCl_2$, 0.2 mg/mL BSA) in a total volume of 200 μL per well. Similarly, somatostatin receptor binding studies used the tracer [^{111}In]-DTPA-[Y^3]-octreotate and CA20948 cell membranes (~25 mg/well). Following incubation for 90 min at room temperature, membranes were filtered and washed with buffer. The filters containing membrane-bound radioactivity were removed from the assay plate and counted using a Parkard Cobra gamma counter (Meriden, CT). IC_{50} values were calculated using a four parameter curve-fitting routine using the program GraFit (Erithacus Software, U.K.). Radiolabeling of DTPA-linked peptides was carried out in 25 mM NaOAc and 12.5 mM sodium ascorbate (pH 5.0, room temperature, 30 min incubation). The specific activity of radiolabeled peptides was >1400 Ci/mmol. Radiochemical yield (>99.5%) and radiochemical purity (>98%) were determined by reverse phase chromatography on a C18 Vydac column using a MeCN/0.1% TFA gradient (5–70% MeCN over 20 min) at a flow rate of 1 mL/min. Binding assays were performed in duplicates per sample, and the experiment was repeated twice. The stock solutions of dye-labeled peptides were prepared by adding an accurate amount of the weighed bioconjugate to 25% DMSO in water, and other concentrations were obtained by serial dilution of aliquots from the stock.

Animal Protocols. All studies were conducted in compliance with Mallinckrodt Inc. Animal Welfare Committee's requirements for the care and use of laboratory animals in research. The rat pancreatic acinar carcinoma (CA20948) expressing the somatostatin receptor was induced by solid implant technique in the rear left flank area. Palpable masses were detected 9 days postimplant. This tumor line has been widely used for somatostatin receptor-positive assays, and the number of binding sites for somatostatin is estimated at 489 fmol mg^{-1}.[48]

The animals were anesthetized with a rat cocktail (xylazine:ketamine:acepromazine 1.5:1.5:0.5) at 0.8 mL/kg via intaperitoneal injection. The area of the tumor (left flank) was shaved to expose the tumor and surrounding surface area. A 21 gauge butterfly infusion set equipped with a stopcock and two syringes containing heparinized saline was placed into the lateral tail vein of the rat. Patency of the vein was checked prior to administration of the new contrast agents via the butterfly apparatus. Each animal weighing about 250 g received 0.5 mL of aqueous solution of ICG (5.4 μM) or cytate (6.0 μM).

Imaging Procedure. A simple noninvasive in vivo continuous wave fluorescence imaging apparatus employed to assess the localization and distribution of contrast agents has been previously described.[27,29] Briefly, laser light of the appropriate incident wavelength to excite the agent fluorescence was launched into a fiber optic bundle. A defocusing lens in position after the bundle expanded the beam such that most of the rat was illuminated. An argon ion laser tuned to 488 nm was used to excite the fluorescein compounds, and a 780 nm laser diode was used for the carbocyanine compounds. The lasers generated a nominal 50 mW of incident power. The laser power at the output of the bundle was approximately one-half of the input power.

The detector was a Princeton Instruments CCD camera. An interference filter in front of the CCD (520 nm for fluorescein compounds and 830 nm for carbocyanine compounds) allowed for detection of the emitted fluorescent light only. Images were acquired and processed using WinView software from Princeton Instruments. Typically, an image of the animal was taken preadministration of contrast agent. Subsequent images were taken post administration of the agent, all performed with the rat in a stationary position. Data analysis consisted of subtracting (pixel by pixel) the preadministration image from the postadministration images and displaying the results in gray scale or false color. For images taken several hours postadministration, the animals were removed from the sample area, returned to their habitat, and then brought back to the sample area. Background subtraction was not performed for these measurements.

References

(1) Shah, N.; Cerussi, A.; Eker, C.; Espinoza, J.; Butler, J.; et al. Noninvasive functional optical spectroscopy of human breast tissue. *Proc. Natl. Acad. Sci. U.S.A.* **2001**, *98*, 4420–4425.

(2) Hawrysz, D. J.; Sevick-Muraca, E. M. Developments toward diagnostic breast cancer imaging using near-infrared optical measurements and fluorescent contrast agents. *Neoplasia* **2000**, *2*, 388–417.

(3) Cheong, W. F.; vanHouten, J. P.; Kermit, E. L.; Macheld, T. R.; Stevenson, D. K.; et al. Pilot comparison of light-based optical tomography versus ultrasound for real-time imaging of neonatal intraventricular hemorrhage. *Pediatr. Res.* **1996**, *39*, 1189–1189.

(4) Rhine, W. D.; Benaron, D. A.; Darceuil, H. E.; deCrespigny, A.; Cheong, W. F.; et al. Simultaneous time of-flight adjusted (TOFA) near-infrared spectroscopy and magnetic resonance imaging of immature rabbit hypoxic-ischemic encephalopathy (HIE). *Pediatr. Res.* **1996**, *39*, 2264–2264.

(5) Wagnieres, G. A.; Star, W. M.; Wilson, B. C. In vivo fluorescence spectroscopy and imaging for oncological applications. *Photochem. Photobiol.* **1998**, *68*, 603–632.

(6) Ntziachristos, V.; Yodh, A. G.; Schnall, M.; Chance, B. Concurrent MRI and diffuse optical tomography of breast after indocyanine green enhancement. *Proc. Natl. Acad. Sci. U.S.A.* **2000**, *97*, 2767–2772.

(7) Cubeddu, R.; Pifferi, A.; Taroni, P.; Torricelli, A.; Valentini, G.; et al. Fluorescence imaging during photodynamic therapy of experimental tumors in mice sensitized with disulfonated aluminum phthalocyanine. *Photochem. Photobiol.* **2000**, *72*, 690–695.

(8) Cerussi, A. E.; Berger, A. J.; Bevilacqua, F.; Shah, N.; Jakubowski, D.; et al. Sources of absorption and scattering contrast for near-infrared optical mammography. *Acad. Radiol.* **2001**, *8*, 211–218.

(9) Hebden, J. C.; Veenstra, H.; Dehghani, H.; Hillman, E. M. C.; Schweiger, M.; et al. Three-dimensional time-resolved optical tomography of a conical breast phantom. *Appl. Opt.* **2001**, *40*, 3278–3287.

(10) Culver, J. P.; Ntziachristos, V.; Holboke, M. J.; Yodh, A. G. Optimization of optode arrangements for diffuse optical tomography: A singular-value analysis. *Opt. Lett.* **2001**, *26*, 701–703.

(11) Hyde, D. E.; Farrell, T. J.; Patterson, M. S.; Wilson, B. C. A diffusion theory model of spatially resolved fluorescence from depth-dependent fluorophore concentrations. *Phys. Med. Biol.* **2001**, *46*, 369–383.

(12) Pogue, B. W.; Geimer, S.; McBride, T. O.; Jiang, S. D.; Osterberg, U. L.; et al. Three-dimensional simulation of near-infrared diffusion in tissue: boundary condition and geometry analysis for finite- element image reconstruction. *Appl. Opt.* **2001**, *40*, 588–600.

(13) McBride, T. O.; Pogue, B. W.; Gerety, E. D.; Poplack, S. B.; Osterberg, U. L.; et al. Spectroscopic diffuse optical tomography for the quantitative assessment of hemoglobin concentration and oxygen saturation in breast tissue. *Appl. Opt.* **1999**, *38*, 5480–5490.
(14) Schotland, J. C. Continuous-wave diffusion imaging. *J. Opt: Soc. Am. A* **1997**, *14*, 275–279.
(15) Lee, J.; Sevick-Muraca, E. Fluorescence-enhanced absorption imaging using frequency-domain photon migration: tolerance to measurement error. *J. Biomed. Opt.* **2001**, *6*, 58–67.
(16) Katzenellenbogen, J. A.; Coleman, R. E.; Hawkins, R. A.; Krohn, K. A.; Larson, S. M.; et al. Tumor receptor imaging: Proceedings of the national cancer institute workshop, review of current work, and prospective for further investigations. *Clin. Cancer Res.* **1995**, *1*, 921–932.
(17) Clauss, M. A.; Jain, R. K. Interstitial Transport of Rabbit and Sheep Antibodies in Normal and Neoplas Tic Tissues. *Cancer Res.* **1990**, *50*, 3487–3492.
(18) Pelegrin, A.; Folli, S.; Buchegger, F.; Mach, J. P.; Wagnieres, G.; et al. Antibody Fluorescein Conjugates for Photoimmunodiagnosis of Human Colon-Carcinoma in Nude-Mice. *Cancer* **1991**, *67*, 2529–2537.
(19) Vogel, C. A.; Galmiche, M. C.; Westermann, P.; Sun, L. Q.; Pelegrin, A.; et al. Carcinoembryonic antigen expression, antibody localisation and immunophotodetection of human colon cancer liver metastases in nude mice: A model for radioimmunotherapy. *Int. J. Cancer* **1996**, *67*, 294–302.
(20) Folli, S.; Westermann, P.; Braichotte, D.; Pelegrin, A.; Wagnieres, G.; et al. Antibody-Indocyanin Conjugates for Immunophotodetection of Human Squamous-Cell Carcinoma in Nude-Mice. *Cancer Res.* **1994**, *54*, 2643–2649.
(21) Ballou, B.; Fisher, G. W.; Deng, J. S.; Hakala, T. R.; Srivastava, M.; et al. Cyanine fluorochrome-labeled antibodies in vivo: Assessment of tumor imaging using Cy3, Cy5, Cy5.5, and Cy7. *Cancer Detect. Prev.* **1998**, *22*, 251–257.
(22) Ballou, B.; Fisher, G. W.; Hakala, T. R.; Farkas, D. L. Tumor detection and visualization using cyanine fluorochrome-labeled antibodies. *Biotechnol. Prog.* **1997**, *13*, 649–658.
(23) Ballou, B.; Fisher, G. W.; Waggoner, A. S.; Farkas, D. L.; Reiland, J. M.; et al. Tumor Labeling in-Vivo Using Cyanine-Conjugated Monoclonal- Antibodies. *Cancer Immunol. Immunother.* **1995**, *41*, 257–263.
(24) Becker, A.; Riefke, B.; Ebert, B.; Sukowski, U.; Rinneberg, H.; et al. Macromolecular contrast agents for optical imaging of tumors: Comparison of indotricarbocyanine-labeled human serum albumin and transferrin. *Photochem. Photobiol.* **2000**, *72*, 234–241.
(25) Bremer, C.; Tung, C. H.; Weissleder, R. In vivo molecular target assessment of matrix metalloproteinase inhibition. *Nat. Med.* **2001**, *7*, 743–748.
(26) Tung, C. H.; Bredow, S.; Mahmood, U.; Weissleder, R. Preparation of a cathepsin D sensitive near-infrared fluorescence probe for imaging. *Bioconjugate Chem.* **1999**, *10*, 892–896.
(27) Achilefu, S.; Dorshow, R. B.; Bugaj, J. E.; Rajagopalan, R. Novel receptor-targeted fluorescent contrast agents for in vivo tumor imaging. *Invest. Radiol.* **2000**, *35*, 479–485.
(28) Becker, A.; Hessenius, C.; Licha, K.; Ebert, B.; Sukowski, U.; et al. Receptor-targeted optical imaging of tumors with near-infrared fluorescent ligands. *Nat. Biotechnol.* **2001**, *19*, 327–331.
(29) Bugaj, J. E.; Achilefu, S.; Dorshow, R. B.; Rajagopalan, R. Novel fluorescent contrast agents for optical imaging of in vivo tumors based on a receptor-targeted dye-peptide conjugate platform. *J. Biomed. Opt.* **2001**, *6*, 122–133.
(30) Raynor, K.; Reisine, T. Analogues of Somatostatin Selectively Label Distinct Subtypes of Somatostatin Receptors in Rat-Brain. *J. Pharmacol. Exp. Ther.* **1989**, *251*, 510–517.
(31) Reubi, J. C.; Waser, B.; Schaer, J. C.; Laissue, J. A. Somatostatin receptor sst1-sst5 expression in normal and neoplastic human tissues using receptor autoradiography with subtype-selective ligands. *Eur. J. Nucl. Med.* **2001**, *28*, 836–846.
(32) Behr, T. M.; Gotthardt, M.; Barth, A.; Behe, M. Imaging tumors with peptide-based radioligands. *Q. J. Nucl. Med.* **2001**, *45*, 189–200.
(33) Janson, E. T.; Westlin, J. E.; Ohrvall, U.; Oberg, K.; Lukinius, A. Nuclear localization of In-111 after intravenous injection of [In-111-DTPA-D-Phe(1)]-octreotide in patients with neuroendocrine tumors. *J. Nucl. Med.* **2000**, *41*, 1514–1518.
(34) Lewis, J. S.; Srinivasan, A.; Schmidt, M. A.; Anderson, C. J. In vitro and in vivo evaluation of Cu-64-TETA-Tyr(3)- octreotate. A new somatostatin analogue with improved target tissue uptake. *Nucl. Med. Biol.* **1999**, *26*, 267–273.
(35) Hoffman, T. J.; Quinn, T. P.; Volkert, W. A. Radiometalated receptor-avid peptide conjugates for specific in vivo targeting of cancer cells. *Nucl. Med. Biol.* **2001**, *28*, 527–539.
(36) Glasspool, R. M.; Evans, T. R. J. Clinical imaging of cancer metastasis. *Eur. J. Cancer* **2000**, *36*, 1661–1670.
(37) Hintz, S. R.; Cheong, W. F.; Van Houten, J. P.; Stovenson, D. K.; Benaron, D. A. Bedside imaging of intracranial hemorrhage in the neonate using light: Comparison with ultrasound, computed tomography, and magnetic resonance imaging. *Pediatr. Res.* **1999**, *45*, 54–59.
(38) Chang, J. W.; Graber, H. L.; Koo, P. C.; Aronson, R.; Barbour, S. L. S.; et al. Optical imaging of anatomical maps derived from magnetic resonance images using time-independent optical sources. *IEEE Trans. Med. Imaging* **1997**, *16*, 68–77.
(39) Edwards, W. B.; Fields, C. G.; Anderson, C. J.; Pajeau, T. S.; Welch, M. J.; et al. Generally Applicable, Convenient Solid-Phase Synthesis and Receptor Affinities of Octreotide Analogues. *J. Med. Chem.* **1994**, *37*, 3749–3757.
(40) Atherton, E.; Sheppard, R. C. *Solid Phase Peptide Synthesis: A Practical Appraoch*; Oxford University Press: Oxford, England, 1989.
(41) Achilefu, S.; Wilhelm, R. R.; Jimenez, H. N.; Schmidt, M. A.; Srinivasan, A. A new method for the synthesis of tri-*tert*-butyl diethylenetriaminepentaacetic acid and its derivatives. *J. Org. Chem.* **2000**, *65*, 1562–1565.
(42) Packard, B. Z.; Komoriya, A.; Toptygin, D. D.; Brand, L. Structural characteristics of fluorophores that form intramolecular H-type dimers in a protease substrate. *J. Phys. Chem. B* **1997**, *101*, 5070–5074.
(43) Reichert, D. E.; Welch, M. J. Applications of molecular mechanics to metal-based imaging agents. *Coord. Chem. Rev.* **2001**, *212*, 111–131.
(44) de Jong, M.; Breeman, W. A. P.; Bernard, B. F.; Bakker, W. H.; Schaar, M.; et al. [Lu-177-DOTA(0), Tyr(3)]octreotate for somatostatin receptor- targeted radionuclide therapy. *Int. J. Cancer* **2001**, *92*, 628–633.
(45) Karra, S. R.; Schibli, R.; Gali, H.; Katti, K. V.; Hoffman, T. J.; et al. Tc-99m-labeling and in vivo studies of a bombesin analogue with a novel water-soluble dithiadiphosphine-based bifunctional chelating agent. *Bioconjugate Chem.* **1999**, *10*, 254–260.
(46) Ntziachristos, V.; Chance, B. Probing physiology and molecular function using optical imaging: applications to breast cancer. *Breast Cancer Res.* **2001**, *3*, 41–46.
(47) Ferone, D.; Kwekkeboom, D. J.; Pivonello, R.; Bogers, A.; Colao, A.; et al. In vivo and in vitro expression of somatostatin receptors in two human thymomas with similar clinical presentation and different histological features. *J. Endocrinol. Invest.* **2001**, *24*, 522–528.
(48) Stolz, B.; Weckbecker, G.; Smith-Jones, P. M.; Albert, R.; Raulf, F.; et al. The somatostatin receptor-targeted radiotherapeutic [Y-90-DOTA- DPhe(1), Tyr(3)]octreotide (Y-90-SMT 487) eradicates experimental rat pancreatic CA 20948 tumours. *Eur. J. Nucl. Med.* **1998**, *25*, 668–674.

JM010519L

Dankwoord

This work would not have been possible without the help and support of many, only some of whom are mentioned below. I do wish to offer my gratitude to all whether mentioned by name or as a group.

First, my most sincere thanks goes to Dr. Marion de Jong, as it was really her idea to persue this as a legitimate thesis project. If it had not been for her on that fateful day in October in the basement labs of Mallinckrodt, this work would likely have remained as a mere footnote in forgotten notebooks. She was the first person to recognize this work as original and defendable, and who made the initial inquiry regarding acceptance to the doctoral program at Erasmus University. Her guidance, insight, encouragement and perseverance are the main reason for it becoming public. Over the past three years, she has been a valuable advisor, co-investigator, and most importantly, a dear friend who has never wavered in support of this work.

To Professor Eric Krenning, the Father of OctreoScan, and the reason why this work was started, for your acceptance of this project and your willingness to serve as Promoter. I am greatly indebted to you for your inspiration, advice and for the example you have set, not only to myself, but to all who labor in „Unclear Medicine".

To the three best co-workers one could ever hope to work with in a laboratory: Drs. Ananth Srinivasan, Jack Erion and Michelle Schmidt. Together we made and evaluated a lot of peptides, injected and scanned many a tumor bearing rat and along the way made a nifty little discovery in Octreotate. I can not really express my full gratitude to the three of you who made this work possible, and who have been so

much a part of its success. It was not always easy working as we did, but somehow we managed to put science first and worry about the politics after. The end result is obvious.

To the BioMedical Optics Team consisting of Drs. Rick Dorshow, Sam Achilefu and Raghavan Rajagopalan who together literally brought light to this project and who gave the world Cytate. I have never worked in a more diverse scientific group, nor have I ever worked in a more diverse group ethnically. In this diversity we created an uncommon bond of trust, dedication and mutual respect. Not only did we also accomplish some fine research, we managed to have a bit of fun and a few laughs along the way. Each of us learned a lot about each other's respective expertise, and in the end we clearly made our mark in the area of targeted peptides for biomedical indications.

To my Paranimf, Bert Bernard, who was always there to lend advice, a helping hand and for just being part of the Octreotate project. You are the true „Maestro", Bert, and you deserve a tremendous amount of credit not only from me, but from many others whom you have helped walk down this difficult path.

To former Mallinckrodt employees, Michael Johnson, Lori Chinen, Betsy Webb, Mary Dyszlewski, and others who helped maintain a challenging and sane environment in which to work.

To other members of the Nuclear Medicine staff at Erasmus Medical Center, most notably Wout Breeman, Willem Bakker and Dik Kwekkeboom, who have been long

standing pioneers in the area of radiolabeled peptides, and more recently for having the foresight to bring Octreotate to a clinical setting.

Lastly, and most importantly I want to reserve a special „thank you" to the two women in my life. First, to my wife of many years, Maggie, who really made this work possible. Without your unconditional support for so many years, it simply could not have happened. You have had to sacrifice for so long, yet you have never questioned why. And to my beautiful daughter, Myrista, I too say thank you. I may not have always been there for you, but you were never far from my thoughts. Unfortunately, I can not turn the clock back and return lost time to either of you, but I promise that, after all these years in the lab, this is my last academic adventure.

Curriculum Vitae

Joseph Thomas Edward Bugaj was born on December 28, 1951 in Huntington Station, New York. He graduated from Honesdale High School (Honesdale, Pennsylvania) in 1969, and then completed studies leading to a Bachelor of Science degree from Black Hills State University (Spearfish, South Dakota) in 1973. He spent the next two and half years in the Philippine Islands (El Salvador, Mindanao) as a Rural Health Assistant as part of the United States Peace Corps. He graduated from the Cincinnati College of Mortuary of Science (Cincinnati, Ohio) in 1977. He then began his career in research in that same year by joining The Procter & Gamble Company in Cincinnati, where he was first introduced to the field of nuclear medicine. He has since worked in nuclear medicine for NeoRx Corporation (Seattle, Washington) and Mallinckrodt Inc. (St. Louis, Missouri). In 1996 he completed a Master of Science degree in Cellular and Molecular Biology from the University of Missouri-St. Louis. For the past two years he has been employed by Schering AG in Berlin, Germany, where he continues research in the area of radiotherapy.

List of Publications

1. VanDuzee, B.F.; Bugaj, J.E.: The Effect of Total Technetium Concentration on the Performance of a Skeletal Imaging Agent, *Technetium and Chemistry in Nuclear Medicine* (1983)

2. Bugaj, J.E.; Esser, P.D.; Tofe, A.J.; Borgia, A.T.; Fawwaz, R.A.: The Effect of DMSO Treatment on the Performance of 99m-Tc HEDP*; Int. J. Nucl. Bio.*, #11, 109-111 (1984)

3. Holland, M.E.; Bugaj, J.E.; Heineman, W.R.; and Deutsch, E.A.: Technetium-99m Complexes of Dimethylaminomethylene Diphosphonate (DMAD)-II. Biological Distributions of 99m-Tc DMAD Components Isolated by Anion Exchange HPLC., *Int. J. Nucl. Med. Bio.*, #16, 313-317 (1989)

4. Rajagopalan, R.; Grummon, G.D.; Bugaj, J.E.; et al.: Preparation, Characterization and Biological Evaluation of Technetium(V) and Rhenium(V) Complexes of Novel Heterocyclic Tetradentate-N_3S Ligands, *Bioconjugate Chemistry*, 8, 407-415 (1997)

5. Dorshow, R.B.; Bugaj, J.E.; Burleigh, B.D.; Duncan, J.R.; Johnson, M.A.; and Jones, W.B.: Non-Invasive Flourescence Detection of Hepatic and Renal Function; *J. Biomedical Optics*, Vol. 3, Issue 3, 340-345 (1998)

6. de Jong, M.; Krenning, E.; Macke, H.; Bugaj, J.E.; Srinivasan, A.; Erion, J.L.; et. al.: Comparison of ^{111}In- Labeled Somatostatin Analogs for Tumor Scintigraphy and Radionuclide Therapy; *Cancer Research*, (58), 437-441, February 1 (1998)

7. Dorshow, R.B.; Bugaj, J.E.: Non-Invasive Fluorescence Detection of Physiological Function, *SPIE*, Vol. 3252, 124-130 (1998)

8. Dorshow, R.B., Bugaj, J.E., Schmidt, M.A., and Srinivasan, A.: Non-Invasive Renal Function Assesment by Fluorescent Detection, *TOPS*, 120-127 (1998)

9. Reubi, J.C.; Waser, B.; Schaer, U.; Srinivasan, A.; Schmidt, M.A.; Erion, J.L.; and Bugaj, J.E.: Unsulfated DTPA and DOTA-CCK Analogs as Specific High Affinity Ligands for CCK- B Receptor-Expressing Human and Rat Tissues *in vitro* and *in vivo*: *European Journal of Nuclear Medicine*, Vol. 25, No. 5, pp.481-490 (1998)

10. Wible, J.H.; Wojdyla, J.K.; Bugaj, J.E.; and Brandenburger, G.H.: Effects of Inhaled Gases on the Ultrasound Contrast Produced by Microspheres Containing Air or Perfluoropropane in Anesthetized Dogs, *Investigative Radiology*, Vol. 33, No. 12, pp.871-879, (1998)

11. Dorshow, R. B., and Bugaj, J.E.; Real-Time Fluorecsent Detection of Dynamic Organ Function, *Optics & Photonic News*, (16), December, 1998

12. Dorshow, R.B., Bugaj, J.E., Achilefu, S.I., Rajagopalan, R., and Combs, A.H.; Monitoring Physiological Function by Detection of Exogeneous Fluorescent Contrast Agents, *SPIE*, Vol. 3599, pp.2-8, (1999)

13. Rajagopalan, R., Bugaj, J.E., Dorshow, R.B., Venkatramani, C.J., et al., Polyionic Fluorescent Bioconjugates as Tracer Agents for Continuous Monitoring of Renal Function, *SPIE*, Vol. 3924, #18, pp.28-34 (2000)

14. Achilefu, S., Dorshow, R.B., Bugaj, J.E., and Rajagopalan, R., Tumor Specific Fluorescent Contrast Agents, *SPIE*, Vol. 3917, #11, pp.80-86, (2000)

15. Rajagopalan, R., Uetrecht, P., Bugaj, J.E., Achilefu, S.A., and Dorshow, R.B.; Stabilization of the Optical Tracer Agent Indocyanine Green Using Noncovalent Interactions, *Photochemistry and Photobiology*, 71 (3), pp. 347-350, (2000)

16. Achilefu, S., Dorshow, R.B., Bugaj, J.E., and Rajagopalan, R.; Novel Receptor-Targeted Contrast Agents for In Vivo Tumor Imaging, *Investigative Radiology*, Vol. 35, No. 8, pp. 479-485, (2000)

17. Bugaj, J.E.; Erion, J.L., Johnson, M.A., Schmidt, M.A., and Srinivasan, A. Radiotherapeutic Efficacy of ^{153}Sm-CMDTPA-Tyr^3-Octreotate in a Rat Tumor Model, *Nuclear Medicine & Biology*, 28, pp.327-334 (2001).

18. Bugaj, J.E.; Achilefu, S.I.; Dorshow, R.B.; and Rajagopalan, R. Novel Fluorescent Contrast Agents for Optical Imaging of in vivo Tumors Based on a Receptor-Targeted Dye-Peptide Platform, *J. Biomedical Optics*, 6, (2) pp.122-133 (2001).

19. De Jong, M.; Breeman, W.A.P.; Bernard, H.F.; Bakker, W.H.; Bugaj, J.E.; Erion, J.L.; Schmidt, M.A.; Srinivasan, A.; and Krenning, E.P. [^{177}Lu-DOTA^0, Tyr^3] Octreotate for Somatostatin Receptor-Targeted Radionuclide Therapy, *Int. J. Cancer*, 92, pp.628-633 (2001)

20. Lewis, J.S.; Wang, M.; LaForest, R.; Wang, F.; Erion, J.L.; Bugaj, J.E.; Srinivasan, A., and Anderson, C.J. Toxicity and Dosimetry of ^{177}Lu-DOTA-Y^3-Octreotate in a Rat Model, *Int. J. Cancer*, 94, pp.873-877 (2001)

21. Kwekkeboom, D.J.; Bakker, W.H.; Kooij, P.M.; Konijenberg, M.W.; Srinivasan, A.; Erion, J.L.; Schmidt, M.A.; Bugaj, J.E.; de Jong, M., and Krenning, E.P. [^{177}Lu-DOTA^0-Tyr^3]Octreotate: Comparison with [^{111}In-DTPA^0]Octreotide in Patients, *Eur. J. Nucl. Med.*, 28, pp. 1319-1325 (2001)

22. Achilefu, S., Jimenez, H.N.; Dorshow, R.B., Bugaj, J.E., Webb, E.G., Wilhelm, R.R., Rajagopalan, R., Johler, J., and Erion, J.L. Synthesis, in vitro receptor binding, and in vivo evaluation of flourescein and carbocyanine Peptide-based optical contrast agents, *J Med Chem*, 9:45, pp. 2003-2015 (2002)

23. Li, W.P.; Lewis, J.S.; Kim, J.; Bugaj, J.E.; Johnson, M.A.; Erion, J.L. and Anderson, C.J. DOTA-D-Tyr^1-Octreotate: A Somatostatin Analogue for Labeling with Metal and Halogen Radionuclides for Cancer Imaging and Therapy, *Bioconjugate Chemistry*, 13, 721-728 (2002)

24. Bugaj, J.E., Friebe, M., Cyr, J.E., Azure, M.T., Lister-James, J., Dean, R.T. and Dinkelborg, L.M. Radiotherapeutic Efficacy of Re-188 P2045 in Small Cell Lung Carcinoma (SCLC) and non-Small Cell Lung Cancer (NSCLC) Mouse Models by Specific SSTR-Targeting, *Technetium, Rhenium and Other Metals in Chemistry and Nuclear Medicine*, 6, 357-362, (2002)